



**HAL**  
open science

# New inhibitors of quinolinate synthase as potential antibacterial drugs

Jaione Saez Cabodevilla

► **To cite this version:**

Jaione Saez Cabodevilla. New inhibitors of quinolinate synthase as potential antibacterial drugs. Bacteriology. Université Grenoble Alpes, 2018. English. NNT : 2018GREAV047 . tel-02065313

**HAL Id: tel-02065313**

**<https://theses.hal.science/tel-02065313>**

Submitted on 12 Mar 2019

**HAL** is a multi-disciplinary open access archive for the deposit and dissemination of scientific research documents, whether they are published or not. The documents may come from teaching and research institutions in France or abroad, or from public or private research centers.

L'archive ouverte pluridisciplinaire **HAL**, est destinée au dépôt et à la diffusion de documents scientifiques de niveau recherche, publiés ou non, émanant des établissements d'enseignement et de recherche français ou étrangers, des laboratoires publics ou privés.

## THÈSE

Pour obtenir le grade de

### **DOCTEUR DE LA COMMUNAUTÉ UNIVERSITÉ GRENOBLE ALPES**

Spécialité : **Chimie Biologie**

Arrêté ministériel : 25 mai 2016

Présentée par

**« Jaione SAEZ CABODEVILLA »**

Thèse dirigée par **Sandrine OLLAGNIER, DR, CNRS**, et  
codirigée par **Yung-Sing WONG, CR, CNRS**

préparée au sein du **Laboratoire de Chimie et Biologie des  
métaux** (CEA, Grenoble) et du **Département de  
Pharmacochimie Moléculaire** (UGA, Grenoble)

dans **l'École Doctorale Chimie et Sciences du Vivant**

## **Nouveaux inhibiteurs de la quinolinate synthase comme potentiels antibactériens**

Thèse soutenue publiquement le « **6 décembre 2018** »,  
devant le jury composé de :

**Monsieur David PIGNOL**

Directeur de Recherches, CEA Cadarache, Président

**Madame Myriam SEEMANN**

Directrice de Recherches au CNRS, Strasbourg, Rapportrice

**Monsieur Erwan GALARDON**

Chargé de Recherches au CNRS, Paris, Rapporteur

**Madame Isabelle SCHALK**

Directrice de Recherches au CNRS, Strasbourg, examinatrice

**Monsieur Nicolas SPINELLI**

Maître de conférences à l'UGA, Grenoble, examinateur

**Madame Sandrine OLLAGNIER**

Directrice de Recherches au CNRS, Grenoble, directrice de thèse

**Monsieur Yung-Sing WONG**

Chargé de Recherches au CNRS, Grenoble, invité

**Monsieur Olivier HAMELIN**

Maître de conférences à l'UGA, Grenoble, invité









# ABBREVIATION LIST

3HP	3-hydroxyphthalic acid
4AP	4-aminophthalic acid
4-DMAP	4-dimethylaminopyridine
4HP	4-hydroxyphthalic acid
4MP	4-mercaptophthalic acid
5MPDC	5-mercaptopyridine-2,3-dicarboxylic acid
5MPzDC	5-mercaptopyrazine-2,3-dicarboxylic acid
6MPDC	6-mercaptopyridine-2,3-dicarboxylic acid
ADP	Adenosine diphosphate
Aib	2-aminoisobutyric acid
AIBN	2,2'-Azo-bis-isobutyronitrile
Ala	Alanine
AMP	Adenosine monophosphate
Arg	Arginine
AS	Ammonium sulfate
Asp	Aparagine
ATP	Adenosine triphosphate
BLY	Bio-Layer Interferometry
Boc	tert-butyloxycarbonyl
BPB	Bromophenol blue
BSA	Bovine serum albumin
cADPR	Cyclic ADP-ribose
CD	Circular dichroism
CHES	N-Cyclohexyl-2-aminoethanesulfonic acid
Cys	Cysteine
DCC	<i>N,N'</i> -Dicyclohexylcarbodiimide
DFT	Density functional theory
DHAP	Dihydroxyacetone phosphate
DMF	N,N-dimethylformamide
DMP	1,2-dimercaptophthalic acid
DMPD	N,N-dimethyl-p-phenylenediamine
DMSO	Dimethyl sulfoxide
DNA	Deoxyribonucleic acid
DTHPA	Dithiohydroxyphthalic acid
DTT	Dithiothreitol
EDCI	1-ethyl-3-(3-dimethylaminopropyl)carbodiimide
EDTA	Ethylenediaminetetraacetic acid
EPR	Electron paramagnetic resonance
Eq	Equivalents
ESI	Electrospray ionization
Et	Ethyl
Et <sub>2</sub> O	Diethyl ether
Et <sub>3</sub> N	Triethylamine

EtOAc	Ethyl acetate
EtOH	Ethanol
FAD	Flavin adenine dinucleotide
G3P	Glyceraldehyde-3-phosphate
Glu	Glutamic acid
h	Hour
HATU	Hexafluorophosphate Azabenzotriazole Tetramethyl Uronium
HEPES	4-(2-hydroxyethyl)-1-piperazineethanesulfonic acid
His	Histidine
HOBt	Hydroxybenzotriazole
HPLC	High performance liquid chromatography
HRMS	High resolution mass spectrometry
Hunig base	N,N-Diisopropylethylamine
IA	Iminoaspartate
IARC	International agency for research on cancer
IPTG	Isopropyl $\beta$ -D-1-thiogalactopyranoside
ITC	Isothermal titration calorimetry
LB	Luria Miller-Broth
Lys	Lysine
M9	Minimal medium
<i>m</i> -CPBA	<i>meta</i> -chloro perbenzoic acid
MDT	Multidrug therapy
Me	Methyl
Me <sub>3</sub> N	Trimethylamine
MeOH	Methanol
min	Minute
MP	Mercaptophthalic acid
MS	Mass spectrometry
Na	Nicotinic acid
NAD	Nicotinamide adenine dinucleotide
NADP	Nicotinamide adenine dinucleotide phosphate
NaNM	Nicotinic acid mononucleotide
Ni-NTA	Nickel nitriloacetic acid
Nm	Nicotinamide
NMN	Nicotinamide mononucleotide
NMNAT	Nicotinamide mononucleotide adenylyltransferase
NMR	Nuclear magnetic resonance
NmR	Nicotinamide riboside
OAA	Oxaloacetic acid
Oac	Acetate
OD	Optical density
PA	Phthalic acid
PCA	Perchloric acid
PEG	Polyethylene glycol
PLP	Pyridoxal-5- phosphate
PMSF	Phenylmethane sulfonyl fluoride

PPI	Proton pump inhibitor
PRPP	Phosphoribosyl pyrophosphate
<i>p</i> -TsCl	<i>para</i> -toluenesulfonyl chlorine
QA	Quinolinic acid
RNA	Ribonucleic acid
ROS	Reactive oxygen species
rt	Room Temperature
SAM	S-adenosyl- <i>L</i> -methionine
SDS	Sodium dodecyl sulfate
SDS-PAGE	Sodium dodecyl sulfate polyacrylamide gel electrophoresis
Ser	Serine
<i>t</i> Bu	<i>tert</i> -butyl
TFA	Trifluoroacetic acid
THF	Tetrahydrofuran
Thr	Threonine
TLC	Thin layer chromatography
TMSCl	Trimethylsilyl chloride
TMSOH	2(trimethylsilyl ethanol
TPI	Triose phosphate isomerase
TRIS	Tris(hidroxymethyl)aminomethane
Trp	Tryptophan
Ts	Tosyl
Tyr	Tyrosine
UV	Ultraviolet
WHO	World health organization



## Résumé

La résistance aux antibiotiques par les micro-organismes est une menace mondiale. C'est pourquoi la recherche de nouveaux médicaments revêt une importance capitale de nos jours.

Le nicotinamide adénine dinucléotide (NAD) est un cofacteur essentiel et un substrat dans de nombreuses réactions biologiques. Pour cette raison, les enzymes qui l'utilisent comme substrat et celles qui participent à sa biosynthèse sont largement étudiées en tant que cibles antibactériennes potentielles. Dans ce contexte, nous nous intéressons au développement de nouveaux agents antibactériens contre la quinolinate synthase (NadA). Cette enzyme participe à la voie de biosynthèse de novo du NAD chez les procaryotes et est essentielle chez deux pathogènes : *Helicobacter pylori*, responsable d'ulcères et de cancers gastriques, et *Mycobacterium leprae*, responsable de la lèpre. Le fait que NadA n'existe que chez les procaryotes et qu'elle est essentielle chez deux agents pathogènes font de NadA une cible intéressante pour la conception de nouveaux antibactériens. La quinolinate synthase est une enzyme [4Fe-4S] où l'un des atomes de Fe est coordonné par une molécule d'eau à l'état de repos et joue le rôle d'acide de Lewis durant la catalyse. La réaction catalysée par NadA consiste en la formation d'acide quinolinique (QA), précurseur du NAD, à partir d'iminoaspartate et de dihydroxyacétone phosphate. Sur la base de la découverte dans notre laboratoire du premier inhibiteur de NadA (le DTHPA), qui agit par coordination irréversible du fer catalytique du cluster, nous avons conçu et synthétisé une famille de molécules pouvant servir d'inhibiteurs plus spécifiques de NadA. Ces molécules contiennent un cycle benzène / pyridine ou pyrazine, deux carboxylates vicinaux et un thiol en tant que groupe coordonnant du fer: l'acide 4-mercaptophthalique (4MP), l'acide 6-mercaptopyridine-2, 3-dicarboxylique (6MPDC), l'acide 5-mercaptopyrazine-2, 3-dicarboxylique (5MPzDC) et l'acide 5-mercaptopyridine-2, 3-dicarboxylique (5MPDC). Nous avons démontré que ces molécules inhibent l'enzyme NadA *in vitro* avec un IC<sub>50</sub> du même ordre de grandeur que celui du DTHPA (dizaine de µM). Par l'utilisation de diverses spectroscopies et de la cristallographie, nous avons démontré que l'inhibition s'effectue par la coordination de ces molécules avec le fer catalytique du cluster via leur groupement thiol. Nous avons également étudié *in vitro* la spécificité de ces molécules. Nous avons montré que les molécules 4MP et 5MPDC étaient des inhibiteurs spécifiques de NadA lorsqu'on les teste sur l'aconitase B, une enzyme [4Fe-4S] bactérienne, dont le cluster présente des propriétés structurales et fonctionnelles similaires à celles du cluster de NadA.

Enfin, nous avons étudié l'activité d'inhibitrice de l'ensemble des molécules *in cellulo* sur de la voie de biosynthèse du QA chez *Escherichia coli* avec le DTHPA comme contrôle. Alors que les molécules 6MPDC et 5MPzDC inhibent la croissance d'*E. coli* de manière indépendante de la voie de biosynthèse du QA, le 4MP et le 5MPDC (les deux inhibiteurs spécifiques *in vitro*) n'ont montré aucune activité inhibitrice *in cellulo*. Ce manque d'activité pouvant être dû à un manque de pénétration des molécules à l'intérieur des bactéries, nous avons envisagé de favoriser la pénétration à l'aide d'un vecteur transmembranaire, un analogue simplifié du tétra-cyclopeptide naturel FR235222. Nous avons synthétisé et couplé le cyclopeptide à l'inhibiteur 4MP. Malheureusement, aucune inhibition de la croissance d'*E. coli* n'a été observée. La thèse s'est terminée en essayant de comprendre la pénétration du tétra-cyclopeptide sur bactérie, en utilisant notamment des agents fluorophores.

## Summary

Resistance to antibiotics is becoming a world-wide threat. Microorganisms are able to withstand drugs leading to persistence of diseases. This is why the research of new drugs is of great importance nowadays.

Nicotinamide adenine dinucleotide (NAD) is an essential cofactor and substrate in numerous biological reactions. For this reason, both the enzymes that use it as a substrate and those participating on its biosynthetic pathway are largely studied as potential antibacterial targets. In this context, we are interested in the development of new antibacterial drugs against quinolinate synthase enzyme (NadA). This enzyme participates in the prokaryotic NAD *de novo* biosynthetic pathway and is essential in two pathogens: *Helicobacter pylori*, cause of gastric ulcers and cancers, and *Mycobacterium leprae*, responsible of leprosy. The fact that NadA only exists in prokaryotes and the fact that it is essential for these two pathogens make it an interesting target for the design of new antibacterial drugs. Quinolinate synthase is a [4Fe-4S] cluster enzyme, where one of the Fe sites is coordinated by a water molecule in the resting state, and plays a Lewis acid role during catalysis. The reaction catalyzed by NadA consists in the formation of quinolinic acid (QA), precursor of NAD, from iminoaspartate and dihydroxyacetone phosphate. Based on the discovery in our laboratory of the first inhibitor of NadA (DTHPA) that coordinates irreversibly the catalytic iron site of the cluster, we designed and synthesized a family of molecules as potential more specific NadA inhibitors. These molecules contain a benzene/pyridine or pyrazine ring, two vicinal carboxylates and a thiol as an iron coordinating group: 4-mercaptophthalic acid (4MP), 6-mercaptopyridine-2, 3-dicarboxylic acid (6MPDC), 5-mercaptopyrazine-2, 3-dicarboxylic acid (5MPzDC) and 5-mercaptopyridine-2, 3-dicarboxylic acid (5MPDC). We demonstrated that these molecules inhibit NadA enzyme *in vitro* in the same range as DTHPA. Using different spectroscopies and crystallography, we demonstrated that inhibition occurs by coordination of the molecules to the catalytic iron site through their thiol group. We investigated also *in vitro* the specificity of these molecules. We demonstrated that 4MP and 5MPDC molecules are specific NadA inhibitors when assayed on bacterial aconitase B, a [4Fe-4S] enzyme, whose cluster displays functional and structural properties similar to those of NadA.

Finally, we investigated the QA pathway inhibition activity of the four molecules *in cellulo*, in an *Escherichia coli* strain. Whereas 6MPDC and 5MPzDC molecules inhibit *E. coli* growth in a QA biosynthetic pathway independent manner, 4MP and 5MPDC (the two *in vitro* specific inhibitors) did not show any *in cellulo* inhibition activity. Since this lack of activity might be due to a lack of penetration of the molecules inside bacteria, we thought about assisting the penetration of the molecules using a transmembrane carrier, a simplified analogue of the tetra-cyclopeptide FR235222 natural product. We synthesized and coupled the cyclopeptide to the 4MP inhibitor. Unfortunately, no *E. coli* growth inhibition was observed. The Ph.D ended by investigating the penetration of the tetra-cyclopeptide inside bacteria, using some fluorophore agents.





# Table of contents

INTRODUCTION .....	15
I. Nicotinamide Adenine Dinucleotide (NAD).....	16
a. Structure .....	16
b. Physical-chemical properties.....	17
c. Functions of NAD/NADH and NADP/NADPH.....	18
(i) Role in redox metabolism.....	18
(ii) Role in non-redox metabolism .....	20
d. NAD physiological concentration and cell localization in eukaryotes.....	23
II. NAD biosynthesis.....	24
a. The <i>de novo</i> pathways .....	24
(i) Upstream pathway in prokaryotes.....	25
(ii) Upstream pathway, in eukaryotes .....	26
(iii) -Downstream pathway: common in prokaryotes and eukaryotes.....	29
b. Salvage and recycling pathways .....	31
(i) Prokaryotes and eukaryotes except mammals .....	32
(ii) Mammals .....	35
c. NAD biosynthesis regulation .....	36
(i) NAD metabolism regulation by NadR.....	36
(ii) NAD metabolism regulation by NiaR.....	37
(iii) NAD metabolism regulation by NrtR .....	37
III. NAD: a pharmacological target.....	38
IV. Quinolinic acid production in prokaryotes: Quinolinate synthase system .....	39
a. Identification of enzymes .....	39
b. Identification of substrates.....	40
c. A NadA-NadB complex?.....	43
d. Characterization of <i>L</i> -aspartate oxidase (NadB).....	44
e. NadA: A [4Fe-4S] <sup>2+</sup> enzyme.....	46
(i) Purification and characterization of NadA apoprotein .....	46
(ii) Purification and characterization of the holoprotein.....	46
(iii) NadA [4Fe-4S] <sup>2+</sup> cluster: sensitivity to oxygen.....	49
f. Structure of Quinolinate synthase NadA.....	52
(i) First structures of apoprotein quinolinate synthase .....	52

(ii)	First structure of holo-protein quinolinate synthase .....	54
g.	Mechanism of Quinolinate synthase .....	57
h.	DTHPA: The first NadA inhibitor .....	63
i.	Structure-activity study based on DTHPA.....	66
V.	Antibiotics in the XXI century .....	68
a.	Antibiotic resistance-historical overview .....	68
(i)	Gram-positive bacteria .....	71
(ii)	Gram-negative bacteria .....	71
(iii)	Mycobacteria .....	71
b.	The search for new antibacterial agents .....	73
(i)	<i>Helicobacter pylori</i> .....	73
(ii)	<i>Mycobacterium leprae</i> .....	74
c.	Across the cell membranes.....	75
d.	Approaches to design and improve membrane permeability.....	76
e.	The natural cyclic tetrapeptide FR235222 and its analogues.....	77
	Ph.D OBJECTIVES .....	81
	RESULTS CHAPTER I: .....	85
	SYNTHESIS OF POTENTIAL QUINOLINATE SYNTHASE INHIBITORS .....	85
I.	Synthesis of 6- mercaptopyridine- 2, 3-dicarboxylic acid (6MPDC) from QA.....	87
II.	Synthesis of 5- mercaptopyrazine- 2, 3-dicarboxylic acid (5MPzDC) from 2- chloroquinoxaline 93	
III.	Synthesis of 5-mercaptopyridine- 2, 3-dicarboxylic acid (5MPDC) from 3-chloroquinoline....	98
	RESULTS CHAPTER II: .....	107
	<i>IN VITRO</i> STUDIES OF 6MPDC, 5MPzDC, 6MPDC AND 4MP ON NadA.....	107
I.	Production of <sup>56</sup> Fe-S NadA, <sup>57</sup> Fe-S NadA and NadB proteins.....	108
a.	<i>E. coli</i> <sup>56</sup> Fe-S NadA and <sup>57</sup> Fe-S NadA.....	108
b.	<i>E.coli</i> NadB .....	110
II.	NadA inhibition with 6MPDC, 5MPzDC, 5MPDC and 4MP .....	111
III.	Study of NadA inhibition mechanism .....	116
c.	Mössbauer spectroscopy.....	116
d.	UV-visible absorption spectroscopy .....	118
e.	Circular dichroism .....	119
f.	Crystal structures of NadA in complex with the molecules.....	122
IV.	Specificity.....	125

V.	Discussion .....	129
a.	NadA inhibition mechanism .....	130
b.	Specificity.....	132
VI.	5MPDC and <i>TmNadA</i> * .....	134
a.	Discussion .....	136
RESULTS CHAPTER III: .....		139
<i>IN CELLULO</i> INHIBITION STUDY OF 6MPDC, 5MPzDC, 5MPDC AND 4MP .....		139
I.	<i>E. coli</i> MG1655 as strain for <i>in cellulosa</i> tests.....	140
II.	<i>In cellulosa</i> tests of the four NadA inhibitors: 6MPDC, 5MPzDC, 5MPDC and 4MP .....	141
a.	Esterification of the carboxylic acids .....	142
b.	Test under anaerobic conditions .....	144
c.	Penetration and drug delivery strategy assisted by FR235222 simplified analogue. 146	
(i)	Synthesis of compound 22 .....	149
	Synthesis of compound 23.....	153
(ii)	Synthesis of compound 24: coupling of 23 and 4MP .....	154
(iii)	<i>E. coli</i> MG1655 growth tests with compounds 22 and 24.....	155
III.	Looking for visual penetration evidence .....	156
a.	Synthesis of compound 40.....	157
b.	Synthesis of compound 41.....	160
c.	<i>In cellulosa</i> assays of fluorophores and their cyclopeptide-analogues 38 and 39; 42 and 40; 50 and 41. ....	162
d.	Fluorescence assays <i>in cellulosa</i> .....	164
IV.	DISCUSSION AND CONCLUSION .....	166
GENERAL CONCLUSION AND PERSPECTIVES.....		169
MATERIALS AND METHODS .....		175
I.	Biological materials.....	176
a.	Bacterial strains .....	176
b.	Plasmids .....	176
c.	Culture media .....	177
II.	Molecular biology methods.....	177
a.	Preparation of competent cells .....	177
b.	Transformation of competent cells .....	177
III.	Biochemical methods .....	178

a.	Protein overexpression.....	178
b.	Protein extraction.....	178
(i)	Freeze-thaw cycles.....	178
(ii)	Sonication.....	178
c.	Protein purification.....	179
d.	Reconstitution of NadB FAD cofactor.....	179
e.	Enzymatic activity measurements.....	179
(i)	<i>in vitro</i> NadA activity.....	179
(ii)	<i>in vitro</i> NadB activity.....	181
(iii)	<i>in vitro</i> AcnB activity.....	182
f.	Biochemical analyses.....	183
(i)	Protein quantification using Bradford method.....	183
(ii)	Protein quantification using Nanodrop.....	183
(iii)	SDS-PAGE: Electrophoresis.....	184
(iv)	Iron content.....	185
(v)	Sulfur content.....	186
IV.	Biological methods.....	187
a.	Functional complementation tests.....	187
b.	<i>E. coli</i> MG1655 bacterial growth in the presence of potential inhibitors.....	188
V.	Spectroscopic, biophysical and analytical methods.....	188
a.	Reversed-phase high performance liquid chromatography (HPLC).....	188
b.	UV-visible absorption spectroscopy.....	190
c.	Mössbauer spectroscopy.....	191
d.	Circular dichroism.....	193
VI.	Protein crystallization and X-Ray structures.....	195
a.	Crystallization.....	195
i.	4MP (4-mercaptopyridine-2,3-dicarboxylic acid) complex.....	195
ii.	6MPDC (6-mercaptopyridine-2,3-dicarboxylic acid) complex.....	195
iii.	5MPDC (5-mercaptopyridine-2,3-dicarboxylic acid) complex.....	196
iv.	TmNadA*-QA Complex (5MPDC-derived).....	196
b.	X-Ray Structure Determination.....	196
VII.	QA Production by 5MPDC and NadA in Solution.....	199
VIII.	Confocal microscopy.....	200
IX.	Buffers.....	200

X.	Chemistry experimental section.....	200
a.	Products and solvents.....	200
b.	Analytic devices .....	201
c.	Synthesis of NadA inhibitors.....	201
	i. 6MPDC: 6- mercaptopyridine- 2, 3-dicarboxylic acid .....	201
	ii. 5MPzDC: 5- mercaptopyrazine- 2, 3- dicarboxylic acid .....	205
	iii. 5MPDC: 5- mercaptopyridine- 2, 3- dicarboxylic acid.....	208
	(i) Alternative synthesis of 5MPDC: 5- mercaptopyridine- 2, 3- dicarboxylic acid 211	
d.	Synthesis of molecules for <i>in cellulo</i> assays.....	212
	ANNEXES.....	233
I.	ANNEX I: Aconitase B enzyme (AcnB).....	234
II.	ANNEX II: NadA, a highly structurally conserved enzyme in different organisms .....	236
a.	Sequence alignment of NadA from different organisms.....	236
	BIBLIOGRAPHY.....	241
	PUBLICATION.....	257



Gizonak badu inguru latz bat menperatzeko premia,  
burruka hortan bizi da eta hori du bere egia.  
Ekin ta ekin bilatzen ditu, saiatze hortan ezin gelditu,  
jakintza eta argia ; bide ilunak nekez aurkitu,  
lege berriak noizbait erditu, hortan jokatuz bizia.

**Xabier Lete**



A ma sœur et mes parents...

... pour leur soutien inconditionnel



## REMERCIEMENTS

Je tiens à remercier tout d'abord mes trois encadrants de thèse. Ma directrice Sandrine Ollagnier ; mon codirecteur Yung-Sing Wong ; et mon co-encadrant Olivier Hamelin.

- Merci Sandrine de m'avoir encadré pendant cinq ans et de m'avoir fait confiance avec Olivier quand j'étais une vraie débutante au labo. Vous m'avez donné la confiance et la motivation pour que je me lance dans cette thèse. Merci de m'avoir appris toute la biochimie que je connais, la rigueur et le compromis au travail. Merci de m'avoir consacré du temps même quand ce n'était pas évident de le faire. Ça a été un vrai plaisir de partager autant d'années avec toi, bien professionnellement comme personnellement. Je garde beaucoup de choses apprises et beaucoup de moments importants partagés.
- Merci Yung de ta patience, d'avoir su me rassurer et me calmer quand j'étais débordée. Merci de toujours arriver à trouver le côté positif de chaque situation, de m'avoir toujours écouté et encouragé. Merci aussi de tout ce que tu as partagé avec moi et ce que tu m'as appris du côté scientifique mais aussi du côté personnelle.
- Olivier, merci pour tout. Sans toi rien aurait été pareil ; ni la thèse, ni ma période grenobloise. Merci de ton soutien, de ta confiance, de ta force, ton savoir être, ton dynamisme, et merci de ta calme et ta pêche à la fois. Merci de chaque moment partagé et de tout ce que tu m'as appris scientifiquement mais surtout dans le personnel. Merci d'avoir été là toujours, dans vraiment tous les moments.

Je remercie également toutes les personnes que j'ai connues pendant ces cinq ans dans mes deux laboratoires :

- Leandro, merci pour le gros travail de synthèse, la rigueur et finesse de ton travail, le compromis avec les dates limites toujours difficiles à tenir et changeants... merci vraiment de ton investissement dans le projet et de tout ce que tu m'as appris.
- Je remercie aussi Stéphane Ménage et Ahcène Boumendjel, les directeurs des deux laboratoires où j'ai travaillé (LCBM et DPM). Merci pour un accueil très chaleureux, l'intérêt toujours montré vers moi et mon travail, et de la bonne humeur.
- Comme j'ai travaillé dans trois équipes différentes et que j'ai interagit vraiment avec tout le monde pour des discussions scientifiques et/ou personnelles, je ne pourrais pas nommer toutes les personnes qui forment ou qui ont fait partie des équipes dans un moment donné pendant ces cinq ans (BioCAT, BioCE et MedChem). Mais je tiens à vous remercier tous. J'ai

été très bien entourée et soutenue tout le temps grâce à vous tous et j'ai fait cette thèse avec plein de conseils de la plupart de vous, merci. Je tiens à remercier en particulier les discussions scientifiques surtout au moment de la rédaction de thèse avec Patrice Cathy, Philippe Carpentier et Vincent Nivière. De la même façon, je tiens à remercier le soutien plutôt personnel de Nicolas Duraffourg, Philippe Carpentier et Christine Cavazza .

- Un petit mot pour remercier les thésards, post-docs et jeunes chercheurs que j'ai côtoyé et dont j'ai trouvé des vrais amis qui ont toujours cru en moi et m'ont toujours soutenu : Marila, Jordan, Émile, Mathieu, Benjamin, Sarah, Lucile, Steve, Leandro, Brayan, Mériem, Lien... merci.

Je remercie tous nos collaborateurs sans lesquels cette thèse n'aurait pas été possible et qui ont apporté un travail crucial qui a permis d'avancer autant ma thèse comme le projet de NadA. Merci pour votre travail, votre temps, votre investissement et votre soutien.

- Spectroscopie Mössbauer : Jean-Marc Latour et Martin Clémencey.
- Spectroscopie UV-visible : Jean-Marc Latour
- Cristallographie : Juan Carlos Fontecilla Camps, Anne Volbeda, Claudine Darnault, Océane Gigarel et Oriane Renoux.
- Docking et calculs théoriques : Patricia Amara
- Microscopie confocale : Claire Durmort

Finalement, je veux remercier les gens qui n'ont pas fait partie de mon environnement professionnel mais qui ont été indispensables pour moi pour leur soutien, force, humeur... grâce auxquels cette thèse a été possible.

- Aita, ama eta Ainhoa. Tengo que ser breve porque si no escribiría otra tesis agradeciéndoos todo lo que sois para mí y hacéis por mí. Si estoy aquí es por vosotros... porque yo me he ocupado del estudio y trabajo, pero esta tesis la he hecho gracias a vuestro apoyo, fuerza, determinación y valores que me habéis transmitido y enseñado toda la vida. ESKERRIK ASKO beroena zuentzako da eta tesi hau ere, zuena da.
- Abuela Petra, gracias por todo el apoyo, por pensar tanto en mí y rezar siempre para que todo me salga bien. No solo durante la tesis, si no durante mis 27 años. Qué suerte tenerte.
- Al resto de mi familia en general y en especial a mi abuela Pili y a todos los que me habéis apoyado tanto e incluso acompañado en Grenoble el día de la lectura: Mariaje, Jose Antonio, Amaya, Cristina, Alex, Maria Eugenia, Aitor e Iñigo.

- Merci de tout mon cœur, Claire. Pour m'avoir accompagné dans ce chemin, pour toujours me soutenir, m'encourager et croire en moi. Mais surtout pour tout ce que vous m'avez appris et montré... tellement précieux. Une de mes plus belles rencontres grenobloises.
- Irakasteko jartzen duzun ilusio, gogo eta energiagatik kimikari gustoa hartu niola ez da sekretu. Bide honi hasiera ematen lagundu zenidan eta nire aurrera-pauso eta lorpen guztiak pozez bizi izan dituzu. "Esker mile" bero-bero bat, Felixe.
- Nire kuadrillari: Bea, Marina, Miren, Ainhoa eta Olaia. Umorea, animoak... ez zaizkit inoiz falta izan. Eskerrik asko neskak, hau ere zuena da parte batean. Amaia, zurea ere bai!
- Maite, Mainer eta Olaia. Zuei ere eskerrik asko, beti hor zaudetelako eta kimikako karrerak eman didan hoberena zaretelako.
- Mezkiritzeko lagunei. Arnas hartu behar izan dudanean leku ederrenean eta konpainia ederrenarekin egin ahal izan dudalako, eskerrik asko.
- I want to thank my American family, the Widemans, for the continued support and prayers and for being my main English teachers.
- And last but definitely not least... to my friends (may I call my family) in Grenoble. Thank you for making these years the best of my life so far, for supporting me, for providing me love, laughter and lots of joy. You will always be part of me. And thank you for the music, for all that singing that put sound to these amazing adventure.



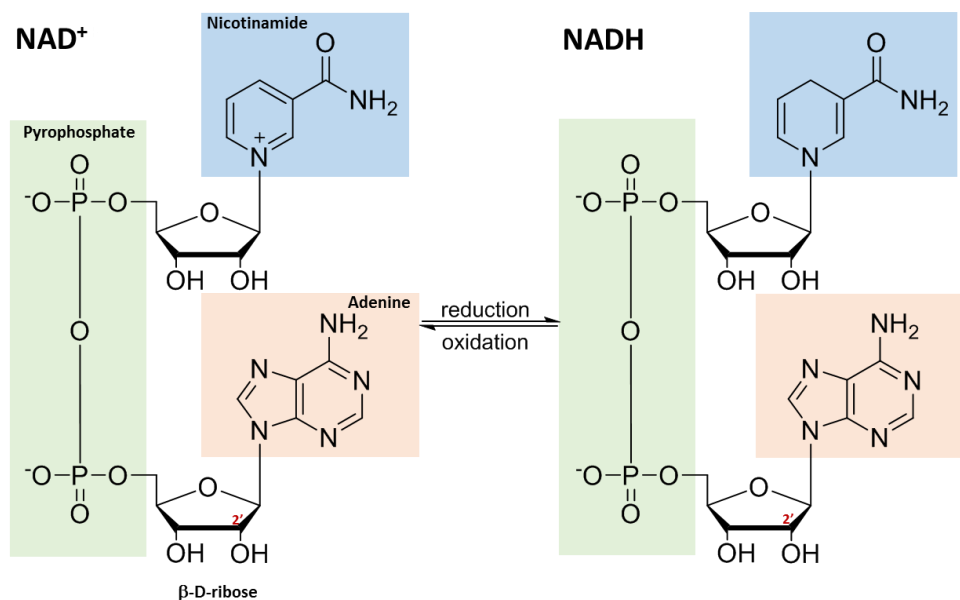
# INTRODUCTION

## I. Nicotinamide Adenine Dinucleotide (NAD)

In 1906 Nicotinamide Adenine Dinucleotide (NAD) was discovered by Arthur Harden in yeast extracts due to its capacity to accelerate alcoholic fermentation<sup>1</sup>. However, its structure remained unknown for 30 years. It was between 1935 and 1936 that Hans Von Euler-Chelpin not only found its structure<sup>2</sup> but Otto Heinrich Warburg also evidenced its redox role<sup>3</sup>. In 1940, nicotinamide adenytransferase enzyme, an enzyme involved in NAD biosynthesis was identified by Arthur Kornberg<sup>4</sup> and became the first identified enzyme in NAD biosynthetic pathway. Since then, the NAD biosynthesis has been and is still widely studied<sup>5,6</sup>. NAD has expanded beyond its role as a redox cofactor, since indeed, NAD<sup>+</sup> and its metabolites also act as degradation substrates for a wide range of enzymes<sup>7</sup>.

### a. Structure

Nicotinamide adenine dinucleotide is formed by two nucleotides bonded by a pyrophosphate bridge. The nitrogenous bases that form these nucleotides are adenine and nicotinamide. NAD refers to the two redox forms which exist in nature: NAD<sup>+</sup> (oxidized form) and NADH (reduced form) (Scheme 1)<sup>8</sup>.

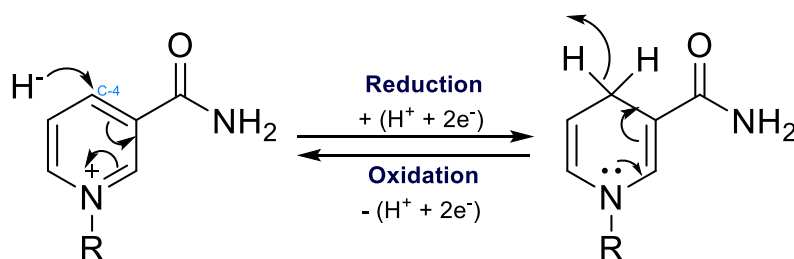


**Scheme 1:** Chemical structure of nicotinamide adenine dinucleotide (NAD).

NAD also exists in a phosphorylated form, NADP. NADP has an additional phosphate group on the 2' position of the ribose ring that carries the adenine moiety. NADP stands for its two redox forms:  $\text{NADP}^+$  and NADPH. Both NAD and NADP have the same redox properties but there is a difference on the way they are used in the cell. Whereas NAD is involved mainly in catabolic reactions, NADP mainly takes part in anabolic reactions.

## b. Physical-chemical properties

NAD(P) is an important redox cofactor in the cell; it can accept or donate electrons in different metabolic reactions. The electron transfer happens at the nicotinamide part. In order to reduce  $\text{NAD(P)}^+$ , a hydride ( $\text{H}^-$ , a proton and two electrons are involved) is transferred to the  $\text{C}_4$  of the nicotinamide base. The aromatization of the system is achieved by reoxidation of the cofactor with the transfer of a hydride ( $2\text{e}^-$ ,  $\text{H}^+$ ) to a substrate (Scheme 2). The standard potential of the  $\text{NAD(P)}^+/\text{NAD(P)H}$  couple is  $E^\circ = -0.32 \text{ V}^9$ .



**Scheme 2:**  $\text{NAD(P)}^+/\text{NAD(P)H}$  redox couple. Only the nicotinamide part is shown in the figure 2, R represents the rest of the skeleton of  $\text{NAD(P)}$ .

The  $\text{NAD(P)}^+/\text{NAD(P)H}$  ratio is known as the redox state of the cell, which is a reflect of the cell metabolic activities as well as an indicator of cell health. In general, the ratio stays constant on a same cell compartment. Under aerobic conditions, the ratio of  $\text{NAD}^+/\text{NADH} = 8\text{-}10$ , which means that the cofactor exists mainly on its oxidized form. However, the ratio of  $\text{NADP}^+/\text{NADPH} = 0.005$ , meaning that in this case the cofactor exists mainly on its reduced form<sup>10</sup>.

Both  $\text{NAD(P)}^+$  and  $\text{NAD(P)H}$  present UV absorption band(s), allowing their identification and quantitation.  $\text{NAD(P)}^+$  has an absorbance peak at 260 nm with a molar extinction coefficient  $\epsilon_{260\text{nm}} = 16900 \text{ M}^{-1}\text{cm}^{-1}$ ;  $\text{NAD(P)H}$  has an additional peak at 340 nm with a molar extinction coefficient  $\epsilon_{340\text{nm}} = 6220 \text{ M}^{-1}\text{cm}^{-1}$ . This difference of absorbance

allows to easily quantify  $\text{NAD(P)}^+$  and  $\text{NAD(P)H}$ , and to easily monitor their conversion during enzymatic reactions.

The two forms also differ with regard to fluorescence.  $\text{NAD(P)}^+$  does not present any fluorescence whereas  $\text{NAD(P)H}$  does at 460 nm. This makes it possible to control the binding of the cofactor to a molecule, for example, a protein.

### c. Functions of NAD/NADH and NADP/NADPH

It has been well known for years that  $\text{NAD(P)}$  is a cofactor that plays a crucial role in the redox metabolism. However, it also plays a role in several non-redox processes such as substrate of bacterial DNA ligases, sirtuins or ADP-ribosyltransferases.

#### (i) Role in redox metabolism

$\text{NAD(P)}$  is the redox cofactor of several oxidoreductases, one of the largest family of enzymes that catalyze electron transfer. Some of the most significant examples are alcohol dehydrogenases, lactate dehydrogenases or NAD-ubiquinone reductases.

$\text{NAD(P)}$  cofactor is bound to proteins through the “Rossmann fold”, a structural motif found in proteins that bind to dinucleotide cofactors (FAD, NAD, NADP). It was first identified by Michael Rossmann in the lactate dehydrogenase enzyme<sup>11</sup> (Figure 1). The Rossmann fold is composed of a series of alternating beta strand ( $\beta$ ) and alpha helical ( $\alpha$ ) segments wherein the  $\beta$ -strands are hydrogen bonded forming a  $\beta$ -sheet. The initial beta-alpha-beta ( $\beta\alpha\beta$ ) fold is the most conserved segment of Rossmann folds<sup>12</sup>.

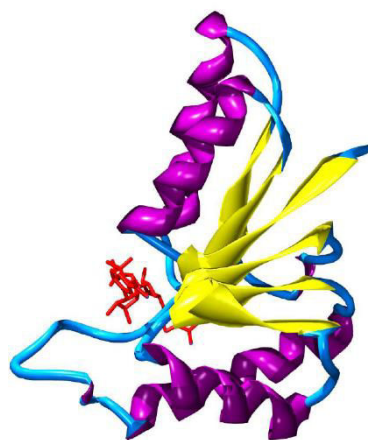


**Figure 1:** NAD-bound Rossmann fold motif. Structure of *Cryptosporidium parvum* lactate dehydrogenase. Red: NAD cofactor; purple:  $\alpha$ -helices; Yellow:  $\beta$ -sheets.

The redox reactions catalyzed by oxidoreductases are essential in cell metabolism with a particular role on the catabolism; in other words, on the break-down of nutrients and energy release. A big part of the energy produced in the catabolic reactions is stored as NADH and converted into ATP during cell respiration in mitochondria. Each molecule of NADH consumed, provides energy to form 3 ATP molecules at the last stage of oxidative phosphorylation (Figure 2)<sup>13</sup>.

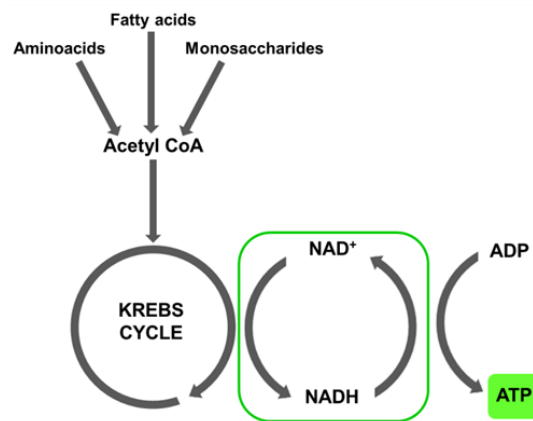


**Figure 2:** Simplified scheme of NAD role in redox metabolism.

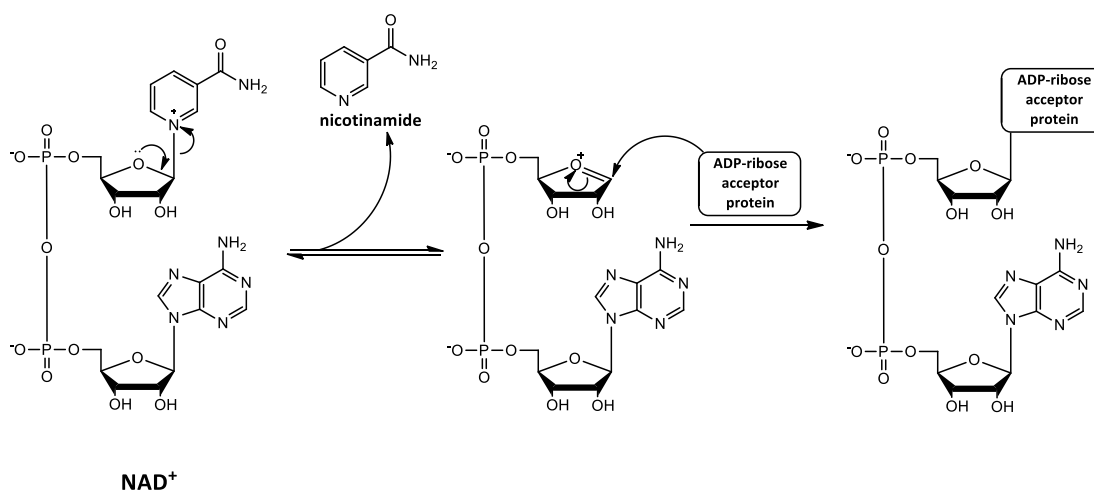
Even though NAD plays an essential role in catabolism, it is also involved in gluconeogenesis (as an electron transporter), which is an anabolic process. It also plays an important role in nitrogen assimilation in nitrifying bacteria<sup>14,15</sup>. In the case of NADP, it is widely used as a reducing agent mainly in anabolic reactions such as fatty acid synthesis or photosynthesis<sup>16</sup>.

A NAD-oxidoreductase that it is worth highlighting at this point is the NAD(P) transdehydrogenase enzyme. It couples the reduction of  $\text{NADP}^+$  to NADPH with the oxidation of NADH to  $\text{NAD}^+$ . This way, it plays a primordial role on maintaining the equilibrium in the cell that exists between the catabolic reactions with NAD production and anabolic reactions with NADPH consumption<sup>17</sup>. The enzyme is present in both prokaryotes and in mitochondria of eukaryotes.

## (ii) Role in non-redox metabolism

### - NAD: substrate in ADP-ribosylation reactions

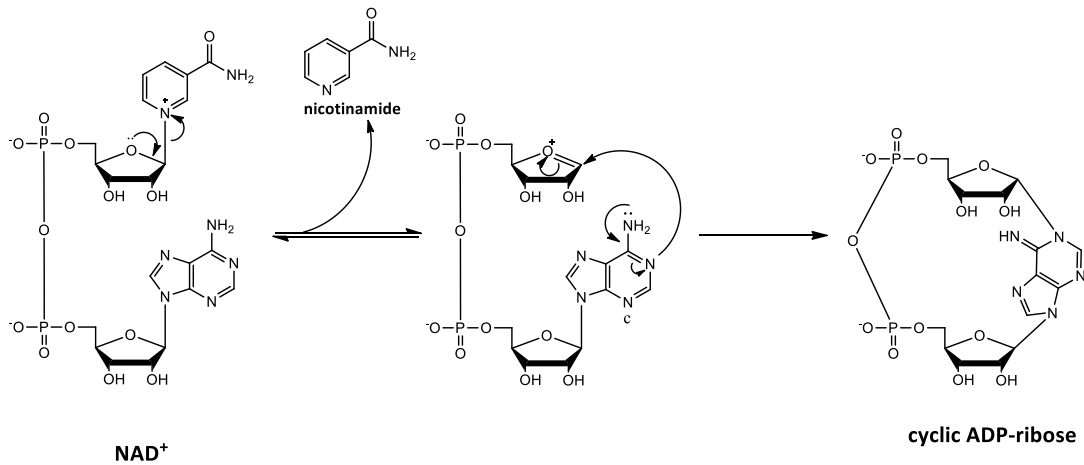
Adenosine diphosphate ribosylation is a reversible post-translational modification reaction that consists in the transfer of an ADP-ribose to a protein and/or the formation of ADP-ribose polymers (Scheme 3). These reactions are performed by ADP-ribosyltransferase (ARTs) or by poly-(ADP-ribose) polymerase (PARPs) enzymes, respectively<sup>18</sup> and are involved in many cellular processes including DNA repair, gene regulation and apoptosis<sup>19</sup>.



**Scheme 3:** ADP-ribosyl transferase reaction. NAD is hydrolyzed by an ART yielding an ADP-ribosylated protein and nicotinamide.

### - NAD: cyclic ADP-ribose precursor

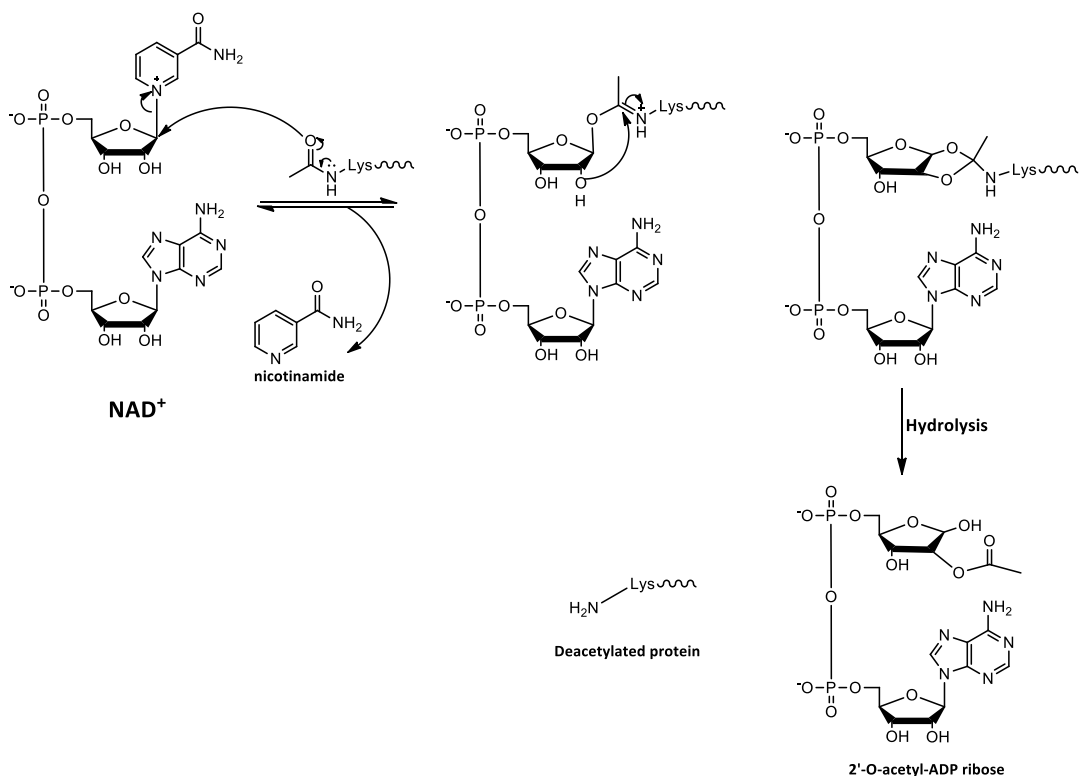
Cyclic ADP-ribose (cADPR) is a potent intracellular calcium releasing agent. This is due to the binding of it to a ryanodine-type receptor. As a consequence, it plays an important role in the maintenance of calcium homeostasis in cells. After the formation of ADP-ribose from NAD<sup>+</sup>, it is cycled through the anomeric carbon of the terminal ribose and the N<sub>1</sub> nitrogen of the adenine ring (Scheme 4)<sup>20</sup>.



**Scheme 4:** Formation of cyclic ADP-ribose from NAD.

- NAD: sirtuin substrate

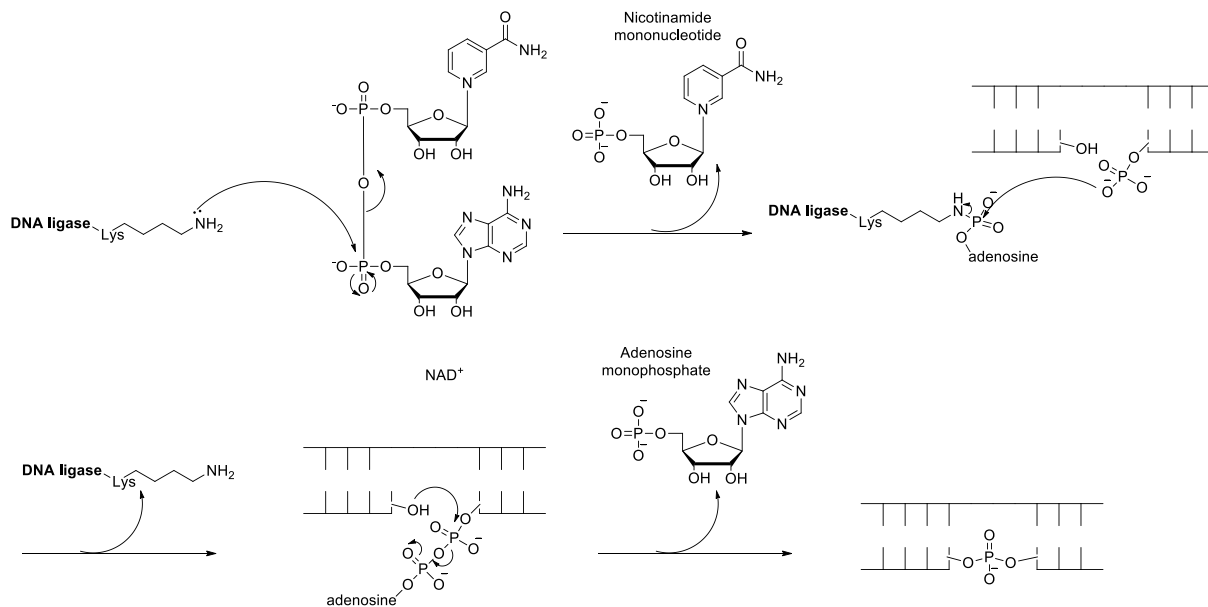
Most of the sirtuins are NAD-dependent protein-deacetylases found in prokaryotes, eukaryotes and archaea. They catalyze the lysine deacetylation coupled to the hydrolysis of NAD and this hydrolysis yields 2'-O-acetyl-ADP-ribose, the deacetylated substrate and nicotinamide<sup>21,22</sup> (Scheme 5). Sirtuins play an important role in the regulation of many biological pathways; the deacetylation of histones is a key part in gene regulation, since it deactivates transcription whereas the acetylation activates it. For this reason, these enzymes are of big importance in processes like apoptosis or cellular aging<sup>23,24</sup>. Eukaryotic cells present seven types of sirtuins whereas prokaryotes and archaea only present one or two<sup>25</sup>.



**Scheme 5:** Reaction catalyzed by a sirtuin that yields 2'-O-acetyl-ADP ribose, nicotinamide and a deacetylated protein.

- NAD: a substrate of NAD-dependent DNA ligases

DNA ligases participate in DNA replication and DNA repair. NAD is a substrate of some of the enzymes of this type in bacteria. In the case of eukaryotes, the substrate of DNA ligases is ATP<sup>26</sup>. They catalyze the phosphodiester bond formation. NAD provides the adenosine monophosphate (AMP) group, which binds to a lysine on the active site of the ligase<sup>27</sup>. The mechanism by which DNA is repaired is shown in Scheme 6.



**Scheme 6:** Reaction catalyzed by a DNA ligase. NAD is the AMP donor which allows the ligation of the two DNA extremities

As shown above, the consumption of NAD in different reactions leads to the formation of nicotinamide (Nm) in most of them. It is important to keep this in mind since this product, along with some others such as nicotinamide mononucleotide (NMN) might be recycled in the cells in order to re-synthesize NAD. This will be explained later on this introduction.

#### d. NAD physiological concentration and cell localization in eukaryotes

As previously explained, NAD plays a crucial role in the redox states and redox processes of the cells as well as in many other different biological processes. For this reason, NAD is found all over the cell in different compartments<sup>28</sup>. Its synthesis is mostly performed in the nucleus where it has an essential role in the regulation of gene expression. It can diffuse through the nuclear pores in order to reach the cytoplasm where it takes part in many different processes. The NADH produced during glycolysis is transported from the cytoplasm into the mitochondrial matrix to provide reducing equivalents for the energy metabolism (Krebs cycle and electron transport chain). The inner membrane of mitochondria is impermeable for NAD<sup>+</sup>, so it can only be imported inside these organelles through membrane carrier proteins called mitochondrial shuttles. The most common ones are malate-aspartate and glycerol-3-phosphate shuttles. Yet, no NAD<sup>+</sup> transporter has been identified in mammals and whether there is a transport through the mitochondrial membrane remains unknown. However, because exogenous NAD<sup>+</sup> was shown to increase mitochondrial NAD<sup>+</sup> level more than cytoplasmic level<sup>29</sup>, it seems conceivable that mitochondrial transport mechanisms might exist for NAD. This seems to be the case also for its precursors or intermediates due to the presence of nicotinamide mononucleotide adenylyltransferase-3 enzyme (NMNAT-3) in the mitochondria, which is the enzyme that catalyzes the formation of NAD from NMN and ATP. This suggests an intramitochondrial NAD biosynthesis<sup>30</sup>.

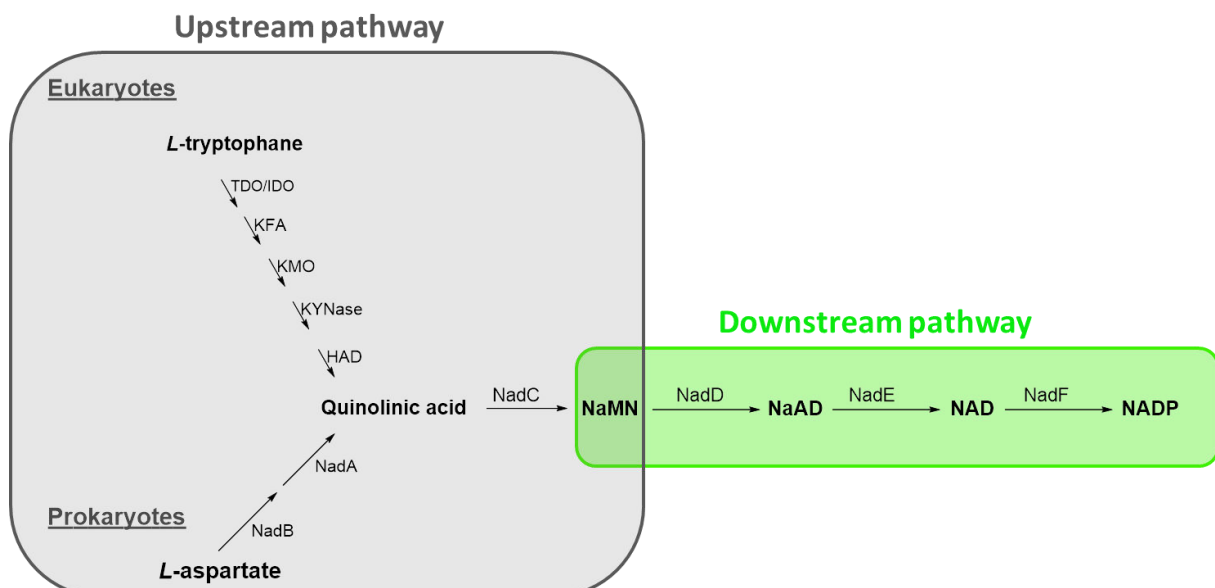
The cellular compartments where the cofactor is found in the largest amounts are mitochondria. Depending on the cell type, up to 70 % of the total NAD of the cell can be found in these organelles<sup>31</sup>. Considering that intracellular NAD level has been estimated to be between 0.2 and 0.5 mM depending on the cell type (levels can change significantly in response to energy stresses), most reports indicate that mitochondrial NAD content is  $\leq 250 \mu\text{M}$ , while nuclear and cytosolic levels seem to be much lower, around  $70 \mu\text{M}$ . It is admitted that the concentration in the nucleus and cytosol is similar<sup>7</sup>.

## II. NAD biosynthesis

Due to its numerous and essential biochemical functions, NAD is an essential molecule in all living organisms. For this reason, organisms have developed different ways of producing it through both *de novo* and salvage pathways. Whereas some organisms are able to synthesize NAD through different ways, some others only possess a single pathway to synthesize it.

### a. The *de novo* pathways

The *de novo* route of NAD is composed of two biosynthetic blocks: (i) The upstream pathway and (ii) the downstream pathway separated by a common molecule, nicotinic acid mononucleotide (NaMN). (i) The upstream pathway yields NaMN from *L*-tryptophan in eukaryotes and from *L*-Aspartate in prokaryotes. The last intermediate of this pathway (quinolinic acid, QA) as well as its last reaction (phosphoribosylation of QA) are common in both prokaryotes and eukaryotes. (ii) The downstream pathway converts NaMN into NAD(P) and is largely conserved in eukaryotes and prokaryotes. For this reason, it is often called “the downstream common pathway”. The separation of the two pathways is illustrated by their different phylogenomic distribution (Scheme 7).



**Scheme 7:** NAD biosynthetic *de novo* pathway in eukaryotes and prokaryotes. They converge in a common intermediate from the upstream pathway, quinolinic acid (QA).

### (i) Upstream pathway in prokaryotes

This three-step pathway is only required for the *de novo* synthesis of NAD. All the three genes involved on it are most of the time dispensable under favorable conditions when nicotinamide (Nm) or nicotinic acid (Na) are present in the growth medium. Many groups of bacteria, mainly Gram-positive pathogens, lack the genes of this biosynthetic pathway and are auxotroph for niacin to produce NaMN<sup>32</sup>.

The conversion of L-Aspartate to NaMN is performed in three consecutive steps by three different enzymes: First, oxidation of L-Aspartate to iminoaspartate catalyzed by L-aspartate oxidase (NadB)<sup>33</sup>; second, condensation of iminoaspartate with dihydroxyacetone phosphate (DHAP, a central glycolytic intermediate) catalyzed by quinolinate synthase (NadA) to yield quinolinic acid (QA)<sup>34</sup>; and last, phosphoribosylation of QA by quinolinate ribosyltransferase (NadC) using phosphoribosyl pyrophosphate (PRPP) as second substrate. Each of these enzymes and corresponding reactions are briefly described below and a general scheme of this pathway is presented in Scheme 8.

#### a. L-aspartate oxidase (NadB)

This enzyme is encoded by *nadB* gene and catalyzes the oxidation of L-aspartate into iminoaspartate (Scheme 8). NadB is a flavoprotein containing a non-covalently bounded FAD (Flavin adenine dinucleotide). Importantly, NadB is able to use different electron acceptors such as oxygen or fumarate showing that NadB is able to work under aerobic and anaerobic conditions<sup>35,36</sup>.

In some organisms like *Thermotoga maritima* or *Acheoglobus fulgidus*, *nadB* gene is not present in their genome. In this case, the conversion from L-aspartate to iminoaspartate is performed by a non-homologous NAD(P)-dependent enzyme, L-aspartate dehydrogenase (NadX)<sup>37</sup>.

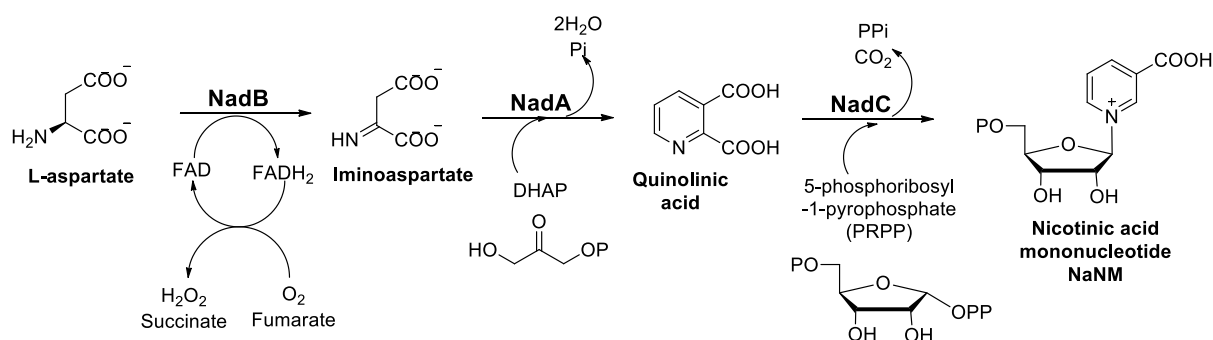
#### b. Quinolinate synthase (NadA)

Encoded by *nadA* gene, quinolinate synthase is a [4Fe-4S]<sup>2+</sup> cluster metalloenzyme<sup>38,39</sup>. It catalyzes a complex reaction which consists in the condensation of two substrates (iminoaspartate and DHAP) to form an aromatic product, quinolinic acid (Scheme 8). The different structural and functional aspects will be detailed further on this

introduction. Very important insights have been understood during my PhD, especially concerning the mechanism.

### c. Quinolinate phosphoribosyl transferase (NadC)

This step is common in both prokaryotic<sup>40</sup> and eukaryotic upstream pathways<sup>41</sup>. NadC enzyme is conserved in the genomes of all species having a *de novo* NAD synthetic pathway. NadC catalyzes the formation of nicotinic acid mononucleotide (NaMN) from quinolinic acid and 5-phosphoribosyl-1-pyrophosphate (PRPP) (Scheme 8). More precisely, it specifically couples the phosphoribosyl group of a 5-phosphoribosyl-1-pyrophosphate (PRPP) with QA. The removal of the pyrophosphate group of PRPP is facilitated by the Mg<sup>2+</sup> metal cofactor of the enzyme, which gives rise to the formation of an oxocarbenium species that is coupled to QA. This coupling yields an instable intermediate which is stabilized by a decarboxylation forming nicotinic acid mononucleotide.



**Scheme 8:** Prokaryotic upstream de novo pathway: From L-aspartate to Nicotinic acid mononucleotide (NaMN).

### (ii) Upstream pathway, in eukaryotes

Eukaryotes and some bacteria (*Pseudomonas aureginosa*, *Burkholderia fungorum*, *Bacillus anthracis*, *Ralstonia metallidurans*...) <sup>42</sup> synthesize quinolinic acid by degradation of L-tryptophan under aerobiosis. This pathway is known as the kynurenine pathway and involves the action of five different enzymes and a final spontaneous cyclisation reaction (Scheme 9). The last step of this upstream pathway is common to the prokaryotic one as previously stated, which consists in the formation of nicotinic acid mononucleotide. This pathway and the enzymes involved on it are detailed below.

a. Tryptophan-2,3-dioxygenase (TDO) or Indoleamine-2,3-dioxygenase (IDO)

This first step may be performed by any of the two enzymes TDO and IDO and consists on the oxidation of *L*-tryptophan to N-formylkynurenine. Tryptophan-2,3-dioxygenase or TDO is able to oxidize only *L*-tryptophan whereas indoleamine-2,3-dioxygenase or IDO oxidizes *L*-tryptophan and some analogues (*D*-tryptophan, tryptamine, serotonin...). Both enzymes contain a heme cofactor which allows the binding and activation of dioxygen and tryptophan<sup>43</sup> (Scheme 9).

b. Kynurenine formamidase (KFA)

The second step of the upstream pathway consists in the deformylation of N-formylkynurenine to *L*-kynurenine and it is performed by kynurenine deformidase (KFA). Different structures of this enzyme have been solved from different organisms and it was demonstrated that the catalysis occurs via a catalytic triad (Ser-Asp-His) where the conserved serine catalyzes the deformylation by participating in a tetrahedral intermediate. Then, a hydrolysis step gives rise to the formation of the product and formic acid<sup>44</sup> (Scheme 9).

c. Kynurenine-3- monooxygenase (KMO)

*L*-kynurenine is oxidized to 3-hydroxykynurenine by kynurenine-3-monooxygenase (KMO) (Scheme 9); a flavoprotein, containing a non-covalently bound FAD. This oxidoreductase enzyme uses NADP in order to regenerate its cofactor. The presence of this enzyme in an organism is not always related to quinolinic acid synthesis. For example, in some insects, the enzyme converts its substrate *L*-kynurenine into xanthurenic acid<sup>45</sup> and in *Pseudomonas*, KMO participates in the formation of an intermediate in the synthesis of quinolobactine-type siderophores<sup>46</sup>.

d. Kynureninase (KYN)

3-Hydroxykynurenine is hydrolyzed by a Kynureninase (KYN) yielding 3-hydroxyanthranilic acid and free *L*-alanine (Scheme 9). This enzyme is the most studied one inside the superfamily of aspartate aminotransferases. This hydrolase is pyridoxal-5-phosphate (PLP) dependent<sup>47</sup>.

e. 3-hydroxyanthranilate-3,4-dioxygenase (HAD)

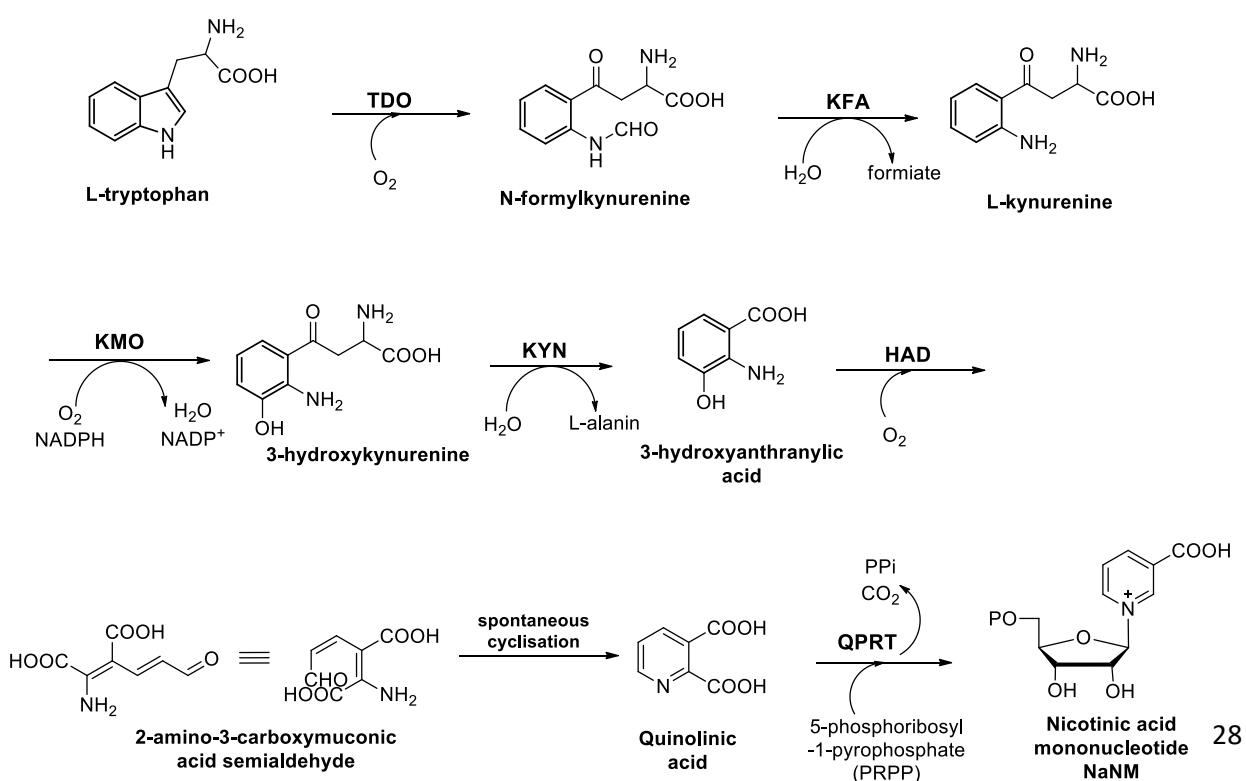
3-Hydroxyanthranilate-3,4-dioxygenase enzyme oxidizes 3-hydroxyanthranilic acid to form 2-amino-3-carboxymuconic acid semialdehyde (Scheme 9). HAD is a Fe-containing extradiol-dioxygenase. Each of the two enzyme subunits has two Fe binding sites. One of them is catalytic and is coordinated by three conserved amino acid residues, two histidines and a glutamate. The other Fe is coordinated by four cysteines forming a [Fe-4S] whose role remains unclear<sup>48</sup>.

f. Spontaneous cyclisation of 2-amino-3-carboxymuconic acid semialdehyde to form Quinolinic acid

This is the only non-enzymatic step in the eukaryotic *de novo* pathway. During this reaction, there is a spontaneous dehydration that gives rise to the cyclisation and aromatization of the product to form quinolinic acid<sup>49</sup> (Scheme 9).

g. Quinolinate phosphoribosyltransferase (QPRT)

The last step of the upstream *de novo* pathway in eukaryotes is common with prokaryotic pathway (Scheme 9). QPRT enzyme is the eukaryotic homologue of the prokaryotic NadC. However, the eukaryotic and prokaryotic enzymes are structurally different. For this reason, NadC became an interesting target for the design of new antibacterial drugs.



**Scheme 9:** Eukaryotic upstream *de novo* pathway: From *L*-tryptophan to Nicotinic acid mononucleotide (NaMN).

The different steps of this *de novo* pathway in eukaryotes have all been characterized at a molecular level, mostly thanks to the crystal structures of all the enzymes<sup>50,51,52,53,54,48</sup>. This pathway is performed under aerobic conditions facilitating the functional and structural studies with regard to the prokaryotic pathway where one of the enzymes, quinolinate synthase, has an oxygen-sensitive Fe-S cofactor.

(iii) -Downstream pathway: common in prokaryotes and eukaryotes

Nicotinic acid mononucleotide (NaMN) is converted during the downstream pathway into nicotinamide adenine dinucleotide (NAD) in two steps. The first step results in adenylation of NaMN catalyzed by NaMN adenytransferase (NadD or NaMNAT) to form Nicotinic acid adenine dinucleotide (NaAD). The second step consists in an amidation of the NaAD by the ATP-dependent NAD synthase enzyme (NadE) to form NAD. NAD may be further phosphorylated by an ATP-dependent kinase (NadK) to form NADP.

The reactions in this pathway are common in prokaryotes and eukaryotes, but the enzymes that catalyze them are not structurally homologous, which make the prokaryotic enzymes interesting targets for the design of antibacterial drugs. This pathway also participates in the NAD salvage and recycling. Below is reported a short description of these enzymes and the corresponding reactions they catalyze.

a. Nicotinic acid mononucleotide adenytransferase (NadD or NaMNAT)

Encoded by *nadD* gene, this enzyme catalyzes the adenylation of nicotinic acid mononucleotide (NaMN) to form nicotinic acid adenine dinucleotide (NaAD) using ATP (Scheme 10). The reaction consists of a nucleophilic attack of the 5'-phosphoribosyl group of NaMN on the  $\alpha$ -phosphate of ATP followed by the departure of the pyrophosphate group. The reaction is  $Mg^{2+}$  dependent and facilitated by two histidine residues of the ATP binding sequence<sup>55</sup>.

It has been shown that the mammal nicotinic acid mononucleotide adenytransferase (NaMNAT) enzyme is able to use both NaMN and its amidated analogue, nicotinamide mononucleotide (NMN) as substrates<sup>56</sup>. However, the high resolution structure of NadD

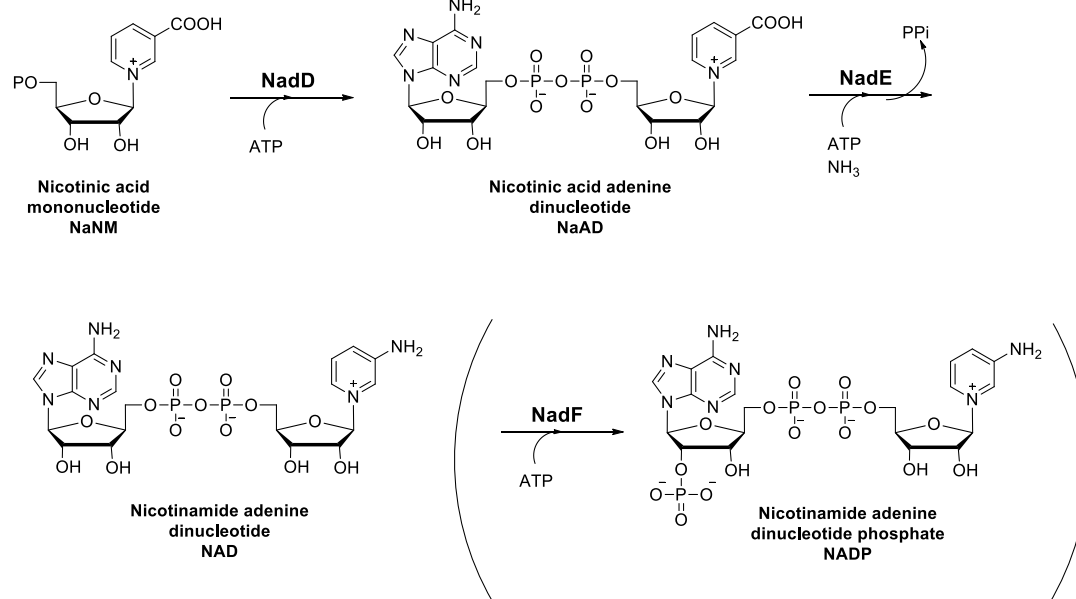
from *E. coli* in complex with NaAD product provided a basis for the interpretation of its strict preference for NaMN as substrate (>1,000- fold based on comparison of  $K_{cat}/K_m$  values for its substrate). This involves some important conformational changes such as H-bonds that favor the deamidated form of the ligand<sup>55</sup>. This preference is conserved in most bacteria and other organisms except mammals.

b. NAD synthetase (NadE or NADS)

The last enzyme participating in NAD biosynthesis is NAD synthetase (NadE in prokaryotes and NADS in mammals) catalyzing the conversion of NaAD to NAD, by transforming the carboxylic acid group of nicotinic acid into an amide (Scheme 10). A  $Mg^{2+}$  cofactor is essential for this activity by activating ATP giving rise to the removal of a pyrophosphate group and formation of an adenylate species, as well as facilitating the nucleophilic attack of ammonia to the carbonyl group of the adenylate intermediate to form an amide<sup>57</sup>. Most of prokaryotes (*E. coli*<sup>58</sup>, *Bacillus subtilis*<sup>59</sup>, *Helicobacter pylori*<sup>60</sup> ...) use ammonia as nitrogen source whereas eukaryotes use glutamine<sup>61</sup> (with *Mycobacterium tuberculosis* as an exception in prokaryotes that can also use glutamine<sup>62</sup>). In this latter case, the protein structure of NADS varies with regard to prokaryotes since these enzymes have to hydrolyze glutamine in order to obtain ammonia<sup>63,64</sup>. They contain an additional N-terminal nitrilase-like domain (Nit) that was shown to hydrolyze glutamine and channel ammonia directly to the amidotransferase domain.

c. From NAD to NADP: NAD kinase (NadF or NadK)

NAD Kinase enzyme is responsible for the phosphorylation of NAD to form NADP (Scheme 10), using ATP that acts as a phosphate donor<sup>65</sup>. The phosphorylation occurs at the hydroxyl group on the 2' position of the ribose ring carried by the adenine nucleotide moiety. The enzyme requires a divalent ion for its activity that varies depending on the organism<sup>66,67,68</sup>. In *Salmonella typhimurium*, an allosteric regulation of the enzyme has been demonstrated which enables the modulation of the equilibrium between NAD and NADP with regard to the cellular need<sup>69</sup>.



**Scheme 10:** Downstream pathway of NAD biosynthesis: from nicotinic acid mononucleotide to NAD/NADP. Common pathway for prokaryotes and eukaryotes.

## b. Salvage and recycling pathways

Under conditions of NAD deficit, organisms still need to keep their NAD pool present (as essential) and this is why most of them, apart from the *de novo* synthetic pathway of NAD, possess salvage or recycling pathways to synthesize the cofactor. These pathways use pyridines and other byproducts of NAD consumption within the cell (recycling) or available on the medium (salvage) that come from the food. These salvage and recycling pathways exist from as many as five salvageable precursors which are nicotinamide (Nm), nicotinic acid (Na), nicotinamide riboside (NmR), nicotinic acid riboside (NaR) and nicotinamide mononucleotide (NMN) (Figure 3). Depending on the organism these pathways can be predominant with regard to the *de novo* pathway. In contrast to NAD biosynthetic pathway, salvage and recycling pathways appear to be subject to considerable variations even between closely related species. Without performing an exhaustive analysis, below, I present a general summary with the main salvage pathways.

Whatever the molecule that is recycled (Nm, Na, NmR, NaR or NMN), these precursors might be outside the cell and they have to pass the membrane through transporters or passive diffusion<sup>70,71,72</sup>. Transporters differ from one organism to another: in the case of pyridine salvage, it exists *NiaX* in *Streptococcus*<sup>73</sup>, *NiaX*, *NiaY* or *NiaP* in

*Mycobacteria*<sup>70,71</sup>, or Tna1 in yeast<sup>74</sup>. PnuC exists in many bacteria and it is also capable to transport nicotinamide riboside (NmR)<sup>75</sup>. For the transport of NmR, yeast have Nrt1<sup>72,71</sup>.

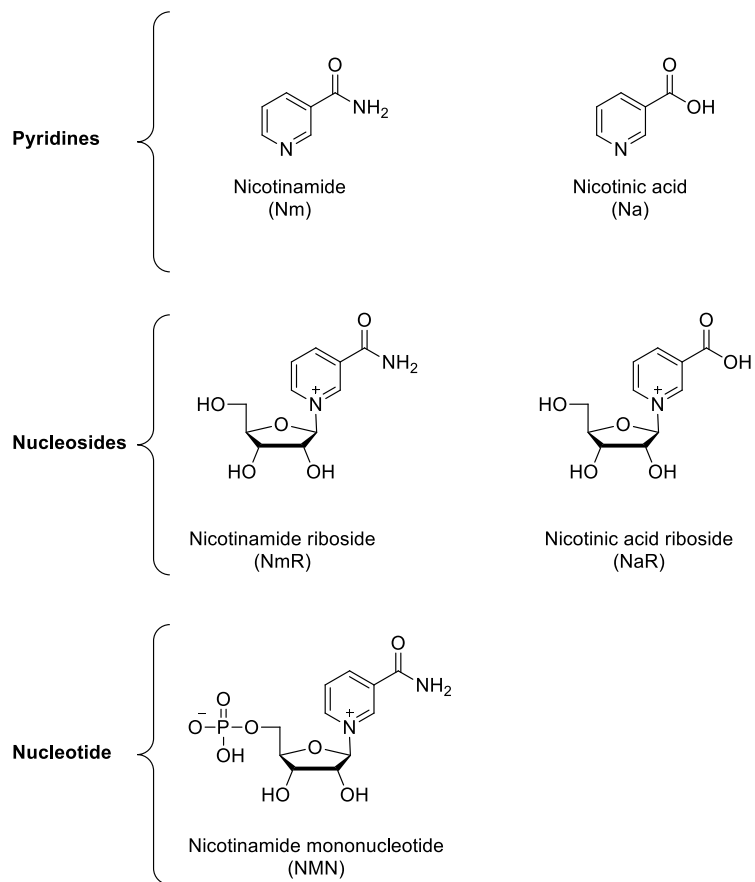


**Figure 3:** Structures of nicotinamide (Nm), nicotinic acid (Na), nicotinamide riboside (NmR), nicotinic acid riboside (NaR) and nicotinamide mononucleotide (NMN).

#### (i) Prokaryotes and eukaryotes except mammals

- Salvage pathway of pyridine ring (Nm and Na)

Many NAD consuming enzymes yield nicotinamide (Nm) as a byproduct and this latter can be recycled in order to synthesize NAD. For this purpose, many bacteria have the following enzymatic pathway (Scheme 11).

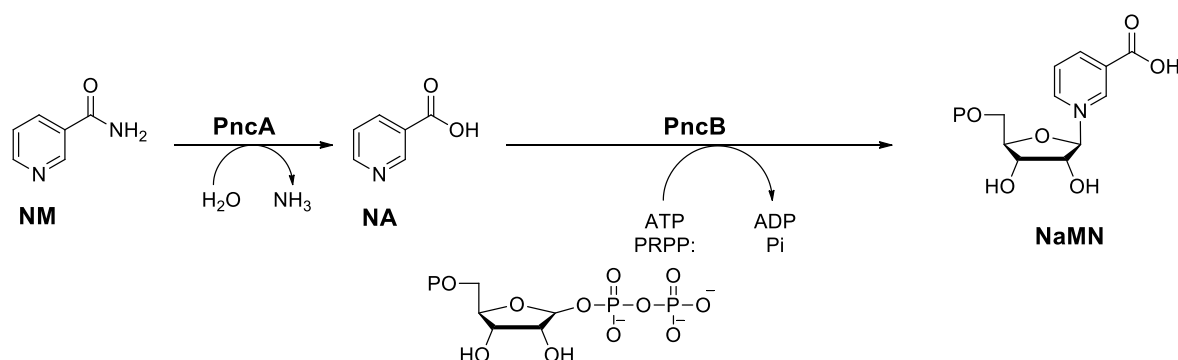
##### a. Nicotinamidase (PncA)

In contrast to mammals, bacteria are unable to transfer any phosphoribosyl group to nicotinamide (Nm)<sup>76</sup>; therefore Nm must be hydrolyzed to nicotinic acid (Na) in order to be used for NAD salvage. The nicotinamidase enzyme PncA catalyzes this hydrolysis reaction

that yields Na and ammonia<sup>77</sup>. The enzyme structure reveals a catalytic triad (Cys-Asp-Lys) and a divalent ion ( $Mn^{2+}$ ,  $Zn^{2+}$ ,  $Fe^{2+}$ ), that plays the role of a Lewis acid, as key elements for the mechanism. The interaction of the divalent ion with the catalytic triad activates the thiolate of the cysteine from the triad which performs a nucleophilic attack to the carbonyl of the amide group giving rise to the formation of Na and ammonia (Scheme 11)<sup>78</sup>.

#### b. Nicotinic acid phosphoribosyltransferase (PncB)

This enzyme is often encoded by the same operon as PncA<sup>32</sup>. It catalyzes the transfer of a phosphoribosyl group from PRPP to nicotinic acid (Na) forming nicotinic acid mononucleotide (NaMN) like NadC does, however without the last decarboxylation step. Even though the enzyme is able to perform this catalysis without ATP, the catalytic efficiency is increased in the presence of ATP by shifting the reaction equilibrium almost fully to the formation of the product (Scheme 11)<sup>79</sup>.



**Scheme 11:** Salvage of nicotinamide and nicotinic acid to form nicotinic acid mononucleotide NaMN that is going to be taken in charge by the enzymes of the *de novo* pathway NadD and NadE.

#### c. From NaMN to NAD

Once NaMN is synthesized, it is taken into the *de novo* pathway enzymes in order to transform it to NAD (NadD and NadE).

- Salvage of pyridine nucleosides (NmR and NaR)

This salvage pathway is less conserved than the pyridine salvage pathway and differs a lot from one organism to another.

In the case of *Escherichia coli*, *Salmonella typhimurium*, or *Haemophilus influenzae*, nicotinamide riboside (NmR) is transformed to nicotinamide mononucleotide (NMN) by NadR enzyme. This last enzyme has also a nicotinamide mononucleotide adenyltransferase activity and allows the production of NAD<sup>80,81,82</sup>. The enzyme is present in many bacteria and it is trifunctional; apart of the described catalytic activities, it also plays a crucial role on NAD metabolism regulation<sup>80</sup>. This will be discussed into more detail further in this introduction.

It is worth noting that this salvage pathway is the only way of NAD production in *Haemophilus influenzae*, that does not possess a *de novo* NAD biosynthetic pathway<sup>83</sup> and which obtains NmR exogenously through the PnuC transporter<sup>84</sup>.

The bacteria *Francisella tularensis* is another particular case, which lacks the *nadD* gene on its genome. Therefore, after the formation of nicotinic acid mononucleotide NaMN, it cannot pursue with the *de novo* pathway. Instead, NaMN is amidated to NMN by NadE and subsequently adenylated to NAD by nicotinamide nucleotide adenyltransferase, NadM<sup>83,85</sup>.

The yeast *Saccharomyces cerevisiae* and *Candida glabrata* transform NmR into NMN using nicotinamide riboside kinase NRK1 enzyme<sup>86,87</sup>. Then, NMN is taken in charge by NadD as in the *de novo* pathway. However, NmR might also be transformed into nicotinamide (Nm) by uridine hydrolase (Urh1) or purine nucleotide phosphorylase (Pnp1) enzymes<sup>88</sup>. Once Nm is formed, it is transformed to nicotinic acid (Na) by nicotinamidase Pnc1 and then to nicotinic acid mononucleotide (NaMN) by nicotinate phosphoribosyl transferase NPT1. Na can also be obtained from the salvage of nicotinic acid riboside NaR with the action of Urh1 and Pnp1 enzymes<sup>88</sup>. At this point, the precursor is taken in charge by the enzymes of the *de novo* pathway to yield NAD.

- Salvage of nucleotides (NMN)

Nicotinamide mononucleotide is a salvageable molecule in the NAD biosynthesis. Some organisms possess a nicotinamide mononucleotide deamidase, PncC, which catalyzes the conversion of NMN to NaMN. NaMN is then taken in charge by the enzymes of the *de novo* pathway. NMN is one of the exceptions of phosphorylated molecules that are able to cross the cell membrane, and it can be also obtained exogenously. However, this is not the case in all organisms. *Salmonella enterica* needs either to cleave nicotinamide (Nm) from NMN in the periplasm and it is Nm that enters the cell<sup>89</sup>; or to transform NMN into NmR

through a periplasmic AphA phosphatase and transport NmR through the membrane by PnuC. Once inside the cell, the NmR salvage route can proceed<sup>73</sup>.

## (ii) Mammals

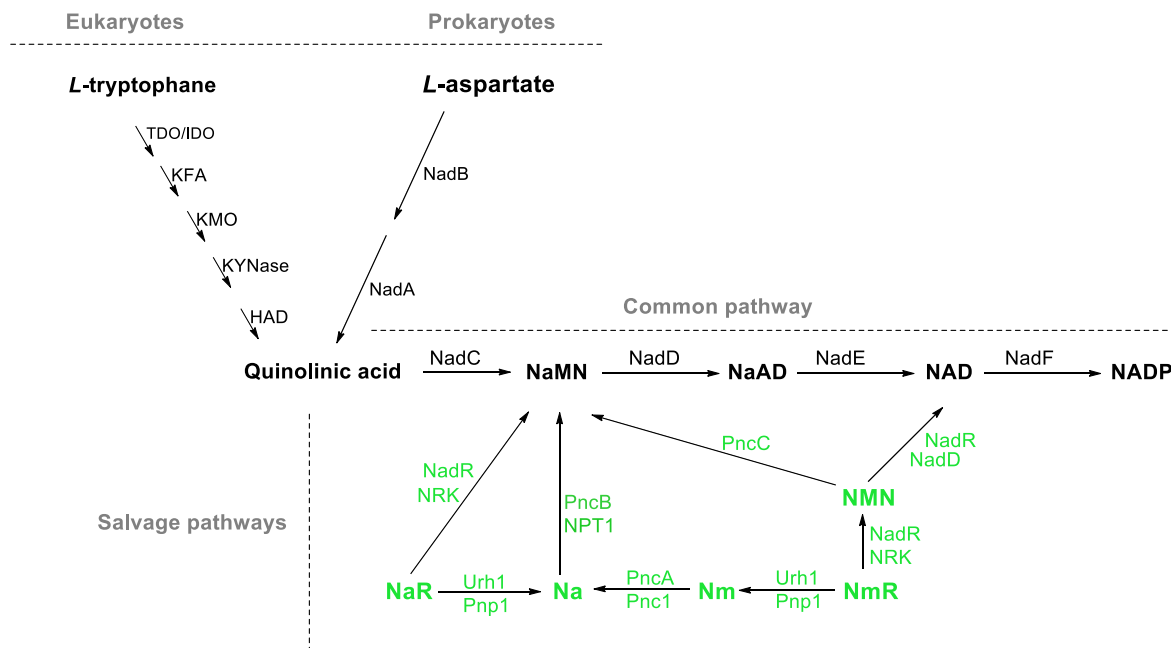
Mammals salvage pathways possess some features with regard to the rest of the organisms. Here are the main differences:

For the recycling of pyridines, mammals do not possess PncA nicotinamidase enzyme in order to hydrolyze Nm into Na. However, Nm might be directly recycled in mammals through its phosphoribosylation by nicotinamide phosphoribosyltransferase enzyme, NadV, with PRPP as second substrate to form NMN. This enzyme is also present in some bacteria like *Haemophilus ducreyi* or in bacteriophages<sup>90,91,92</sup>. The enzyme is able to couple the PRPP with Na to form NaMN. NadV is the equivalent to PncB in bacteria, except that it can couple PRPP to both Na and Nm, whereas PncB is specific for Na.

Concerning the recycling of NMN and NaMN, mammals possess a nicotinamide adenyltransferase enzyme which exists in three isoforms in humans, depending on the compartment: NMNAT-1 in the nucleus; NMNAT-2 in Golgi apparatus; and NMNAT-3 in mitochondria. Compared to prokaryotes, it is the equivalent of NadD and NadR. However, once again, no substrate specificity is found in the mammal one, being able to transfer the adenylyl group to both NaMN and NMN. This yields directly NAD from NMN but NaAD from NaMN. The amidation of NaAD in order to obtain NAD is performed by NAD synthetase NadE<sup>93</sup>.

For the salvage of NmR and NaR, nicotinamide ribose kinase NRK catalyzes their transformation to NMR and NaMN respectively. The enzyme exists in two isoforms; NRK-1 is present in every tissue whereas NRK-2 is present in only some tissues. After phosphorylation, NMN and NaMN are taken in charge by the enzymes described above for the salvage of pyridine nucleotides.

To conclude this part of the introduction, I present a general view summarizing the NAD biosynthetic pathways (de novo and salvage/recycling) in Figure 12.



**Scheme 12:** *de novo* and salvage NAD production pathways. In black: the *de novo* pathway in prokaryotes and eukaryotes as well as their common pathway. In blue: different NAD salvage pathways in eukaryotes and prokaryotes.

### c. NAD biosynthesis regulation

Bacteria possess different NAD biosynthesis regulation systems depending on the type of organism (NadR, NiaR or NrtR/Nudix). The existence of various regulatory mechanisms reflects the importance of maintaining NAD homeostasis in a variety of growth conditions.

#### (i) NAD metabolism regulation by NadR

This tri-functional protein regulator NadR is present in enterobacteria (*E. coli*, *Salmonella*, *Yersinia*, *Shigella*). The N-terminal domain (NadR\_R) with a helix-turn-helix DNA binding motif provides the protein with a regulation activity; the nucleotide binding central domain (NadR\_A) displays a nicotinamide mononucleotide (NMN) adenylyltransferase activity; the C-terminal domain (NadR\_K) displays nicotinamide ribose kinase activity.

The basis of this transcriptional regulation is the following one: In the presence of NAD, the dinucleotide binds to the enzyme through its NadR\_A domain. This interaction leads to the dimerization of the protein that can bind to DNA through the helix-turn-helix DNA-binding domain (NadR\_R) in the specific site where the promoter of genes *nadA*, *nadB*,

*pnuC*, *pncB* and *nadR* is found. This way, the transcription of the genes involved in NAD biosynthesis is repressed as well as the transcription of the regulatory protein itself. However, in the absence of NAD, ATP binds to the protein on the same NAD binding domain (NadR\_A) than NAD and the protein remains as a monomer unable to bind DNA. As a consequence, *nadA*, *nadB*, *pnuC*, *pncB* and *nadR* genes are transcribed and the NAD biosynthesis occurs<sup>94</sup>.

#### (ii) NAD metabolism regulation by NiaR

This second regulation system is present in some bacteria (*Bacillus*, *Clostridium*, *Streptococcus*, *Thermotoga*). The regulator NiaR (**N**iacin **R**epressor) was originally named YrxA<sup>95</sup>. NiaR is a transcriptional repressor that binds to DNA through its helix-turn-helix domain. In contrast to NadR, it is the nicotinic acid (Na) and not NAD that binds to the protein and induces its dimerization and therefore its interaction with DNA. In this case, the transcription of *nadA*, *nadB*, *nadC*, *pncA*, *pncB*, *pnuC* *niaP* (the last one identified as a nicotinic acid and nicotinamide transporter in bacteria) is repressed. In the absence of Na, the protein remains on its monomeric form unable to bind DNA. In this case, there is a derepression of the genes mentioned above<sup>96</sup>.

#### (iii) NAD metabolism regulation by NrtR

Some bacteria like *Vibrio*, *Pseudomonas*, *Mycobacterium* or *Shewanella* possess this last type of regulation system. The regulator is called NrtR for “**N**udix-related **t**ranscriptional **R**egulator”, where Nudix refers to (**N**ucleoside **D**iphosphate linked to a **x** part, a motif found in a family of enzymes that catalyze the hydrolysis of several nucleoside diphosphate derivatives)<sup>97</sup>. The Nudix domain is found on the N-terminal part of the protein whereas the C-terminal contains a helix-turn-helix DNA-binding domain. In contrast to the two previous regulators (NadR and NiaR), the protein is in a dimeric form in the absence of ADP-ribose and bound to DNA. In the presence of ADP-ribose, the protein becomes monomeric and under this form it dissociates from DNA. In this case, the transcription of the genes *nadA*, *nadB*, *nadC*, *nadD*, *nadE*, *pncA*, *pncB*, *niaP*, *pnuC*, *nadR*, *nadM*, *nadV* and *prs* (protein participating in the synthesis of PRPP) is possible. Since ADP-ribose is a NAD degradation product, it functions as a signal for the cell indicating that NAD must be resynthesized<sup>98</sup>.

### III. NAD: a pharmacological target

Nicotinamide adenine dinucleotide plays crucial roles in cellular processes as explained above. Maintenance of the NAD pool is of extreme importance for the good health of cells. Many diseases are associated to perturbations on the concentration levels of NAD coming either from a dysfunction in the NAD biosynthesis enzymes or in the NAD consuming enzymes. For this reason, any of these two kinds of enzymes are interesting targets for the design of pharmacological agents against a large variety of diseases.

Targeting the enzymes involved on NAD biosynthesis is particularly interesting because the NAD biosynthesis pathway of mammals differs from that of bacteria, and therefore, inactivation of the bacterial pathway has no impact on the eukaryotic one (human). However, due to the complexity and diversity of NAD biosynthesis and the presence of different salvage pathways which differ from one organism to another, this antibacterial strategy, despite being promising, is more complex than expected.

Currently, prokaryotic enzymes from both upstream and downstream pathways are explored as potential antibacterial targets. The enzymes driving the downstream conversion of nicotinic acid mononucleotide (NaMN) to NAD are present in almost all analyzed genomes and therefore represent promising broad-spectrum antibacterial targets<sup>32</sup>. Progress have been made in the development of bacterial NadD, NadE and NadK enzyme inhibitors<sup>99,100,101,102</sup>. The upstream NAD biosynthetic pathway is not conserved in all bacteria. Yet, it is a particularly interesting target for the design of new drugs since it allows targeting specific pathogens that lack all kind of NAD salvage pathway and for whom the *de novo* biosynthetic pathway of NAD is essential. From this point of view, two organisms have been proved to have only the *de novo* pathway: *Helicobacter pylori* (cause of gastroduodenal disease) and *Mycobacterium leprae* (cause of leprosy disease).

The main objective of my PhD was to find new antibacterial drugs against these pathogens by targeting quinolinate synthase or NadA, the enzyme responsible of quinolinic acid formation (NAD precursor). The essential nature of NadA was confirmed in *H. pylori* since a *nadA* mutation is lethal to this organism<sup>103</sup>(and unpublished data). Similarly, it has been validated that NAD biosynthesis is a drugable pathway in Mycobacteria such as *M. leprae*<sup>101</sup>. In the following two chapters of this introduction, I will perform a deep description of the

NadA enzyme concerning its structure, function and mechanism as well as an evaluation of the pertinence of looking for new antibacterial drugs against the targeted pathogens and the challenge associated to this.

The enzymes that use NAD either as a redox cofactor or as substrate can also be targeted to design new therapeutic agents. In the first case, where NAD is used as a redox cofactor and where it is bound to the highly conserved Rossmann motif, the strategy consists of occupying the NAD site by an analogue of the cofactor. A significant example that is worth noting here is the case of IMP (Inosine-5'-monophosphate) dehydrogenase enzyme. IMP dehydrogenase is of great importance in purine metabolism and its inhibition is interesting for cancer chemotherapy<sup>104</sup>. Two NAD analogues, tiazofurin and benzamide riboside were shown to inhibit this enzyme<sup>105</sup>. In the case where NAD is a substrate, sirtuins constitute a significant example where this time the enzyme activation (instead of inhibition) may suppose an improvement on life expectancy. Resveratrol is a compound that activates sirtuins and has been shown to retard cell aging in several organisms<sup>106,107</sup>.

#### IV. Quinolinic acid production in prokaryotes: Quinolinic acid synthase system

Several labelling experiments demonstrated that prokaryotes do not synthesize NAD from *L*-tryptophan like eukaryotes<sup>108</sup>. Andreoli A.J. observed that the addition of quinolinic acid (QA) to *E. coli* cell extracts allowed the formation of nicotinic acid mononucleotide (NaMN), and therefore NAD<sup>109</sup>. This suggested that QA was likely to be an intermediate in the prokaryotic biosynthetic pathway of NAD<sup>109</sup>.

##### a. Identification of enzymes

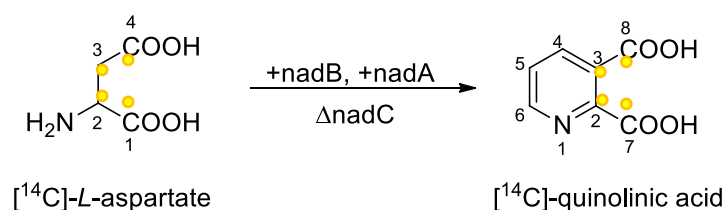
Three genes involved in the *de novo* synthesis of NAD in *E. coli* were discovered based on microbiological experiments. The corresponding *E. coli* mutant strains were able to grow in minimal media in the presence of nicotinic acid (Na)<sup>110</sup>. These genes named *nicA*, *nicB* and *nicC* (for **n**icotinic **a**cid) were renamed later as *nadA*, *nadB* and *nadC* for **n**icotinamide **a**denucleotide<sup>111,112</sup>.

*In vitro* studies performed by the same authors demonstrated that NadA and NadB proteins are both indispensable for quinolinic acid biosynthesis. For this,  $^{14}\text{C}$ -QA formation was monitored by mixing bacterial extracts containing overexpressed NadA but not NadB ( $\Delta\text{nadB}$ ) with bacterial extracts containing NadB but not NadA ( $\Delta\text{nadA}$ ). With the extracts containing only one of these two enzymes (either NadA or NadB) or none, no QA formation was detected<sup>111</sup>.

In the case of NadC, it was observed that a  $\Delta\text{nadC}$  *E. coli* mutant accumulates QA but is not able to produce nicotinic acid mononucleotide (NaMN). For this reason, NadC protein was proposed to be involved downstream QA formation for NaMN production<sup>113</sup>.

### b. Identification of substrates

The research of the substrates to form quinolinic acid was performed through labelling-experiments. An *E. coli* strain deleted in *nadC* (but containing *nadA* and *nadB* genes, which means that it accumulates QA), was mixed with  $^{14}\text{C}$ -L-Aspartate for 5 hours. Degradation of [ $^{14}\text{C}$ ]-quinolinic acid formed from labeled [ $^{14}\text{C}$ ]-L-aspartate showed that a quarter of the radiation was localized on the C<sub>7</sub> carboxylate; another quarter on the carboxylate C<sub>8</sub>; and the rest of the radiation was localized on the C<sub>2</sub> and C<sub>3</sub> of the aromatic part of the molecule. This experiment clearly proved that L-aspartate is a QA precursor<sup>113</sup> (Scheme 13).

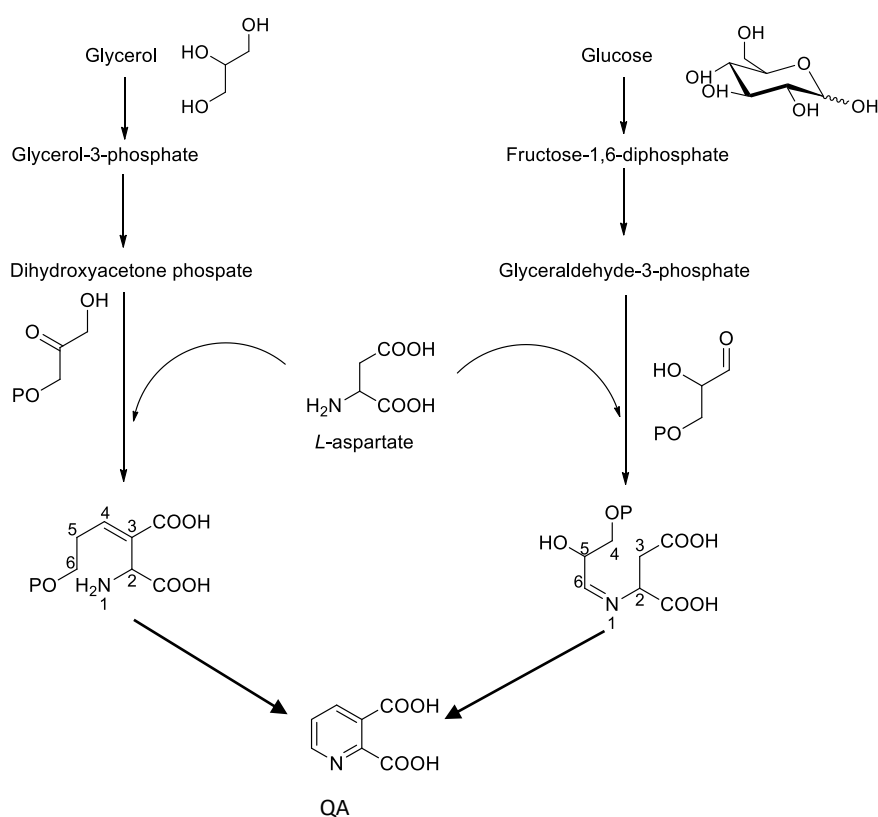


**Scheme 13:** Positions of the labelled carbons in [ $^{14}\text{C}$ ]-quinolinic acid formed from [ $^{14}\text{C}$ ]-L-aspartate and *E. coli* extracts.

In order to determine the origin of the rest of the carbons of QA (C<sub>4</sub>, C<sub>5</sub> and C<sub>6</sub>), *E. coli*  $\Delta\text{nadC}$  extracts were incubated in the presence of L-aspartate and  $^{14}\text{C}$ -labelled potential substrates: [1-(3)- $^{14}\text{C}$ ]-glycerol, [1- $^{14}\text{C}$ ]-glucose, [2- $^{14}\text{C}$ ]-glucose and [6- $^{14}\text{C}$ ]-glucose<sup>114</sup>. In all cases, formation of labelled QA acid was observed in similar amounts. From all the tested substrates and taking into account the repartition of the labelling incorporated in QA

carbons (dosed after degradation of QA like previously described) it was concluded that the molecules must be transformed before being condensed with *L*-aspartate<sup>114</sup>. Dihydroxyacetone phosphate (DHAP) and glyceraldehyde-3-phosphate (G3P) were proposed as molecules that fulfill these conditions: 1) they can be formed from glucose and glycerol respectively and 2) they are able to condense with *L*-aspartate in order to form QA.

Two mechanisms of *L*-aspartate condensation were proposed depending on the triose phosphate nature<sup>114</sup>, as shown in Scheme 14:

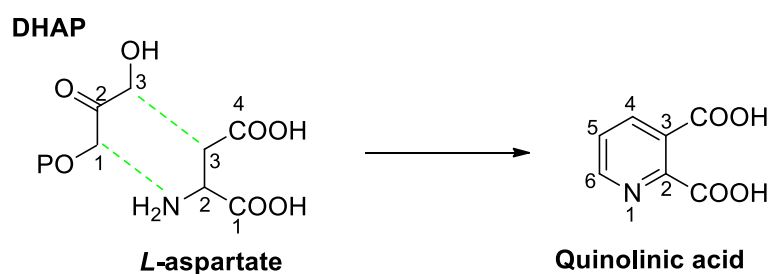


**Scheme 14:** Hypothesis proposed by Chandler J.L.R. in 1970 about the nature of the product that condenses with *L*-aspartate to form quinolinic acid.

In order to know which product condenses with *L*-aspartate (DHAP or G3P), the following experiment was then carried out: partially purified NadA and NadB proteins, <sup>14</sup>C-*L*-aspartate and products resulting from glycolysis (DHAP, G3P, glyceraldehyde, dihydroxyacetone, 3-phosphoglyceric acid,  $\alpha$ -glycerophosphate or glycerol) were mixed.

Among these molecules only G3P and DHAP appeared to be involved in  $^{14}\text{C}$ -QA formation in the presence of  $^{14}\text{C}$ -L-aspartate. These two products are the substrates of triose phosphate isomerase (TPI) enzymes. Therefore, an inhibitor of this enzyme, chloroacetol phosphate was used in the experiment, in order to investigate i) whether QA formation might be due to a TPI-like activity coming from a contaminant and ii) to discriminate in this case between DHAP and G3P as substrates. This way, it was shown that the QA synthesis from G3P and L-aspartate was absent, whereas with DHAP and L-aspartate, the QA occurred. This experiment showed that the molecule that condenses with L-aspartate is likely DHAP and therefore, the activity observed with G3P is likely due to a protein contamination providing TPI activity. From this paper, it was more or less established that quinolinic acid is formed from L-aspartate and DHAP<sup>115</sup>.

An *in vitro* experiment with partially purified NadA and NadB enzymes in the presence of [ $^{14}\text{C}$ ]-dihydroxyacetone phosphate and L-aspartate showed that C<sub>3</sub> of DHAP condenses with C-3 of L-aspartate and as a consequence of that, a bond between C<sub>1</sub> of DHAP and the amine of L-aspartate is formed<sup>116</sup>. This experiment along with the previously described one with [ $^{14}\text{C}$ ]-L-aspartate allowed the attribution of all of the carbons of QA. (Scheme 15).



**Scheme 15:** Condensation mode of L-aspartate and DHAP proposed by Wicks F.D in 1977, after DHAP-labelling.

Even though labelling studies had shown that NadA and NadB catalyze the formation of QA from L-aspartate and dihydroxyacetone phosphate<sup>34</sup> (Figure 4 b), their action remained unknown (which enzymes works before the other). The following experiment allowed to address this question (Figure 4 a). Each protein was placed separately on each side of a dialysis membrane, both in the presence of DHAP and [ $^{14}\text{C}$ ]-L-aspartate. Labelled

QA was found in both compartments. However, since a larger amount of labelled QA was found in the compartment of NadA, it was proposed that NadB first converts *L*-aspartate into iminoaspartate and then NadA condenses iminoaspartate and DHAP to form QA<sup>34</sup>.

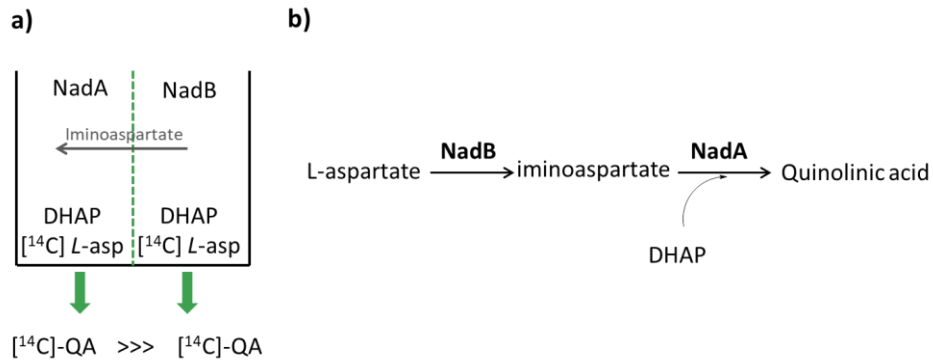


**Figure 4:** **a)** Experiment that allowed the determination of the order in which NadA and NadB enzymes might work. **b)** Proposal of the working order of enzymes.

### c. A NadA-NadB complex?

The hypothesis of an existing “quinolinate synthase complex” formed by NadA and NadB enzymes has been latent since 1970. This hypothesis is based on the facts that:

- Both proteins are implicated in quinolinic acid biosynthesis in the upstream pathway<sup>111</sup>.
- In most bacteria, *nadA* and *nadB* genes are present in the same operon.
- The particular instability of iminoaspartate (the product of NadB enzyme), would support the idea of an existing NadA-NadB complex, which would protect IA and enable its utilization by NadA (see characterization of *L*-aspartate oxidase paragraph).

However, two experiments question the existence of a NadA-NadB complex:

- The experiment described in Figure 4 with partially purified NadA and NadB separated by a dialysis membrane. The fact that formation of [<sup>14</sup>C]-QA was observed in both compartments shows that a NadA-NadB complex is not necessary for the formation of QA.
- NadA is able to form QA from chemically generated IA (from oxaloacetic acid (OAA) and ammonium sulfate (AS))<sup>117</sup>. This proved that NadA may be active without NadB.

However, it is worth noting that this experiment was performed *in vitro* and that formation of IA from OAA and AS likely does not occur *in vivo*.

These experiments suggest that there is no NadA-NadB complex; however the formation of a transient complex cannot be completely excluded.

#### d. Characterization of *L*-aspartate oxidase (NadB)

The first studies that attributed a role to each of the enzymes NadA and NadB were performed in the 70s. Concerning NadB, Wicks F.D. established a relationship between the enzyme and the conversion of *L*-aspartate. He showed that NadB is able to use *L*-aspartate as substrate and that the consumption of *L*-aspartate depends on FAD. This led to propose that NadB catalyzes the dehydrogenation of *L*-aspartate to form the very unstable intermediate, iminoaspartate (IA) and FADH<sub>2</sub>. In 1982, Nasu S. purified for the first time NadB from *E. coli*<sup>33</sup>. He demonstrated the *L*-aspartate oxidase activity of NadB *in vitro* using [<sup>14</sup>C]-*L*-aspartate and its dependence for FAD.

The reaction product was characterized and demonstrated to be iminoaspartate (IA), that decomposes to oxaloacetate and ammonia within seconds<sup>117</sup>. The stability of IA was also studied as following: NadB enzyme was incubated for 100 seconds with [<sup>14</sup>C]-*L*-aspartate and then inhibited by mesotartrate<sup>33</sup>. The stability of the formed IA (the amount accumulated during the 100 seconds) was evaluated by the addition of NadA protein and DHAP at different times after the addition of mesotartrate ( $t_0$ ,  $t_{60s}$ ,  $t_{120s}$ ...). QA was quantified after 5 min incubation. A decrease in the amount of QA formation was observed with regard to the NadA/DHAP addition time. In other words, later NadA and DHAP were added, less QA was formed. This decrease on QA formation within time belongs to the iminoaspartate intrinsic decomposition and this allows the calculation of the IA half-life time: 144 seconds<sup>33</sup>. Another study concluded identically with a half-life time of 150 seconds. The assay was performed as follow: IA was produced chemically by mixing oxaloacetic acid and ammonium sulfate, at 25°C and pH 8 (note that the stability of IA is temperature and pH dependent)<sup>117</sup>. Then [<sup>14</sup>C]-*L*-aspartate was added and detection of [<sup>14</sup>C]-oxaloacetic acid performed allowing to measure the different kinetic constants of NadB for its substrate and FAD. As observed in Figure 5, *L*-aspartate oxidase shows an atypical behavior with regard to the substrate concentration. Two  $K_m$  values were determined for the enzyme and its substrate:  $K_{m1}=0.63$

mM between 0.25 mM and 1.25 mM of *L*-aspartate;  $K_{m2}=3.3$  mM for concentrations of *L*-aspartate higher than 2 mM. Concerning FAD, a  $K_m=2.5$  mM was determined when *L*-aspartate concentration is 0.5 mM. The values were calculated from Lineweaver-Burk curves<sup>33</sup>. It is worth noting that such a  $K_m$  value for FAD is higher than what is usual to find for other flavoproteins, with  $K_m$  values in the range of tens of micromolar<sup>118</sup>.

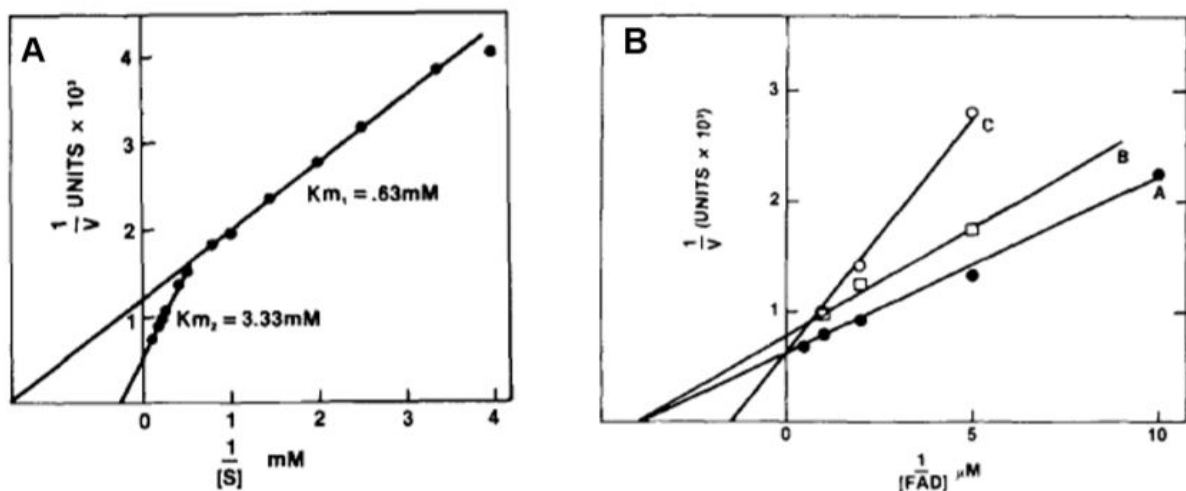


**Figure 5:** **A.** Lineweaver-Burk representation of the initial-velocity of NadB as function of *L*-aspartate concentration (9  $\mu\text{g}$  NadB, 60 minutes). **B.** Lineweaver-Burk representation of the initial-velocity of NadB apoprotein as function of FAD concentration (4.5  $\mu\text{g}$  NadB, 0.5 mM *L*-aspartate, different concentrations of FAD between 1-20  $\mu\text{M}$ ). A: without inhibitor; B: 45  $\mu\text{M}$  of Cibacron blue (a non-competitive FAD inhibitor); C: 2 mM  $\text{NAD}^+$  (a competitive FAD inhibitor).

It was observed that for a same quantity of *L*-aspartate, the increase of NadB enzyme concentration does not imply a proportional formation of IA. A hypothesis to explain this lack of correlation is the existence of an equilibrium between an active monomeric form of NadB (at lower concentrations) and an inactive dimeric form (at higher concentrations)<sup>33</sup>. In 1996, Montarino M. confirmed the existence of a change in oligomerization state as a function of protein concentration, but attributed the lack of linearity between the enzyme activity and protein quantity to an inhibition of the enzyme by its own product IA. This inhibition that is completely avoided in the presence of NadA, led to propose that it could be due to the formation of a NadB-IA complex. This way, the addition of NadA would allow to take in charge IA as soon as it is formed, allowing NadB to be functional again<sup>119</sup>.

### e. NadA: A [4Fe-4S]<sup>2+</sup> enzyme

*E. coli* nadA gene was identified in 1967<sup>111</sup> but its cloning and sequencing were only performed in 1988<sup>120</sup>. Even though it took a long time to characterize the protein for the first time, the use of partially purified NadA *in vitro* or the use of bacterial extracts overexpressing NadA early suggested that the protein likely has an oxygen sensitive [4Fe-4S]<sup>2+</sup> cluster since it lost its activity when extracts were exposed to air, with regard to extracts that were manipulated inside a glove box<sup>121</sup>.

#### (i) Purification and characterization of NadA apoprotein

The first characterization of NadA was done in 2000 by the group of Ceciliani, F. that overexpressed and purified *E. coli* NadA under aerobic conditions<sup>122</sup>. After overexpression the protein was insoluble (inclusion bodies) and it had to be denatured and re-natured before purification. No cofactor was detected<sup>121</sup>. The specific activity of that preparation of NadA was determined to be 0.6  $\mu\text{mol}/\text{min}/\text{mg}$  when NadA was incubated with NadB (purified enzyme), *L*-aspartate and DHAP<sup>121</sup>. The activity was measured by quantifying the phosphate released from DHAP during condensation with IA<sup>122</sup>. As reported on the publication, the main drawback of this method was that DHAP spontaneously hydrolyzes producing phosphate, which might explain the activity found for the apoenzyme<sup>122</sup>. Booker's group reported that this activity is likely a typographical error<sup>39</sup>. An apo-NadA from *Pyrococcus horikoshii* was purified some years later with a specific activity of 2.2  $\mu\text{mol}/\text{min}/\text{mg}$ , determined by measuring the formation of QA from IA and DHAP by high performance liquid chromatography<sup>123</sup>. The activity remains particularly high for an apo-form (we will see later that the NadA enzyme is active under a holo-form) and it is possible that a quantification error was performed, due to the overlapping of QA and fumarate peaks on the HPLC chromatogram.

#### (ii) Purification and characterization of the holoprotein

The first purification and characterization of quinolinate synthase from *E. coli* on its holo-form (with an Fe-S cluster) was reported in 2005 by our laboratory<sup>38</sup> and by the group of Squire Booker<sup>39</sup>. The holo-form could be obtained because the protein was purified under anaerobic conditions. Since then, many purifications of NadA from different organisms (P.

horikoshii<sup>124</sup>, *M. tuberculosis*<sup>124</sup>, *A. thaliana*<sup>125</sup>, *T. maritima*<sup>126</sup> ...) have been performed and these have demonstrated the presence of a Fe-S cluster in the protein<sup>38,39,124,125</sup>.

#### a. Biochemical properties

The as-purified protein presents a brown-yellowish color, indicative of a  $[4\text{Fe-4S}]^{2+}$  cluster. The Fe and S amount varies between  $3.1\text{-}3.6 \pm 0.4$  Fe and  $2.7\text{-}3 \pm 0.4$  S atoms per monomer also in agreement with a  $[4\text{Fe-4S}]^{2+}$  cluster<sup>124,126</sup>. Sometimes, the cluster is lost during purification and as a consequence the Fe-S content is low ( $0.5 \pm 0.5$  iron per monomer; for NadA from *M. tuberculosis*<sup>124</sup>, *A. thaliana*<sup>125</sup>, *T. maritima*<sup>126</sup>, *P. horikoshii*<sup>124</sup>, *P. furiosus*<sup>127</sup> and *B. subtilis*<sup>36</sup>). In these cases, the cluster is chemically reconstituted afterwards.

The measure of the enzymatic activity of the holo-NadA was performed by two different techniques<sup>38,39</sup>. Squire Booker's group measured it by quinolinic acid quantification using HPLC. This way, a specific activity of 15 nmol QA/min/mg protein was found<sup>39</sup>. In our laboratory, a previous assay consisted in the measurement of the remaining DHAP after the enzymatic reaction. This was done using  $\alpha$ -glycerophosphate dehydrogenase that catalyzes the oxidation of DHAP by NADH into  $\alpha$ -glycerophosphate and  $\text{NAD}^+$ . The total amount of  $\text{NAD}^+$  formed, determined from the light absorption at 340 nm, is identical to the remaining DHAP<sup>38</sup>. Currently, we are measuring QA formation using HPLC as described by S. Booker's lab. Our protein preparations display activities in the range of 50-60 nmol/min/mg. Our best preparation displays a specific activity of 90 nmol/min/mg.

#### b. Spectroscopic properties

##### UV-visible absorption spectroscopy of holo-NadA

The UV-visible spectrum of holo-NadA recorded inside the glove box after purification of the enzyme displayed absorption bands at 280 nm and 420 nm. The band at 280 nm corresponds to the aromatic amino acids of the protein. The absorption band at 420 nm is characteristic of a ligand to metal charge-transfer band (S to  $\text{Fe}^{3+}$ ). The lack of any bands at 320 nm and 460 nm (characteristic  $[2\text{Fe-2S}]^{2+}$  clusters) strongly suggested the presence of a  $[4\text{Fe-4S}]^{2+}$  cluster (Figure 6).

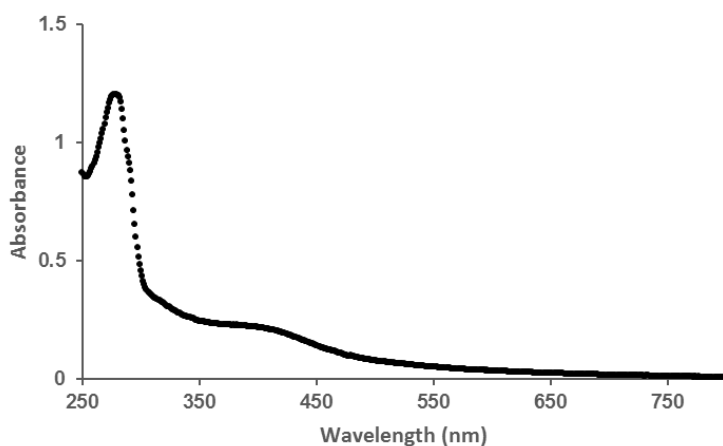


**Figure 6:** UV-vis. spectrum of *E. coli* NadA (13  $\mu$ M) measured in a 1 mm cell under anaerobic conditions in buffer A.

### Mössbauer spectroscopy of holo-NadA

The Mössbauer spectrum of anaerobically purified  $^{57}\text{Fe}$ -S NadA from *E. coli* consists of a quadrupole doublet (almost symmetrical) which can be simulated with two doublets of similar intensity, belonging to two species. Each one corresponds to a mixed valence Fe pair ( $\text{Fe}^{2+}$  and  $\text{Fe}^{3+}$ ). The parameters of the first doublet are  $\delta=0.43$  mm/s and  $\Delta_{\text{EQ}}=0.94$  mm/s; the parameters of the second doublet are  $\delta=0.44$  mm/s and  $\Delta_{\text{EQ}}=1.27$  mm/s. The average of these measured parameters ( $\delta=0.43$ - $0.44$  mm/s and  $\Delta_{\text{EQ}}=1.11$  mm/s) are consistent with a  $[\text{4Fe-4S}]^{2+}$  cluster <sup>126</sup> (Figure 7).

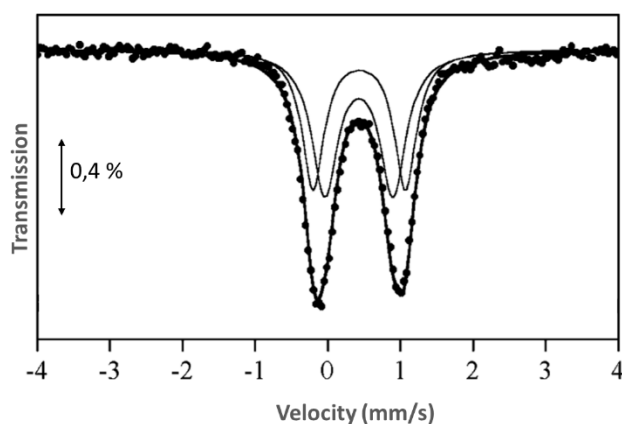


**Figure 7:** Mössbauer spectrum of *E. coli* NadA (560  $\mu$ M, 3.2 Fe per monomer), purified under anaerobic conditions. The spectrum is recorded at 4.2 K and under a 600 G magnetic field. Dotted line corresponds to the experimental spectrum; plain lines represent the two simulated species.

## EPR spectroscopy of holo-NadA

The EPR spectrum of as-purified holo-NadA does not display any EPR signal in agreement with the presence of a  $[4\text{Fe-4S}]^{2+}$  cluster. However, after one electron reduction by dithionite, a rhombic EPR signal with g values of 2.03 and 1.93 was observed, whose temperature dependence and microwave power saturation properties are characteristic of a  $[4\text{Fe-4S}]^{1+}$  cluster ( $S=1/2$ ) (Figure 8). The double integration of the signal and quantification using a Cu-EDTA standard show that 80 % of the total iron is present in the  $[4\text{Fe-4S}]^{1+}$  form<sup>126</sup>.

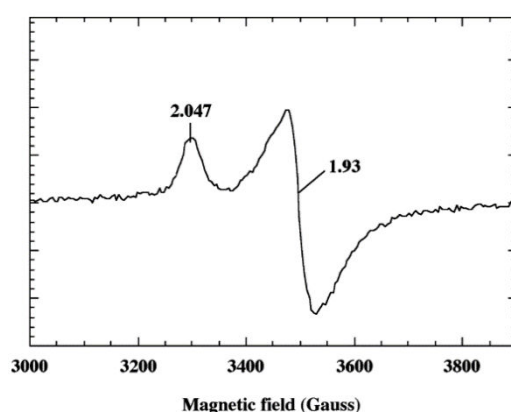


**Figure 8:** EPR spectrum of anaerobically as isolated *E. coli* NadA (200  $\mu\text{M}$ ) reduced with 2 mM of dithionite for 15 min. T = 5 K; P = 0.1 mW; gain =  $2 \times 10^5$ ; amplitude modulation: 10 mT<sup>-38</sup>.

### (iii) NadA $[4\text{Fe-4S}]^{2+}$ cluster: sensitivity to oxygen

The existence of an oxygen-sensitive enzyme in NAD biosynthetic pathway was suggested<sup>128</sup> early since it was observed that  $\text{O}_2$  played a bacteriostatic role in *E. coli* growth<sup>128</sup> and considerably decreased the cell NAD(P) pool<sup>129</sup>. Later, quinolinate synthase was found to be this oxygen sensitive enzyme<sup>115,130</sup>.

Several spectroscopic studies performed with holo-NadA have demonstrated the  $\text{O}_2$ -sensitivity of the cluster. Herein, I report these studies:

The UV-visible spectrum of the as-purified holo-NadA presents a characteristic band at 420 nm that comes from the cluster as previously explained. After 30 minutes incubation in the presence of oxygen, the intensity of this band considerably decreases and the protein solution color changes. Two new absorption bands appear at 320 and 460 nm. These bands

are typical signatures of a  $[2\text{Fe-2S}]^{2+}$  cluster. This experiment strongly suggested the degradation of the  $[4\text{Fe-4S}]^{2+}$  into a  $[2\text{Fe-2S}]^{2+}$  under aerobic conditions. Note that the band at 420 nm cannot be recovered after incubation of the protein under anaerobic conditions<sup>126</sup> (Figure 9; part A).

Mössbauer spectra of purified NadA after  $\text{O}_2$ -exposure are reported in figure 9 (Part B). The spectrum at  $t=0$  (spectrum **a**) corresponds to the one previously described for NadA, i.e. a  $[4\text{Fe-4S}]^{2+}$  cluster that accounts for 100 % of total iron present in the protein.

Spectra **b** and **c** (Figure 9, Part B) were recorded after thawing the sample and exposure to air for 20 and 80 minutes, respectively. Significant changes were observed confirming that the  $[4\text{Fe-4S}]^{2+}$  ( $S=0$ ) cluster is air sensitive. The deconvolution of the spectra **b** and **c** was performed assuming that these spectra accounted for ~50 % of the iron relative to the **a** spectrum. The absorption area in the  $\sim+1.0$  mm/s region gradually decreases indicating a degradation of the  $[4\text{Fe-4S}]^{2+}$  ( $S=0$ ) clusters. In the simulation of the spectra **b** and **c** was included a doublet with parameters taken from the analysis of the spectrum **a** corresponding to intact residual  $[4\text{Fe-4S}]^{2+}$  ( $S=0$ ) center. It was therefore estimated that the iron in  $[4\text{Fe-4S}]^{2+}$  ( $S=0$ ) form is 20-25 % in **b** and <10 % in **c**. The decrease of the  $[4\text{Fe-4S}]^{2+}$  ( $S=0$ ) doublet is accompanied by the appearance of new species with one of the absorption lines at 0.5 – 0.6 mm/s. These new features were simulated assuming two nested doublets **I** and **II** with parameters  $\delta(\text{I}) = 0.29(\pm 0.01)$  mm/s,  $\Delta_{\text{EQ}}(\text{I}) = 0.45(\pm 0.03)$  mm/s;  $\delta(\text{II}) = 0.30(\pm 0.02)$  mm/s,  $\Delta_{\text{EQ}}(\text{II}) = 0.80(\pm 0.07)$  mm/s. The values of the parameters for doublets **I** and **II**, and more specifically the isomer shift, strongly suggested tetrahedral high spin ferric ions, most probably in a diamagnetic environment. Combination of the above information suggests that doublets **I** and **II** arise from  $[2\text{Fe-2S}]^{2+}$  ( $S=0$ ) clusters (25-30 % of the iron in **b** and ~40 % in **c**). In summary, Mössbauer spectroscopy indicates that the anaerobically isolated protein contains one  $[4\text{Fe-4S}]^{2+}$  ( $S=0$ ) per monomer that after the exposure to air leads to a gradual degradation of this cluster to yield new species most probably in the  $[2\text{Fe-2S}]^{2+}$  ( $S=0$ ) form.

EPR spectroscopy was also used to study NadA [4Fe-4S]<sup>2+</sup> cluster degradation in the presence of oxygen. After 10 min exposure to O<sub>2</sub>, a new EPR signal appears different to that of the reduced holo-NadA with the following values: g = 2.03, 2.01 and 1.95. These parameters, in addition to the behavior of the signal with temperature and microwave power saturation properties match with a [3Fe-4S]<sup>+</sup>. A longer exposition to oxygen gives an EPR silent species which is in agreement with the formation of a [2Fe-2S]<sup>2+</sup> cluster<sup>126</sup> (Figure 29; Part C).

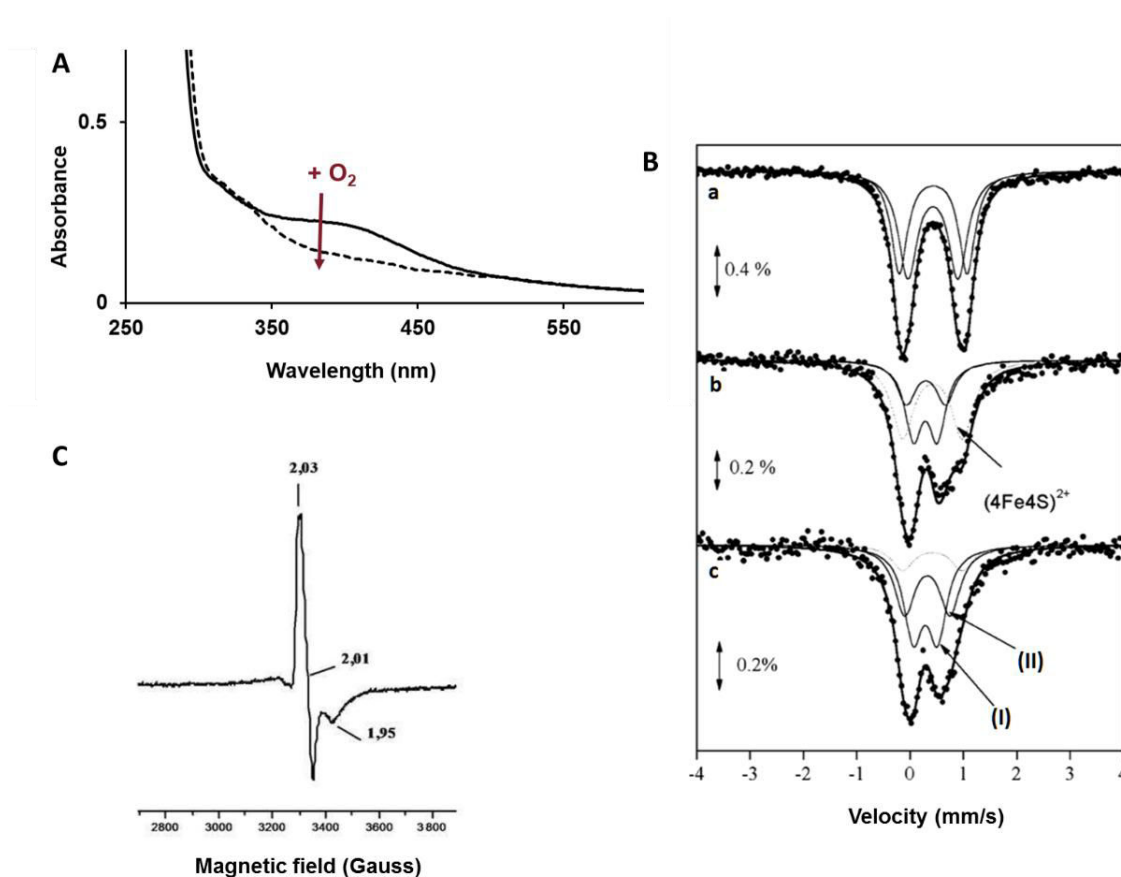
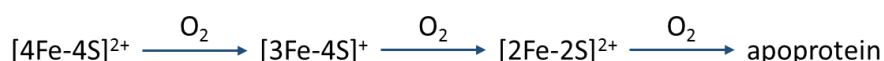


**Figure 9:** **A.** *E. coli* holo-NadA UV-visible spectrum (18 μM) under anaerobic conditions (black) and after 30 minutes of exposure to oxygen (dotted line). **B.** *E. coli* <sup>57</sup>Fe-S NadA Mössbauer spectra (560 μM, 3.2 Fe/monomer of protein) measured at 4.2 K A) before; B) 20 min after; C) 80 min after O<sub>2</sub> exposure. The dotted lines correspond to experimental spectra and bold lines correspond to simulations<sup>38</sup>. **C.** *E. coli* NadA EPR spectrum (260 μM) after 10 min O<sub>2</sub> exposure, recorded at T:10 K, P: 0.1 mW, modulation amplitude: 10 Gauss, gain: 2.10<sup>126</sup>.

The use of all these three different spectroscopies allowed to understand the mechanism of NadA [4Fe-4S]<sup>2+</sup> cluster degradation upon O<sub>2</sub> exposure (Scheme 16).



**Scheme 16:** NadA [4Fe-4S]<sup>2+</sup> cluster conversion upon O<sub>2</sub> exposure.

## f. Structure of Quinolinate synthase NadA

Despite the importance of NadA protein in the synthesis of NAD, it is the only enzyme of the pathway whose structure and mechanism remained unknown until very recently. Two structures of apo NadA from thermophilic organisms were solved<sup>123,127</sup>. In 2014, our collaborator Juan Carlos Fontecilla Camps (IBS Grenoble) solved the first crystal structure of NadA from *T. maritima* organism on its holo-form; i.e. on its active form<sup>131</sup>. Here is a chronological summary starting from the apo NadA structures until the solving of the first holo NadA structure.

### (i) First structures of apoprotein quinolinate synthase

#### The structure of Sakuraba - a particular folding

The first quinolinate synthase structure was solved in 2005 by Sakuraba H. *et al.*<sup>123</sup>. The *P. horikoshii* NadA protein was crystallized at 2 Å resolution as a monomer without the presence of its [4Fe-4S]<sup>2+</sup> cluster. The overall structure includes a central region plus N- and C- terminal helical segments ( $\alpha_1$  and  $\alpha_{14}$  respectively). The central region forms a unique triangular convexo-concave structure and is composed of three analogous domains, which relate to a pseudo-3-fold symmetry and exhibit similar folds: a four-stranded parallel  $\beta$  sheet flanked by two  $\alpha$  helices on either side, forming a three layer ( $\alpha\beta\alpha$ ) sandwich. The three domains are separated by three surface loops where two of them were found disordered on the structure<sup>123</sup>.

This structure was obtained in the presence of malate, an analog of iminoaspartate (IA), one of the substrates of NadA. The amino acids involved in the interaction with malate were proposed to be those involved in the interaction with IA (Figure 10).

The organization of the enzyme in three similar domains was unique until the resolution of two other  $[4\text{Fe-4S}]^{2+}$  containing enzymes: IspH, an enzyme involved in the last step of isoprenoid biosynthesis<sup>132</sup> and Dph2, a radical-SAM enzyme involved in the first step of diphthamide biosynthesis (a post-translationally modified histidine residue in translation elongation factor 2)<sup>133</sup>.

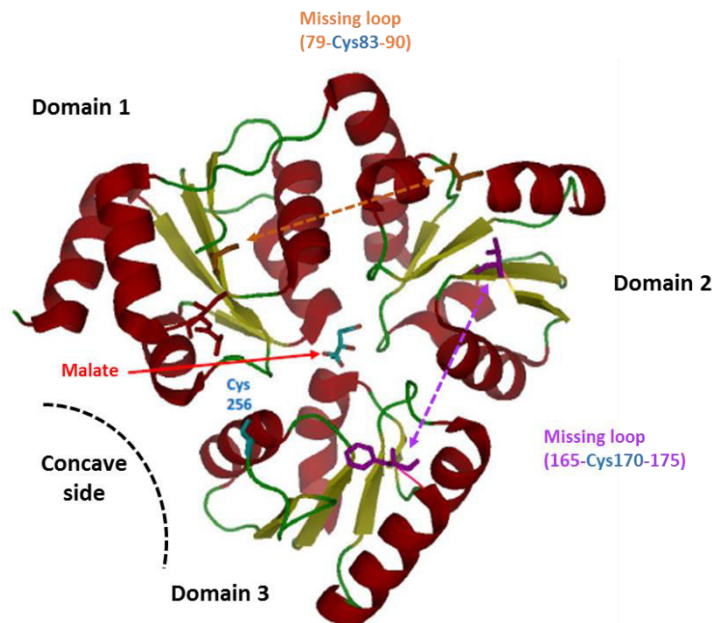


**Figure 10:** Ribbon diagram of the first NadA structure (apo-protein) solved by Sakubara H. *et al*<sup>123</sup>. The bound malate molecule is shown.

### The structure of Soriano – active site models

A second structure of apo-NadA from *P. furiosus* was solved by Soriano E. V. *et al.* at 2.8 Å resolution<sup>127</sup>. The global structure matches that of Sakuraba's one with the three  $\alpha\beta\alpha$  folded domains. However, in contrast to the previous structure, the *P. furiosus* structure was crystallized as a dimer and two out of the three domain-binding loops are observable.

Using structures of holo-IspH and holo-Dph2 (in the presence of their  $[4\text{Fe-4S}]^{2+}$  cofactor) some docking experiments allowed the authors to place a  $[4\text{Fe-4S}]^{2+}$  on the apo-enzyme structure of *P. furiosus* NadA and to propose functional amino acids in the active-site<sup>127</sup>.

## (ii) First structure of holo-protein quinolinate synthase

In our laboratory, two approaches were used in order to obtain holo-NadA structure: (i) the use of NadA protein from different organisms in order to increase the chances of crystallization and (ii) the use of surface mutants of *T. maritima* NadA in order to change the stacking of crystals. The use of *T. maritima* NadA with a surface mutation on the lysine 219 (K219R) allowed to obtain the crystal structure of NadA at 1.6 Å resolution<sup>131</sup>. *TmNadA* K219R exhibits biochemical and spectroscopic properties as the wild-type NadA and displays identical *in vitro* and *in cellulo* activities with regard to NadA wild-type<sup>131</sup>. Since that time, it is considered as the “wild-type” in our crystallographic studies and we refer to it in the thesis manuscript as *TmNadA\**.

The *TmNadA\** structure has provided the following information:

### a. The particular folding of NadA

The holo-NadA structure confirms the unique triangular architecture of NadA in three domains ( $\alpha\beta\alpha$  structure on each domain) encountered in the two previous apo-NadA structures<sup>123,127</sup>. As previously stated, such structure is only found in two other Fe-S enzymes: IspH and Dph2<sup>132,133</sup> which are not dehydratases like NadA but which both possess a catalytic  $[4\text{Fe-4S}]^{2+}$  coordinated by three cysteine residues and a exchangeable non-cysteinylligand. In these enzymes, the iron coordinated by the non-cysteinylligand is the catalytic site of the Fe-S cluster.

### b. The fourth ligand of NadA $[4\text{Fe-4S}]^{2+}$ cluster

The structure of *TmNadA\** holo-protein revealed that the  $[4\text{Fe-4S}]^{2+}$  cluster is coordinated by three strictly conserved cysteines (Cys<sub>81</sub>, Cys<sub>168</sub> and Cys<sub>254</sub> in *T. maritima* and Cys<sub>113</sub>, Cys<sub>200</sub> and Cys<sub>297</sub> in *E. coli*) and that the fourth ligand of the  $[4\text{Fe-4S}]^{2+}$  cluster is a water molecule. This is also the case for aconitase<sup>134</sup> (Annex I) and most of the dehydratase enzymes in which the Fe-S cluster plays a catalytic role through the iron coordinated by the exchangeable ligand (H<sub>2</sub>O).

### c. A tunnel connects the $[4\text{Fe-4S}]^{2+}$ with the surface

The structure reveals a tunnel that connects the  $[4\text{Fe-4S}]^{2+}$  with the surface of the molecule. Interestingly, the catalytic iron site (coordinated by the water molecule) points

towards the entrance of the tunnel, in agreement with the catalytic role of the Fe-S cluster through this Fe site. Such a tunnel is not common in  $[4\text{Fe-4S}]^{2+}$  proteins. This structure with the opened tunnel<sup>131</sup> will be later referred in the manuscript as the opened NadA structure (Figure 11).

Some docking studies of the last QA precursor intermediate 5-hydroxy-4,5-dihydroquinolinate (named **Y**, Figure 12) in holo-*TmNadA*\* were performed and one of its two isomers, (R)-**Y**, satisfied well the anchoring requirements and provided structural basis for catalysis. Indeed, the -OH from Tyr21 is properly positioned to become the nucleophile that deprotonates C4, a step required in the dehydration of **Y** to form QA. Incidentally, it was seen that the long tunnel that connects the catalytic unique iron ion of the  $[4\text{Fe-4S}]^{2+}$  cluster to the molecular surface collapses in the *TmNadA* model in which **Y** intermediate was docked (Figure 11). This suggests that the substrate binding controls the opening and closure of the tunnel. In other words, the entrance of substrates may reorganize the three domains by modifying the tunnel in a way where it becomes closed, protecting the intermediates and substrates (especially IA). This structure corresponds and will be referred as the closed NadA structure.

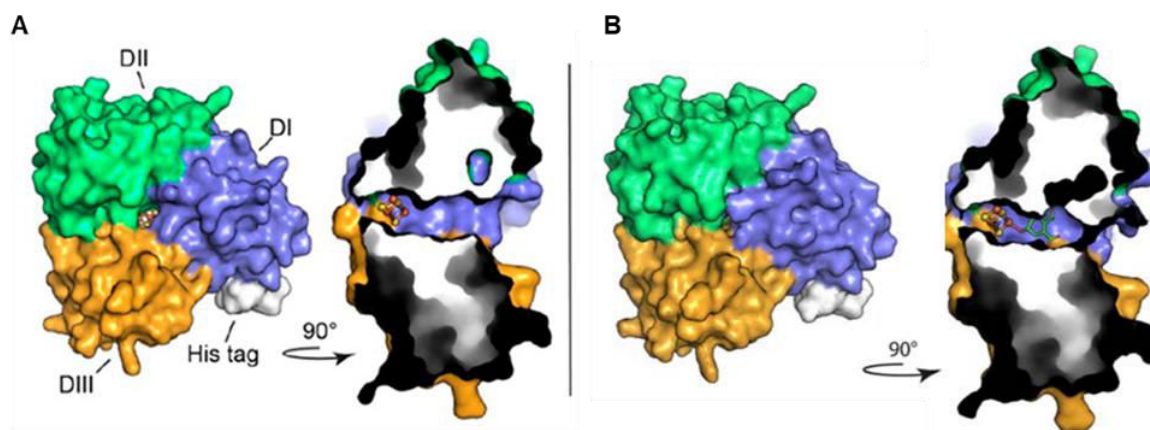


**Figure 11: A-left:** Structure of *TmNadA*\*. Three domains (green, purple and gold) define a tunnel that connects the  $[4\text{Fe-4S}]^{2+}$  cluster to the molecular surface. **A-right:** Section through the long tunnel of the structure rotated by  $90^\circ$  about the vertical axis. **B-left:** Structure of the modeled **Y** intermediate bound to *TmNadA*\*. The long tunnel of the structure is closed. **B-right:** Section through the long tunnel of the modeled-structure rotated by  $90^\circ$  about the vertical axis.

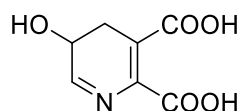


**Figure 12:** Structure of 5-hydroxy-4,5-dihydroquinolinic acid (Y), the last precursor before the formation of quinolinic acid (QA).

#### d. NadA catalytic triade

The docking of the Y intermediate in the *TmNadA*\* structure also revealed the existence of a catalytic triad (Thr229-His171-Glu195) in the active site that might be involved in a charge-relay system able to deprotonate the tyrosine 21 residue. All these residues are strictly conserved (Annex II). Triad mutants were generated in the *E. coli* NadA enzyme, as well as the tyrosine 49 mutant. All these mutants display a drastically reduced activity compared to the wild-type showing that the triad residues and the tyrosine are crucial for catalysis (Table 1).

	Specific activity (nmoles/min/mg)	
	NadB	OAA/AS
<i>TmNadA</i> wt	-	10.3
<i>TmNadA</i> Y21F	-	n.d
<i>EcNadA</i> wt	176.2	64.1
<i>EcNadA</i> Y49F	13	n.d
<i>EcNadA</i> E228A	9	-
<i>EcNadA</i> H205F	n.d	-
<i>EcNadA</i> T262V	15	-

**Table 1:** Specific activity of NadA proteins from *E. coli* and *T. maritima*. No QA was formed using *TmNadA*Y21F. The crucial role of the tyrosine residue in NadA activity was verified by assaying the corresponding *E. coli* (Ec) Y49F mutant. The role of the Thr-His-Glu triad residues was also checked by measuring the NadA activity of *E. coli* E228A, H205F and T262V mutants<sup>131</sup>.

The catalytic mechanism proposed for the triad in *TmNadA*\* was the following one: glutamate residue deprotonates histidine; histidine snatches a proton from threonine and threonine deprotonates the Y21, which in the form of a phenoxide is able to perform a nucleophilic attack at C<sub>4</sub> proton of the intermediate facilitating the last dehydration reaction (second dehydration) that gives rise to the formation of QA and the regeneration of the free enzyme (Figure 13).

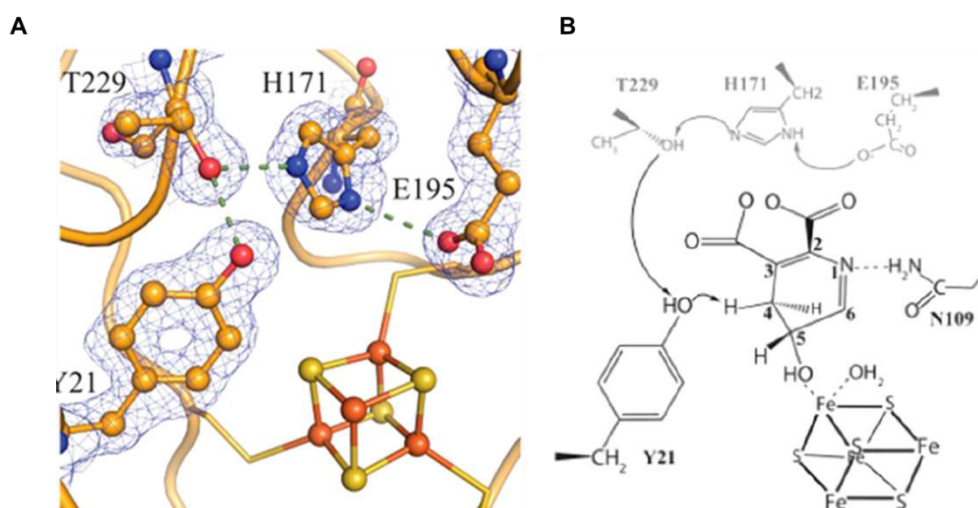


**Figure 13:** A. Charge-relay triad (Thr229-His171-Glu195) and Tyr21 at the NadA active site. B. Schematic view of the active site of *TmNadA* and proposed catalytic mechanism of the triad and tyrosine 21 for the last dehydration step of Y before QA formation<sup>131</sup>.

### g. Mechanism of Quinolinate synthase

As already mentioned, labelling experiments demonstrated that in order to form quinolinic acid, two substrates have to condense: iminoaspartate (IA) and dihydroxyacetone phosphate (DHAP)<sup>34</sup>. Having a bimolecular reaction that yields an aromatic molecule reflects the complexity of the reaction catalyzed by NadA.

Before my arrival at the laboratory, two mechanisms had been proposed for the synthesis of QA from DHAP and IA, based on chemistry rules (A and B) and on previous experiments with G3P<sup>114</sup> (B) (Scheme 17).

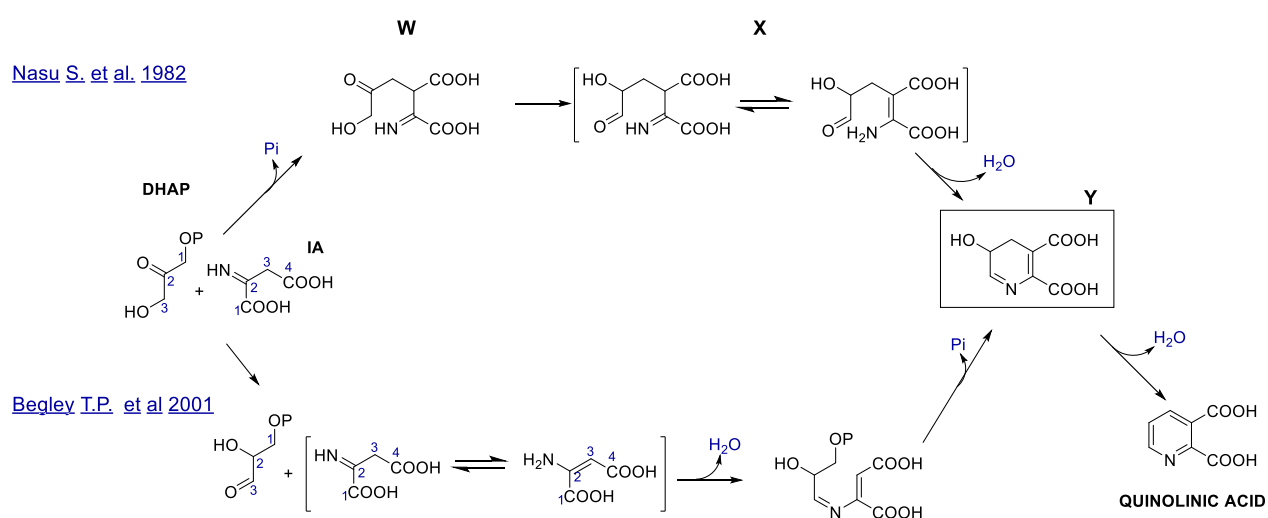
#### A. The mechanism proposed by Nasu S. in 1982<sup>33</sup>

In a first step, electron-withdrawing groups in IA facilitate removal of a proton from the C<sub>3</sub>. The resulting species, having partial carbanion character, carries out a nucleophilic

attack on C<sub>1</sub> of DHAP with the elimination of inorganic phosphate. A keto-aldo isomerization followed by two dehydrations gives rise to the formation of quinolinic acid<sup>135</sup> (Scheme 17 higher part).

B. The mechanism proposed by Begley in 2001<sup>136</sup>

In contrast to the previous mechanism, Begley T.P. hypothesized another mechanism where DHAP is first isomerized to glyceraldehyde-3-phosphate (G3P) before condensation with IA. In this case, the condensation reaction occurs between the amine (IA tautomer) and the aldehyde group of G3P resulting in the removal of a water molecule. A cyclisation of the formed intermediate involves the release of an inorganic phosphate. Then, a final dehydration allows the aromatization of the molecule forming quinolinic acid (Scheme 17 lower part).



**Scheme 17: Higher part:** NadA mechanism proposed by Nasu S. in 1982. **Lower part:** NadA mechanism proposed by Begley T.P. in 2001.

In order to gain insight into NadA reaction mechanism and in particular determine which mechanism (Nasu's or Begley's one) occurs, a comparison of the NadA activity using G3P versus DHAP was performed in our laboratory using pure enzymes, in contrast to the previous experiments performed with partially purified ones<sup>114</sup>.

First, NadA (*E. coli* or *T. maritima*) was incubated in the presence of IA and DHAP or G3P. A similar activity was detected with both molecules in agreement with the results

obtained with labelling experiments performed with NadA and NadB enriched extracts in the presence of *L*-aspartate and [<sup>14</sup>C]-DHAP or [<sup>14</sup>C]-G3P<sup>115</sup>.

Second, it was shown that NadA displays a triose phosphate isomerase (TPI) activity. Indeed, the enzyme is able to convert G3P into DHAP and DHAP into G3P<sup>137</sup>. These results revealed a new activity for NadA, but did not provide any information as to which molecule, DHAP or G3P, condenses with IA to form QA, i.e, whether Nasu's or Begley's mechanism is occurring (Scheme 17).

Third, NadA activity was monitored using phosphoglycolic acid (PGA), an inhibitor of TPI activity. When NadA was incubated with IA, DHAP and PGA, formation of QA was observed. In contrast, when NadA was incubated with IA, G3P and PGA, no QA formation was observed, showing that QA can only be formed from DHAP and IA. These data allowed to discriminate between the two proposed mechanisms, in favor of Nasu's mechanism (Scheme 17 higher part)<sup>137</sup>.

In 2016, our collaborators (the group of Juan Fontecilla Camps, IBS Grenoble) solved the structure of *TmNadA*\* Y107F variant in complex with the first intermediate of NadA mechanism **W** (Figure 31A) at 1.9 Å resolution resulting from the condensation of its two substrates, DHAP and IA<sup>138</sup>. The crystals of the *TmNadA*\*Y107F-**W** complex were obtained after overnight incubation of *TmNadA*\*Y107F with DHAP, oxaloacetic acid and ammonium ions at neutral pH in the glovebox. Tyrosine 107 is a conserved amino-acid of the active-site and its mutation was likely responsible for the trapping of the **W** intermediate. From the obtained X-ray structure, the electron density for **W** fitted with **W** in two conformations: a major called **W'** (2-imino, 3-carboxy, 5-oxo, 6-hydroxy hexanoic acid) and a minor called **W''** (**W'** 2-amino tautomer) (Figure 14A). In both conformations, **W** binds NadA mainly through its two carboxylate groups and through its C<sub>6</sub>-O<sup>-</sup> to the catalytic iron site of the [4Fe-4S]<sup>2+</sup> cluster (Figure 14A). The structure revealed that the enzyme was in its closed form. The obtained structure showed that the **W** intermediate has no phosphate group and therefore that the condensation of the two substrates causes dephosphorylation, in agreement with Nasu's mechanism. A role for the tyrosine 107 in the protonation state of glutamate 195 was proposed. In the absence of the hydroxyl group of the tyrosine, there is no interaction between Tyr107 and Glu195 and the active site conformation changes rendering *TmNadA*\*Y107F unable to catalyze the isomerization of **W** to **X** (Figure 14A).

A complex of *TmNadA*\*Y21F variant with substrate-derived QA was solved at 1.9 Å resolution by our collaborators (Figure 14B). Tyrosine 21 is another conserved active-site amino acid (see above) and its mutation renders the reaction very sluggish but possible (30% of product form relative to the control after 35 h<sup>138</sup>). The crystals were obtained after incubation of the enzyme *TmNadA*\*Y21F in the presence of the substrates as above. QA appears bound to the accessible iron of the [4Fe-4S]<sup>2+</sup> cluster in a bidentate mode through its nitrogen and the adjacent carboxylate.

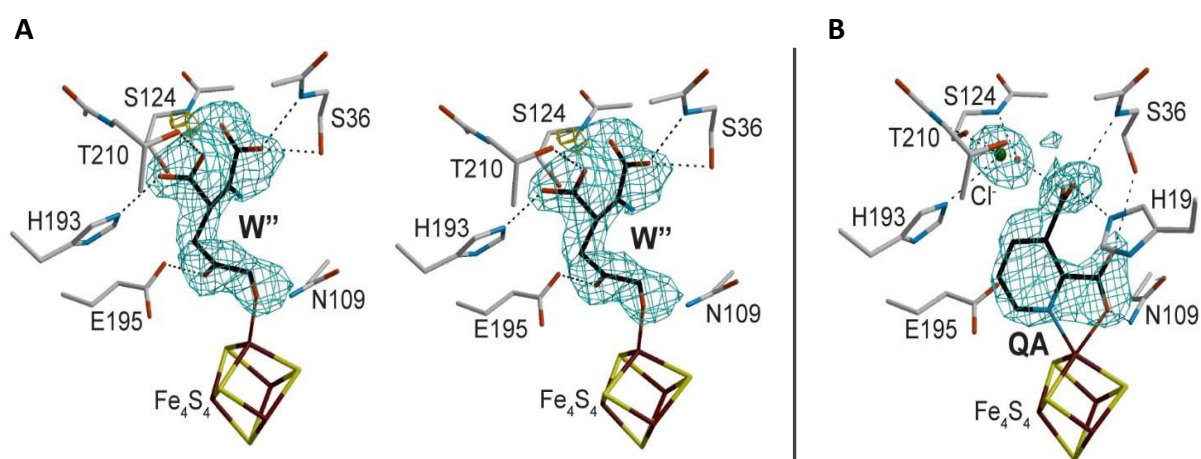


**Figure 14:** **A.** Stereo view of the model and electron density ‘omit’ map (in blue mesh) of a *TmNadA* complex with **W'** and **W''**. **B.** Stereo view of the model and electron density ‘omit’ map (in blue mesh) of a *TmNadA* complex with QA<sup>138</sup>.

These results imply that formed QA (originating from **W''** transformation) rotates in *NadA* active-site to form the bidentate complex with the catalytic iron site of the cluster.

In 2018, we reported with our collaborators a new structure of the slowly reacting *TmNadA*\*Y21F variant in the presence of substrate-derived products **X** and **Y** (Figure 15)<sup>139</sup>. The crystals were obtained by incubating *TmNadA*\*Y21F enzyme with DHAP, oxaloacetate and ammonium ions in the glove box at pH 7.5 and then a pH shift to 7.1 was performed. In such conditions, wild-type *NadA* displays very little activity and as a consequence its *TmNadA*\*Y21F variant is even less efficient<sup>139</sup>. X-ray data from a crystal grown under these “pH shifted” conditions showed a density peak in the active site where intermediates **X** and **Y** could be built with a remarkably good match (Figure 15). They interact with the enzyme through the carboxylates groups and coordinate the catalytic iron of the [4Fe-4S]<sup>2+</sup> through their C<sub>5</sub>-O<sup>-</sup> group.

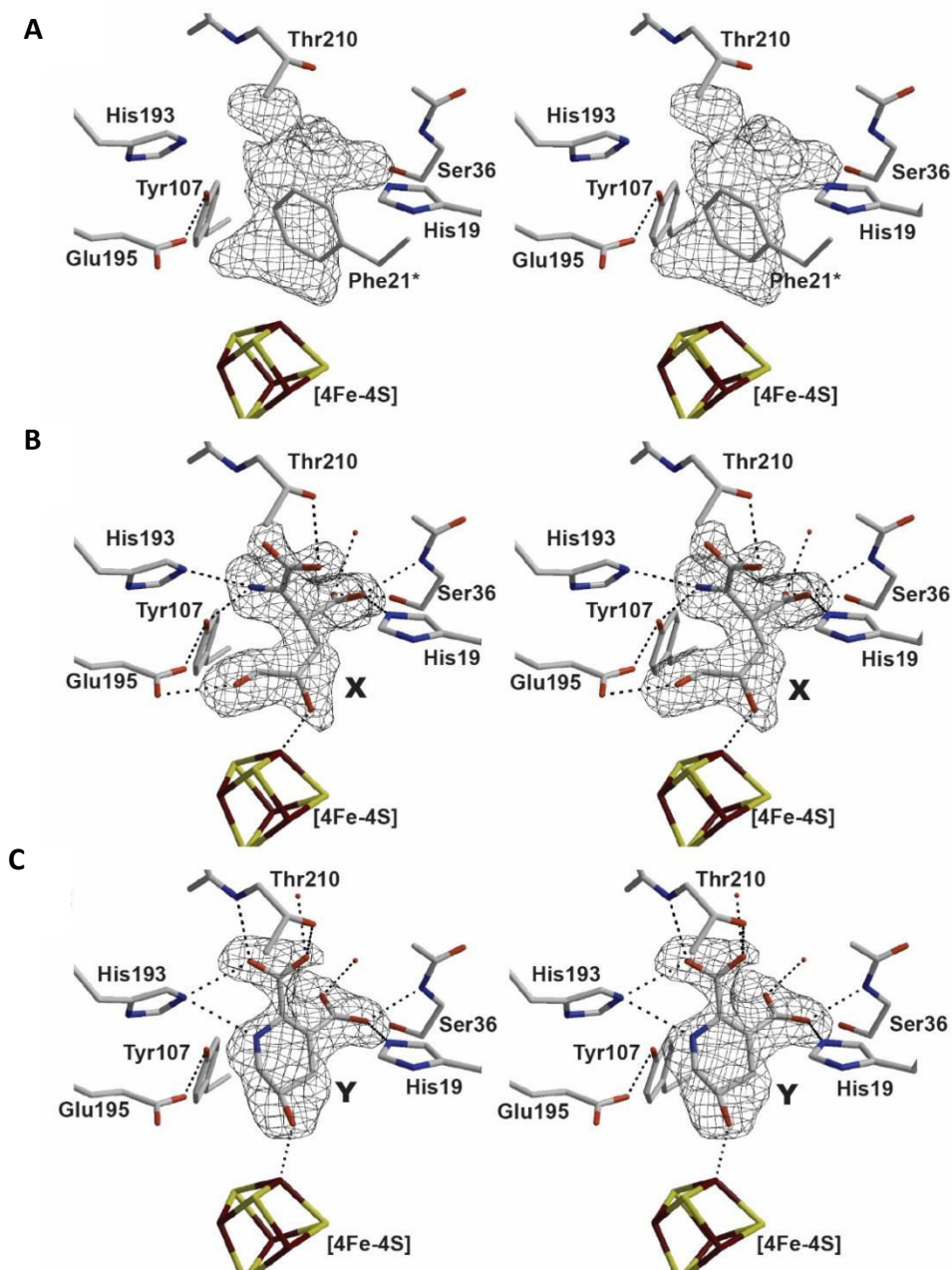


**Figure 15:** **A.** Stereo image of the electron density omit map calculated with diffraction data at 1.5 Å resolution from a crystal grown from a *TmNadA*\*Y21F. This electron density has been modeled as a combination of the **X** and **Y** intermediates (40% each) and solvent (20%). **B.** Stereo image of the **X** intermediate in a partial electron density omit map calculated after adding a 40% occupied **Y** intermediate and four 20% occupied water molecules to the calculated phases and structure factors. **C.** Stereo pair of the **Y** intermediate in an equivalent omit map obtained after adding instead 40% **X** and 20% occupied water to the model phases and structure factors<sup>139</sup>.

The comparison of the *TmNadA*\*Y107F-**W** intermediate obtained in 2016 with the *TmNadA*\*Y21F-**X** intermediate indicates that the former binds in an approximately 180°-rotated position relative to the latter. This likely explains why catalysis stops at **W** in

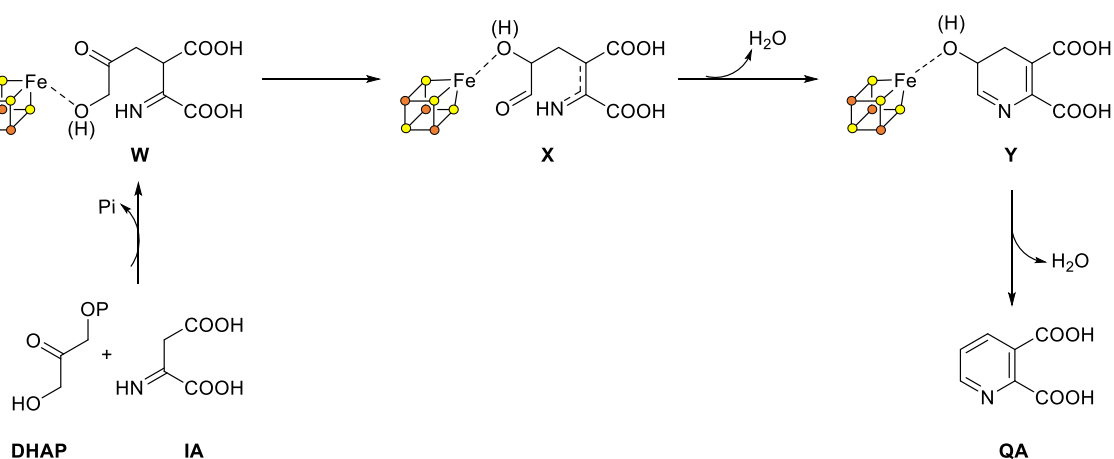
*TmNadA*\*Y107F mutant. It was also noted that in the structure of *P. horikoshii* NadA reported recently by Ealick<sup>140</sup>, DHAP binds in an orientation that is consistent with **X** and consequently, rotated relative to our previously reported **W**.

The difference between the structure of **W** and **X** is the nature of the NadA protein: Y107F vs Y21F, suggesting that the mutation at the tyrosine 107 might be responsible for the conformation of **W** in the crystal. In order to see if **W** is able to bind to NadA on a different conformation, **W** was docked into *TmNadA*\*. The docking experiment showed that **W** in *TmNadA*\* active site is in a position different to the one obtained in the *TmNadA*\*Y107F-**W** complex. Its orientation is consistent with that of the **X** and **Y** intermediates found in the *TmNadA*\*Y21F-**X/Y** complex<sup>139</sup> as well as with the one found for *PhNadA*-DHAP complex<sup>140</sup>.

These observations indicate that the NadA active site can lodge the same molecule in different orientations depending on Tyr107 mutation and that the Tyr107 induces a **W** unproductive conformation. In addition, this configuration induces a partially closed form of NadA (in the *TmNadA*\*Y107F-**W** complex) whereas *TmNadA*\*Y21F-**X/Y** structure is in an opened form like in ligand-free *TmNadA*\*.

Finally, in the productive **W** model and due to its orientation in the active site, the Tyr21 is well placed to function in the first dehydration reaction with the deprotonation of the Schiff base and the protonation of the O that will become the leaving water molecule upon cyclisation. Tyr21 was postulated in 2014 to assist the second dehydration but these recent results strongly suggest that it likely assists the first dehydration whereas the second is probably spontaneous.

Taken together, these results provide a structure-based sequence for all the catalytic steps of QA synthesis by NadA (Scheme 18).



**Scheme 18:** Proposed NadA mechanism involving **W**, **X** and **Y** intermediates before the formation of QA. The cluster is illustrated and positioned according to the newly obtained structures in the presence of the intermediates. The catalytic iron appears coordinating the intermediates.

#### h. DTHPA: The first NadA inhibitor

We designed and synthesized an analogue of the last intermediate **Y** (Figure 12): dithiohydroxyphthalic acid, DTHPA, as a potential NadA inhibitor<sup>141</sup> (Figure 16). It consists of a benzenic ring with two neighboring carboxylic acids and two neighboring thiol groups at positions 4 and 5 with regard to the carboxylic acids. We expected from this molecule to bind irreversibly to the accessible iron site, preventing the substrates and intermediates to access the catalytic iron site, and therefore inhibiting QA formation. We used a combination of *in vitro* and *in cellulo* studies to investigate DTHPA effect on NadA activity along with UV-visible and Mössbauer experiments.

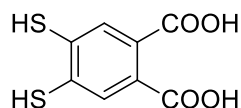


**Figure 16:** Dithiohydroxyphthalic acid (DTHPA).

NadA activity was assayed in the presence of increasing concentrations of DTHPA. It can be seen in Figure 17, a loss of NadA activity as a function of increasing concentrations of DTHPA. An  $IC_{50}$  value of 7  $\mu M$  was determined (for 7  $\mu M$  of protein).

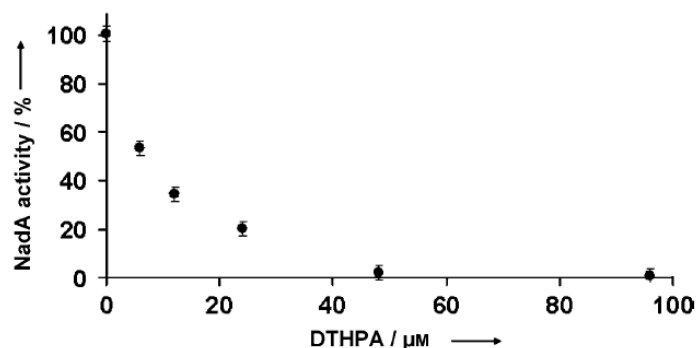


**Figure 17:** Enzymatic activity of 7  $\mu M$  *E. coli* NadA in the presence of increasing concentrations of DTHPA<sup>141</sup>.

The inhibition mechanism was investigated using UV-visible and Mössbauer spectroscopies. Upon addition of 6 equivalents of DTHPA, the UV-visible spectrum of NadA was modified (Figure 18A). The prominent S to  $Fe^{3+}$  charge transfer band at 420 nm, which is characteristic of a NadA  $[4Fe-4S]^{2+}$  cluster, was less defined and slightly blue-shifted compared to that obtained in the absence of DTHPA. Furthermore, a small absorption band around 500 nm appeared in the presence of DTHPA. The change in the UV-visible spectrum indicated that DTHPA interacts with the NadA  $[4Fe-4S]^{2+}$  cluster.

Next, Mössbauer spectroscopy of the protein in the presence of DTHPA was performed. The spectrum was drastically modified compared to that of the enzyme before DTHPA addition (Figure 7). After the addition of 6 equivalents of DTHPA, the spectrum could be fitted with three components in a 2:1:1 ratio (Figure 18B and 18C). The most populated species belongs to a mixed valence  $Fe^{+2.5}$  pair; the other two correspond to a fixed valence ferric ion and a fixed valence ferrous ion. The Mössbauer parameters of the ferrous ion are almost identical to those reported by Ciurli et al<sup>142</sup> for a  $[4Fe-4S]^{2+}$  model containing a differentiated iron site coordinated by 4-toluene-1,2-dithiolate (a dithiolate like DTHPA) through the two sulfur atoms. Thus, Mössbauer spectroscopy showed that the  $[4Fe-4S]^{2+}$  of NadA has an accessible iron site on which DTHPA binds. This occurs through the two thiolate groups of DTHPA as confirmed by DFT calculations<sup>141</sup>.

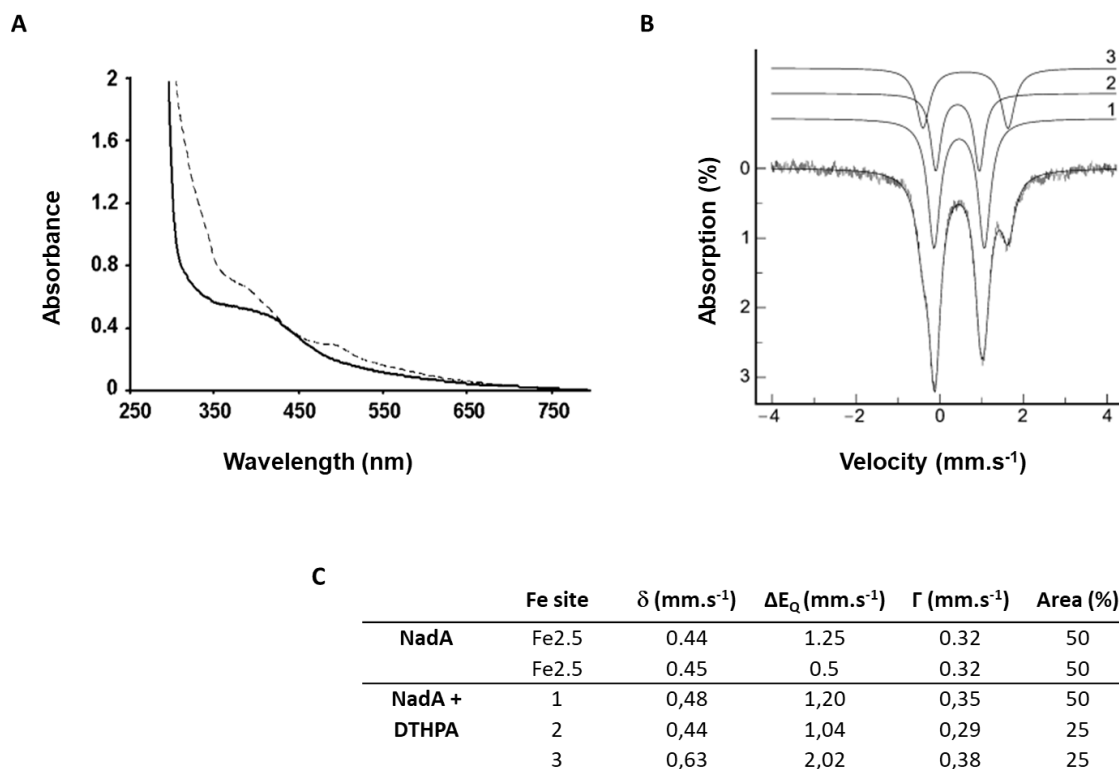


**Figure 18:** **A.** UV-vis. spectrum  $^{57}\text{Fe-S-NadA}$  (300  $\mu\text{M}$ ) in 100 mM Tris-HCl, pH 7.5, 50 mM NaCl without (bold line) or with (dotted line) 1.8 mM DTHPA. **B.** Mössbauer spectrum of  $^{57}\text{Fe-S NadA}$  in the presence of DTHPA (6 equivalents). Mössbauer spectrum was recorded at 4.2 K with an external magnetic field of 0.06 T applied parallel to  $\gamma$  rays. Traces 1, 2, and 3 represent component contributions. **C.** Mössbauer parameters of NadA in the absence and in the presence of 6 equivalents of DTHPA<sup>141</sup>.

DTHPA was also tested *in cellulo*. A  $\Delta\text{nadA}$  MG1655 *E. coli* strain is unable to grow in M9 minimal media (devoid of NAD precursors) but the growth can be rescued by addition of QA. An *E. coli* MG1655 strain containing a nonfunctional or inhibited NadA enzyme behaves similarly. The growth of an *E. coli* MG1655 strain was monitored in the presence of increasing concentration of DTHPA. The bacterial growth was inhibited since 10  $\mu\text{M}$  of DTHPA and it could be rescued by the addition of QA until 20  $\mu\text{M}$ , which means that DTHPA is a specific inhibitor of QA biosynthetic pathway at these concentrations. However, at higher concentrations of DTHPA (beyond 20  $\mu\text{M}$ ), the growth inhibition couldn't be rescued by the addition of QA suggesting that at these concentrations, specificity is lost and that DTHPA inhibits other essential (metallo)enzymes (Figure 19A)<sup>141</sup>, such as Fe-S enzymes or other metalloenzymes acting as a chelate to their metal site.

Due to structural and functional similarities between AcnB and NadA (Annex I), we thought that AcnB is a good model enzyme to test DTHPA specificity *in vitro*. Thus, AcnB

activity was tested in the presence of DTHPA. DTHPA inhibited AcnB (Figure 19B, black bars): indeed, 50 % of the enzyme activity is inhibited with 5 equivalents of DTHPA, and 80 % with 20 equivalents. When NadA and AcnB were incubated in a 1:1 ratio, AcnB activity was also inhibited by DTHPA but at higher concentrations. There was less than 50 % of inhibition of AcnB activity with 20 equivalents of DTHPA (Figure 19B, grey bars).

These data showed that DTHPA inhibits NadA preferentially but that it is also able to inhibit AcnB (Saez Cabodevilla et al.; submitted to Chem. Comm.).

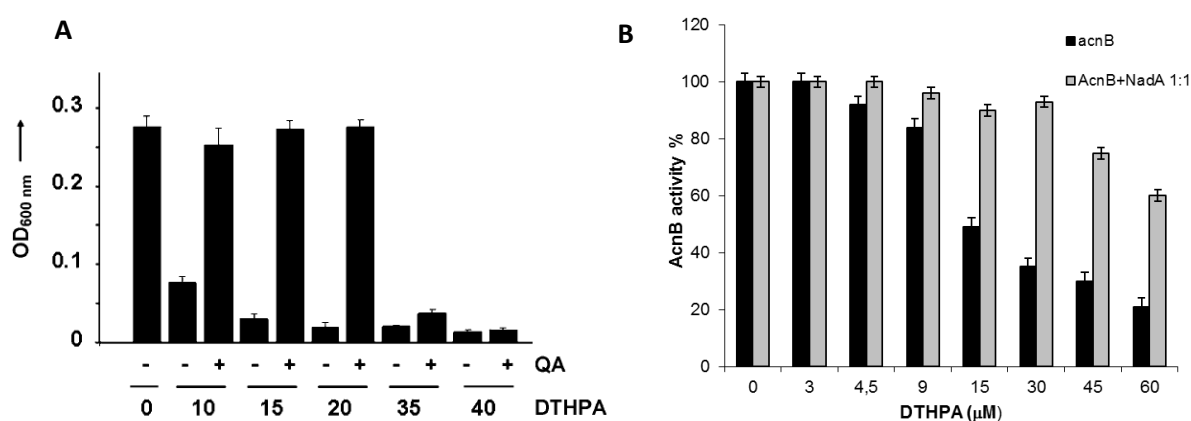


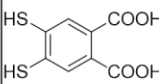
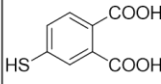
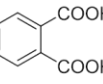
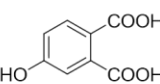
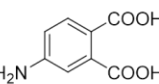
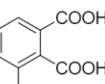
**Figure 19: A.** *In cellulo* assay with MG1655 *E. coli* strain. OD<sub>600 nm</sub> was measured after 16 h of growth in M9 at 37°C in the presence of increasing amounts of DTHPA (µM) and in the presence or absence of QA<sup>141</sup>. **B.** Black bars: *In vitro* AcnB activity (%) in the presence of increasing amounts of DTHPA. Grey bars: *In vitro* AcnB activity in the presence of NadA enzyme (1:1 ratio) and increasing amounts of DTHPA. AcnB: 3 µM; NadA: 3 µM.

### i. Structure-activity study based on DTHPA

Results obtained from DTHPA led to a structure-activity study that was started just before my arrival to the laboratory by the PhD Alice Chan. A structure activity study aimed at identifying the chemical functions of a molecule required for a biological activity; in our case this study aimed at identifying chemical functions of DTHPA derivatives for an inhibition on NadA activity. Such a study should provide important information in order to design stronger and more specific NadA inhibitors based on DTHPA.

DTHPA molecule consists of a benzenic ring, two carboxylic acids and two thiol groups. The influence and role of these chemical functions were evaluated testing different

DTHPA derivatives on *in vitro* NadA activity. Table 2 shows the most significant results obtained from this structure-activity study.

	DTHPA	DMB	MB	4MP	PA	4HP	4AP	3HP
								
IC <sub>50</sub> (μM)	10	52	No inhibition	32	No inhibition	135	No inhibition	No inhibition

**Table 2:** Structure-activity study performed with DTHPA and some of its derivatives. The IC<sub>50</sub> values are given in μM and correspond to the concentration of a molecule needed to inhibit 50% the NadA activity. The IC<sub>50</sub> values are given for 10 μM of enzyme (A. Chan's PhD).

The removal of the carboxylate groups of DTHPA results in 1,2-dimercaptobenzene (DMB). This molecule inhibits the enzyme activity with an IC<sub>50</sub> value of 52 μM. However, UV-visible and Mössbauer analyses show a degradation of the cluster by DMB. Degradation of the cluster was also observed after ion exchange chromatography. In the absence of DMB, the chromatogram of the protein shows the presence of the holo-protein as the major species; whereas in the presence of DMB (5 equiv.), the chromatogram shows that apo-protein predominates, demonstrating that the protein has lost the majority of its cluster in the presence of DMB. One explanation is that the two thiols groups of DMB chelate the catalytic site of NadA [4Fe-4S]<sup>2+</sup> cluster leading to demetallation of the protein. We hypothesized that such a molecule could demetallate the cluster of other Fe-S enzymes and therefore that it is not an interesting inhibitor. To have a specific inhibition of NadA, carboxylates groups are likely required (DTHPA does not demetallate de cluster).

Mercaptobenzene (MB) which contains a single thiol group and no carboxylates was also tested. No inhibition of NadA activity was found. In addition, MB does not degrade the cluster (not shown) compared to DMB which contains an additional neighboring thiol.

By keeping a single thiol (4' position of the ring) and adding two carboxylates like in DTHPA, 4-mercaptophthalic acid (4MP) is obtained. With this molecule an IC<sub>50</sub> value of 32

$\mu\text{M}$  was determined and it did not degrade the cluster. These results revealed that in order to have a NadA inhibition, a single iron coordinating group is enough in addition with two carboxylates. Indeed, phthalic acid (PA) that contains only two carboxylates on a benzene ring does not inhibit NadA activity.

The nature of the iron coordinating group was also tested with 4-hydroxyphthalic acid (4HP) and 4-aminophthalic acid (4AP). As expected, they displayed less inhibitory effect ( $\text{IC}_{50-4\text{HP}} = 135 \mu\text{M}$  and no inhibition for 4AP) than 4MP in agreement with the thiolate being the best iron coordinating atom ( $\text{IC}_{50-\text{THPA}} = 32 \mu\text{M}$ ).

The position of the iron coordinating group with regard to the carboxylates was finally tested using 3-hydroxyphthalic acid (3HP). This molecule did not inhibit NadA activity whereas its isomer 4HP did, showing that the position 4' of the benzene ring with regard to the carboxylates is the essential position for the iron coordinating group in order to have an inhibition of NadA.

As conclusion, from this non-exhaustive structure-activity study based on DTHPA derivatives, it seems that an inhibitor of NadA activity should have at least one Fe coordinating thiol group on the aromatic benzene ring as well as two carboxylate groups that likely help anchoring the molecule in NadA active site and therefore stabilizing the molecule in the active site, inhibiting the enzymatic activity. The thiol should be positioned in position 4' of the ring with regard to the carboxylates.

## V. Antibiotics in the XXI century

### a. Antibiotic resistance-historical overview

Antibiotics have revolutionized and transformed modern medicine as well as saved a countless number of lives. However, the success of these drugs is compromised by the potential development of resistance from their very first use.

We have been aware of bacterial resistance since the beginning of the antibiotic era. Penicillin (a  $\beta$ -lactam antibiotic which inhibits the formation of peptidoglycan cross-links in the bacterial cell wall) was discovered in 1928<sup>143</sup> and by 1940 (years before its introduction

as a therapeutic), an enzyme able to destroy penicillin had already been discovered; penicillinase<sup>144</sup>. Once the antibiotic was used widely, resistant strains capable of inactivating the drug became prevalent. To face the problem, new  $\beta$ -lactam antibiotics were discovered<sup>143</sup> which helped restoring confidence but again, in the early 1960, the first resistance to one of these drugs, methicillin was identified. Later, resistance has been observed for almost all of the antibiotics that have been commercialized.

Antibiotics target essential bacteria physiology and biochemistry, causing their death or inhibiting their growth. There are five major antibiotic targets: the bacterial cell wall, the cell membrane, protein synthesis, DNA and RNA synthesis, and folic acid (vitamin B9) metabolism. These bacterial targets are different or do not exist in eukaryotic cells. Resistance to antibiotics occurs through four general mechanisms which are target modification, efflux, immunity and bypass, and enzyme-catalyzed inactivation. The main antibiotic targets as well as the antibiotic resistant ways are summarized on Figure 20, taken from *Wright G.D. BMC Biology 2010*<sup>145</sup>.

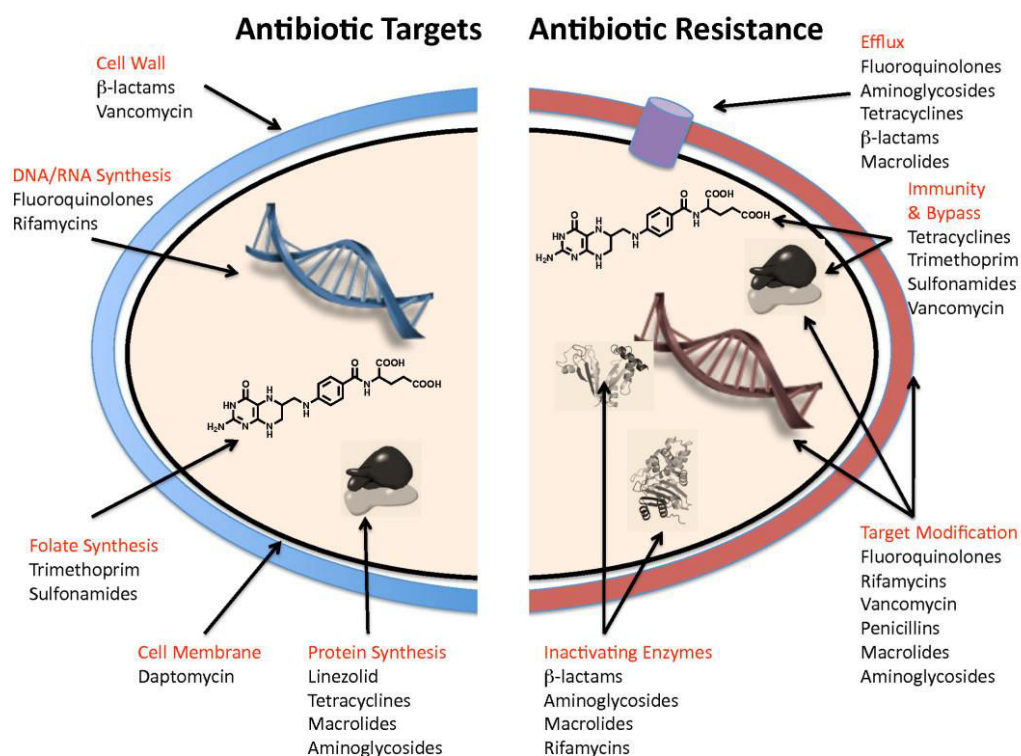


**Figure 20:** Antibiotic targets and mechanisms of resistance of the main current antibiotics<sup>145</sup>.

The traditional answer to this problem has been to introduce new antibiotics. However, nowadays, the pharmaceutical industry is producing too few antibiotics, particularly against gram-negative organisms, to replace antibiotics that are no longer effective for many types of infection. For this reason bacterial infections have become a threat and many people already claim the start of a post-antibiotic era. It is expected that by 2050, 10 million people worldwide will die per year from drug-resistant bacterial infections<sup>146</sup>.

In February of 2017, the World Health Organization (WHO) published the first ever list of bacteria for which new antibiotics are urgently needed with the aim of guiding and promoting research and development of new antibiotics<sup>147</sup>. The list is divided in three categories (critical, high and medium priority) classified by criteria such as deadliness, facility to spread or remaining treatment options (Table 3).

<b>PRIORITY 1: CRITICAL</b>	
<i>Acinetobacter baumannii</i>	Carbapenem-resistance
<i>Pseudomonas aeruginosa</i>	Carbapenem-resistance
<i>Enterobacteriaceae</i>	Carbapenem resistance, 3 <sup>rd</sup> generation cephalosporin resistance
<b>PRIORITY 2: HIGH</b>	
<i>Enterococcus faecium</i>	Vancomycin-resistance
<i>Staphylococcus aureus</i>	Methicillin-resistance, Vancomycin resistance
<i>Helicobacter pylori</i>	Clarythromycin-resistance
<i>Campilobacter spp</i>	Fluoroquinolone-resistance
<i>Salmonellae</i>	Fluoroquinolone-resistance
<i>Neisseria gonorrhoeae</i>	Fluoroquinolone-resistance, 3 <sup>rd</sup> generation cephalosporin - resistance
<b>PRIORITY 3: MEDIUM</b>	
<i>Streptococcus pneumonia</i>	Penicillin-non-susceptibility
<i>Haemophilus influenzae</i>	Ampicillin-resistance
<i>Shigella spp</i>	Fluoroquinolone-resistance
* Note that Mycobacteria were excluded from the list because they are targeted by other dedicated programs. However, they present a high resistance to traditional treatment and represent a threat to public health, especially the pathogen <i>Mycobacterium tuberculosis</i> .	

**Table 3:** Priority pathogen list for R&D of new antibiotics, published by WHO in February 2017.

Nine out of the twelve pathogens listed above (Table 3) are gram-negative bacteria including all the critical priority pathogens. It is particularly difficult to find new antibiotics against gram-negative pathogens mainly due to their difficulty to penetrate membranes which make them naturally resistant to many antibiotics. The arising resistance to current antibiotics and the lack of new ones especially against gram-negative organisms highlights the particular threat of gram-negative organisms nowadays.

Below, I make a non-exhaustive description of the different bacterial cell walls which shows how gram negative bacteria or mycobacteria cell structure constitutes a great barrier of entrance in the cell, which is particularly concerning for antibiotics with cytosolic targets since they need to penetrate the cell in order to be active. All the figures of the different cell walls were taken from *Brown, Nature reviews 2015, 13:620*.

(i) Gram-positive bacteria

Gram-positive bacteria have a single lipid bilayer which is surrounded by a thick wall of peptidoglycan layers where teichoic acids and lipoteichoic acids are embedded. The peptidoglycan layer is linked to the membrane by lipoproteins. Since peptidoglycan is relatively porous, many substances can pass through the gram positive cell wall without difficulty (Figure 21A)<sup>148</sup>.

(ii) Gram-negative bacteria

Gram-negative bacteria possess two membranes (phospholipid bilayers); an inner plasma membrane and an outer membrane. The additional membrane makes up the bulk of the gram negative cell wall and represents a formidable penetration barrier. The outer membrane contains lipopolysaccharides which are anchored into the outer layer of the outer membrane and project from the cell into the environment. This membrane also possesses channels, such as porins or specific transporters, for the transport of different molecules. In the periplasmic space between the two membranes there is a thin porous peptidoglycan layer that is linked to the outer membrane by lipoproteins (Figure 21B)<sup>148</sup>.

(iii) Mycobacteria

A thick cell wall surrounds the single cell membrane (lipid bilayer) of mycobacteria. The wall is formed by three main compounds: A thin layer of peptidoglycans, linked to the membrane by lipoproteins; arabinogalactan bonded to the peptidoglycan layer; and mycolic

acids (long fatty acids) that extend perpendicular to the arabinogalactan/peptidoglycan. Other cell wall-associated glycolipids intercalate into the mycolic acid layer to form a 'pseudo' lipid layer. There are porins that assist the transport of different molecules through the thick wall. An additional compound anchored to the cell membrane is lipoarabinomannan. It is implicated as a key surface molecule involved in the mycobacterial diseases (Figure 21 C)<sup>149</sup>. The unusual structure of the thick wall of mycobacteria results in extremely low permeability.

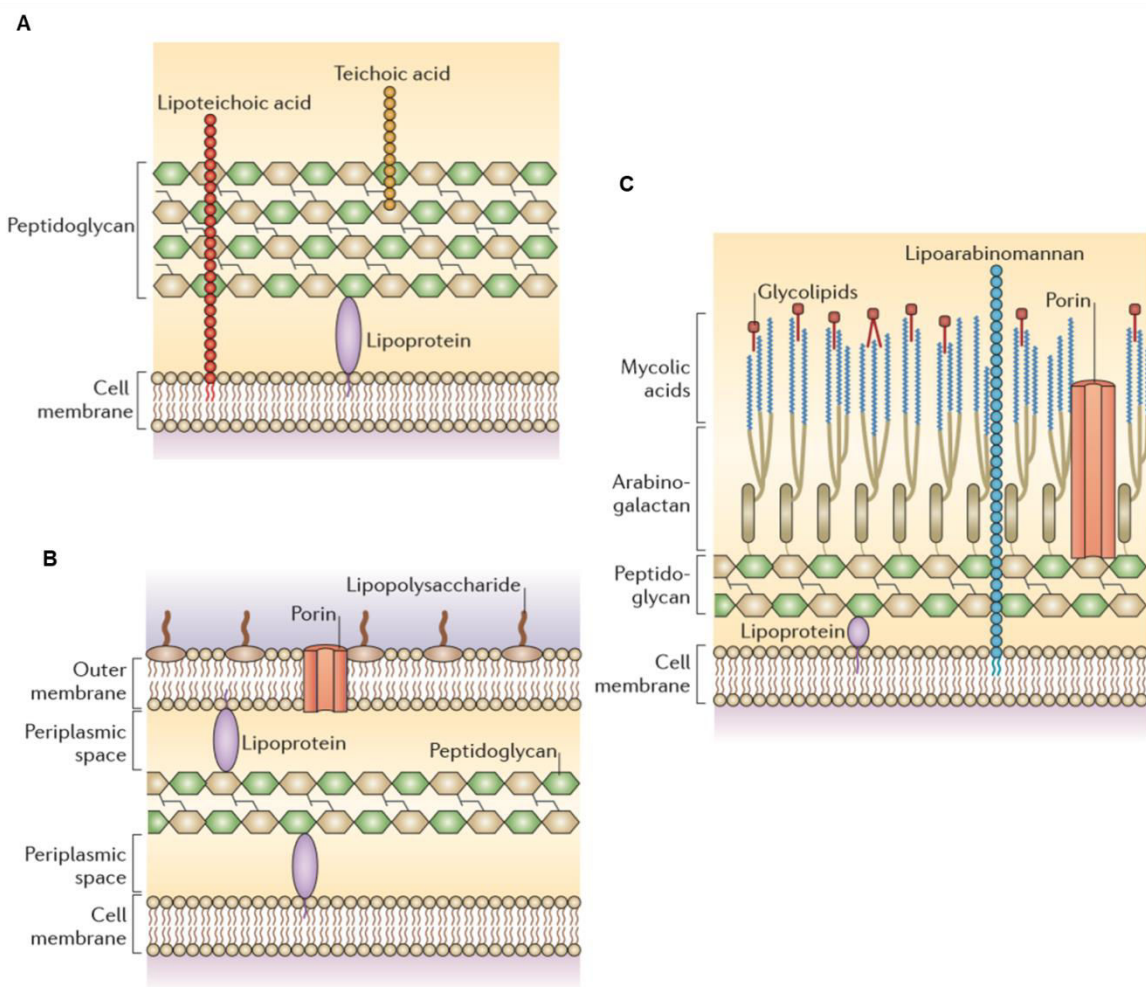


**Figure 21:** A. Gram-positive cell wall. B. Gram-negative cell wall. C. Mycobacteria cell wall<sup>150</sup>.

Thus, gram-negative bacteria and mycobacteria represent a big challenge in terms of cell penetration and this fact is particularly worrying concerning antibiotics.

## b. The search for new antibacterial agents

For the design of new antibiotics, historically, there has been higher chances of success with the development of compounds that belong to already established antibiotic classes<sup>151</sup>. In addition, there is a lack of diversity in the cellular targets of antibiotics. These were summarized above. Approximately half of the existing antibiotics target the cell wall<sup>152</sup>. However, this strategy of modifying existing antibiotics contains a main drawback, which is that the new antibiotics obtained that belong to the existing families are often subject to at least some of the same resistances observed for previous members.

Lately, more effort is being made for the design of completely novel antibiotics which at some point were discarded due to narrow activity spectrum. Nowadays, it is argued that specific antibiotics to some bacterial species may offer some significant advantages<sup>153</sup>. Indeed, their cellular targets are less likely to overlap with those of eukaryotic cells or other bacteria and resistance is believed to be slower to develop, as resistance genes would likely have to be originated. An effort is made to find new antibiotics but also to find new targets. Many of the most promising new targets are bacterial enzymes which are not conserved in eukaryotes.

This latter strategy concerns my Ph.D work where we are targeting specifically quinolinate synthase, an enzyme that is essential in two pathogens: *Helicobacter pylori* and *Mycobacterium leprae*. But what is the current treatment situation for this two pathogens?

### (i) *Helicobacter pylori*

*Helicobacter pylori* is a microaerophilic, spiral-shaped, gram-negative bacterium with several polar flagella for mobility (Figure 22)<sup>154</sup>. *H. pylori* lives in the human stomach and it is the only organism known to able to live in such an acidic pH (average pH in the human stomach ~1.4)<sup>155</sup>.

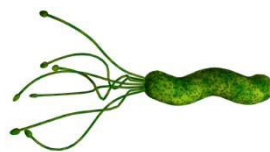


**Figure 22:** *Helicobacter pylori*.

Nearly half of the world human population is infected by *H. pylori* but often, it is asymptomatic. However, it is the cause of several gastric diseases, such as gastro-duodenal ulcers, chronic gastritis or gastric mucosa associated lymphoma<sup>156,157</sup>. In addition, the infection leads to a considerably increased risk of developing precancerous gastric conditions<sup>158</sup>. In 1994, the International Agency for Research on Cancer (IARC) classified *H. pylori* as a class I carcinogen to humans<sup>159</sup>. It is the only bacterium that has been recognized to be a cancer-causing agent until now.

The first-line treatment for the eradication of *H. pylori* has been a triple therapy consisting on clarithromycin, a second antibiotic (amoxicillin or metronidazole) and a PPI (proton pump inhibitor)<sup>160</sup>. However, its efficacy is seriously challenged due the growing resistance of these bacteria towards clarithromycin<sup>161</sup>. Levofloxacin was proposed in 2000 as an alternative to clarithromycin but resistance has also been observed for this antibiotic<sup>162</sup>. A quadrupole bismuth-based therapy, consisting in bismuth, metronidazole, tetracycline and a PPI is an interesting option for clarithromycin-resistant *H. pylori* treatment<sup>163</sup>. However, bacterial resistance to metronidazole has also been reported<sup>164</sup>.

As it can be observed, there is a particularly worrying problem concerning *Helicobacter pylori* treatment and eradication and thus, this pathogen was included in the WHO list as a “high priority” pathogen (Table 3). It is of high priority to find new treatments against *Helicobacter pylori*.

#### (ii) *Mycobacterium leprae*

*M. leprae* is an aerobic, rod-shaped bacterium with parallel sides and rounded ends. It is sometimes considered as a gram-positive bacterium due to its ability to retain the Gram stain but its cellular wall is different to the rest of gram positive bacteria as explained above (Figure 23) and thus, it is usually excluded from this classification and referred as gram-indeterminate bacteria not responding predictably to Gram staining.



**Figure 23:** *Mycobacterium leprae*.

*M. leprae* causes leprosy, which is an infectious chronic disease that affects mainly the skin, the peripheral nerves, mucosal surfaces of the upper respiratory tract and the eyes. Inside their hosts (humans and armadillos), bacteria live inside of Schwann cells and macrophages<sup>165,166</sup>.

The first antibiotic to be widely used for leprosy treatment was dapsone in the 1950 which had to be taken over several years later due to the increasing bacterial resistance<sup>167</sup>. In 1981, WHO recommended that leprosy should be treated by a combination therapy of three antibiotics: rifampicin, dapsone and clofazimine<sup>168</sup>. In 1985, 5.3 million patients were receiving multidrug therapy (MDT) and by 1991 the number decreased to 3.1 million (42 %). Furthermore, by 2000, the number was 597 232, which belongs to a 90% decrease with regard to the number of 1985<sup>168</sup>.

However, in spite of the encouraging reports, bacteria resistance is a cause of concern and threat concerning *M. leprae*, especially at this stage, where a dramatic decline in prevalence and new case detection has been achieved. Reports and publications have indicated rifampicin resistance in several endemic areas<sup>169</sup>. Rifampicin being the MDT backbone, it is important to monitor the arising resistance. Resistant to dapsone was also reported since the late 1960s.

No resistance to clofazimine has yet been reported but still, with the challenge of containing the disease and sustaining the on-going declining trend of leprosy, the WHO calls to promote research on developing new drugs for patients who relapse after completing the MDT treatment or those who do not respond to it.

### c. Across the cell membranes

Despite the fact that several inhibitors that were active on targets *in vitro* were found, providing promising new antibacterial agents, most of them have lacked an *in vivo* activity. In many cases, cellular permeability is the reason for this lack of activity, especially in the case of gram negative bacteria and mycobacteria<sup>170,171</sup>.

For this reason, and not less importantly than looking for new antibiotics, there is a lot of effort being done in developing technologies for delivering impermeable molecules into the cell across the different hard-to-permeate membranes. These are based on the

natural membrane transport mechanisms that cells possess in order to deliver substances/antibiotics into the cell.

#### d. Approaches to design and improve membrane permeability

Nowadays, there are numerous approaches to deliver molecules into the bacterial cells based on the cell natural permeation systems; in other words, that take advantage of the cell transport mechanisms in order to enter cargos into the cells. However, many of them are designed for eukaryotic targets that possess easier to penetrate membranes and a larger number of targetable transport forms than bacteria<sup>172</sup>. For example, the largely studied cell penetration peptides often cross the membranes through endocytic pathways or direct translocation, both involving the formation of different types of vesicles that do not exist in bacteria<sup>173</sup>. This is the case of the widely used and studied cell penetrating peptides Penetratin or TAT<sup>174,175</sup>.

In order to design cell penetration systems for bacteria the strategies to take into account are either to take advantage of the existing transporters or to design molecules that will penetrate the membranes passively.

In the first case, there are different reported strategies such as the use of siderophores as shuttle vectors for active transport of antibiotics through the bacterial membrane<sup>176,177</sup>, or the use of designed antibiotics with high resemblance to specific solute transporters. Examples of the latter are streptozotocin antibiotic, which contains structural resemblance to N-acetyl-D-glucosamine to be transported by the phosphoenolpyruvate-phosphotransferase system, or D-cycloserine which is recognized by the D-alanine proton motive force dependent transport system<sup>178</sup>.

For the second case, the passive permeation, the most significant examples are cyclic peptides. Several cyclic peptide natural products have proved high penetrating performance. This is suggested to be due to these molecules' conformational flexibility that allows them to form intramolecular hydrogen bonds in a low dielectric environment by reducing their surface polarity, or to point these towards the surface by making the surface polar in more polar environments<sup>172</sup>. This is the case of the immunosuppressant Cyclosporin A which is

suggested to traverse the cell membrane passively (even though in this case the target are eukaryotic cells)<sup>179</sup>.

### e. The natural cyclic tetrapeptide FR235222 and its analogues

FR235222 is a natural cyclic tetrapeptide which was isolated from the fermentation broth of a fungus, *Acremonium sp* in 2003<sup>180</sup> (Figure 24A). It has proven to be isoform selective Histone deacetylase (HDAC) inhibitor, of class I<sup>181</sup>, which are localized in the nucleus<sup>182</sup>.

FR235222 and its simplified analogue I (Figure 24A) can be divided into two structural parts: (i) the tetra-cyclopeptide that could be responsible for the cell permeability since it shares features with other uncharged cyclopeptides that have passive membrane permeability properties; and (ii) the zinc binding group involved in the HDAC activity. Both were highly bioactive in cell assays<sup>183</sup>.

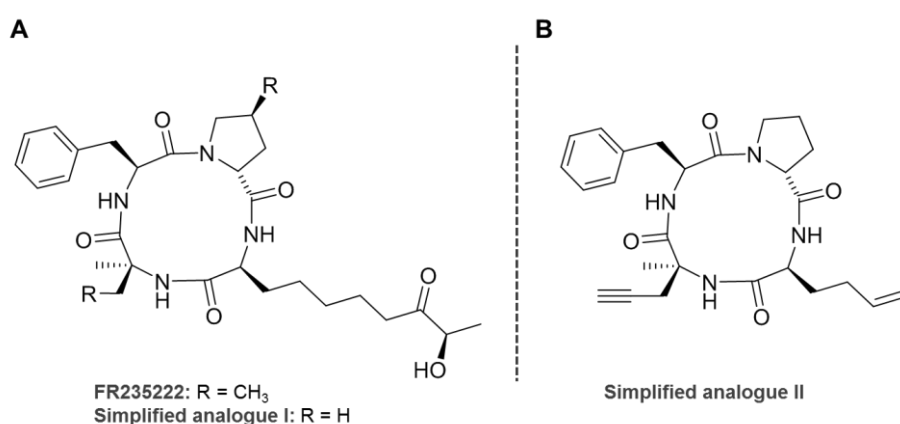


**Figure 24:** **A.** FR235222 natural product (R = CH<sub>3</sub>) and its simplified analogue I (R = H). **B.** FR235222 simplified analogue II, which keeps the central core as close as possible to FR25222 and contains a terminal alkyne and olefin for orthogonal ligation of two groups.

The pharmacophore triazole aminocoumarin (Figure 25 A (1)) is known to induce reactive oxygen species (ROS) in *Cryptococcus*<sup>184</sup> and it can be traced in cells as a fluorescent molecule<sup>185</sup>. Treatment of HeLa cells with this molecule showed poor permeability and it was not visible inside the cells after one hour of treatment (Figure 25 A). However, once coupled to FR232555 analogue II (Figure 24 B) and treatment of HeLa cells

with the resulting molecule (Figure 25 B **(2)**), rapid cell fluorescence labeling was observed, proving the cell permeability properties of the tetra-cyclopeptide (Figure 25 B)<sup>183</sup>.

Evidence of intracellular penetration was provided by the heterogeneous distribution of **(2)** (Figure 25 B **(2)**) inside the cell where high fluorescence signals were located at the perinuclear area without labeling the nucleus and the cytoplasm, a phenomenon that has already been observed for aminocoumarins. To overcome the limitation of further evaluating subcellular membrane permeability like the nucleus, the HDAC' zinc binding motif  $\alpha$ -hydroxyl ketone was added to compound **(2)** (Figure 25 C **(3)**) on the terminal olefin, to address the molecule to the nucleus. Indeed, both compounds **(2)** and **(3)** clearly accumulate at specific intracellular organelles confirming the internalization in the cell. Focusing in the nucleus, compound **(3)** was visible inside even though the large majority of it remained in perinuclear organelles (Figure 25 C). In addition, the staining of HeLa cells with Draq5 to visualize DNA allows to observe that compound **(3)** does not seem to label DNA, indicating that the compound is concentrated in the nucleoplasm, where HDAC inhibitors affect transcription regulation<sup>183</sup>.

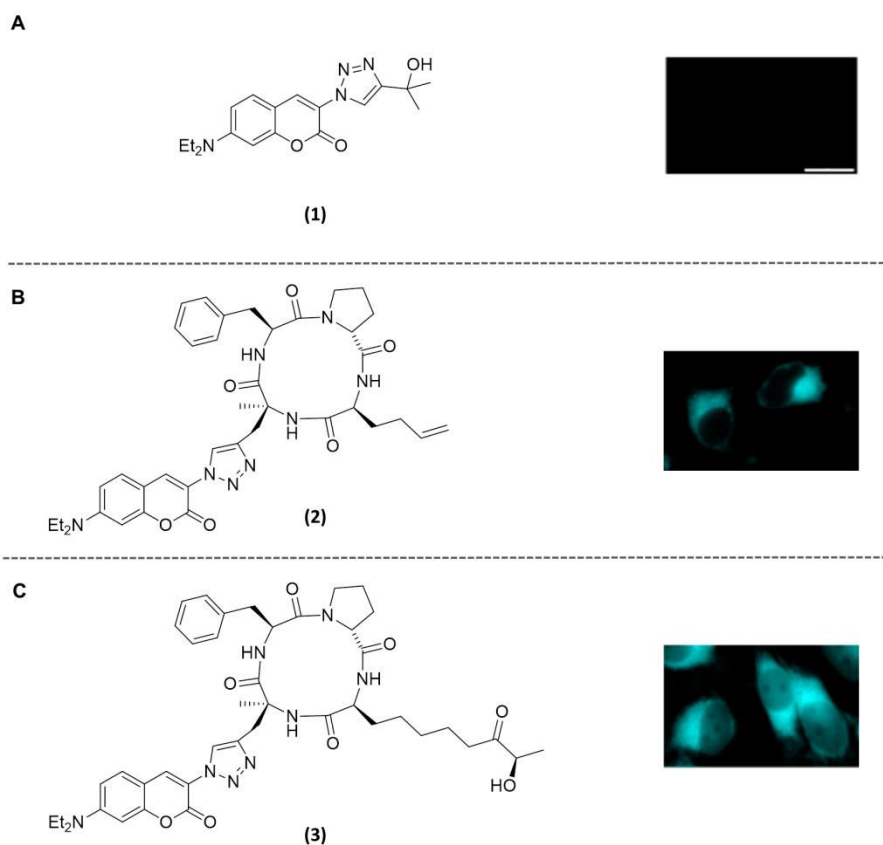


**Figure 25:** Global cell distribution of compounds under live cell microscopy conditions. Compounds: triazole aminocoumarin alone (**A**); coupled to FR235222 simplified analogue II (**B**); and coupled to  $\alpha$ -hydroxyl ketone zinc binding motif containing analogue II (**C**). Conditions: HeLa cells were incubated with 160 nM compounds for 1 hour at 37 °C.

These results show the ability of the simplified FR235222 tetra-cyclopeptide scaffolds to increase the permeability of the triazole aminocoumarin making them interesting transmembrane carriers, yet to explore. Furthermore, the fact that their targets are nuclear (HDAC class I) shows their high performance on permeating several membranes (cell membrane and nuclear membrane).

In recent studies, six new cyclic tetrapeptides have been isolated from the termite-associated fungus *Pseudoxylaria sp. X802*, which share much structural resemblances with FR235222<sup>186</sup>. Four out of the six cyclic tetrapeptide showed antimicrobial activity against gram-negative *Pseudomonas aeruginosa* (Figure 26). This suggests that these types of scaffolds are able to permeate even the bulky gram-negative bacteria cell walls. This fact makes them first-row candidates for the challenge of bringing drugs into bacteria<sup>186</sup>.

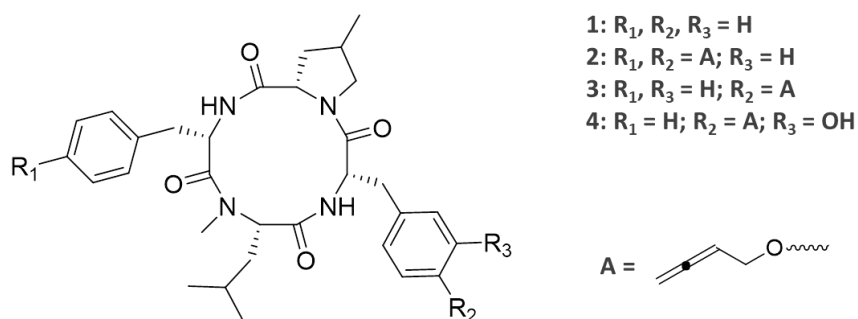


**Figure 26:** Structure of pseudoxyllallemycins (cyclic tetrapeptides) 1-4 that showed antimicrobial activity against Gram-negative human-pathogenic *Pseudomonas aeruginosa*.



# Ph.D OBJECTIVES

As I have shown during the introduction, NAD is an essential cofactor in every living organism and its biosynthesis presents substantial variations between prokaryotes and eukaryotes. For these two reasons, the NAD pathway is a very interesting target for the design of new antibacterial drugs and it has been and still is largely studied.

In our laboratory, we are interested by the inhibition of quinolinate synthase (NadA), one of the enzymes of the bacterial QA biosynthetic *de novo* pathway that is essential in *Helicobacter pylori* and *Mycobacterium leprae*. The first NadA inhibitor (DTHPA) was reported by our group in 2012, but it presents a lack of specificity both *in vitro* and *in cellulo* likely due to its two chelating thiol groups.

In order to find more specific NadA inhibitors, we used a rational approach by investigating DTHPA derivatives. For this, we used the structure-activity study presented in the introduction as basis. An aromatic ring with two neighboring carboxylates and an iron coordinating thiol group were proved to be necessary for NadA inhibition.

We also took into account the docking experiment where **Y** intermediate (the last intermediate before QA formation, Figure 12) was docked into the structure of NadA<sup>131</sup>. This experiment showed key interactions of this molecule with NadA active site: the carboxylates interact with Thr210 and Ser124; the hydroxyl group coordinates the catalytic Fe of the cluster; while the nitrogen from the pyridine interacts with Glu109.

This way, we designed and proposed the following family of molecules as potential NadA inhibitors expected to be more specific than DTHPA. We expect these molecules to target NadA from *H. pylori* and *M. leprae* (Figure 27).

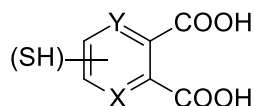


**Figure 27:** Family of potential NadA inhibitors. X= C or N; Y = C or N.

My Ph.D project was therefore divided in three main objectives: synthesis of these potential inhibitors, *in vitro* study of these inhibitors on NadA from *E. coli* and *in cellulo* activity of these molecules on an *E. coli* strain in M9 medium.

### 1. Synthesis of potential NadA inhibitors

Whereas one molecule of this family, 4MP (Figure 28) was commercial, the other three were not and their synthesis was not described in the literature. Therefore, the first objective was to synthesize 6-mercaptopyridine-2, 3-dicarboxylic acid (6MPDC), 5-mercaptopyrazine-2, 3-dicarboxylic acid (5MPzDC) and 5 mercaptopyridine-2, 3-dicarboxylic acid (5MPDC) (Figure 28).

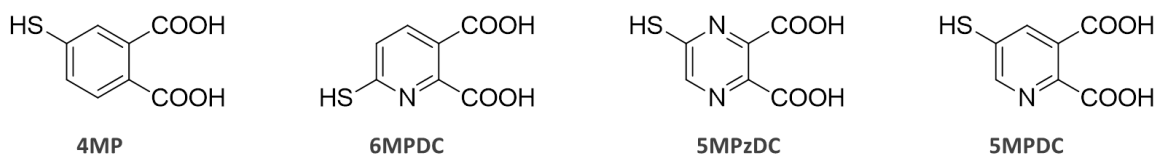


**Figure 28:** Potential NadA inhibitors: 4MP, 6MPDC, 5MPzDC and 5MPDC.

### 2. In vitro study of the potential NadA inhibitors on E. coli NadA

The next goal was to test NadA enzymatic activity in the presence of the four potential NadA inhibitors as well as to perform a spectroscopic and structural characterization of NadA in their presence.

### 3. In cellulo inhibition assays on MG1655 E. coli strain

The last part of my PhD was to test NadA inhibitors *in cellulo* on an *E. coli* MG1655 strain that cultivated in M9 mimics our pathogens of interest *H. pylori* and *M. leprae*. We anticipated some cell penetration assistance by a natural tetra-cyclopeptide analogue (see introduction) because i) every molecule of the new family contains two carboxylates whose charge might result on a difficult cell penetration, and ii) the targeted pathogens as well as *E. coli* are gram-negative organisms or mycobacteria which are highly impermeable and for which drug delivery is known to be difficult. Therefore, the synthesis of the transmembrane carrier as well as the coupling to the inhibitors were part of the objectives of the third part of my Ph.D too.

Information from the sequence alignment and the superposition of the two available NadA structures are indicative of a high conservation of NadA in different organisms and therefore, this justifies the fact that we work with *E. coli* and *T. maritima* NadA in the

laboratory to look for new antibacterial drugs against *H. pylori* and *M. leprae* by targeting their quinolinate synthase enzyme (Annex II).

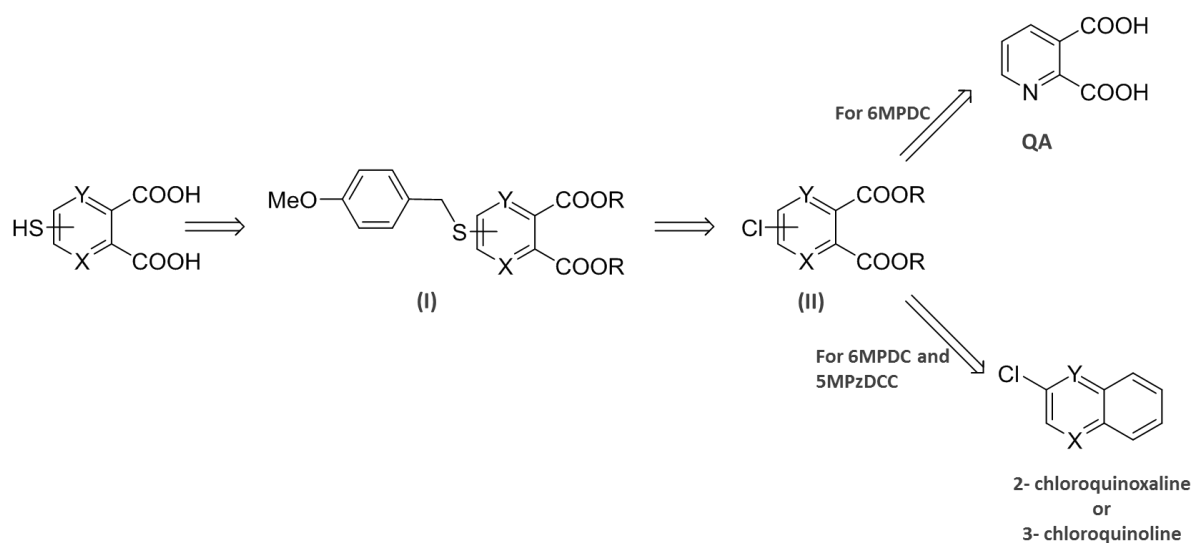
**RESULTS CHAPTER I:  
SYNTHESIS OF POTENTIAL  
QUINOLINATE SYNTHASE  
INHIBITORS**

The following table shows the three aromatic heterocyclic compounds that were targeted as potential NadA inhibitors for our research (Table 4). Their syntheses are reported in this chapter.

6MPDC	5MPzDC	5MPDC

**Table 4:** Three potential NadA inhibitors. 6MPDC: 6-mercaptopyridine-1,2-dicarboxylic acid; 5MPzDC: 5-mercaptopyrazine-1,2-dicarboxylic acid; 5MPDC: 5-mercaptopyridine-1,2-dicarboxylic acid.

In order to simplify the synthesis of these structurally close molecules, a general strategy was developed. The general retrosynthesis is shown below and involves two main steps (Scheme 19). First, the thiol group is introduced via the formation of a benzyl thioether as intermediate **I** which is obtained by a nucleophilic substitution of a chloro-pyridine/pyrazine derivative. The second key step is related to the formation of the corresponding chloro derivatives **II**. In the case of 6MPDC, it was thought that intermediate **II** could be obtained from commercial quinolinic acid (pyridine-2,3-dicarboxylic acid; (QA)); while 5MPzDC and 5MPDC, could be obtained from the 2-chloroquinoline and 2-chloroquinoxaline, respectively by oxidative cleavage using potassium permanganate<sup>187</sup>.



**Scheme 19:** Retrosynthetic pathway of 6MPDC (X = N, Y = C), 5MPzDC (X = N, Y = N) and 5MPDC (X = C, Y = N) showing the two main intermediates **(I)** and **(II)**.

## I. Synthesis of 6- mercaptopyridine- 2, 3-dicarboxylic acid (6MPDC) from QA

The synthesis of the intermediate **II** was first investigated and involves two consecutive steps. The first one was the protection of the two carboxylic acids in their ester form in order to avoid undesired reactions as well as obtaining easier to handle products during all the synthesis. The second step is related to the regioselective introduction of the chloro substituent at the position 6 of the pyridine ring.

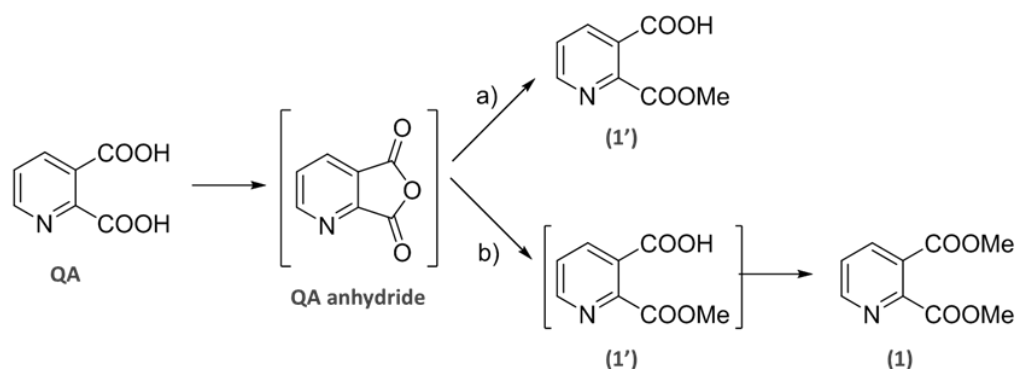
Numerous procedures are reported in the literature to perform esterification reactions<sup>188,189,190</sup>. With the aim of performing the double esterification of QA (Scheme 20), a standard procedure using DCC in MeOH was first used<sup>188</sup>. Surprisingly, after 2 h at room temperature as reported for another similar aromatic diacid, monoester sub product **1'** was obtained as a unique product (position 2' of the pyridine) (Scheme 21)<sup>188</sup>. Increasing the reaction time from 2 h to overnight yielded to the formation of the desired diester **1** but as a minor product (less than 10 %). Silica gel column chromatography afforded the desired product in only 5 % yield. Consequently, another classical approach was used using thionyl chloride. Thus, a solution of quinolinic acid in MeOH was refluxed in the presence of an excess (18 equivalents) of thionyl chloride<sup>189</sup>. Unfortunately, despite all our efforts the monoesterified product **1'** was obtained as the unique product.

Finally, it was found that harsher acid esterification conditions (sulfuric acid in refluxing MeOH for 24 h)<sup>190</sup> afforded the desired diester **1** with a 78 % yield from quinolinic acid.



**Scheme 20:** First step: double esterification of QA.

From these results, on the contrary to what was expected, the behavior of such particular diacid cannot be correlated to usual diacids such as phthalic acid. Indeed, while phthalic acid in the presence of thionyl chloride in MeOH affords the corresponding diester in high yield<sup>191</sup>, it was observed that, in our case, such conditions yield to the selective monoesterification of the acid function at the C-2 position of the pyridine. We observed that the esterification of only the acid function at the C-2 position proceeds with much more ease than the other. On the basis of literature<sup>192</sup> we may suggest that firstly, thanks to the vicinal proximity of the two carboxylic groups a cyclic anhydride intermediate is formed, QA anhydride, (Scheme 21). Thanks to this activation of the acid groups, a regioselective opening of the anhydride by MeOH would afford the pyridine-2-(methoxycarbonyl)-3-carboxylic acid monoester product **1'**. It can be assumed that this could be due to electronic effects, the carboxyl in C-2 of the ring being more electrophilic than the one at C-3. In contrast, the second esterification comes to be more difficult due to a lack of intramolecular activation of the second acid. However, we still do not understand why the second carboxylic acid cannot be activated enough with an excess of SOCl<sub>2</sub> to be esterified as well while it is efficiently done in the case of phthalic acid. Fortunately, the use of H<sub>2</sub>SO<sub>4</sub> helps overcoming this difficulty and obtaining the desired compound **1**.



**Scheme 21:** a) DCC, MeOH, reflux or SOCl<sub>2</sub>, MeOH, reflux. Both conditions yield only the monoester species **1'**; b) H<sub>2</sub>SO<sub>4</sub> and MeOH in reflux allows to obtain the diester pyridine derivative **1**.

Introduction of the thioether at the C-6 position has to be done via the formation of the corresponding chloro intermediate. However this first step could not be achieved directly from the synthesized diester. An activation of the pyridine ring through its pyridine-

N-oxide intermediate is required in order to enhance the electrophilic character at the C-6 position<sup>193</sup>.

The oxidation of pyridine to afford pyridine-N-oxide (Scheme 22) might be achieved by different methods<sup>190,194,195,196</sup>. We chose *m*-CPBA as oxidant in refluxing chloroform<sup>190</sup>. Surprisingly, following the reported procedure (reflux overnight), we were not able to obtain the desired product and longer reaction times did not help on its obtaining either. A larger excess of *m*-CPBA compared to that described on the protocol was the key to allow the completion of the reaction. However, even if the reaction proved to be completed, the main difficulties relied on the purification. A first purification attempt was done by a simple recrystallization in CH<sub>2</sub>Cl<sub>2</sub>: Et<sub>2</sub>O (1:1), affording the pure pyridine-2, 3-dicarboxylic acid dimethyl ester N-oxide (**2**) in only 14 % yield. Silica gel chromatography of the mother liquor allowed the isolation of additional 12 % of pure product (26 % total yield). Unfortunately, a big part of the oxidized pyridine came out from the column along with impurities.



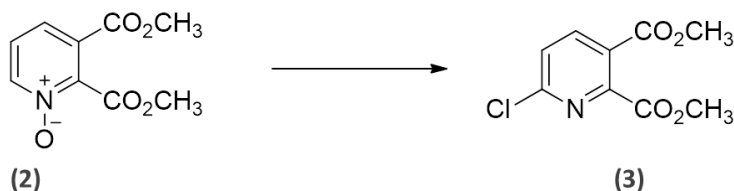
**Scheme 22:** Pyridine-N-oxide derivative formation.

In order to avoid an important loss of the product, the next step was attempted on the crude oxidized product but unfortunately this attempt had no success.

As purification seemed to be the major reason to explain the moderate yield, improvement of this step was assayed. First, a major part of the *m*-chlorobenzoic acid by-product was eliminated by filtration of the crude mixture. It was found that after concentration of the filtrate, solubilization of the resulting sticky paste residue in a minimum volume of CH<sub>2</sub>Cl<sub>2</sub> and subsequent precipitation in Et<sub>2</sub>O, compound **2** could be obtained in a 51 % reasonable yield.

Compound **2** was then allowed to react with refluxing phosphorous oxychloride<sup>190</sup> in order to introduce the chloro substituent in a regioselective manner (Scheme 23). The

reaction was completed in 8 h and pure 6-chloropyridine-2, 3-dicarboxylic acid dimethyl ester (**3**) was obtained in 70 % yield after purification by silica gel column chromatography achieving a considerably better yield than the one described in the literature (53 %).

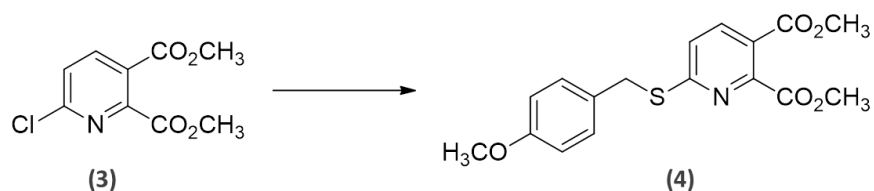


**Scheme 23:** Pyridine-N-oxide derivative substitution by chlorine.

The next key step of the synthesis was the introduction of the thiol group from the obtained chloro derivative **3** (Scheme 24). After bibliographic research, it was seen that a benzylthioether derivative is a frequently encountered intermediate to achieve such a transformation<sup>197,198,199</sup>. In particular it was reported that (4-methoxyphenyl)-methanethiol could be a reagent of choice for two main reasons<sup>200</sup>. First, compared to phenylmethanethiol, this chemical should be more reactive towards **3** due to a higher nucleophilicity. Secondly, we thought that making the aromatic ring richer in electrons should facilitate a latter deprotection in Lewis acid conditions. This could be helpful to increase the reactivity both for its introduction and for its cleavage.

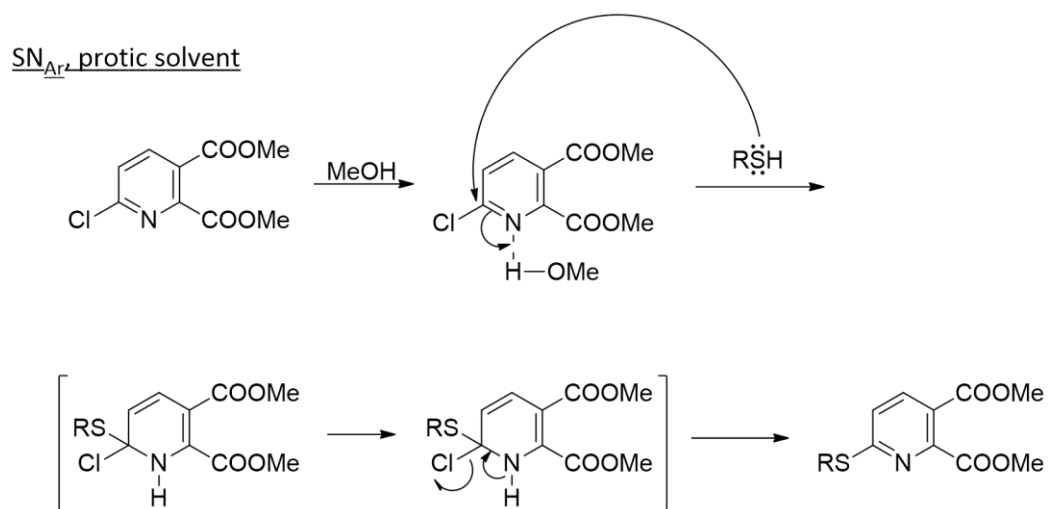
(4-methoxyphenyl)methanethiol and compound **3** were allowed to react with three different combinations of base/solvent:  $K_2CO_3/DMF$ <sup>198</sup>,  $DBU/CH_3CN$ <sup>199</sup> and  $Et_3N/MeOH$ <sup>197</sup>. In all cases the reaction mixtures were refluxed under argon atmosphere in order to avoid the oxidation of the thiol reagent. Different quantities of thiol and base as well as different reaction times were assayed. However, only the use of  $Et_3N/MeOH$  (with 2 equivalents of both base and thiol with regard to the pyridine derivative) during 3-day reflux proved to be efficient for the desired substitution and obtaining of compound **4** with a fair yield (53 %) whereas the other two combinations came to be unproductive (6 % of yield with  $K_2CO_3/DMF$  and ~10 %  $DBU/CH_3CN$ ). It is important to note that in such conditions a reflux for 3 days was required for complete conversion under such a condition emphasizing the low reactivity

of compound **3**. Without any doubt, a longer time would have been needed with phenylmethanethiol.



**Scheme 24:** Chlorine substitution by (4-methoxyphenyl)methanethiol.

In addition, we suggest that the difference in the observed reactivity in the different conditions could come from the different nature of the solvents (protic vs aprotic). Thus, whereas the expected mechanism for all the three cases is a common  $S_N_{Ar}$ , we may assume that the methanolic media increases the reactivity of **3** due to the formation of a hydrogen bond (Scheme 25).



**Scheme 25:**  $S_N_{AR}$  mechanism in a protic solvent (MeOH) for the substitution of compound **3**.

With compound **4** in hands, there were two options to get to the desired product 6MPDC: (i) performing hydrolysis of both esters first followed by deprotection of the thiol; or (ii) performing these two steps on a reverse way. In order to avoid the formation of the

disulfide by air oxidation which could be favored in basic conditions during saponification, we decided to perform thiol deprotection at the final step.

Saponification of the two ester groups (Scheme 26) was achieved with ease in an Et<sub>2</sub>O/H<sub>2</sub>O biphasic system using NaOH at 40 °C in an almost quantitative yield to achieve compound **5**<sup>201</sup>.



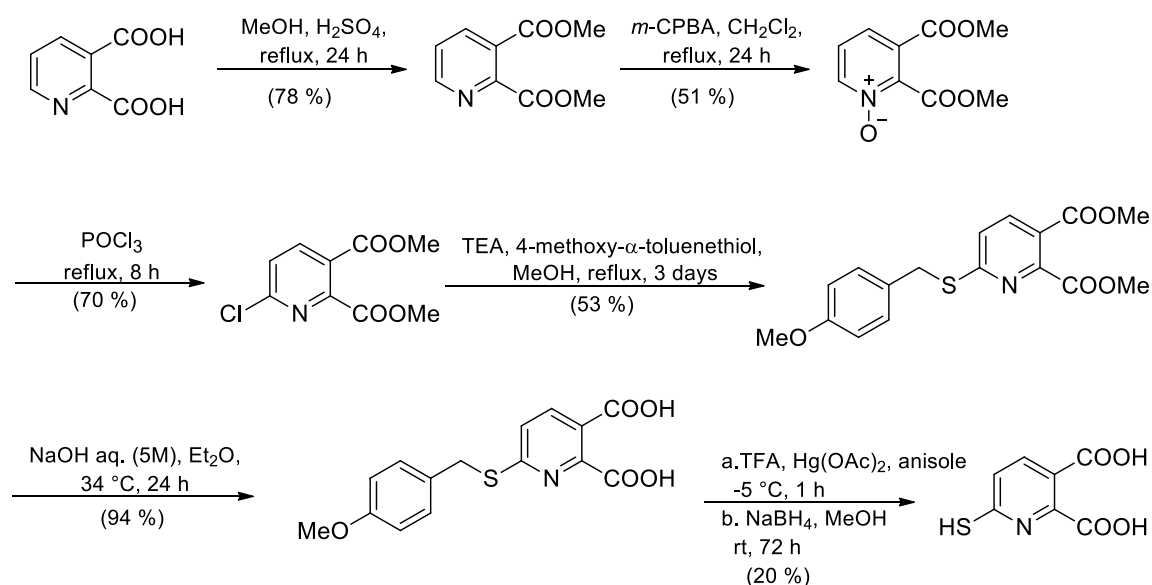
**Scheme 26:** Saponification of esters.

Finally, the last step proved to be more problematic than expected. A protocol which consisted in the deprotection of the thiol in acidic medium (mixture of TFA, triflic acid, 5:1) was first attempted<sup>198</sup>. <sup>1</sup>H-NMR spectrum of the resulting mixture showed the presence of desired product in a weak proportion. Despite all our efforts (selective extraction, cation/anion exchange column chromatographies), we were unable to obtain the final product.

Hydrogenolysis using Pd/C as catalyst<sup>202</sup> was then investigated despite the fact that thiols are known to poison the Pd catalysts<sup>203, 204</sup>. Unfortunately, and as a little bit expected, only the 4-methyl anisole protecting group was recovered in the solution confirming the loss of the final product by coordination to the catalyst.

Finally, the deprotection was succeeded following a two-step procedure<sup>205</sup>. Firstly, the thioether derivative was allowed to react in acid media (TFA) in the presence of anisole and mercury (II) acetate as a Lewis acid salt. This first step allowed the removal of the anisole derivative and led to a thiol-Hg complex. Mercury was removed by NaBH<sub>4</sub> reduction. The obtained product was then solubilized in EtOAc and precipitated into a large volume of hexane in order to obtain the pure product for characterization, biochemical and biological tests.

Finally, 6MPDC (**6**) was obtained in 6 steps from quinolinic acid in a low overall yield of 3 % (Scheme 27) but with enough material to perform the biochemical and biological tests. In addition, as the main objective of this thesis was, in part, the discovery of potential inhibitors, optimization of this synthesis was not a priority.

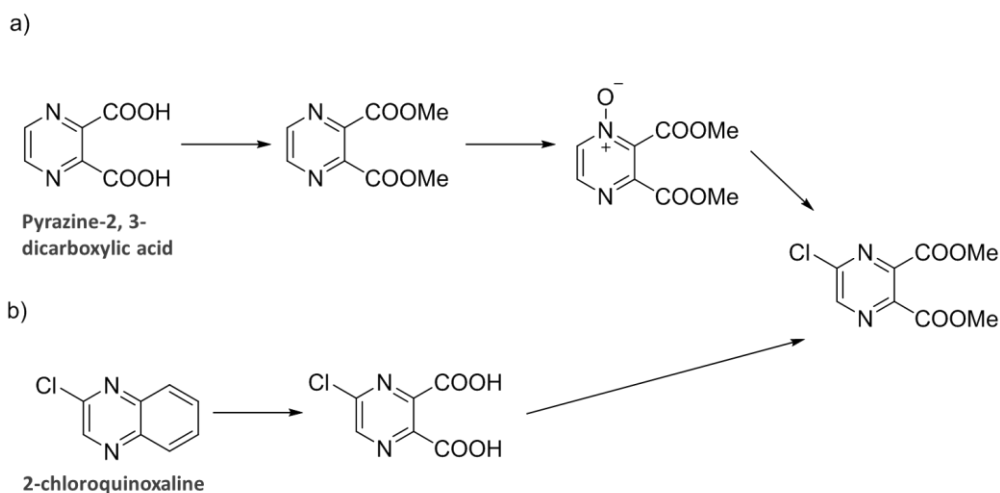


**Scheme 27:** Synthetic pathway of 6MPDC.

The synthesis of 6MPDC allowed us to pave a synthetic pathway for the other two analogues 5MPzDC and 5MPDC.

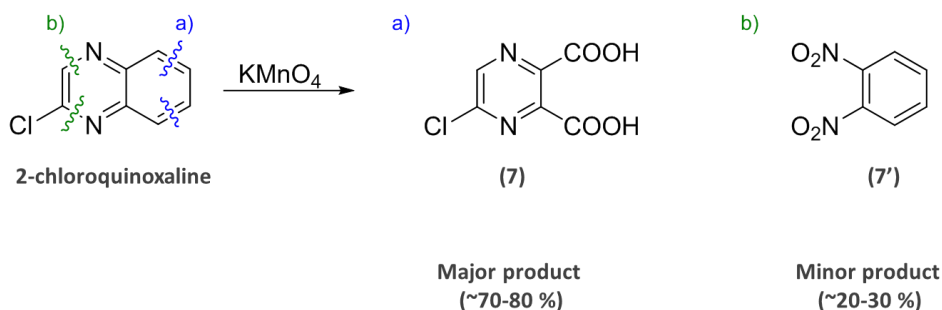
## II. Synthesis of 5-mercaptopyrazine-2,3-dicarboxylic acid (5MPzDC) from 2-chloroquinoxaline

In order to synthesize 5MPzDC, most of the steps were based on the synthesis of its analogue 6MPDC at the exception of the way to synthesize the intermediate **II** (scheme 19). To synthesize the chloro diester compound **8**, we decided to generate 5-chloropyrazine-2,3-dicarboxylic acid **7**, in a single step from 2-chloroquinoxaline as it was reported by Obafemi, C.A. and Pfeleiderer, W.<sup>187</sup> followed by a double esterification. This two-step strategy seemed to be more direct than the one used for 6MPDC (double esterification, N-oxide formation and addition of the chloride) and probably more efficient as well (Scheme 28).



**Scheme 28:** The two considered strategies a) and b) in order to obtain **8** intermediate for the synthesis of 5MPzDC. a) strategy based on the synthesis of 6MPDC; b) was designed after literature research in order to simplify the synthesis of 5MPzDC and improve the overall yield.

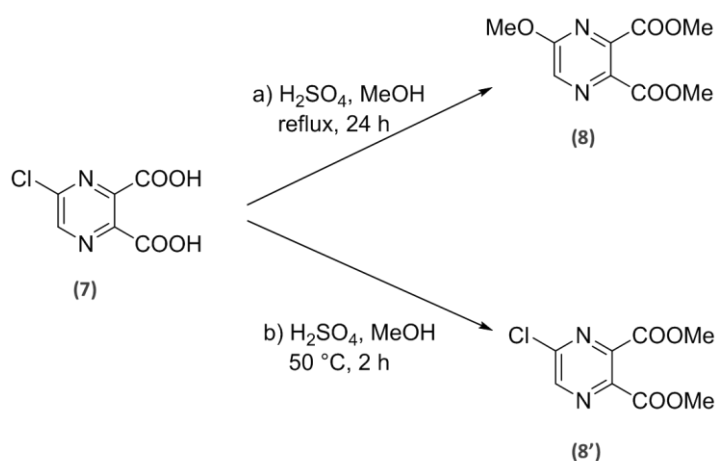
The first step consists in an oxidative cleavage of 2-chloroquinoxaline with a highly concentrated aqueous solution of a large excess of  $\text{KMnO}_4$  (5 equiv.) added dropwise in a refluxing solution of the starting material. This strategy, while a bit hazardous afforded the desired product **7** in an efficient manner but, in the presence of a non-negligible amount of impurities (20-30%).  $^1\text{H-NMR}$  analysis of this by-product showed the presence of two doublets in the aromatic region of the spectrum which could be consistent with the formation of 1, 2-dinitrobenzene. This could likely be due to a non-selective oxidative cleavage of the quinoxaline with however, a preference for the cleavage of the benzenic ring (Scheme 29).



**Scheme 29:** Two possible oxidative cleavages of 2-chloroquinoxaline by  $\text{KMnO}_4$ .

In contrast to what it is reported<sup>187</sup> even though a large part of the impurities on the final residue can be removed by precipitation and crystallization, it was not possible to obtain the pure desired product. However, the impurity did not bother in the subsequent step and the recuperated whole mixture was used without further purification in the next step.

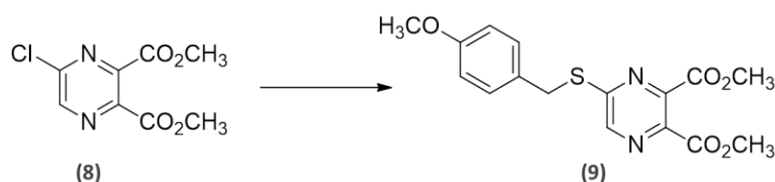
In the synthesis of 6MPDC, we observed that the protection of the two carboxylic acids (as esters) of quinolinic acid was efficiently achieved in acidic conditions (1.25 equivalents of H<sub>2</sub>SO<sub>4</sub>) but required 24 h at reflux for completion<sup>190</sup>. Under the same conditions, compound **7** was totally converted in a unique product. However, <sup>1</sup>H-NMR analysis showed the presence of an additional methoxy group resulting of the substitution of the chloride by a MeOH molecule of the solvent. Fortunately, by checking the progress of the reaction we found that milder heating (50°C) and a shorter reaction time (2 h) was enough to obtain **8** without any formation of the side product (Scheme 30). This difference in terms of reactivity could probably be explained by the higher electrophilic nature of the pyrazine ring compared to that of the pyridine one.



**Scheme 30:** a) Double esterification conditions used during the synthesis of 6MPDC that lead to complete formation of a non-desired byproduct in the synthesis of 5MPzDC. b) Optimized conditions for the double esterification of the pyrazine derivative that allow to obtain the desired product without formation of other side products.

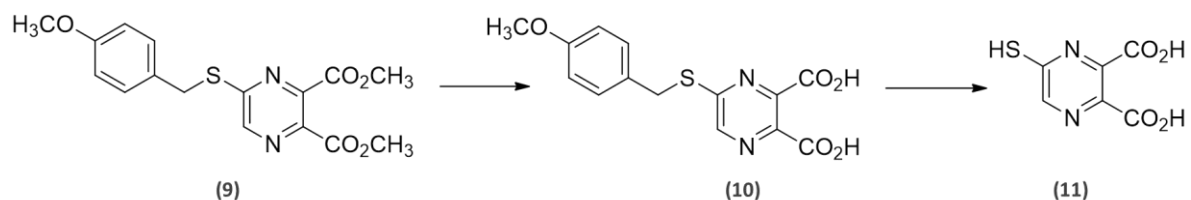
Finally, compound **8** was obtained after two steps in a moderate 35 % yield. We may assume that a big percentage of the product was lost on the first oxidative step.

For the introduction of 4-methoxy- $\alpha$ -toluenethiol in compound **8** by nucleophilic substitution of the chloride (Scheme 31), the same conditions as for 6MPDC were assayed (2 equivalents of thiol and base and 3 day reflux). Surprisingly, while 3 days at reflux were required to convert **3** into **4**, here, only 2 h at 50°C allowed the total conversion, highlighting once again the important effect of the nitrogen on the reactivity of such molecules. Moreover, only one equivalent of the base and thiol was needed instead of two, which made the final purification step easier and allowed to obtain the desired thio-ether molecule, (**9**), in an almost quantitative yield.



**Scheme 31:** Substitution of the chlorine by (4-methoxyphenyl)methanethiol.

As for 6MPDC, the deprotection of the carboxylic acids was performed before the deprotection of the thiol (Scheme 32), in order to avoid the possible formation of disulfide bridges. Without any surprise, saponification of the ester groups was efficiently achieved as for the previous molecule yielding compound **10** in 85% yield<sup>201</sup>.

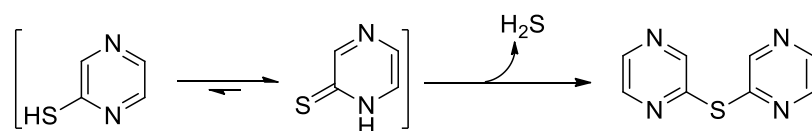


**Scheme 32:** Deprotection of esters followed by deprotection of thiol.

Finally, intermediate **10** was engaged in the deprotective step using the previously used procedure. Unfortunately, even if the final compound 5MPzDC, (**11**), was efficiently

formed in 55 % yield, a slow degradation of the product in solution (acetone) and even as a solid was observed.

According to literature, 2-thiopyrazines exist predominately in the thione form and their decomposition to dipyranizyl sulfide derivatives with the release of H<sub>2</sub>S gas is favored under atmospheric conditions (Scheme 33)<sup>206</sup>.



**Scheme 33:** 2-thiopyrazines degradation mechanism under atmospheric conditions<sup>206</sup>.

On the basis of <sup>1</sup>H-NMR analysis and our literature research<sup>206</sup>, we suggest that one of the degradation products observed could be 5, 5'-thiobis(pyrazine-2,3-dicarboxylic acid) (**11'**). Our pyrazine derivative might follow the described decomposition mechanism and form compound **11'** with generation of H<sub>2</sub>S resulting from the condensation of two 5MPzDC molecules (Figure 29). The addition of DTT reducing agent allowed us to conclude that a degradation process was happening and not an oxidation to form disulfide dimers, as could have been expected. Consequently, once obtained, the final product has to be stored at -80 °C in order to prevent its degradation.

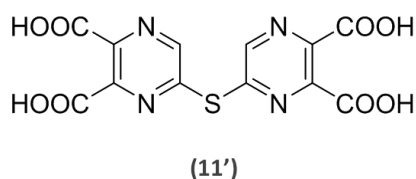
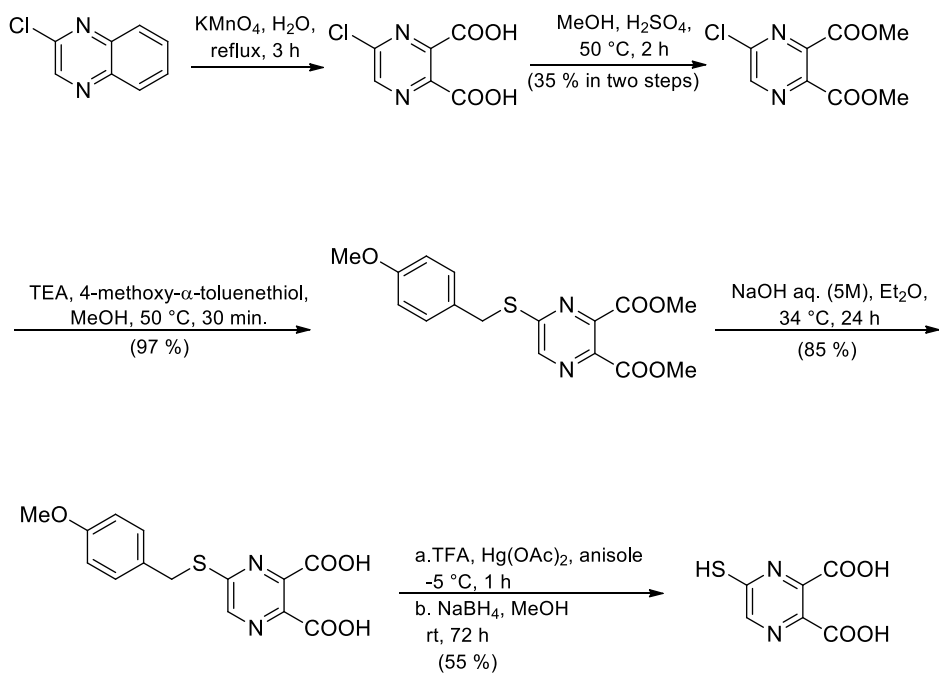


**Figure 29:** Proposed compound as degradation product of 5MPzDC.

Finally, 5MPzDC (**11**), was obtained in 5 steps from 2-chloroquinoxaline in reasonable 16 % overall yield (Scheme 34).



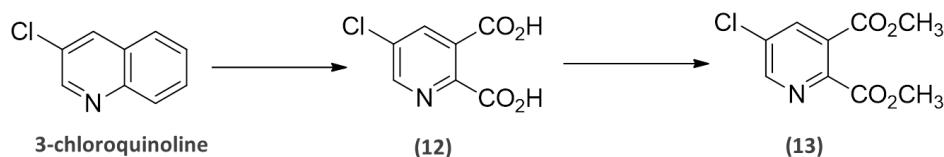
**Scheme 34:** Synthetic pathway of 5MPzDC.

### III. Synthesis of 5-mercaptopyridine- 2, 3-dicarboxylic acid (5MPzDC) from 3-chloroquinoline

The thiol substituent in 5MPzDC is on the C-5 position of the pyridine ring. Due to the electronic effect of the nitrogen on the ring, the position 5 is a less electrophilic position. Consequently, the introduction of either the chloro or the thioether substituent by a nucleophilic process should be less favorable than it was for 6MPzDC and 5MPzDC. For this reason, in order to overcome the first difficulty namely the introduction of the chloro substituent, we decided to start from the commercially available 3-chloroquinoline and proceed with the oxidative cleavage by  $\text{KMnO}_4$  as for the synthesis of 5MPzDC.

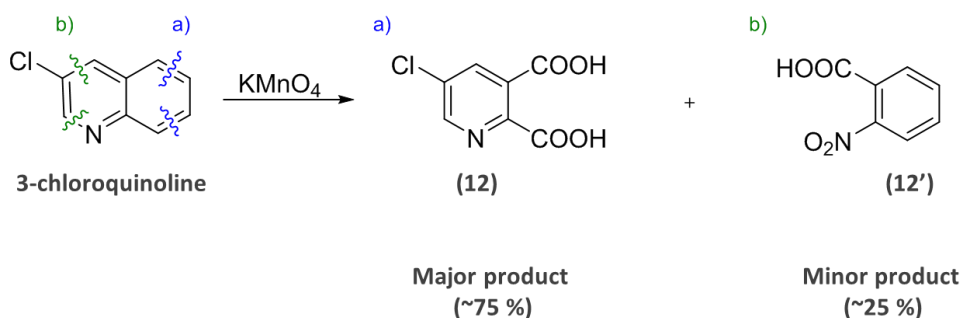
We followed the oxidation protocol described above for 5MPzDC<sup>187</sup>, starting from 3-chloroquinoline. Once again, in contrast to what it is described in literature, even if a large part of impurities could be removed by precipitation and crystallization, it was not possible to obtain the desired product in a pure manner. Fortunately, as for the previous case, the obtained residue **12** was pure enough to be used in the next step without any further purification (Scheme 35). The double esterification was achieved after 24 h reflux to afford

**13** (Scheme 35) as it was the case for the other pyridine derivative in the synthesis of 6MPDC, in contrast to the pyrazine derivative that required milder conditions for completion during the synthesis of 5MPzDC (50 °C and 2 h). As predicted, no chloro substitution by MeOH was observed due to the deactivation of the position 5.



**Scheme 35:** Obtaining and protection of carboxylic acids.

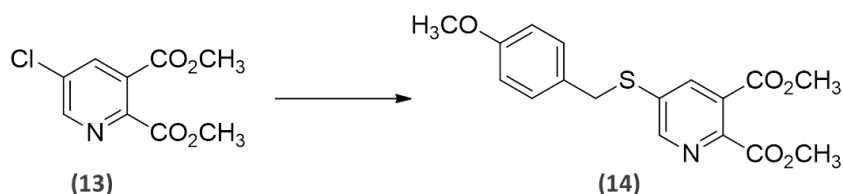
Once again, the overall yield of these two steps is particularly low (24 %). After  $^1\text{H-NMR}$  analysis, it was determined that a big part of the loss comes from the first oxidative cleavage with  $\text{KMnO}_4$ . Indeed, the spectrum of the resulting mixture showed the formation of two species, a major (the desired product) and a minor whose signal matches with a 2-nitrobenzoic acid species in a 75:25 ratio (**12:12'**)(Scheme 36).



**Scheme 36:** The two oxidative cleavages of 2-chloroquinoline by  $\text{KMnO}_4$ .

Being aware that the substitution of the chlorine atom by the thiol group (Scheme 37) could be difficult, different conditions were assayed. First, the conditions used in the previous syntheses ( $\text{Et}_3\text{N}/\text{MeOH}$ ) did not lead to any formation of the product even using a larger excess of reactants and longer reactions times. We thought that the fact of using a stronger base that ensures the thiolate form to enhance its nucleophilicity (with regard to the thiol form) could afford the desired product. Consequently,  $\text{NaH}$  in THF was assayed<sup>207</sup>.

An excess of both base and thiol (1.5 equivalents) yielded the desired product at room temperature but completion in such a condition was not observed. These conditions probably could have been optimized but meanwhile we found that the use of  $\text{Cs}_2\text{CO}_3$  (1.05 equivalents) in DMSO in the presence of a small excess of thiol afforded the product **14** in an efficient manner after 48 h even at room temperature<sup>208</sup>.



**Scheme 37:** Chlorine substitution by (4-methoxyphenyl)methanethiol.

In terms of pKa,  $\text{Cs}_2\text{CO}_3$  is not as strong base as  $\text{NaH}$ ; however, we may assume that the carbonate counter ion  $\text{Cs}^+$  has an important Lewis acid role interacting with the nitrogen and enhancing the electrophilic character of the aromatic ring (Figure 30).

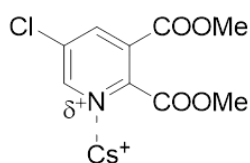
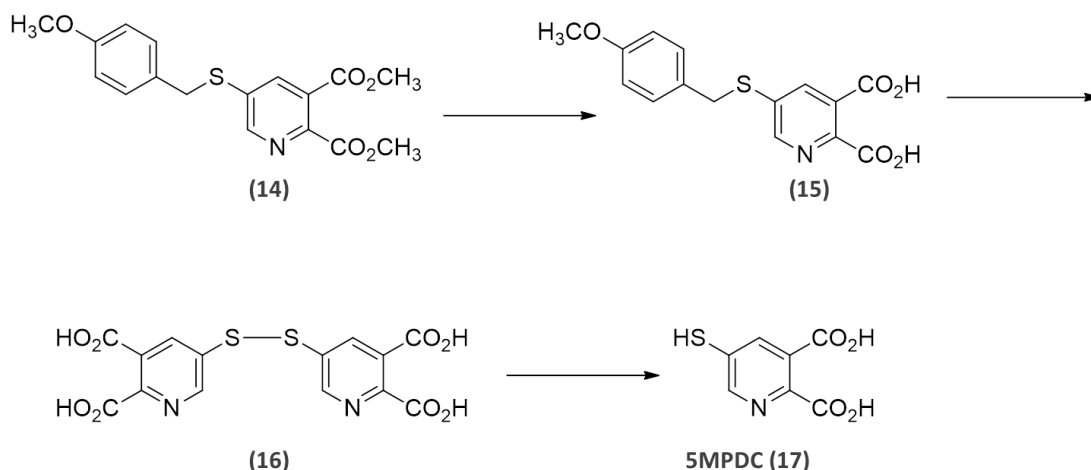


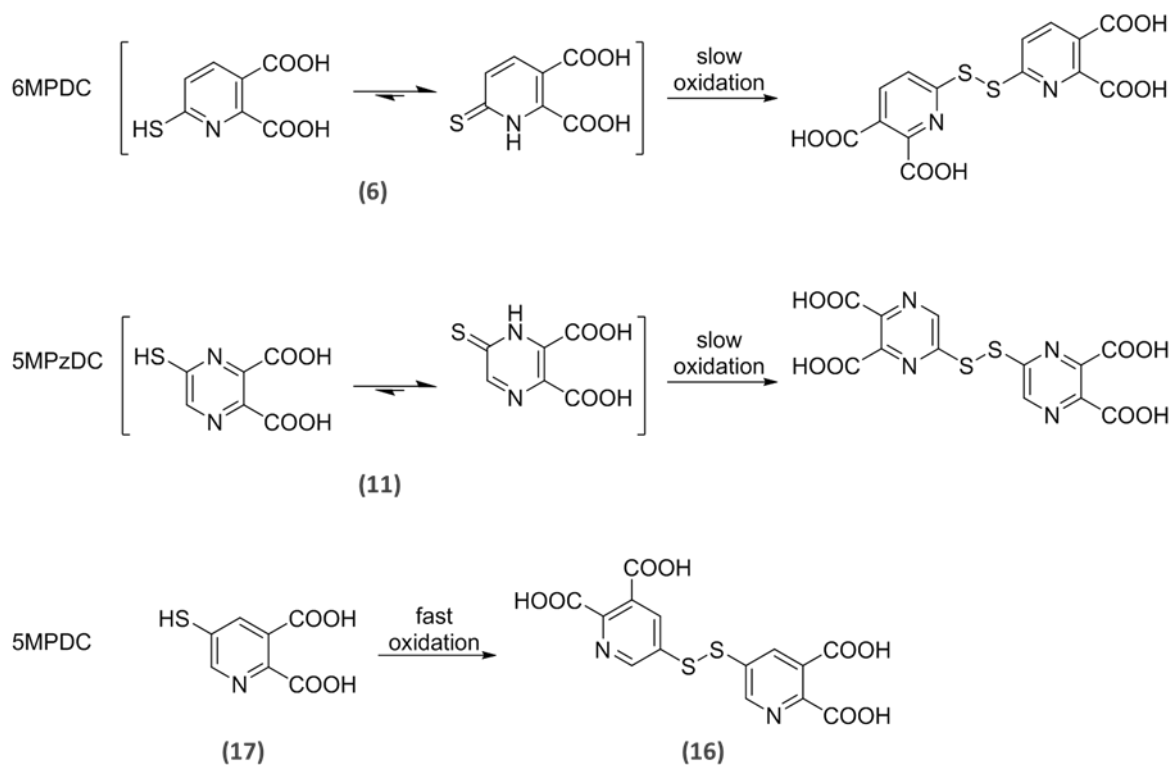
**Figure 30:** Activation of the pyridine derivative by  $\text{Cs}^+$  renders the substitution of the chlorine easier.

The saponification of the esters was performed as for the two previous molecules and the desired compound **15** was obtained in similar yield (Scheme 38). However, with the aim of improving the last step, the deprotection procedure of the thiol was modified a little bit with regard to the previous molecules. It was decided to remove the mercury salt by  $\text{H}_2\text{S}$  bubbling instead of  $\text{NaBH}_4$  as it was the case for the previous molecules. Unfortunately, the yield remained considerably low (9%). 5MPDC was obtained as a disulfide dimer **16**, and its reduction with DTT allowed to obtain 5MPDC, (**17**) (Scheme 38).



**Scheme 38:** Synthesis of 5MPDC (**17**) from **14**, after deprotection of carboxylic acids (**15**) and thiol (**16**), followed by reduction to yield the desired molecule as a monomer.

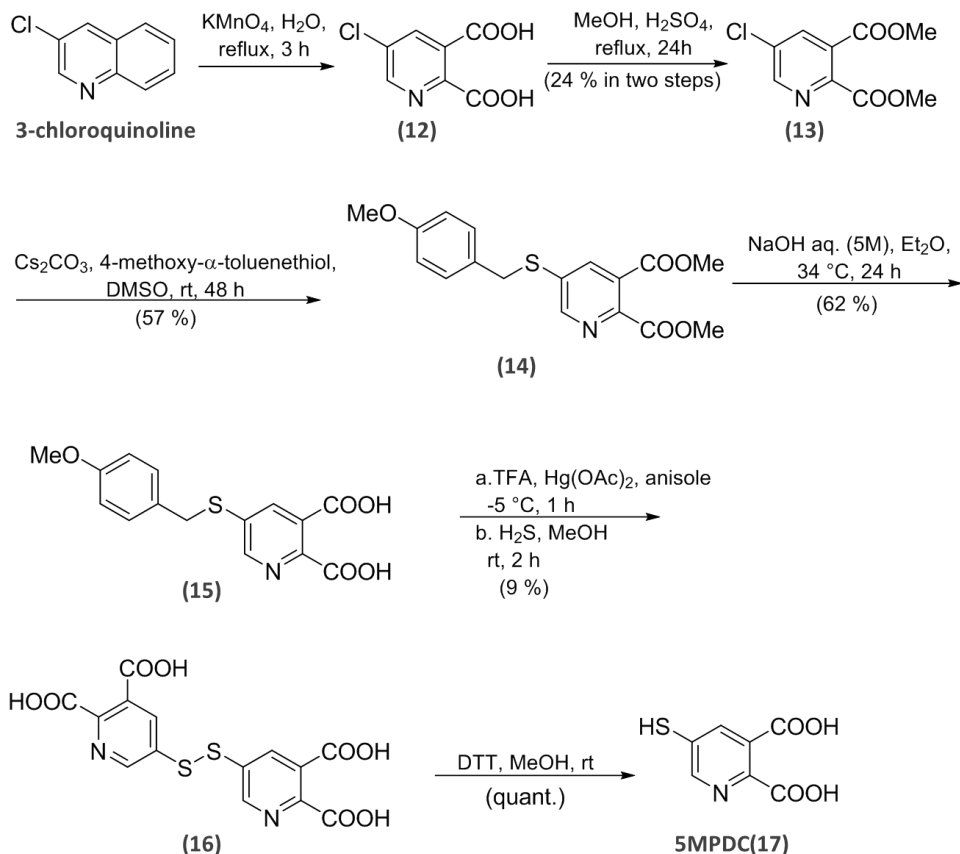
It is noteworthy the fact that 5MPDC was obtained as a disulfide dimer **16** in contrast to the two other molecules 6MPDC and 5MPzDC. This suggests that 5MPDC is much easier oxidizable than the two others. The main difference between the three molecules is related to the thiol position with regard to a nitrogen atom (position 2 vs 3). Consequently, it is highly probable that, for 6MPDC and 5MPzDC, a 2-pyridinethiol/2-pyridinethione tautomeric equilibrium exists as it is known for 2-pyridinethiol and 2-pyridone (Scheme 39)<sup>209</sup>. This equilibrium is not possible with 3-mercapto pyridine derivatives. Due to the charge delocalization, the thiol is reasonably less oxidizable.



**Scheme 39:** 6MPDC and 5MPzDC are slowly oxidized due to the thiol-thione tautomerism that renders the thiol less oxidizable. The thiol of 5MPDC does not exist in the previous form and is more oxidizable.

Thus, the obtaining of the desired molecule was achieved by DTT reduction of compound **16** which yields 5MPDC (**17**) in quantitative yield.

Finally, 5MPDC targeted molecule was obtained after 6 steps with an optimizable 1 % overall yield (Scheme 40).



**Scheme 40:** Synthetic pathway of 5MPDC.

The three molecules were achieved with particularly low yields. It is noteworthy that despite the small size of the molecules which only contain 15 atoms, 40 % of these are heteroatoms of three different nature (S, N, O) presented in four different chemical functions (carboxylic acid, heteroaromatic ring, thiol/thione). Thus, these molecules display important amphoteric, tautomeric and redox properties. In addition to this multi-faced reactivity, the formation of disulfide dimers and different side products especially concerning the chlorine introduction have been observed.

Particularly, in all three cases, it was during the thiol deprotection last step that a big amount of product was lost. In fact, we believe that this is due to the extremely strong affinity between thiol and mercury salt. Despite numerous attempts such as exposure to  $\text{H}_2\text{S}^{205}$  and even with an excess of  $\text{NaBH}_4^{210}$ , a large amount of the desired product still remains bonded to the metal and only a small part of desired molecule can be isolated pure.

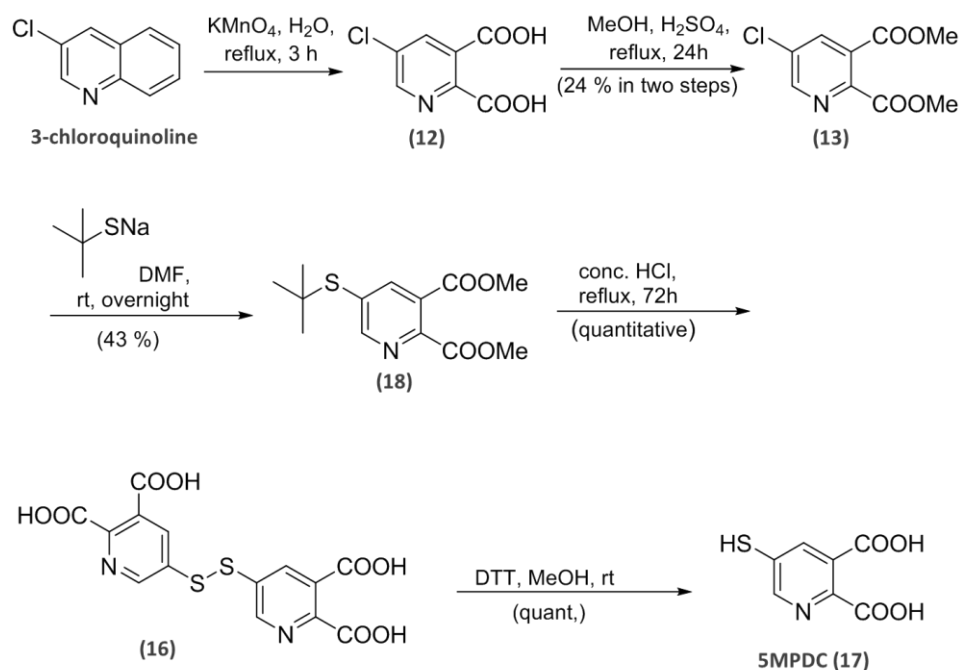
In addition to this, the use of Hg is hazardous for its manipulation and for the environment due to its toxicity. Furthermore, since the obtained molecules are going to be used for *in vitro* and *in cellulo* inhibition tests, the presence of mercury in the product, in case of a non-effective purification, might distort the results.

We ensured that mercury salt was absent by high resolution mass spectrometry and therefore the characterization of the compounds could be performed, as well as the biochemical tests. However, for the reasons mentioned above, at the late stage of the thesis, we performed some literature research in order to develop a Hg-free synthetic pathway for the molecules. It was found that, *a posteriori*, the use of 4-methoxy- $\alpha$ -toluenethiol to introduce the thiol function was not the best choice. A recent paper showed that the use of tertbutylate could be a good substitute<sup>211</sup>. Indeed, its deprotection does not only avoid the use of Hg, but it could also allowed the orthogonal deprotection of both the esters and the thiol at the same time and should increase considerably the overall yield of the synthesis. Due to a lack of time such a protocol was assayed only for the synthesis of 5MPDC.

Starting from compound **13**, addition of sodium *tert*butylthiolate in DMF resulted in the formation of the desired thioether **18** obtained with an unoptimized 43 % yield after purification which is a lower yield than the one obtained with the former protecting group.

After saponification of the esters, the thiol deprotection was attempted: both AlCl<sub>3</sub> in toluene<sup>212</sup> and TFA in CH<sub>2</sub>Cl<sub>2</sub><sup>213</sup> at room temperature did not yield the desired product even after an overnight reaction time. However, it was found that concentrated HCl at overnight reflux allowed to obtain the desired product in a quantitative yield. As it was considered to do, in order to both save a step and improve the yield even more, we found that the deprotection of both the carboxylic and thiol substituents could also be achieved simultaneously using such a procedure after a three-day reflux and in a quantitative manner (Scheme 41).

Finally, using such an approach, 5MPDC was synthesized in 4 steps with a better overall yield of 10 % instead of 1 % using the previous strategy (Scheme 41). If required, this approach will have to be tested for the synthesis of the two others molecules 6MPDC and 5MPzDC.



**Scheme 41:** Hg-free synthetic pathway of 5MPDC.

In conclusion, the syntheses and characterization of the three desired molecules that we wanted to test as potential NadA inhibitors were performed: 6MPDC, 5MPzDC and 5MPDC. The main drawback of these syntheses was their poor yield and the use of a Hg reactant which is toxic and should be avoided at the largest extent possible. For this reason, a new easier, safe and efficient synthetic pathway was determined for one of the molecules, 5MPDC. This avoids the use of mercury salt, removes one step and at the same time increases considerably the overall yield. This new pathway was not developed for 6MPDC and 5MPzDC for a matter of time but could be considered for further syntheses of the molecules or new analogues.



RESULTS CHAPTER II:

*IN VITRO* STUDIES OF 6MPDC,  
5MPzDC, 6MPDC AND 4MP ON  
NadA

In this chapter, we study the inhibition of the family of molecules that we identified as potential NadA inhibitors.

## I. Production of $^{56}\text{Fe-S}$ NadA, $^{57}\text{Fe-S}$ NadA and NadB proteins

Purifications of both NadA and NadB enzymes from *E. coli* have been described for several years (Materials and Methods). I have used these described protocols to produce  $^{56}\text{Fe-S}$  NadA,  $^{57}\text{Fe-S}$  NadA (for Mössbauer analyses) and NadB.

### a. *E. coli* $^{56}\text{Fe-S}$ NadA and $^{57}\text{Fe-S}$ NadA

*E. coli* BL21(DE3) bacteria were transformed with pT7-7NadAEcWT. Cultures were performed in LB medium or in M9 medium in the presence of  $^{57}\text{Fe}$  for Mössbauer study. Thanks to the His-tag in the N-terminal of NadA, the purification was easily performed through a Ni-NTA column under anaerobic conditions. Both  $^{56}\text{Fe-S}$  NadA and  $^{57}\text{Fe-S}$  NadA proteins were obtained with high purity as judged by SDS-PAGE analysis (Figure 31A). The average yield of our  $^{56}\text{Fe-S}$  NadA preparations was 10 mg/L of culture and 4.5 mg/L in the case of  $^{57}\text{Fe-S}$  NadA. As purified  $^{56}\text{Fe-S}$  NadA and  $^{57}\text{Fe-S}$  NadA proteins were brownish due to the presence of the  $[\text{4Fe-4S}]^{2+}$  cluster. We determined a Fe and S content of  $3.1\text{-}3.6 \pm 0.4$  iron and  $2.7\text{-}3 \pm 0.5$  sulfur per monomer for  $^{56}\text{Fe-S}$  NadA protein. Surprisingly but reproducibly,  $^{57}\text{Fe-S}$  NadA contained higher amounts of Fe and S, with  $3.8\text{-}4 \pm 0.4$  iron and  $3.1\text{-}3.5 \pm 0.5$  sulfur per monomer. All these results are in agreement with those obtained previously<sup>126,38,39</sup>.

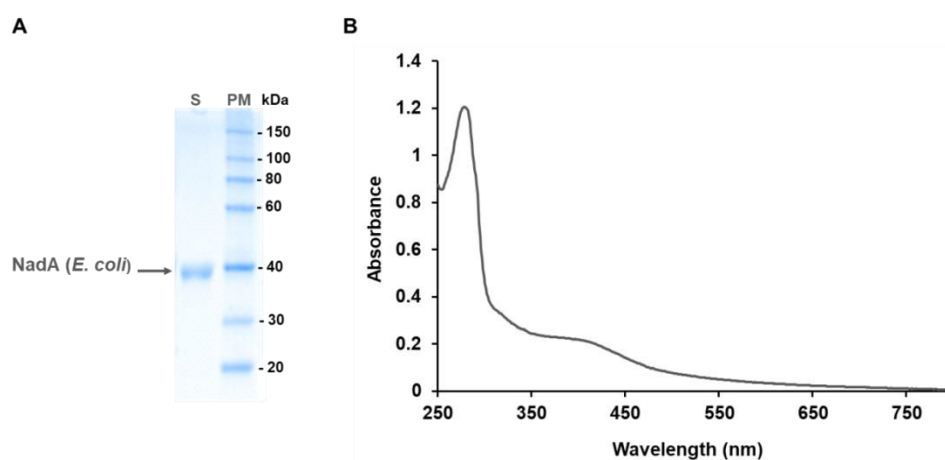


**Figure 31:** **A.** SDS-PAGE under denaturing conditions where PM are protein markers and S the loaded sample corresponding to as-purified  $^{56}\text{Fe-S}$  NadA. **B.** UV-visible spectrum of  $^{56}\text{Fe-S}$  NadA protein (21  $\mu\text{M}$ ) in buffer A.

UV-visible spectra of purified  $^{56}\text{Fe-S}$  NadA and  $^{57}\text{Fe-S}$  NadA were recorded in the glove box between 250 and 800 nm. Since they were identical in shape, I just show the spectrum corresponding to  $^{56}\text{Fe-S}$  NadA. The spectrum presents two absorption bands at 280 nm and at 420 nm (Figure 31B). The former belongs to the aromatic amino acids of the protein whereas the latter belongs to the  $[\text{4Fe-4S}]^{2+}$  cluster, more specifically to a ligand-to-metal ( $\text{S}^{2-} \rightarrow \text{Fe}^{3+}$ ) charge transfer. The absorbance at 420 nm allowed to estimate the amount of cluster per protein. Indeed, for a protein containing 4 atoms of Fe per monomer, the ratio between the absorption at 420 nm and absorption at 280 nm is 0.25. The smaller the ratio, the smaller the Fe-S content per monomer. In our  $^{56}\text{Fe-S}$  NadA preparation (Figure 31B) a ratio of 0.192 was calculated corresponding to 3.1 Fe/protein.

Mössbauer spectrum of as-purified  $^{57}\text{Fe-S}$  NadA (Figure 32) recorded at 4.2 K consisted of a quadrupole doublet (almost symmetrical) which was simulated with two doublets of similar intensity, belonging to two species. Each one corresponds to a mixed valence Fe pair ( $\text{Fe}^{2.5+}$  and  $\text{Fe}^{2.5+}$ ) typical for  $[\text{4Fe-4S}]^{2+}$  clusters. Mössbauer parameters (Table 5) were in agreement with those already described for NadA enzyme (see introduction)<sup>38</sup>.

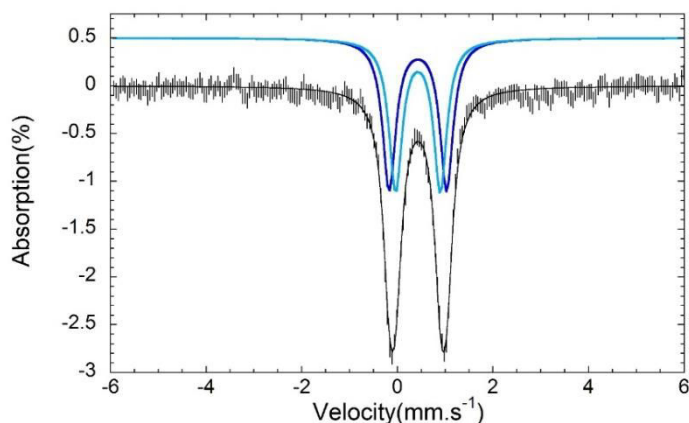


**Figure 32:** Experimental Mössbauer spectrum of  $^{57}\text{Fe-S}$  NadA protein (200  $\mu\text{M}$ ) in buffer A (black line) and simulations (light and dark blue). Spectrum was recorded at 4.2 K with an external magnetic field of 0.06 T applied parallel to  $\gamma$ -rays.

Species	$\delta$ (mm.s <sup>-1</sup> )	$\Delta E_Q$ (mm.s <sup>-1</sup> )	$\Gamma$ (mm.s <sup>-1</sup> )	Area (%)
Fe2.5	0.43	1.20	0.33	50
Fe2.5	0.43	0.93	0.33	50

**Table 5:** Mössbauer parameters.

The specific activity of *E. coli*  $^{56}\text{Fe}$ -S NadA was measured *in vitro* (see Materials and Methods) and was found to be 60 nmol/min/mg as average.  $^{57}\text{Fe}$ -S NadA specific activity is similar with an average of 64 nmol/min/mg. These values are above the one found in literature (15 nmol/min/mg)<sup>39</sup> but in agreement with previous NadA preparations obtained in our laboratory (60 nmol/min/mg)<sup>126</sup>.

### b. *E. coli* NadB

*E. coli* BL21(DE3) bacteria were transformed with the plasmid pET-22b-nadBEc. The culture and purification steps were performed under aerobic conditions in contrast to NadA, since NadB does not contain any oxygen-sensitive cofactor. The N-terminal His-tag allowed the purification through a Ni-NTA column, and a colorless protein was obtained, due to the loss of its FAD cofactor. 5 mg of protein were obtained per liter of culture with a purity of 95 % as judged by SDS-PAGE analysis (Figure 33A).

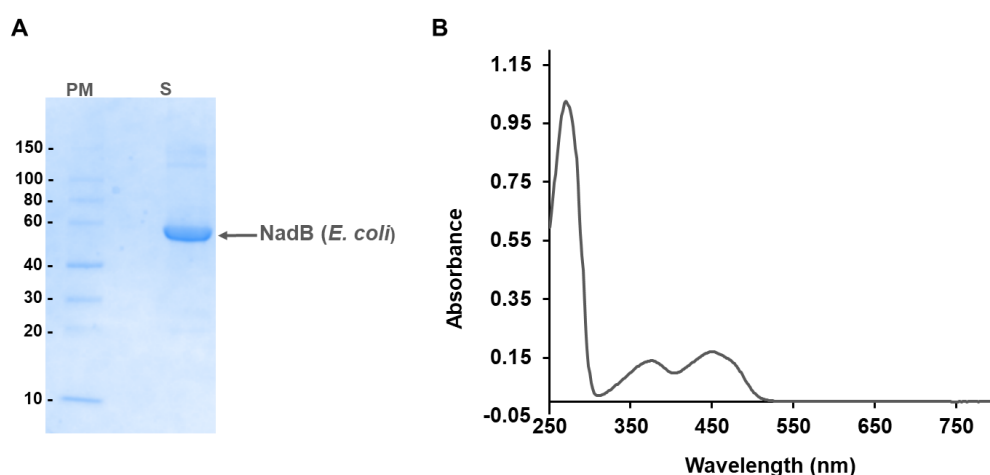


**Figure 33:** **A.** SDS-PAGE under denaturing conditions where PM are protein markers and S the loaded sample corresponding to purified NadB. **B.** UV-visible spectrum of NadB protein (13.25  $\mu\text{M}$ ) in buffer A after FAD reconstitution.

After FAD reconstitution, the protein was yellow, in agreement with the presence of the cofactor. The FAD content was determined by UV-visible absorption spectroscopy. The UV-visible spectrum of NadB after reconstitution was recorded between 250 and 800 nm. It displays three absorption bands: one at 280 nm which corresponds to the aromatic amino acids of the protein and two others at 360 and 450 nm that come from FAD cofactor (Figure

33B). Quantification of FAD, obtained by measuring the absorbance at 450 nm ( $\epsilon_{450\text{nm}} = 11300 \text{ M}^{-1} \cdot \text{cm}^{-1}$ ) was determined to vary between 1 and 1.3 FAD per protein, depending on the preparation. In this case (Figure 33B), for an  $A_{450\text{nm}} = 0.171$ , the FAD concentration is  $15.13 \mu\text{M}$ , that corresponds to 1.15 FAD per protein.

NadB oxidizes *L*-aspartate into iminoaspartate by forming  $\text{FADH}_2$  from FAD. To measure NadB specific activity, we used cytochrome c as electron acceptor that allowed to regenerate the FAD cofactor (see Materials and Methods). The reduction of cytochrome c was monitored by UV-vis. at 550 nm as a function of time. This resulted in an increase in the absorption at 550 nm as a function of time. The slope of the linear part allowed to calculate the concentration of reduced cytochrome c formed per minute and therefore the concentration of iminoaspartate formed. After calculation, the specific activity of the NadB preparation was  $0.62 \mu\text{mol}/\text{min}/\text{mg}$ , a value smaller to preparations obtained in our laboratory by other students ( $1.06 \mu\text{moles}/\text{min}/\text{mg}$ ) but acceptable for enzymatic assays with NadA (Figure 34).

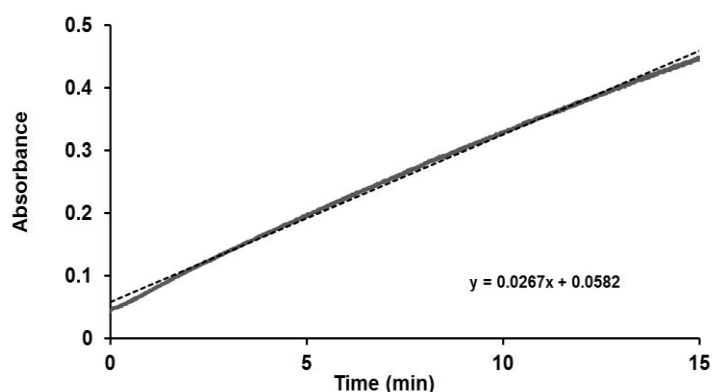


**Figure 34:** Determination of *L*-aspartate oxidase specific activity ( $15 \mu\text{M}$ ) by the reduction of cytochrome c. The grey line corresponds to the experimental data; the dotted line corresponds to the fit of the line allowing the calculation NadB activity.

## II. NadA inhibition with 6MPDC, 5MPzDC, 5MPDC and 4MP

Once the three molecules 6MPDC, 5MPzDC and 5MPDC synthesized (Results chapter I) and the NadA, NadB proteins produced under an active form, we performed NadA enzymatic assays in the presence of the molecules to determine if they present an inhibitory effect towards NadA or not. Even though 4MP (commercial) had already been tested during

the Ph.D of Alice Chan, we included it in the present study as it belongs to the family of molecules that we are interested in, and also because it is important to have results made by the same experimenter.

The inhibition assays were performed as explained in Materials and Methods. Briefly, NadA (10  $\mu$ M) was incubated with the molecules-to-test (0-1 mM) in buffer B for 15 min. before the addition of the premix containing the substrates and fumarate. After 15 min. of incubation at 37 °C, the reaction was started by addition of NadB, quenched 20 min later and QA formation analyzed by HPLC.

As control, each molecule was injected onto the HPLC column under identical conditions, in order to check that their retention time is different to that of QA and thus, that their presence does not interfere with QA quantification.

All four molecules inhibited NadA activity *in vitro* (Figure 35). Indeed, we observed a decrease in the activity as a function of molecule concentration. An IC<sub>50</sub> value could be calculated for each molecule (Table 6).

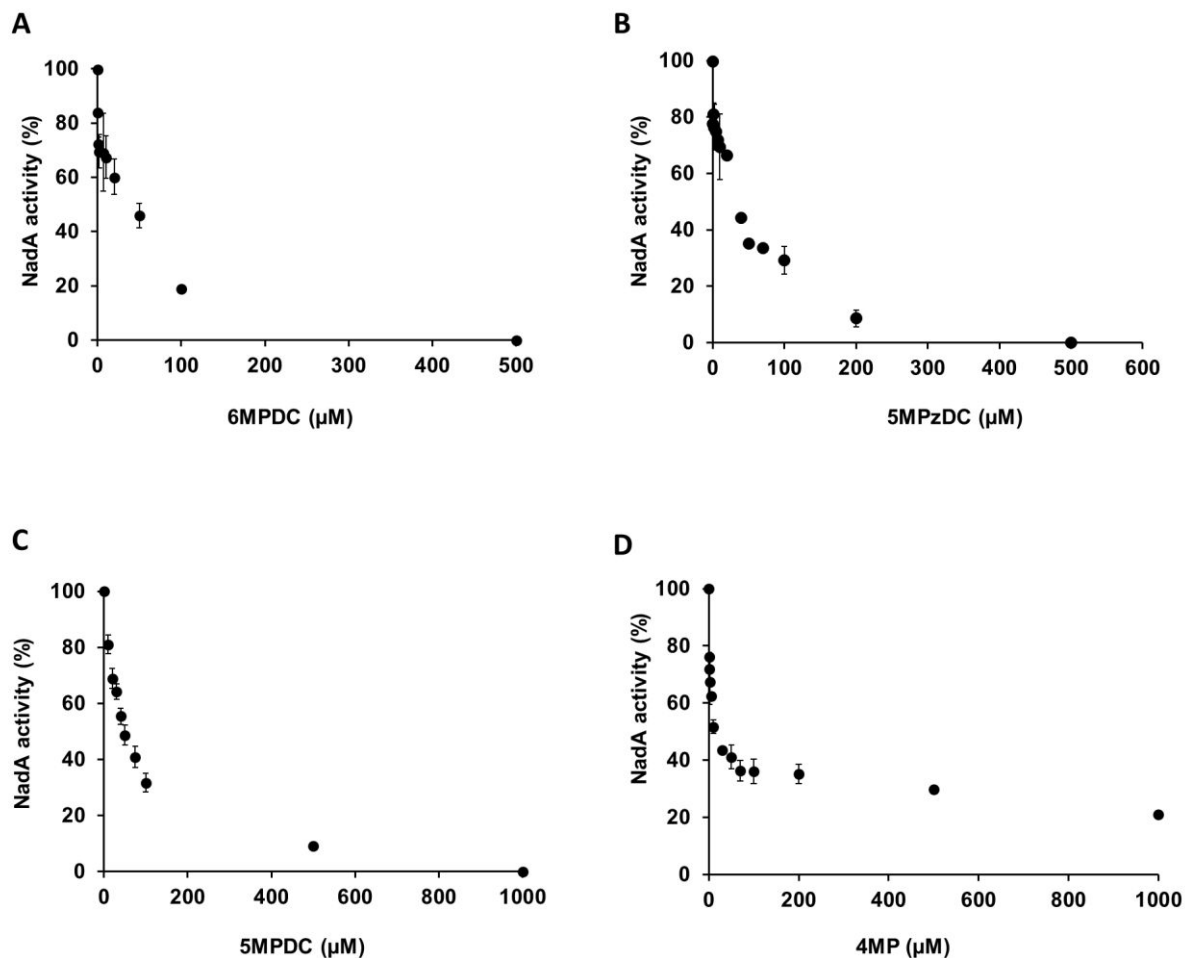


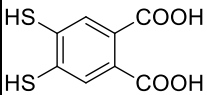
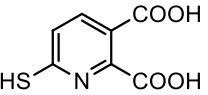
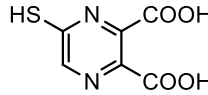
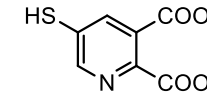
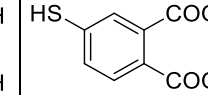
**Figure 35:** NadA Activity (%) in the presence of increasing concentrations ( $\mu\text{M}$ ) of 6MPDC (**A**), 5MPzDC (**B**), 5MPDC (**C**) and 4MP (**D**). NadA: 10  $\mu\text{M}$ .

In more detailed concerning each molecule. The addition of an equimolar amount of 6MPDC to NadA resulted in a loss of 30 % of the activity. An inhibition of 50 % was obtained with 40  $\mu\text{M}$  of 6MPDC. The addition of 10 equivalents of 6MPDC (100  $\mu\text{M}$ ), led to the loss of 80 % of the enzyme activity which was completely inhibited at 500  $\mu\text{M}$  (Figure 35A). An  $\text{IC}_{50}$  of 40  $\mu\text{M}$  was calculated (Table 6).

5MPzDC at equimolar amount with regard to the enzyme inhibited 30 % of the enzyme activity like 6MPDC. However, 50 % of enzyme activity was inhibited at 32  $\mu\text{M}$  of the molecule. At 100  $\mu\text{M}$ , 30 % of the enzyme activity remained and a complete inhibition was observed at 500  $\mu\text{M}$  of 5MPzDC (Figure 35B). An  $\text{IC}_{50}$  of 32  $\mu\text{M}$  was calculated (Table 6).

10  $\mu\text{M}$  of 5MPDC inhibited almost 30 % of the enzyme activity. It took more than 4 equivalents of 5MPDC to inhibit 50 % of NadA activity (45  $\mu\text{M}$ ). Only 10 % of activity remained at 500  $\mu\text{M}$  concentration and we observed a complete inhibition at 1 mM (Figure 35C). An  $\text{IC}_{50}$  of 45  $\mu\text{M}$  was calculated (Table 6).

Concerning 4MP, we found different results to those obtained by A. Chan. (2014). Reproducibly, at 10  $\mu\text{M}$  (a 1:1 ratio with NadA) almost 50 % of the enzyme activity was inhibited. Despite this strong inhibition at low concentrations of 4MP, at 50  $\mu\text{M}$ , 60 % of the activity was inhibited and 64 % at 100  $\mu\text{M}$ . Even at 1 mM (100 equiv with NadA), we still found 20 % of the activity (Figure 35D). An  $\text{IC}_{50}$  of 13  $\mu\text{M}$  was calculated (Table 6).

	DTHPA	6MPDC	5MPzDC	5MPDC	4MP
					
$\text{IC}_{50}$ ( $\mu\text{M}$ )	10	40	32	45	13

**Table 6:**  $\text{IC}_{50}$  ( $\mu\text{M}$ ) values determined on *E. coli* NadA (10  $\mu\text{M}$ ) for DTHPA, 6MPDC, 5MPzDC, 5MPDC and 4MP ( $n \geq 4$ ). DTHPA was used as a control.

Quinolate synthase activity/inhibition assays were performed in the presence of a second enzyme, L-aspartate oxidase that produces from L-aspartate iminoaspartate, one of the substrates of NadA. For this reason, before going further on the inhibition study of the different molecules, we had to make sure that the inhibition we observed was due to an inhibition of NadA and not NadB.

For this reason, the activity of NadB was tested *in vitro* in the presence of all molecules (4MP, 5MPzDC, 6MPDC and 5MPDC). Briefly, the different molecules were incubated in buffer B with NadB and cytochrome c before adding L-aspartate. The enzymatic activity of NadB was determined by quantification of the reduced cytochrome c as explained before. We tested the molecules at 50  $\mu\text{M}$  (3.3 equivalents with regard to NadB enzyme), a concentration that inhibits more than 50 % of NadA activity in all cases.

No inhibition of NadB was observed by any of the tested molecules (Table 7). Even, for some of them, a stimulatory effect was observed (5MPDC and 4MP). The fact that we did not observe any NadB inhibition shows that the inhibition of QA formation comes from the inhibition of NadA and not NadB, and thus that the four molecules can be defined as NadA inhibitors.

	Control	6MPDC (50 $\mu$ M)	5MPzDC (50 $\mu$ M)	5MPDC (50 $\mu$ M)	4MP (50 $\mu$ M)
NadB activity (%)	100	100 $\pm$ 10	100 $\pm$ 15	125 $\pm$ 5	175 $\pm$ 13

**Table 7:** *E. coli* NadB activity at 15  $\mu$ M in the presence of the different molecules at 50  $\mu$ M. NadB activity is given as percentages in comparison with NadB activity in the absence of the molecules (control, 100 %).

Before going further, we tried to understand the reason of the NadB activity stimulation by 5MPDC and 4MP. As explained on the previous chapter, 6MPDC and 5MPzDC contain hardly oxidizable thiol groups. Indeed, due to their neighboring nitrogen, they can exist on a thiol-thione equilibrium where the electrons are delocalized and less available for an oxidation (Figure 39). The thiol from 5MPDC and 4MP does not have a neighboring nitrogen and therefore does not exist under this equilibrium becoming easier oxidizable (Figure 39). This was described for 5MPDC, but it is also the case of 4MP. Therefore, it could be possible that oxidized cytochrome c might be reduced by 5MPDC and 4MP yielding disulfide dimers. In this case, the amount of reduced cytochrome c is increased leading to incorrect NadB activity.

To address that, we incubated each of the four molecules (50  $\mu$ M) in the presence of oxidized cytochrome c (100 $\mu$ M) in buffer B (without NadB), and monitored the absorbance at 550 nm as a function of time. No cytochrome c was reduced in the presence of 6MPDC and 5MPzDC. In contrast, we observed a linear increase of the absorbance at 550 nm with time (i.e the formation of reduced cytochrome c) in the presence of 4MP and 5MPzDC (Figure 36) showing that 4MP and 5MPzDC are able to reduce cytochrome c forming disulfide dimers. This stimulatory effect cannot occur in the NadA enzymatic assay since there is no cytochrome c present.

We can conclude from these experiments that i) none of the four molecules inhibit NadB activity; ii) all four molecules are NadA inhibitors.

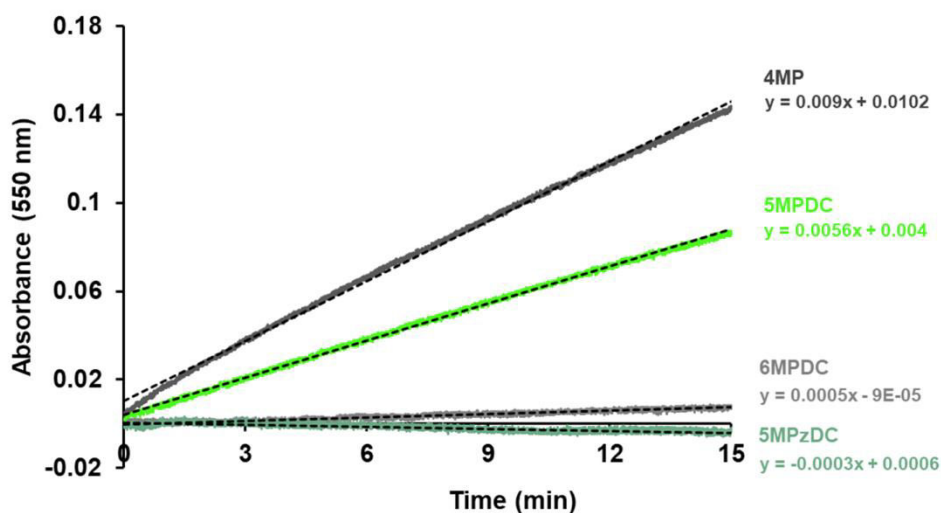


**Figure 36:** Cytochrome c reduction in the presence of 50  $\mu$ M of 4MP (dark grey), 5MPDC (light green), 6MPDC (light grey) and 5MPzDC (dark green). Trend lines of each of the four lines are represented in dotted lines and the corresponding equation is shown at the same color as their line.

### III. Study of NadA inhibition mechanism

#### c. Mössbauer spectroscopy

The family of molecules was designed with a thiol in order to coordinate the accessible ( $H_2O$ -coordinated) Fe site of NadA cluster. Therefore, we considered that Mössbauer spectroscopy would be an appropriate spectroscopy to detect an interaction between the cluster and the inhibitors and understand the inhibition at a molecular level.

Mössbauer spectra of *E. coli*  $^{57}Fe$ -S NadA incubated with 5-5.7 equivalents of 4MP, 6MPDC, 5MPzDC and 5MPDC were recorded at 4.2 K (Figure 37). All spectra were very similar to the as-isolated NadA spectrum (Figure 32)<sup>38</sup>. They all consist of a main quadrupole doublet that can be fitted with two components of equal intensity whose parameters (Table 8) are characteristic of delocalized mixed valence  $Fe^{2.5+}$  pairs within diamagnetic  $[4Fe-4S]^{2+}$  clusters.

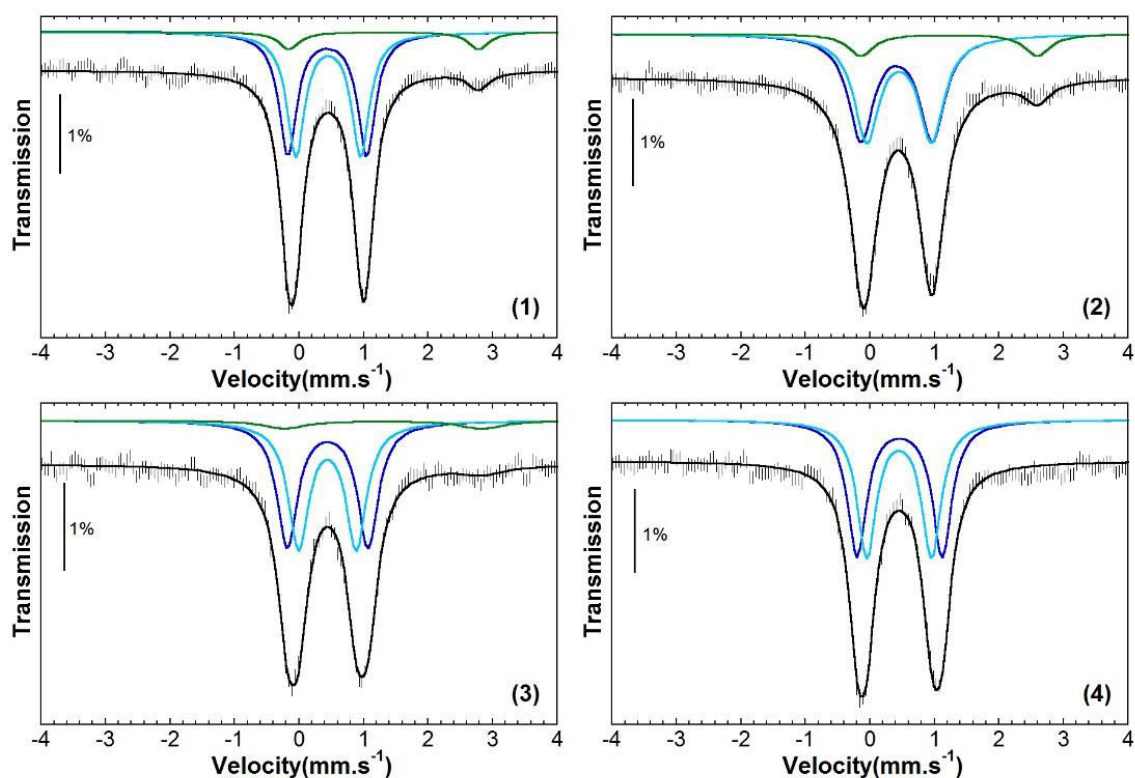


**Figure 37:** Mössbauer spectra of *E. coli*  $^{57}\text{Fe}$ -S NadA with 5-5.7 eq of 6MPDC **(1)**; 5MPzDC **(2)**; 5MPDC **(3)** and 4MP **(4)**. Mössbauer spectra were taken at 4.2 K with an external magnetic field of 0.06 T applied parallel to  $\gamma$ -rays.

Sample	Molecule	Species	$\delta$ (mm.s $^{-1}$ )	$\Delta E_Q$ (mm.s $^{-1}$ )	$\Gamma$ (mm.s $^{-1}$ )	Area (%)
NadA as-purified	-	4Fe-4S	0.43	1.20	0.33	100
			0.43	0.93	0.33	
1	6MPDC	4Fe-4S	0.43	1.23	0.33	92
			0.45	1.01	0.33	
		Fe $^{II}$	1.31	2.94	0.38	8
2	5MPzDC	4Fe-4S	0.41	1.10	0.47	91
			0.45	1.01	0.47	
		Fe $^{II}$	1.23	2.74	0.48	9
3	5MPDC	4Fe-4S	0.44	1.26	0.38	94
			0.44	0.90	0.38	
		Fe $^{II}$	1.30	3.06	0.80	6
4	4MP	4Fe-4S	0.46	1.32	0.36	100
			0.45	1.01	0.36	

**Table 8:** Experimentally determined Mössbauer parameters for NadA in the presence of 6MPDC **(1)**, 5MPzDC **(2)**, 5MPDC **(3)** and 4MP **(4)**. Parameters of as-purified NadA were added to the table for comparison.

Mössbauer data demonstrated that the cluster was not degraded by the molecules. In addition, analyses of the Mössbauer parameters (Table 8) did not clearly reveal a change in the coordination number of the catalytic iron site in contrast to DTHPA<sup>141</sup> (Figure 18B), suggesting that the catalytic Fe site remained tetraordinated. A pentacoordination through the thiol and the nitrogen in the case of 5MPzDC and 6MPDC was therefore excluded. It is possible that the four molecules interact through their thiol with the Fe catalytic site without changing the symmetry of the catalytic iron that remains tetra-coordinated. Indeed, the exchange of the oxygen atom of the coordinating water molecule (present in the resting state) by the thiol moiety of the molecules could lead to the obtained Mössbauer parameters. Another possibility is that there is no or a very weak interaction between the molecules and the Fe catalytic site of the cluster.

Therefore, even though Mössbauer technique didn't prove an interaction of the four molecules with the cluster as for DTHPA, it didn't exclude one either. In addition, it has allowed us i) to exclude some coordination modes and ii) to observe that all these molecules do not degrade the Fe-S cluster.

#### d. UV-visible absorption spectroscopy

UV-visible absorption spectroscopy is a more sensitive spectroscopy than Mössbauer one for evaluating ligation changes on a metal. Thus, we recorded UV-vis. spectra of *E. coli* NadA (18-21 $\mu$ M) before (black solid lines) and after addition of 5 equivalents of 6MPDC (A), 5MPzDC (B), 5MPDC (C) and 4MP (D) (black dashed lines) and 15 min. incubation. UV-vis. spectra of 5 equivalents of 6MPDC, 5MPzDC, 5MPDC and 4MP without NadA were also recorded (gray lines) (Figure 38).

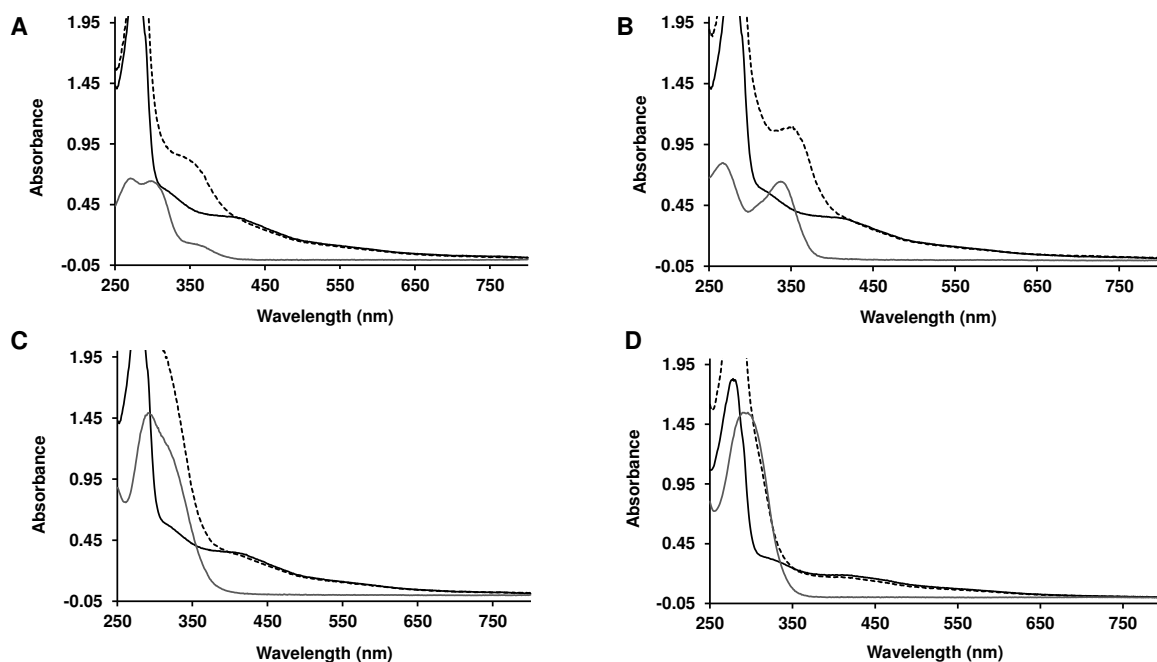


**Figure 38:** NadA (18-21 $\mu$ M) UV-visible spectra before (black solid lines) and after addition (black dashed lines) of 5 eq. of 6MPDC (**A**), 5MPzDC (**B**), 5MPDC (**C**) and 4MP (**D**) and 15 min. incubation. UV-vis. spectra of 5 eq. of 6MPDC, 5MPzDC, 5MPDC and 4MP without NadA (gray lines).

As a reminder, DTHPA modifies UV-visible spectrum of NadA with a blue-shift of the characteristic  $S^{2-} \rightarrow Fe^{3+}$  charge transfer band and a new absorption at 500 nm (Figure 18A)<sup>141</sup>. UV-visible analyses of NadA in the presence of 6MPDC, 5MPzDC, 5MPDC and 4MP did not reveal major changes in the cluster region (400-500 nm) making it impossible to unambiguously demonstrate an interaction of these molecules with the cluster. Indeed, at first sight, the spectra of NadA in the presence of the different molecules could be the resulting of the addition of the NadA spectrum alone with that of the different molecules alone, suggesting no interaction or weak interactions between the molecules and the cluster. Thus, it was not possible to easily demonstrate an interaction of the four molecules with the cluster by UV-visible absorption spectroscopy.

#### e. Circular dichroism

As just discussed above, by UV-visible spectroscopy, it was hard to determine whether molecules interact with the cluster. For this reason, we decided to use circular dichroism to investigate the interaction between NadA and the four molecules. Circular dichroism is also a UV-visible technique but the difference is that the recorded spectra

represent the differential absorption of left- and right- handed circularly polarized light. This is an advantage since we see in the recorded spectrum just the protein (the chiral solute) and what it is bound to it, regardless of what remains in solution. First, we recorded the CD spectra of NadA (8.2  $\mu\text{M}$ ) (black lines) alone and in the presence of 5 equivalents (41  $\mu\text{M}$ ) of DTHPA (green line) as control, which had never been done before (Figure 39A). Then, the same was done with NadA (8.2  $\mu\text{M}$ ) (black lines) before and after the addition of 5 equivalents (41  $\mu\text{M}$ ) of 6MPDC (B), 5MPzDC (C), 5MPDC (D) and 4MP (E) (green lines) (Figure 39B-E).

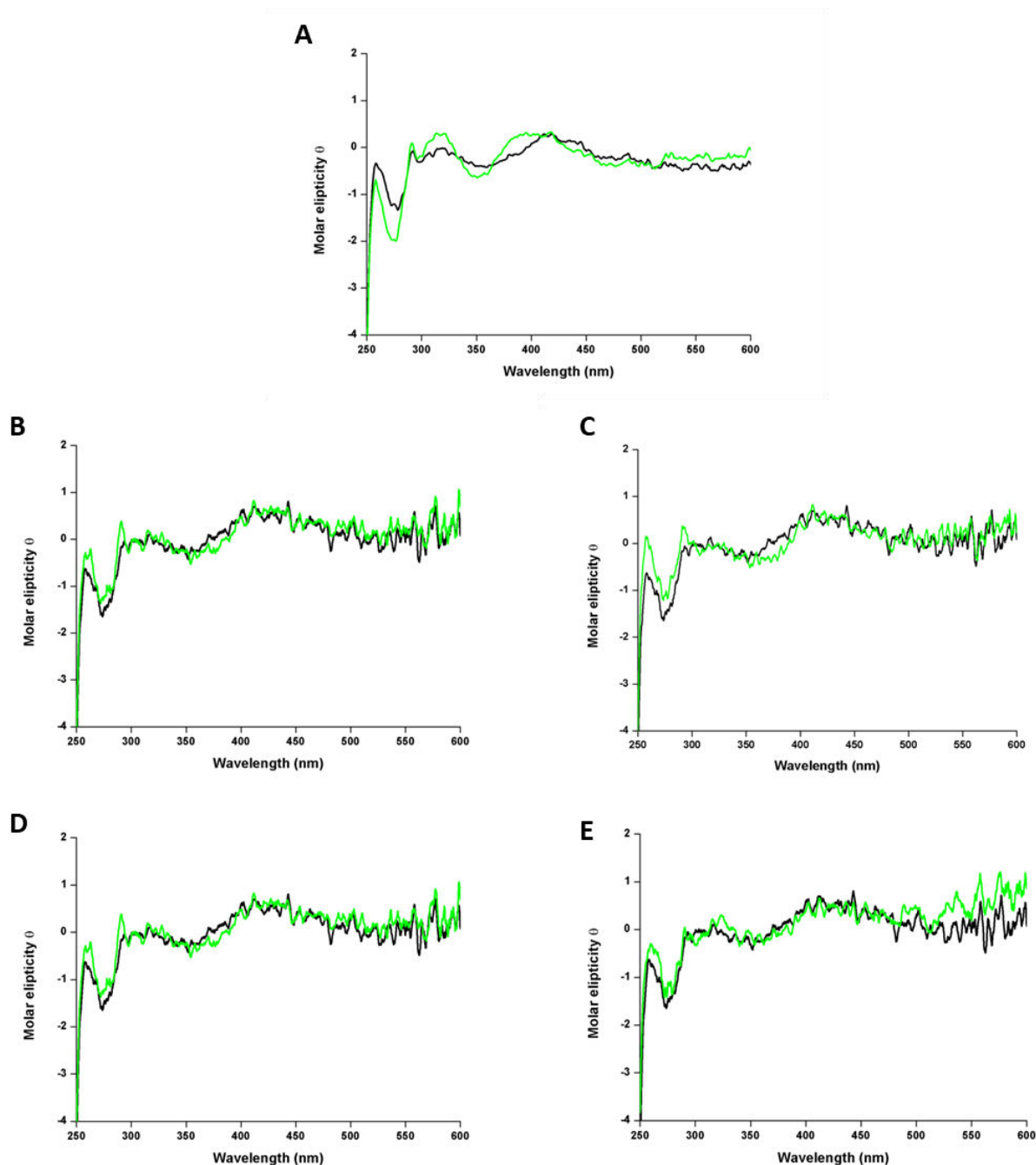


**Figure 39:** Circular dichroism spectra of NadA (8.2  $\mu$ M) before (black lines) and after addition (green lines) of 5 eq. (41  $\mu$ M) of DTHPA (A), 6MPDC (B), 5MPzDC (C), 5MPDC (D) and 4MP (E) (10 accumulations). (A) was recorded every 1 nm whereas (B), (C), (D) and (E) were recorded every 0.1 nm.

In the case of spectrum A, we observed that the CD signal of NadA is significantly modified in the presence of 5 equivalents of DTHPA, especially in the cluster region (300-450 nm). This shows that DTHPA interacts with the protein, likely through the cluster in agreement with the other techniques used before<sup>141</sup>. Spectra B, C, D and E presented small

changes, which are slightly more pronounced in the case of 5MPzDC and hardly detectable in the case of 4MP (Figure 39C and 39B). This makes it difficult to conclude if the observed changes are due to a weak interaction of the molecules with the protein or not. Spectra B, C, D, and E are noisier than that of DTHPA (due to the interval of the recording that was increased by a factor of 10 (0.1 nm for B-E, 1 nm for A) which does not help to see subtle changes. We considered that it was not worth repeating experiments under identical conditions as for DTHPA since changes are extremely small and the technique is protein-consuming (1 mg/one experiment).

#### f. Crystal structures of NadA in complex with the molecules

Crystal structures of *T. maritima* NadA\*Y21F variant in complex with 6MPDC, 5MPDC and 4MP were obtained at 1.8 Å, 2.1 Å and 1.64 Å, respectively (Juan Carlos Fontecilla Camps and Anne Volbeda, IBS, Grenoble). Due to the instability of 5MPzDC, this molecule was not given to crystallographers. Indeed, a night at 20°C is enough to degrade more than 50 % of 5MPzDC and the time scale to obtain crystals with NadA is usually in the order of days or weeks. We have used the NadA\*Y21F variant because i) we had a lot; 2) it crystallizes easily and crystals diffract very well; and 3) it is an active enzyme (even if it is slower than wild-type). The preparation of the NadA\*Y21F protein was performed by Deborah Reichmann (Post-doc in 2014-2015 in our laboratory).

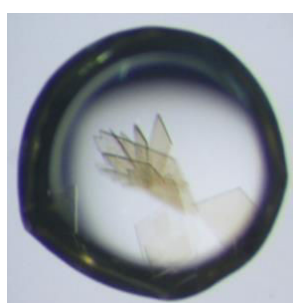


**Figure 40:** NadA\*-5MPDC crystals. For crystallization conditions, see Materials and Methods.

Brown crystals of the three complexes, NadA\*Y21F-**6MPDC**, NadA\*Y21F-**5MPDC** and NadA\*Y21F-**4MP** were obtained by incubating the enzyme under anaerobic conditions with a small excess of the molecules (2-3.5 equivalents). The brown color comes from the  $[4\text{Fe-4S}]^{2+}$  cluster (Figure 40). In the three structures, the three molecules fitted well to omit  $F_{\text{obs}} - F_{\text{calc}}$  electron density maps calculated with phase information from refined models (Figure 41).

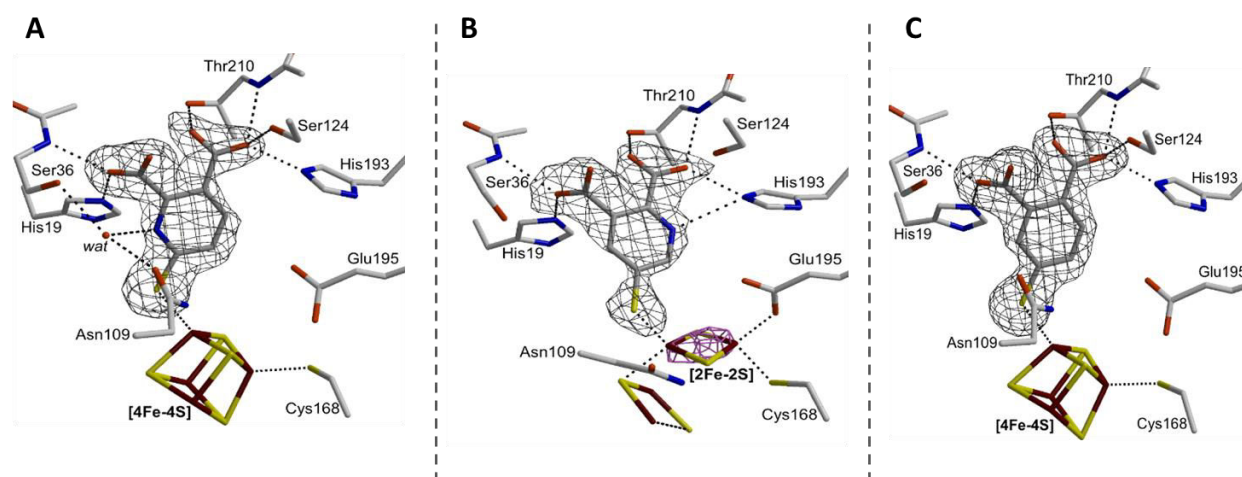


**Figure 41:** Electron density ( $F_{\text{obs}} - F_{\text{calc}}$ ) omit maps for three NadA-bound molecules. **A.** 6MPDC. **B.** 5MPDC and **C.** 4MP. The omit maps are indicated with a black mesh contoured at 4.0 times their r.m.s. ( $\sigma$ ) level in **(C)** and  $3.5\sigma$  in **(A)** and **(B)**. In **(B)** an anomalous difference map shown in pink and contoured at  $3.5\sigma$  indicates that the  $[4\text{Fe-4S}]$  cluster has been converted to a relatively well-defined 100% occupied  $[2\text{Fe-2S}]$  cluster.

All NadA-complexes display similar interactions with *Tm*NadA\*Y21F enzyme. In all cases, carboxylates of the three molecules interact with active site amino acids from three different protein domains: His19 and Ser36 (domain 1), Ser124 (domain 2) and His193 and Thr210 (domain 3), like QA and the reaction intermediates **W**, **X** and **Y** do<sup>138,139</sup>. In addition, the three molecules are coordinated to the catalytic iron of the  $[4\text{Fe-4S}]^{2+}$  through their thiol moiety and they present Fe-S distances of 2.3, 2.5 and 2.2 Å for 6MPDC, 5MPDC and 4MP, respectively.

It can be observed that there is no binding between the cluster and the nitrogen atom of the ring of 6MPDC and 5MPDC, as it was the case in two reported QA-bound NadA structures where the nitrogen and its neighboring carboxylate coordinate the catalytic iron site<sup>138,214</sup>. This is in agreement with our Mössbauer spectroscopy data that excluded a pentacoordination of the catalytic iron in the presence of any of the four molecules.

Structures of *TmNadA*\*Y21F-**4MP** and *TmNadA*\*Y21F-**6MPDC** (Figures 41A and 41C) were superposed for comparison (Figure 42A). We observed that the two structures are quite identical. The *TmNadA*\*Y21F-**6MPDC** complex has an additional hydrogen bond between the nitrogen of the pyridine from 6MPDC and a water molecule which at the same time forms another hydrogen bond with Ser36 and Asp109. This likely helps stabilizing the complex (Figure 42A).

The superposition of *TmNadA*\*Y21F-**5MPDC** to any of the other two structures leads to the observation of some differences (Figure 42B). In fact, in the *TmNadA*\*Y21F-**5MPDC** complex (Figure 41B) there is a hydrogen bond interaction between the nitrogen atom of the pyridine ring with His193. This way, the thiol from 5MPDC coordinates the catalytic iron site of the cluster. If we compare it to the structure with 6MPDC, we find that the pyridine ring is 180° rotated. Because of this rotation, the sulfur group in 5MPDC shifts by 2.1 Å on the enzyme active site (Figure 42B), inducing an important structural constraint for iron binding that leads to cluster degradation. An anomalous difference map calculated for the 5MPDC complex suggests that the cluster degradation involves the formation of a  $[2\text{Fe}-2\text{S}]^{2+}$  form in which one Fe is bound to the thiol of 5MPDC and the other to the carboxylate of Glu195.

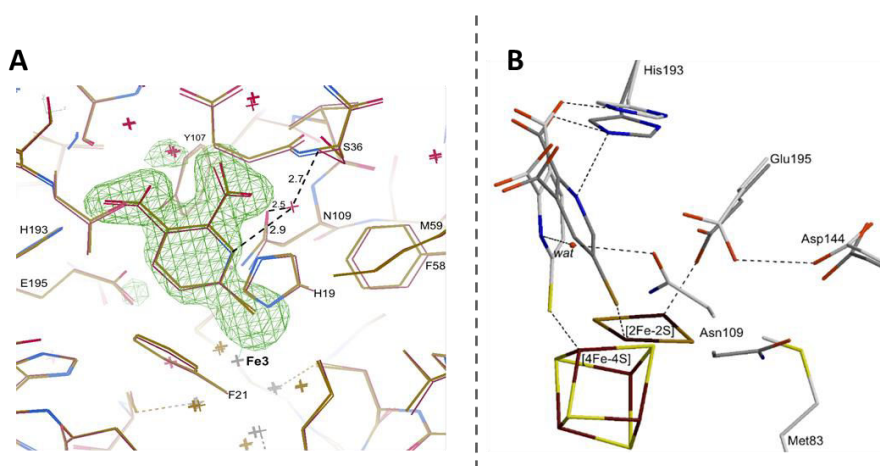


**Figure 42:** **A.** Superposition of electron density ( $F_{\text{obs}}-F_{\text{calc}}$ ) omit maps of *TmNadA*\*Y21F-**4MP** and *TmNadA*\*Y21F-**6MPDC**. The omit maps are indicated with a green mesh contoured at  $3.5\sigma$ . **B.** Stereo image of superposition of 6MPDC (white carbons) and 5MPDC (grey carbons) complexes in an approximately perpendicular view related to Figure 41, highlighting residues with significantly different conformations. Only  $[2\text{Fe}-2\text{S}]^{2+}$  fragment is shown in the *TmNadA*\*Y21F-**5MPDC** complex.

#### IV. Specificity

For DTHPA, we have shown that it is not a specific inhibitor of NadA *in cellulo* at high concentrations (above 20  $\mu\text{M}$ ) likely inhibiting other essential pathways (introduction)<sup>141</sup>. In order to evaluate DTHPA specificity *in vitro*, we tested it on the Aconitase B (AcnB) enzyme, a Fe-S enzyme model for the reasons explained in the Annex I. Aconitase activity was measured anaerobically by a coupled reaction involving the NADP(H) dependent isocitrate dehydrogenase enzyme, and monitoring the NADPH formation (see Materials and Methods). Fe-S AcnB enzyme was prepared by Sandrine Ollagnier.

While 1 equivalent of DTHPA inhibited 50 % of NadA activity<sup>141</sup>, it took 5 equivalents of DTHPA to inhibit 50 % of AcnB activity (Figure 43, black bars). When NadA and AcnB were incubated in a 1:1 ratio in the presence of increasing amounts of DTHPA, we observed 30 % inhibition of AcnB activity for 20 equivalents of DTHPA (Figure 43, grey bars). All together, these results show that DTHPA is able to inhibit AcnB, even though it is more specific to NadA, explaining partly *in cellulo* results.

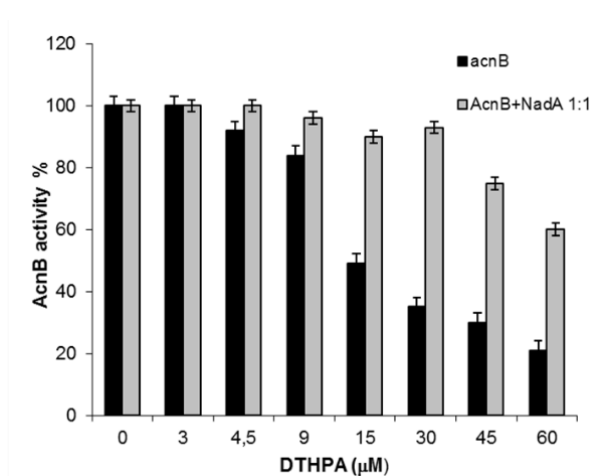


**Figure 43:** *In vitro* AcnB activity. Black bars: in the presence of increasing amounts of DTHPA; grey bars: in the presence of NadA enzyme (1:1 ratio) and increasing amounts of DTHPA. AcnB: 3  $\mu\text{M}$ ; NadA: 3  $\mu\text{M}$ .

The same *in vitro* experiment was used to evaluate the specificity of the four NadA inhibitors (6MPDC, 5MPzDC, 6MPDC and 4MP).

We observed that 6MPDC (Figure 44A) does not inhibit AcnB activity until 5 equivalents and more than 90 % of the enzyme activity remained in the presence of 10

equivalents. However, 50 % of AcnB activity was inhibited at 20 equivalents and at the highest concentration used, 50 equivalents, 60 % of activity was inhibited.

Concerning 5MPzDC, (Figure 44B) more than half of the enzyme activity was inhibited at 10 equivalents and no activity at all remained using 50 equivalents.

In the case of 5MPDC (Figure 44C) and 4MP (Figure 44D), no inhibition of AcnB was observed using 50 equivalents.

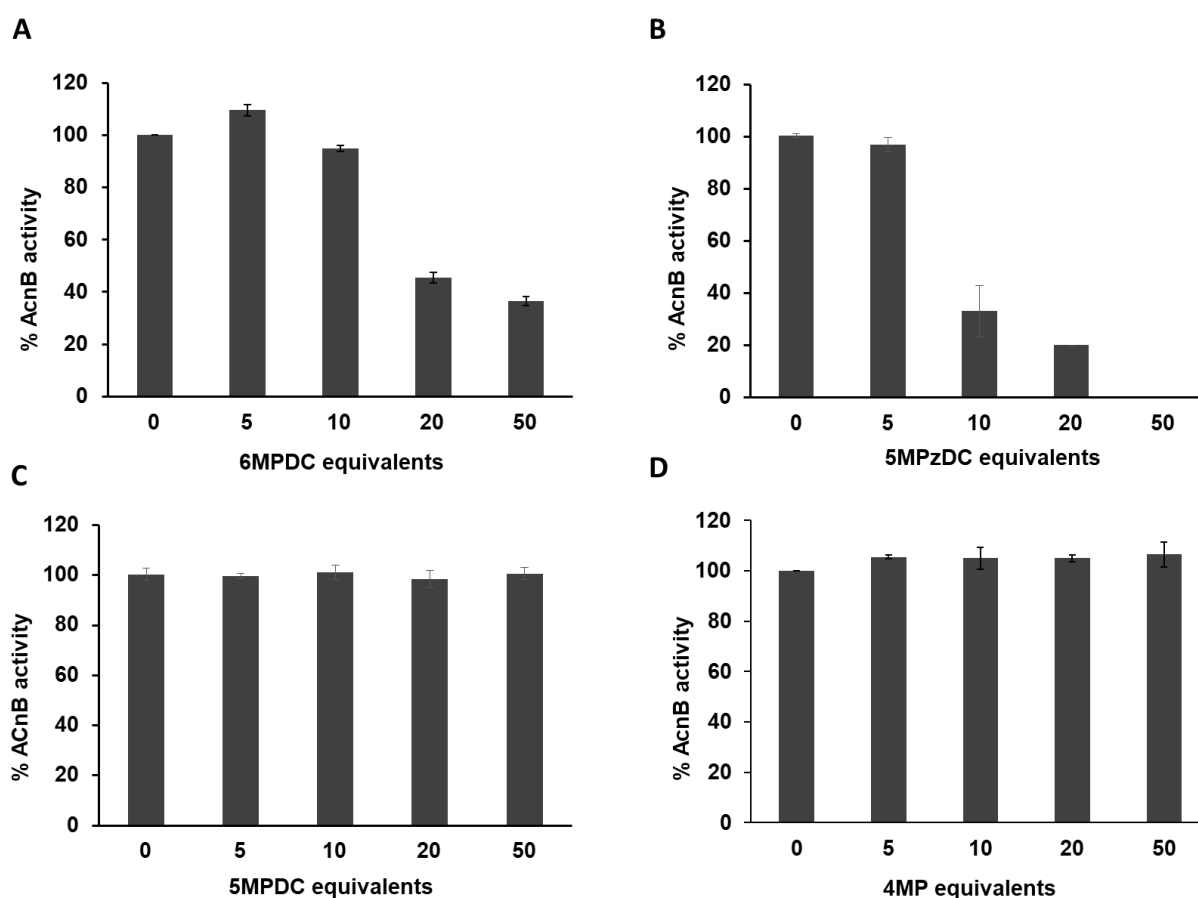


**Figure 44:** Aconitase B activity (%) in the presence of increasing amounts of 6MPDC (A), 5MPzDC (B), 5MPDC (C) and 4MP (D) (0-50 equivalents). AcnB was used at 3  $\mu$ M.

These results show that out of the four NadA inhibitors, two molecules, 5MPDC and 4MP, are likely specific towards our NadA target enzyme. It is noteworthy that even if 6MPDC and 5MPzDC inhibit AcnB activity, the inhibition starts at high concentrations of the molecules (at 10 equivalents for 6MPDC and at 5 for 5MPzDC), whereas in the case of

DTHPA, at 1.5 equivalents, some AcnB inhibition could already be observed. Thus, 6MPDC and 5MPzDC are likely not specific at high concentrations but at low concentrations are more specific than DTHPA.

With the aim of further studying and understanding the inhibition specificity of the four NadA inhibitors, we decided to perform a more exhaustive and fine UV-visible spectroscopy analysis with our collaborator Jean-Marc Latour (LCBM, PMB, Grenoble). For this, we selected 6MPDC which inhibits AcnB activity and 4MP which does not.

We recorded spectra of Fe-S NadA, Fe-S AcnB and apo AcnB at low concentration in order to be under non-saturating conditions. Indeed, for deconvoluting UV-spectra and be able to perform subtractions, the UV-visible spectra must not be saturated. A concentration of around 10  $\mu\text{M}$  of enzyme was chosen.

Addition of 5 equivalents of 4MP to the three proteins (Fe-S NadA, apo and Fe-S AcnB) did not give clear-cut spectroscopic changes (Figure 45, main graphs). However, a close examination of the proteins spectra with and without 4MP revealed a small but significant modification in the case of Fe-S NadA; a substantial shoulder in the range 300-330 nm (Figure 45C, main graphs). This is absent in AcnB samples (Figure 45A and 45B, main graphs). That this effect is real is supported by the observation of the difference between the spectra of 4MP (5 eq.) and those from the subtraction of “(protein + 4MP) - protein” spectra, which show a significant shift of the absorption maximum (ca 300  $\text{cm}^{-1}$ ) that is absent for AcnB samples (Figure 45, inserts).

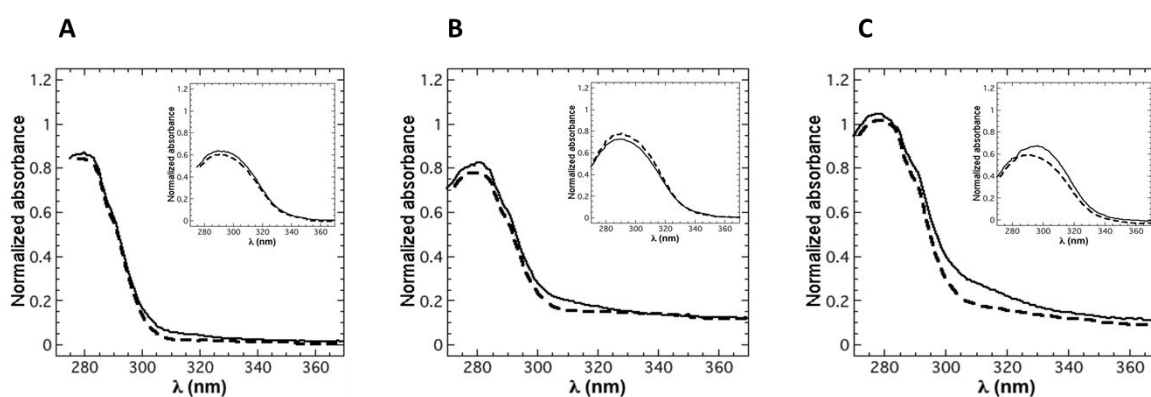


**Figure 45:** Panels (A-C) present the respective UV-visible spectra of proteins ApoAcnB (A), Fe-S AcnB (B) and Fe-S NadA (C) in absence (dotted line) and presence of 5 eq of 4MP (solid line). Insets represent the comparison between the spectrum of 4MP (5 eq) (dotted line) and the subtraction of the spectra “(protein + 4MP) - protein” (solid line).

To analyze the interaction of Fe-S NadA with 4MP, the data were treated as absorbance vs energy and the absorption maxima were simulated with a gaussian function to obtain a precise estimation of the absorption maximum (Figure 46). The values of the maxima are gathered in Table 9 and a close examination of the table revealed that for the three determinations of free 4MP and 4MP in presence of Fe-S and apo AcnB, the absorption maxima were at  $34.403 \pm 80 \text{ cm}^{-1}$ . By contrast, a ca  $400 \text{ cm}^{-1}$  difference in the energy maxima was observed in presence of Fe-S NadA which supports the occurrence of an interaction between 4MP and the protein cluster.

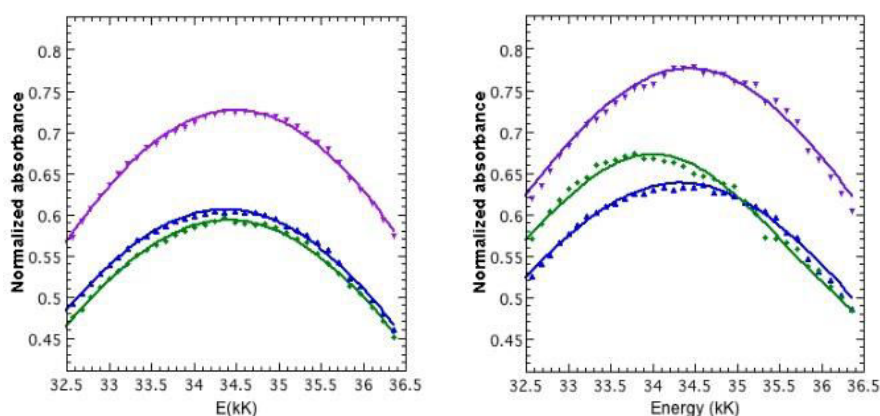


**Figure 46:** Experimental UV-visible spectra (dots) and gaussian simulations (solid lines) of 4MP in absence (left) and in presence (right) of proteins: apo AcnB (blue), Fe-S AcnB (violet) and Fe-S NadA (green).

	4MP	4MP + protein	Energy difference
Fe-S AcnB	34.482	34.434	0.048
Apo AcnB	34.367	34.326	0.041
Fe-S NadA	34.405	34.010	0.395

**Table 9:** Energies of the absorption maxima of solutions of 4MP (5eq.) in absence and in presence of protein (10-12  $\mu\text{M}$ ). Energies are given in kiloKaiser; 1 kK =  $1\,000 \text{ cm}^{-1}$ .

The modification on the UV-visible spectrum produced by 4MP in the case of Fe-S NadA, absent in AcnB samples, confirms the specificity of 4MP for NadA inhibition and also that the inhibition likely occurs through coordination to the  $[4\text{Fe-4S}]^{2+}$  cluster.

Addition of 5 equivalents of 6MPDC to Fe-S AcnB and Fe-S NadA induced a new absorption band close to ca 350 nm with similar intensity. It is noteworthy that 6MPDC

exhibits two absorption bands in the same region (300 and 360 nm) albeit with lower intensity. Surprisingly, the same band appeared on adding 6MPDC to apoAcnB, which rules out that it originates from binding of 6MPDC to the [4Fe-4S] cluster, suggesting that the interaction of 6MPDC occurs with the protein backbone (Figure 47).

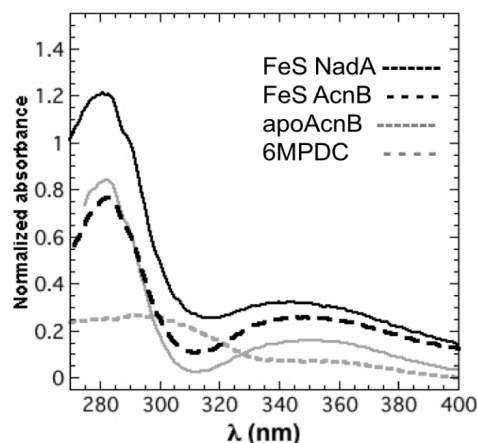


**Figure 47:** Experimental UV-visible spectra of Fe-S NadA, Fe-S AcnB and ApoAcnB (10-12  $\mu\text{M}$ ) in the presence of 6MPDC (5 eq.) and 6MPDC alone (5 eq.).

A similar treatment (as for 4MP) of the data obtained with 6MPDC failed to reveal a specific interaction with the Fe-S clusters (either NadA or AcnB clusters). These results are in agreement with inhibition assays which show that 6MPDC is non-specifically interacting with both NadA and AcnB.

## V. Discussion

A single NadA inhibitor had been described and studied before my Ph.D: DTHPA<sup>141</sup>. With an  $\text{IC}_{50}$  value of 10  $\mu\text{M}$  (for 10  $\mu\text{M}$  of enzyme), the inhibition mechanism has been well studied and understood<sup>141</sup>. However, despite its promising inhibitory effect it was shown to be not specific of NadA *in cellulo* at concentrations above 20  $\mu\text{M}$  and preliminary *in vitro* experiments demonstrated that it inhibits another [4Fe-4S]<sup>+2</sup> containing enzyme, the aconitase B from *E. coli*. This non-specificity was attributed to the presence of its neighboring thiols that likely chelate metal ions from other enzymes (Fe-S enzymes with catalytic Fe site such as aconitase; Zn enzymes; Cu enzymes; ...). In this context, we decided

to assay 4MP, a DTHPA derivative that contains only one thiol group. We also designed, synthesized and assayed as potential specific NadA inhibitors three other analogs of DTHPA (6MPDC, 5MPzDC and 5MPDC) that contain also a single thiol group but also one or two nitrogen(s) atom(s) in their ring.

The four molecules (4MP, 6MPDC, 5MPzDC and 5MPDC) were assayed on NadA activity *in vitro*. We found out that three of them (6MPDC, 5MPzDC and 5MPDC) inhibit NadA activity with  $IC_{50}$  values between 30 to 45  $\mu$ M (for 10  $\mu$ M of enzyme). None of them displayed an inhibitory effect as strong as that of DTHPA, but on the other hand, the  $IC_{50}$  values are on the same range of tens of  $\mu$ M. Surprisingly, we reproducibly found that 4MP, the only molecule with a benzenic ring, has an  $IC_{50}$  value of 13  $\mu$ M, being the best inhibitor of the family. This way, 4MP displays an inhibitory power similar to that of DTHPA (10  $\mu$ M). Thus, although the addition of a nitrogen (or two) to the aromatic ring mimics better intermediates (with regard to DTHPA), this does not improve the inhibitory power of the molecules.

#### a. NadA inhibition mechanism

To study a protein inhibition by a molecule and understand the inhibition mechanism, the determination of the inhibition constant ( $K_i$ ) and the type of inhibition (reversible (competitive, noncompetitive, and uncompetitive) or irreversible) are the typical parameters to get. However, in our case, determining such parameters is extremely complicated for the following reasons: 1/ NadA has two substrates; 2/ one of the substrates, iminoaspartate, is highly unstable and therefore has to be produced continuously *in situ* by L-aspartate oxidase (NadB) using large amounts of L-aspartate (10 mM). For these reasons, we couldn't determine such parameters for our inhibitors.

However, in order to get some information concerning the inhibition by the 4 molecules we thought about determining  $K_d$  value for our inhibitors on NadA. We were not equipped anaerobically on the laboratory with ITC or BLI devices and we couldn't perform such experiments. Therefore, we used some spectroscopies and X-ray crystallography to get some information that could explain  $IC_{50}$  values. UV-visible absorption spectroscopy and Mössbauer spectroscopy have allowed the non-ambiguous characterization of NadA

inhibition mode by DTHPA<sup>141</sup> and we could expect the same with 4MP, 6MPDC, 5MPzDC and 5MPDC molecules.

All four inhibitors contain a single thiol which was designed with the aim of interacting specifically with the catalytic iron site of NadA and not with other metalloenzymes. However, the presence of a single thiol could make the interaction of the molecules with the catalytic iron site of NadA cluster weaker than in the case of a dithiol (DTHPA). This is probably what happens since the studies of the molecules with NadA cluster using spectroscopies were not conclusive. Indeed, we were not able to clearly prove nor exclude an interaction of the molecules with the cluster. UV-visible spectroscopy did not show clear changes on NadA spectrum in the presence of 5 equivalents of the four different molecules. Having the free molecules in solution, that absorb also in the UV-visible region made it even harder to find on the spectra significant changes associated to the cluster. Even using circular dichroism we couldn't make a clear discrimination towards an interaction or a lack of interaction of the molecules with NadA since very slight or subtle changes were observed. Mössbauer spectroscopy allowed us to get some important information: (i) molecules do not degrade the  $[4\text{Fe-4S}]^{2+}$  cluster and (ii) the geometry around the catalytic iron does not change, remaining tetracoordinated. The Mössbauer parameters can fit with a tetracoordination by either 4 sulfur atoms (3 cysteines from the protein and one thiol from the inhibitor) or 3 sulfur and 1 oxygen atoms (from the 3 cysteines of the protein and the water molecule). Therefore, like other spectroscopies, Mössbauer spectroscopy couldn't demonstrate neither exclude an interaction of inhibitors with the NadA Fe-S cluster.

Structures of NadA in complex with 3 inhibitors were obtained after having performed spectroscopic studies. Structures of 6MPDC, 5MPDC and 4MP in complex with *TmNadA*\*Y21F variant showed that the molecules interact similarly on NadA active site through the coordination of the catalytic iron site of the cluster via their thiol group.

Therefore, X-ray crystallography demonstrated that the presence of nitrogen(s) in the ring and its position with regard to the thiol are not key factors for inhibition since the thiol always points towards the catalytic iron, no matter in which position it is and if nitrogen(s) is(are) present. Even though the nitrogen atom provides extra interactions in the active site of NadA (6MPDC, 5MPDC compared to 4MP) they are not crucial for inhibition. This suggests that the interaction between the catalytic iron and the thiol of the different molecules is the

guiding force for the positioning of the molecules in the active site along with the interactions of the carboxylates, which help anchoring the molecules in the active site and stabilizing them (through interactions with Ser36, His19, Thr210, Ser124 and His193).

X-ray structures showed that all molecules bind Fe-S cluster similarly, but they don't explain us the difference in the  $IC_{50}$  values that we obtained in solution. The observed difference between 4MP and 6MPDC ( $IC_{50}$ : 13  $\mu$ M for 4MP and  $IC_{50}$ : 40  $\mu$ M for 6MPDC) could be related to the existence of a thiol-thione equilibrium in solution in the case of 6MPDC. We expect a thione to be less coordinating than a thiol, resulting on a weaker interaction with the iron.

4MP and 5MPDC, none of both exist in the thione form but their  $IC_{50}$  values are quite different ( $IC_{50} = 13 \mu$ M and  $IC_{50} = 45 \mu$ M, respectively). As it was observed in the *TmNadA*\*Y21F-**5MPDC** crystal structure, 5MPDC fits worse on the active site, with the thiol group 2.1 Å shifted with regard to 4MP structure (Figure 42). This could be at the origin of a less efficient inhibition and thus of a higher  $IC_{50}$  value.

Concerning the structure of *TmNadA*\*Y21F-**5MPDC** complex, a degradation of the cluster was observed. The cluster degradation may be a relatively slow process, since no  $[4Fe-4S]^{2+}$  cluster conversion or degradation was observed in the short time scale of minutes in Mössbauer, UV-visible or circular dichroism studies. Inhibition studies are performed under similar conditions (20 min) and therefore, we believe that the *NadA* inhibition by 5MPDC cannot be due to cluster degradation.

To conclude, X-ray crystallography demonstrated the binding of all inhibitors on the iron catalytic site of the cluster; that is likely at the origin of the inhibition of *NadA* activity. However, X-ray didn't allow us to explain the difference in the  $IC_{50}$  values; but note that crystallization was performed under different conditions, at high concentration of protein and without substrates.

## b. Specificity

Our chosen model enzyme in order to test the specificity was *AcnB* for the reasons explained in the Annex I. We thought about using other  $[4Fe-4S]$  containing enzymes with a catalytic and available iron site such as Radical-SAM enzymes<sup>215,216</sup>. However, these enzymes

are redox [4Fe-4S] enzymes that use S-adenosylmethionine cofactor and a reducing agent to perform a radical chemistry. We believed that the use of such systems would have complicated analyses of the results and lead to artifacts. Using AcnB, a non-redox [4Fe-4S] enzyme, we showed that DTHPA *in vitro* inhibits Fe-S AcnB since 1.5 equivalents, confirming *in cellulo* data. DTHPA is not a specific inhibitor of NadA. AcnB activity tests in the presence of the 4 molecules (4MP, 6MPDC, 5MPzDC and 5MPDC) revealed that 6MPDC and 5MPzDC inhibit AcnB at high concentrations whereas 5MPDC and 4MP don't inhibit it at all. UV-visible spectroscopy deconvolution was of great importance in this study since it has shown that 4MP interacts with Fe-S NadA specifically whereas 6MPDC does not. The deconvolution was not performed with the other two molecules for time constraints but we believe that 5MPDC should behave similarly to 4MP (both molecules were shown not to inhibit AcnB activity) and 5MPzDC similarly to 6MPDC (they both inhibit AcnB enzyme). 6MPDC and 5MPzDC that inhibit AcnB activity exist under a thiol-thione equilibrium (Chapter I). Therefore their thiols are considerably less coordinating than those of 5MPDC and 4MP and thus, their strongest interactions are likely not with the thiol group and therefore probably with the protein's backbone (holo-NadA, holo-AcnB, apo-AcnB), rather than with the cluster specifically. This is what UV-vis spectroscopy taught us with holoNadA, apoAcnB and holoAcnB. However, the structure of NadA\*Y21F-6MPDC complex shows that 6MPDC interacts with the Fe-S cluster of NadA. Currently, we have no explanation.

To conclude on this chapter dedicated to *in vitro* studies of NadA inhibitors, I would like to remind that our goal was to find new and specific NadA inhibitors. From these studies, two interesting candidates emerged: 5MPDC and 4MP.

## VI. 5MPDC and *TmNadA*\*

As part of our ongoing efforts to obtain crystal structures of NadA in the presence of the inhibitors, an unexpected result was obtained by crystallographers with NadA\* cocrystallized with 5MPDC. A structure of *TmNadA*\* was solved at 2.3 Å resolution. Surprisingly, in this structure there was no 5MPDC, but instead we could clearly see QA in the active site of *TmNadA*\* bound through its carboxylates to residues His193, Thr210, Ser36 and His19 and through its nitrogen to His193 (Figure 48). QA did not bind the [4Fe-4S] cluster. It was in a position completely different from the one previously observed where QA was bound as a bidentate to the catalytic Fe of the cluster through its nitrogen and the neighboring carboxylate<sup>140,214,138</sup>. In addition, in this new structure of NadA with QA, the amide fragment of Asn109 was missing and the [4Fe-4S] cluster appeared to be partially disrupted (Figure 48).

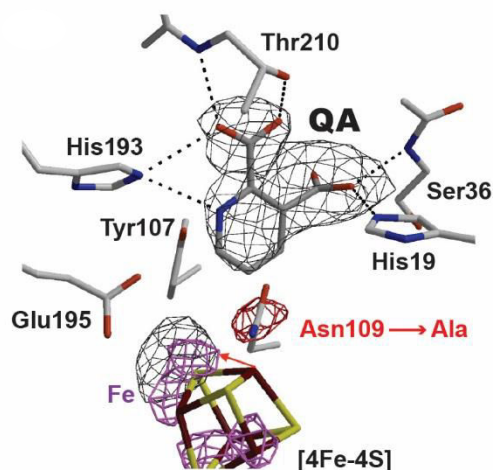


**Figure 48:** *TmNadA*-QA structure. Electron density ( $F_{obs} - F_{calc}$ ) omit map in the crystal structure of the *TmNadA*\*- 5MPDC-derived QA complex. The positive black mesh at the top of the figure has been modeled as QA, whereas the one at the bottom, and based on a coinciding peak in the anomalous scattering difference map (shown as a pink mesh), is thought to correspond to a Fe ion displaced from the [4Fe-4S] cluster. The negative red mesh in the center of the figure indicates the missing amide group of Asn109. The omit, the  $F_o - F_c$  around Asn109 and the  $\Delta_{anom}$  maps were contoured at  $3.3\sigma$ ,  $-3.3\sigma$ , and  $4\sigma$ , respectively.

To test whether the transformation of 5MPDC into QA might have been a crystallographic artifact or whether it might also occur in solution, *TmNadA*\* (430  $\mu$ M) and 5MPDC (3.5 equivalents) were incubated in the crystallization buffer and the formation of

QA was monitored every 2-5 days by HPLC (see materials and methods for more details). No QA was observed (at 12.8 min. on the HPLC chromatogram) for the first 25 days, but after 35 days, a small peak at 12.8 min., indicative of QA was detected by HPLC (Figure 49). After quantitation, the QA concentration corresponded to 1/100 of the NadA concentration and 1/330 of the initial 5MPDC equivalents. The control experiment without NadA did not produce any QA after 35 days. These data were in agreement with crystallographic ones and show that 5MPDC, can convert to QA in a long incubation time in the crystallization buffer (35 days in solution, 5 months in crystallography).

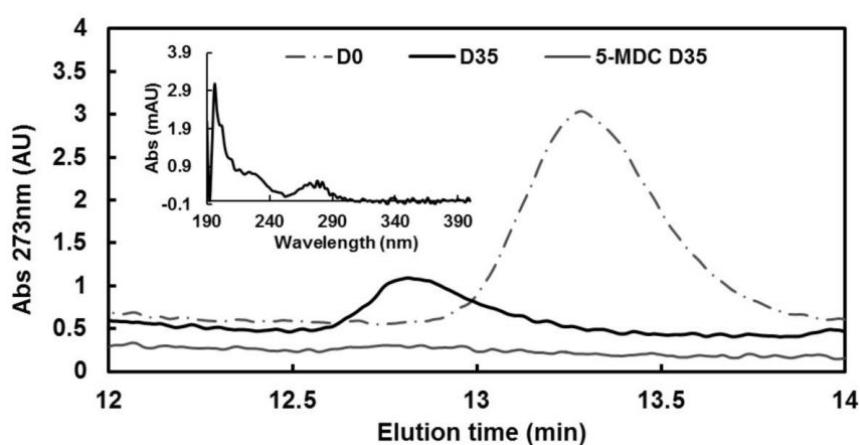
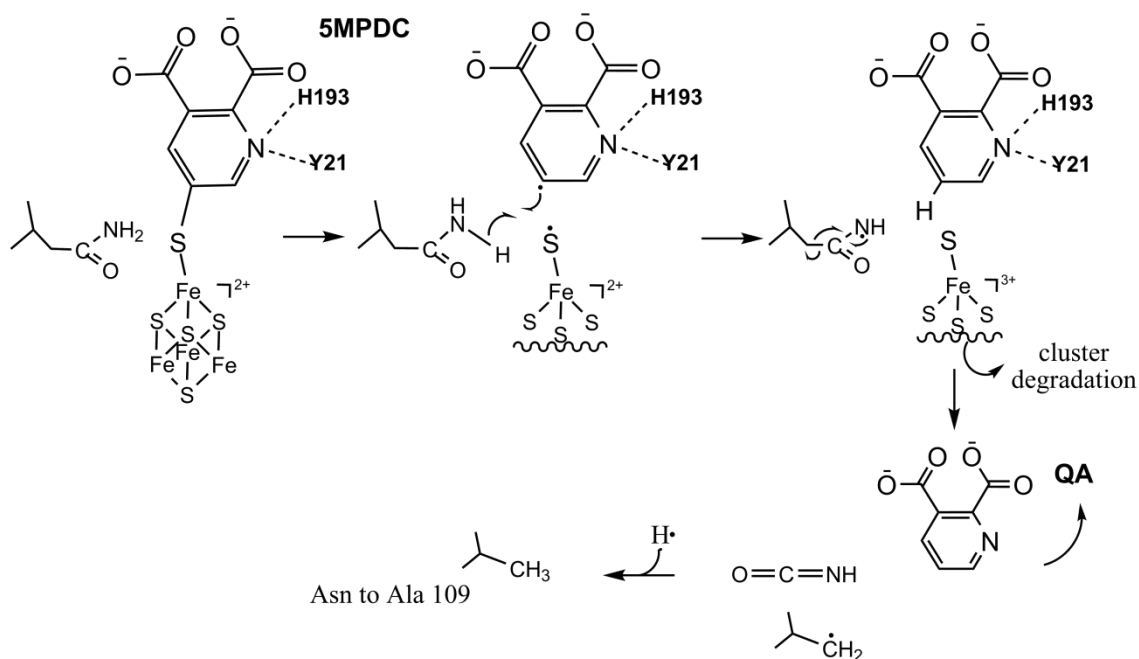


**Figure 49:** HPLC chromatograms (12-14 min) of *TmNadA*\*- **5MPDC** at day 0 (D0; dashed-dot line) and day 35 (D35; black line) and of the 5MPDC control without protein at D35 (gray line). The small peak at 13.3 min (dashed-dot line) corresponds to the CHES buffer. Insert: UV-visible spectrum of the peak eluted at 12.8 min for the D35 sample. See materials and methods for QA UV-visible spectrum.

We tried to confirm the conversion of Asn109 to Ala 109 by MS experiments but we did not see the expected peak. Nevertheless, relative to the total amount of added protein in the solution experiment the reacted fraction was small, which makes its detection difficult. We also considered the possibility that the reacted protein could have precipitated (due to the radical chemistry).

Conversion of 5MPDC to QA corresponds to the loss of the sulfur group of 5MPDC. A plausible explanation for the desulfurization reaction mechanism that must have generated QA from 5MPDC would be the homolytic cleavage of the 5MPDC's S-C bond followed by H atom abstraction from the amide group of Asn109 by the nascent QA radical (Scheme 42).

The resulting radical amide group will rearrange causing the cleavage of the Asn109 C $\beta$ -C $\gamma$  bond and the release of isocyanate. Finally, the generated Ala109 radical will abstract an H atom from a component of the solution. Conversely, the thiyl radical probably oxidizes the [4Fe-4S] cluster causing its observed changes that, however, cannot be unambiguously modeled (Scheme 42). Homolytic cleavage of an aromatic C-S bond while bound to a sulfur-metal cluster was already observed<sup>217</sup>.



**Scheme 42:** Proposed desulfurization reaction mechanism of 5MPDC at the TmNadA\* active site.

## a. Discussion

*TmNadA\** was cocrystallized with 5MPDC and the structure of the obtained crystals was solved. In this structure there is no 5MPDC within the active site in contrast with the recent structure of *TmNadA\**Y21F-5MPDC that we obtained (Figure 41B). Instead, a QA molecule was observed as well as a partial cluster degradation and a residual amino acid transformation, Asn109 to Ala. We proposed a desulfurization reaction of 5MPDC on *TmNadA* active site based on a similar example described in literature<sup>217</sup> that explains the missing amino acid fragment on NadA active site and the partial cluster degradation.

This structure was obtained with the *TmNadA\** enzyme in contrast to the described *TmNadA* structure in complex with **5MPDC** that was obtained with the NadA\*Y21F variant.

In addition, the *TmNadA*\*-QA structure was obtained during the first crystallization assays without optimized crystallization conditions and it took 5 months to obtain these crystals in contrast to the 10 days that were needed in general to grow *NadA*\*Y21F-5MPDC crystals. We believe that such process of QA formation from 5MPDC might be due to the long incubation time, in agreement with the results obtained from the experiment in solution where only after 35 days of incubation of *TmNadA*\* and 5MPDC, a small amount of QA was formed.

The new QA position within *NadA* active site is interesting in terms of understanding *NadA* mechanism. QA, the *NadA* product, now points at the tunnel that leads to the solvent medium and its position coincides with the equivalent fragment in **Y**, the last intermediate before QA formation in *NadA* mechanism (Figure 16). Although the desulfurization of 5MPDC and the dehydration of **Y** are not chemically related reactions both involve the loss of a ring substituent to produce QA (Figure 50).

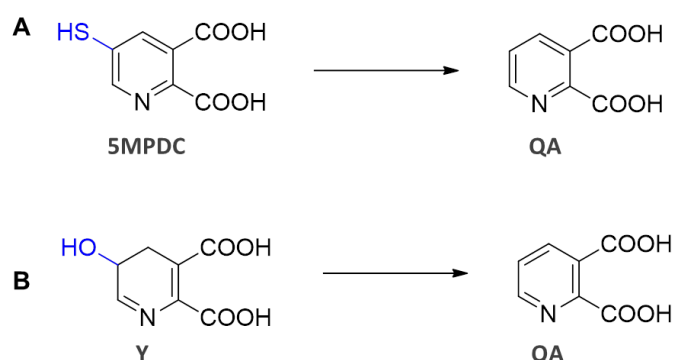


**Figure 50:** A. 5MPDC transformation to QA. B. Y transformation to QA.

The functional relevance of this new QA position is also supported by the reported crystal structure of a *TmNadA*\*Y21F-phthalate complex where this QA analogue occupies the same position as the *NadA* reaction product and establishes the same interactions with the protein, with only one exception due to the missing N atom in the phthalate ring<sup>139</sup>.

Finally, the previously observed QA position bound as a bidentate ligand to the [4Fe-4S] cluster was in a closed form of *NadA* and it was difficult to conclude about the release of the reaction product from the enzyme<sup>138</sup>. Based on our new result, we believe that the bidentate binding to the cluster does not belong in the catalytic sequence; instead it is an *in vitro* artifact caused by either an excess of added QA or crystal packing effects.

Thus, this new structure provided insights of NadA mechanism, more precisely, of the substrate release.

**RESULTS CHAPTER III:**  
***IN CELLULO*** INHIBITION STUDY  
**OF 6MPDC, 5MPzDC, 5MPDC**  
**AND 4MP**

## I. *E. coli* MG1655 as strain for *in cellulo* tests

For *in cellulo* assays we used the *E. coli* MG1655 strain. Unlike *H. pylori* and *M. leprae*, it contains a salvage pathway for NAD cofactor biosynthesis and therefore in this strain NadA is not essential<sup>141</sup>. However, *E. coli* MG1655 strain cultivated in minimal (M9) medium that is devoid of Na, Nm and QA is unable to use its salvage pathway and therefore mimics our pathogens *M. leprae* and *H. pylori* for which NadA is an essential enzyme. Indeed, an *E. coli* MG1655  $\Delta$ NadA strain in M9 is unable to grow (Figure 51). Addition of QA (1.4 mg/mL final concentration) can restore its growth (Figure 51). See Materials and Methods for further details.

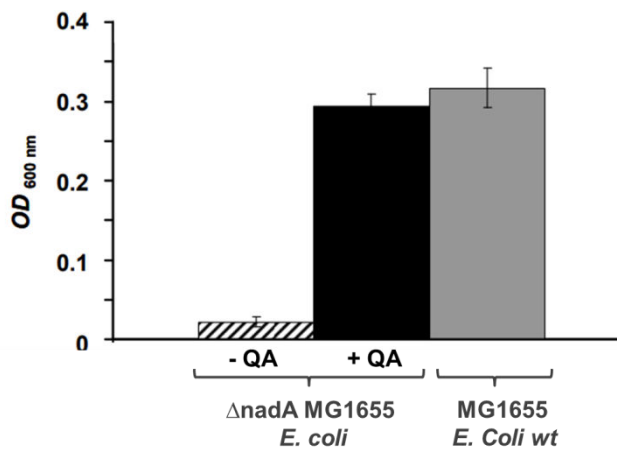


**Figure 51:** Growth of  $\Delta$ nadA MG1655 *E. coli* strain in M9 medium in the absence (hatched bar) and presence (black bar) of QA (1.4 mg/mL). Growth of the wild-type MG1655 *E. coli* strain in M9 is shown for comparison (grey bar).

These are the experimental conditions that we have used to test our inhibitors. *E. coli* MG1655 bacteria strain were cultivated in M9 in the presence of different concentrations of molecules (potential inhibitors). Duplicates were performed in the presence of QA. In case of inhibition of MG1655 growth (as for *E. coli* MG1655  $\Delta$ NadA strain) and if this inhibition is reversed by QA addition, that means that the molecule is an inhibitor of QA formation pathway (NadA and/or NadB enzymes). If the growth is not restored by addition of QA that means that the molecule has inhibited another pathway.

## II. *In cellulo* tests of the four NadA inhibitors: 6MPDC, 5MPzDC, 5MPDC and 4MP

We performed bacterial growth assays with the four inhibitors that were active *in vitro* on NadA enzyme (Figure 52).

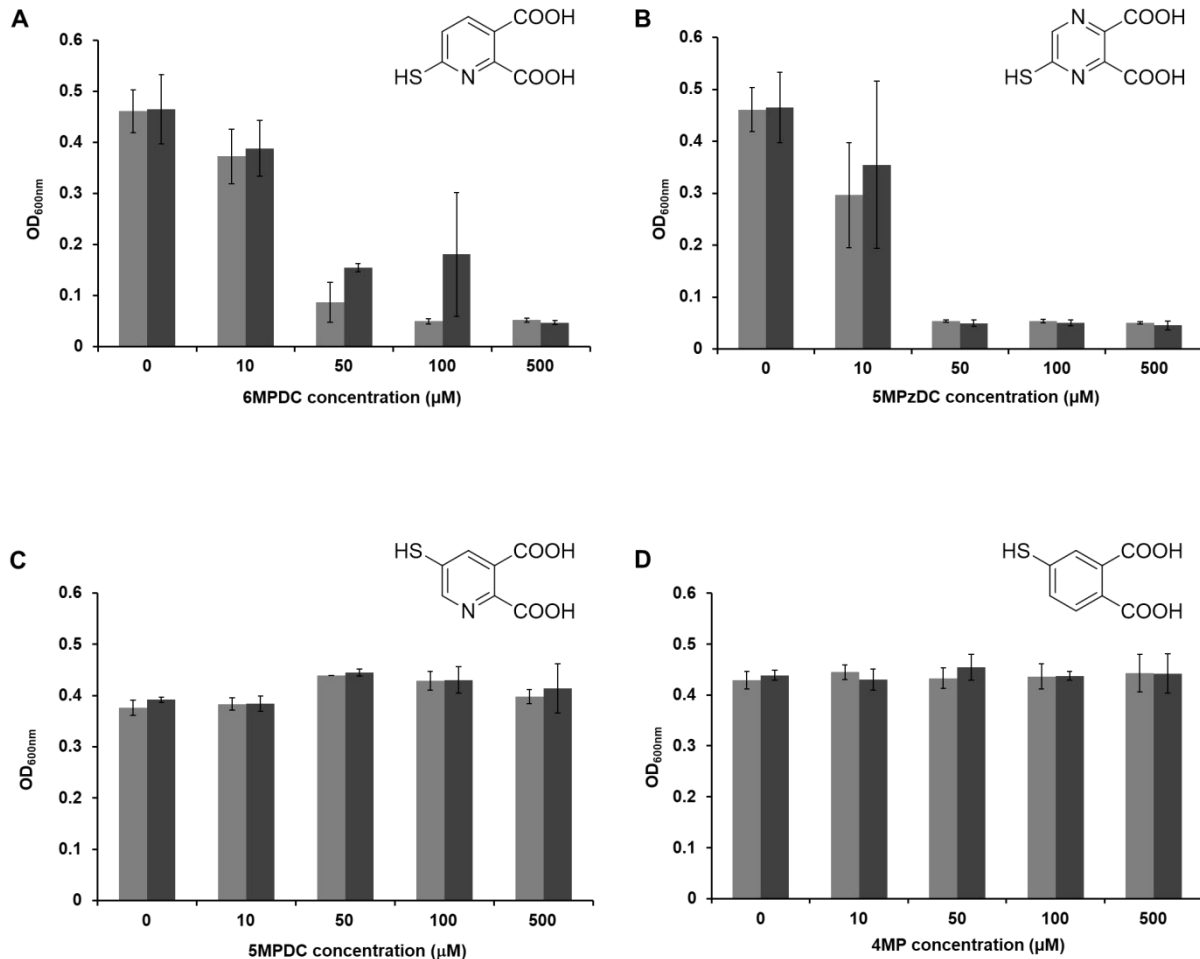


**Figure 52:** *E. coli* MG1655 growth in M9 in the presence of increasing concentrations of molecules with (dark grey bars) or without (light grey bars) QA (1.4 mg/mL). **A:** 6MPDC; **B:** 5MPzDC; **C:** 5MPDC; and **D:** 4MP.

Bacterial growth was inhibited at 10 μM of 6MPDC and 5MPzDC and a complete inhibition was observed using 50 μM of both molecules. In the case of 6MPDC, the bacterial growth was partially reversed by the addition of QA until 100 μM of 6MPDC whereas for 5MPzDC the addition of QA did not have any effect at any concentration of 5MPzDC. In contrast to 6MPDC and 5MPzDC, no inhibition of the bacterial growth was observed in the presence of 5MPDC and 4MP, even at the highest concentration tested (500 μM).

The fact that growth inhibition by 6MPDC and 5MPzDC is not reversed by the addition of QA strongly suggests that these two molecules inhibit other enzymes or other pathways than the QA pathway to which we are interested in. These results are in agreement with *in vitro* ones, where we observed that both 6MPDC and 5MPzDC inhibit NadA but also AcnB, another [4Fe-4S] enzyme (Annex I). For this reason, these two were not considered for further studies in our research on antibacterial drugs against NadA. In the case of 5MPDC and 4MP, we do not observe any *in cellulo* inhibition. This is surprising because they are NadA inhibitors *in vitro* with interesting IC<sub>50</sub> values (45 μM for 5MPDC and 13 μM for 4MP).

As explained in chapter I and discussed several times in chapter II, 5MPDC and 4MP contain easy oxidizable thiols. Since the growth assays were performed aerobically, it is possible that the lack of *in cellulo* activity of these two molecules could be due to their oxidation forming disulfide dimers unable to penetrate bacterial cell. Such oxidized molecules contain 4 carboxylates becoming extremely charged and bigger than the monomers, probably resulting in a weaker penetration or no penetration.

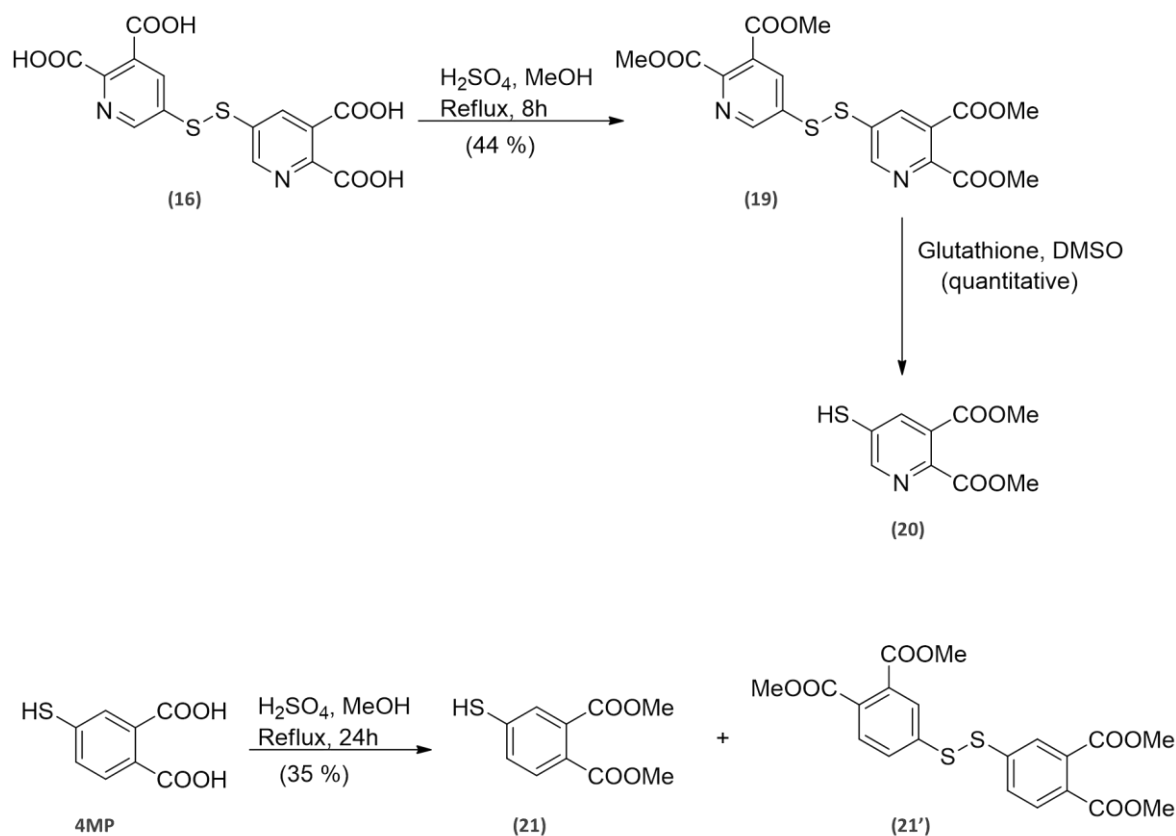
To test this hypothesis, we considered the three following approaches.

#### a. Esterification of the carboxylic acids

One of the considered approaches was to esterify the two carboxylic acids of both molecules 5MPDC and 4MP. There are examples in the literature (eukaryotic cells) where drugs containing carboxylic acid or alcohol functions have been transformed to esters forming prodrugs that once inside the cells are released in the active form thanks to the esterase activity<sup>218</sup>. This approach allows neutralizing the negative charges (carboxylates) of 4MP and 5MPDC and we expected that cell penetration of the resulting molecules should be considerably easier and that once inside the cells they will be delivered under the active form by esterase activity. In addition, even if the oxidation forming disulfide dimers is still likely to happen, it is known that within bacterial cells some enzymes and molecules like glutathione provide a reducing intracellular environment allowing reduction of the disulfide<sup>219,220,221</sup>.

Esterification of compound **16** was obtained after 24 h reflux in MeOH and H<sub>2</sub>SO<sub>4</sub>. The resulting compound **19** was reduced by glutathione allowing formation of the desired diester **20** (Scheme 43).

The same esterification conditions were used to esterify 4MP. The reaction yielded a mixture of the desired dimethylester **21** and its disulfide dimer **21'**. Compound **21** was isolated by column chromatography (Scheme 43).



**Scheme 43:** Synthesis of compounds **20** and **21**.

Then, compounds **20** and **21** were tested *in cellulo* on *E.coli* MG1655, as described previously (Figure 53).

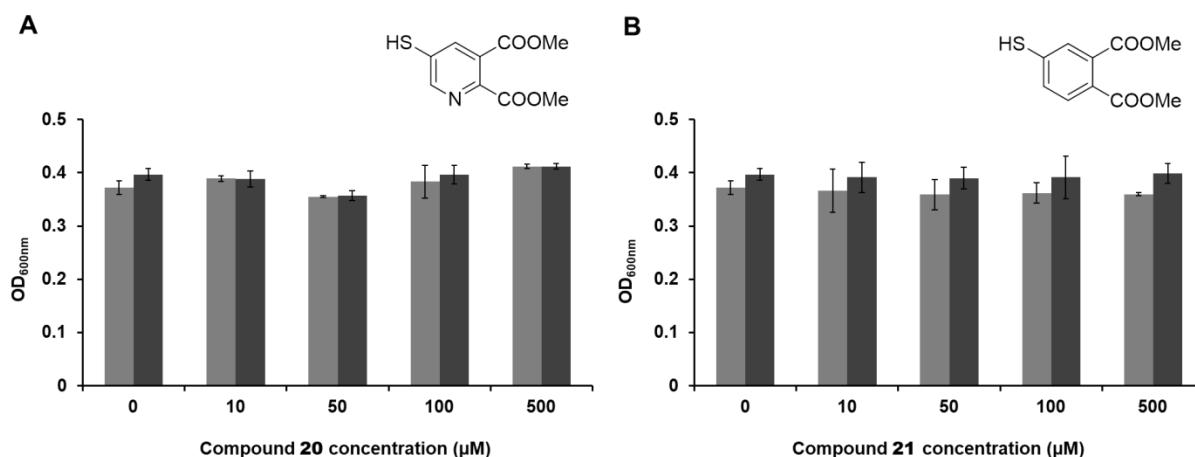


**Figure 53:** *E. coli* MG1655 growth in M9 in the presence of increasing concentrations of esterified molecules with (dark grey bars) or without (light grey bars) QA (1.4 mg/mL). **A:** esterified 5MPDC (compound **20**); **B:** esterified 4MP (compound **21**).

No effect was observed in the bacterial growth by any of the molecules **20** or **21**, even at very high concentrations (500 μM). Even longer incubation times (12 h and 24 h) did not lead to any inhibition of the bacterial growth. This can be due to a lack of penetration. However, we cannot exclude that molecules **20** and **21** penetrate bacterial cells but that esters were not removed and therefore that the molecules have no inhibitory action on NadA.

#### b. Test under anaerobic conditions

Another approach was to perform *in cellulo* tests under anaerobic conditions, inside a glove box. Indeed, if the lack of *in cellulo* activity of 5MPDC and 4MP is due to the bulky and very charged molecules as a consequence of their oxidation under aerobic conditions, we would expect that anaerobic conditions would avoid this and that we might observe an *in cellulo* activity of the molecules.

*E. coli* are facultative anaerobic bacteria, able to live under anaerobic conditions thanks to the fermentation metabolism<sup>222</sup>. Thus, bacteria should be able to grow and 5MPDC and 4MP should not oxidize under these conditions.

To start, we performed the bacterial growth assays in the presence of 0, 10 and 20 μM of DTHPA that inhibits the bacterial growth under aerobic conditions at 10 μM and

whose action is reversed by the addition of QA until 20  $\mu\text{M}$  (Figure 54). Addition of QA does not reverse the growth inhibition using higher concentrations of DTHPA (intro)<sup>141</sup>.

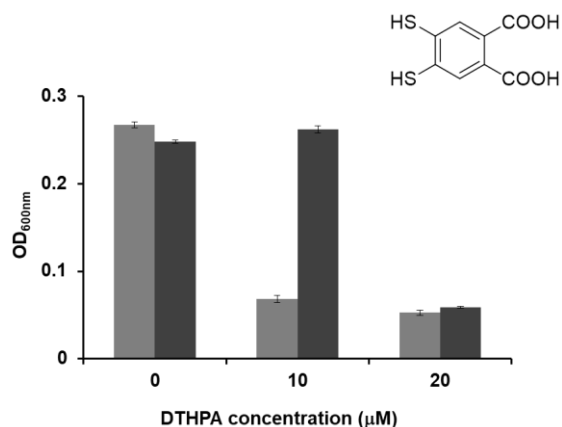


**Figure 54:** *E. coli* MG1655 growth in M9 under anaerobic conditions, in the presence of increasing concentrations of DTHPA ( $\mu\text{M}$ ) with (dark grey bars) or without (light grey bars) QA (1.4 mg/mL).

First, we observed that the OD at 600 nm of the culture without DTHPA under fermentation conditions is lower than that under aerobic conditions: 0.25-0.30 vs 0.40-0.50 under aerobic conditions. This is in agreement with the lower energy production during fermentation with regard to the aerobic metabolism which results on slower growth of the bacteria<sup>223</sup>. Second, inhibition of the bacterial growth by DTHPA was non-ambiguously observed and similar to the described one under aerobic conditions<sup>141</sup>. Thus, we proceeded to test 5MPDC and 4MP *in cellulo* under anaerobic conditions (Figure 55).

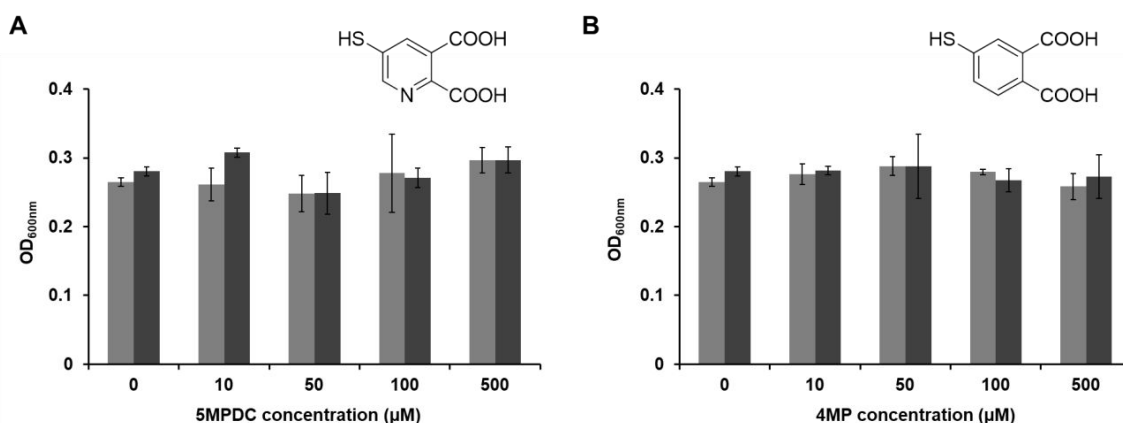


**Figure 55:** *E. coli* MG1655 growth in M9 under anaerobic conditions, in the presence of increasing concentrations 5MPDC (A) and 4MP (B) ( $\mu\text{M}$ ) with (dark grey bars) or without (light grey bars) QA (1.4 mg/mL).

We observed no effect of any of the two molecules even at high concentrations (500  $\mu\text{M}$ ).

Compounds **20** and **21** were also tested under fermentation conditions to study if avoiding the formation of disulfide dimers and having neutral compounds could lead to an *in cellulo* activity (Figure 56). However, no effect was observed for any of the two compounds **20** and **21** neither, even at 500  $\mu\text{M}$ . Once again, we don't know whether the lack of activity of the molecules *in cellulo* is due to a lack of penetration into the bacterial cells or whether the esters are not cleaved by esterases.

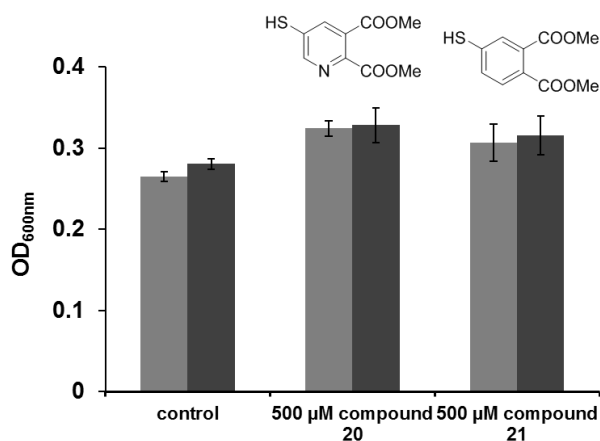


**Figure 56:** *E. coli* MG1655 growth in M9 under anaerobic conditions, in the absence and presence of 500  $\mu\text{M}$  esterified 5MPDC (**20**) and esterified 4MP (**21**) with (dark grey bars) or without (light grey bars) QA (1.4 mg/mL).

### c. Penetration and drug delivery strategy assisted by FR235222 simplified analogue

Another strategy consisted in assisting the cell penetration by a transmembrane carrier-by using compound **22** (Figure 57), a simplified analogue of the previously described natural product, FR235222 tetra-cyclopeptide (see introduction)<sup>224</sup>.

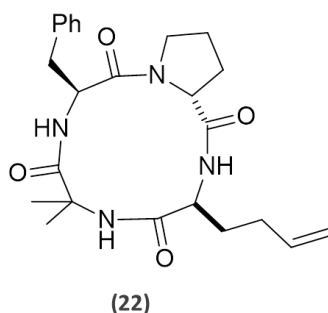


**Figure 57:** Compound **22**, analogue of natural product FR235222.

Compound **22** contains a final functionalizable olefin which is designed to allow the coupling of molecules. The used coupling should consist of a chemical bond, cleavable in intracellular media (by either enzymatic or non-enzymatic activity) allowing the release of the molecules on their active form once inside the cell (prodrug). According to this, we considered the following coupling strategies: (i) formation of an amide or ester/thioester bond through the carboxylic acids of 5MPDC and 4MP which should be cleavable by proteases or esterases/thioesterases<sup>225</sup>; (ii) formation of a disulfide bridge or a thioester through the thiol of 5MPDC and 4MP; the former should be cleavable by reducing agents in the cell such as glutathione, and the latter by thioesterase activity<sup>219,221,225</sup>.

A lot of examples are available in the literature concerning the disulfide bond approach, cleavable by the reducing conditions of the cytoplasm, especially by glutathione<sup>221,219</sup>. This is the strategy we chose for coupling 5MPDC and 4MP molecules to compound **22** (Figure 58).

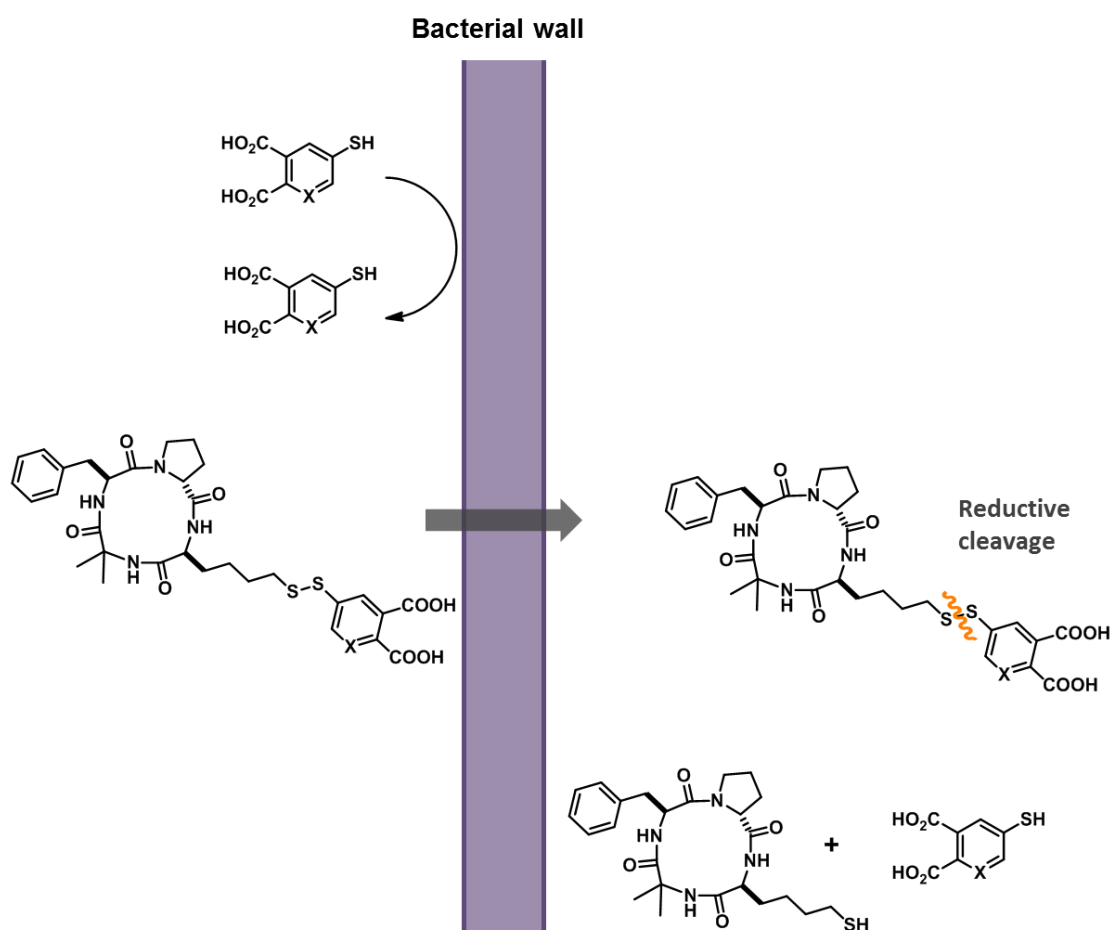
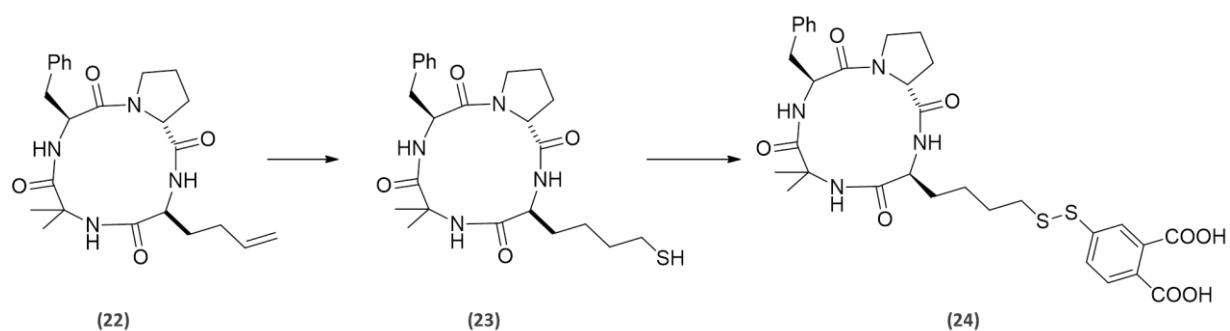


**Figure 58:** Strategy for cell penetration and drug delivery: disulfide bond cleaved by the reducing medium. X = N or C.

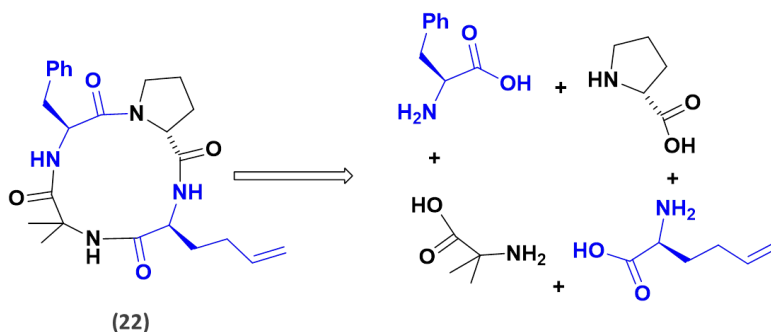
For this strategy, the olefin of compound **22** must be transformed into a terminal thiol, compound **23**. The coupling of the latter with 4MP allows to obtain the desired molecule **24** (Figure 44).



**Scheme 44:** Coupling of compound **22** with 4MP through intermediate **23** yields compound **24**.

(i) Synthesis of compound **22**

The synthesis of compound **22** was described in the DPM laboratory in 2013<sup>224</sup>. It derives from four amino acids (Scheme 45).



**Scheme 45:** The four amino acids forming compound **22**.

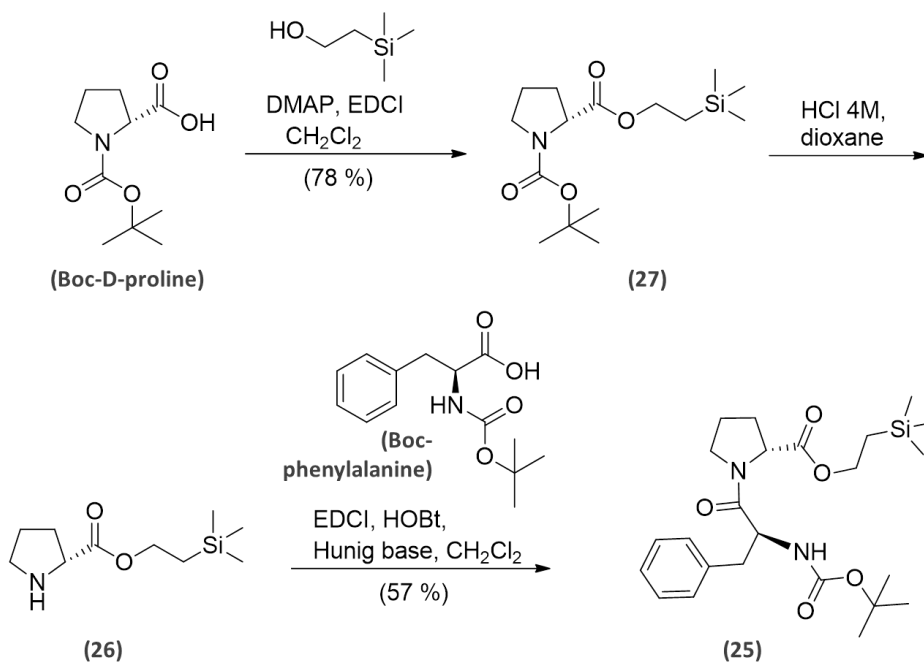
We explored a slightly modified synthetic pathway of compound **22** with regard to the literature<sup>224</sup>, by changing the protecting group of D-proline carboxylic acid from *tert*-butyl (*t*Bu) to trimethylsilyl ethyl (TMSE). In this way, a complete Boc strategy for the protection of the amine groups can be used all along the peptide synthesis, by deprotecting simply with 4 M HCl. In addition, we also changed the solvent (CH<sub>2</sub>Cl<sub>2</sub> instead of DMF) during the whole synthesis with regard to the described pathway in literature<sup>224</sup> that is DMF and involves long times of evaporation for treatment.

Below I report the linear synthesis of compound **22**, starting from Boc-D-proline and Boc-phenylalanine.

Synthesis of dipeptide **25**

Dipeptide **25** was obtained by a peptidic coupling of compound **26** with commercial Boc-phenylalanine.

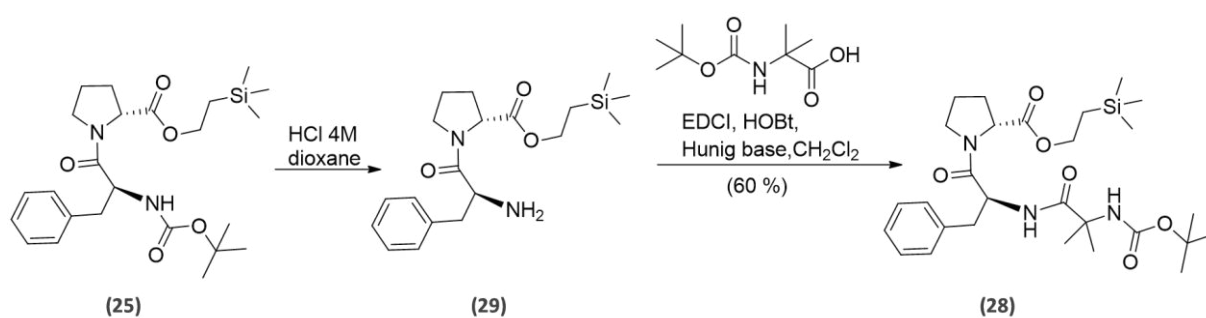
Compound **26** was obtained from commercial Boc-D-proline. Protection of the carboxylic acid of commercial D-proline with trimethylsilyl ethanol following a described synthesis yielded compound **27**<sup>226</sup>. After removal of the Boc protecting group to afford compound **26**, the condensation between **26** and Boc-phenylalanine allowed to obtain dipeptide **25** with 57 % of yield (Scheme 46).



**Scheme 46:** Synthesis of dipeptide **25** from Boc-D-proline and Boc-phenylalanine.

### Synthesis of tripeptide **28**

After the deprotection of the Boc of dipeptide **25** with HCl to obtain the free-amino dipeptide **29**, the coupling with commercial (Boc-amino)isobutyric acid allowed to obtain tripeptide **28** with 58 % of yield (Scheme 47).

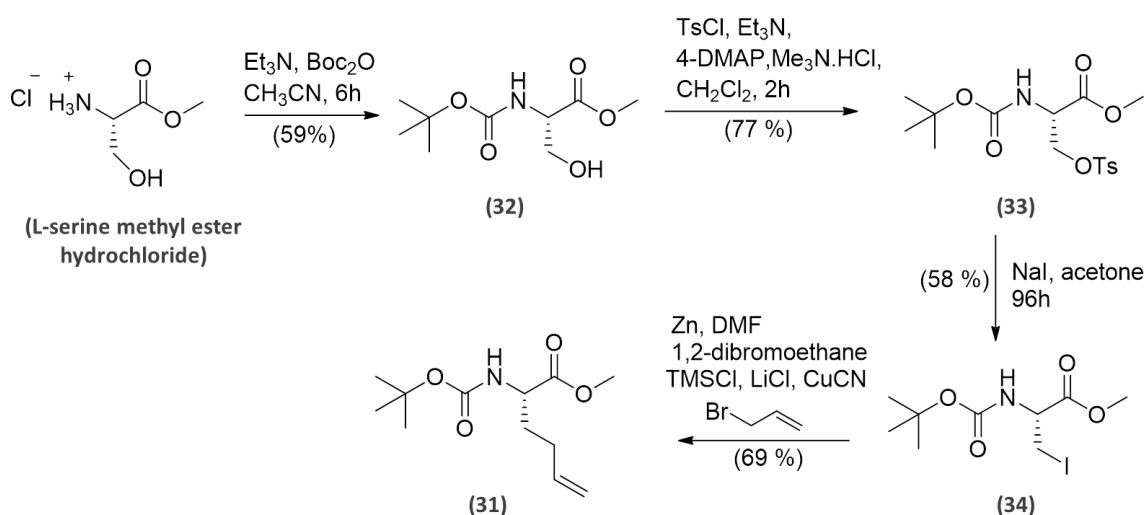


**Scheme 47:** Synthesis of tripeptide **28** from dipeptide **25** and (Boc-amino)isobutyric acid.

### Synthesis of the tetrapeptide **30**

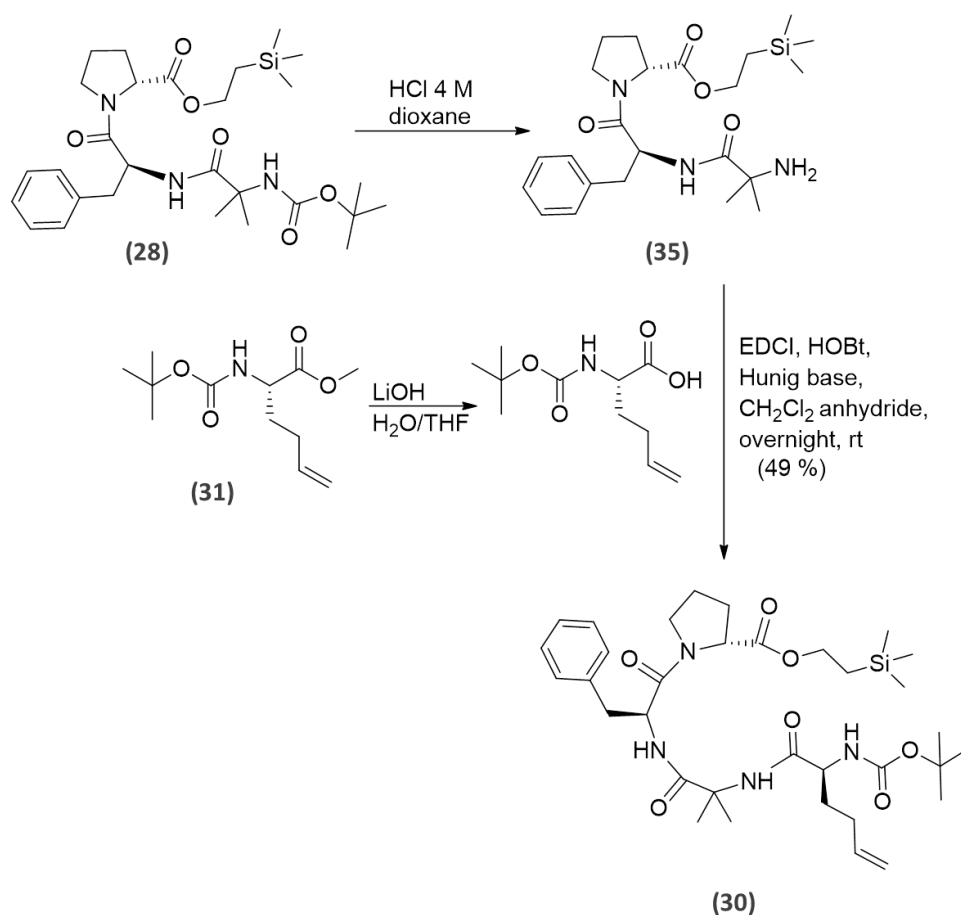
The linear tetrapeptide **30** was obtained by coupling tripeptide **28** with compound **31**.

Compound **31** was obtained in four steps from commercial L-serine methyl ester hydrochloride (Scheme 48). After protection of the amine group by Boc (**32**), the hydroxyl group was transformed into a tosyl group to form compound **33**. Tosyl being a particularly good leaving group, its substitution by an iodine using NaI is possible with 58 % yield to obtain compound **34**. The introduction of a Cu-Zn in the carbon-iodine bond of **34** renders that carbon a good nucleophile and it allows the nucleophilic attack to allyl bromide yielding compound **31** at 69 % (Scheme 48).



**Scheme 48:** Synthesis of compound **31** from L-serine methyl ester hydrochloride in four steps.

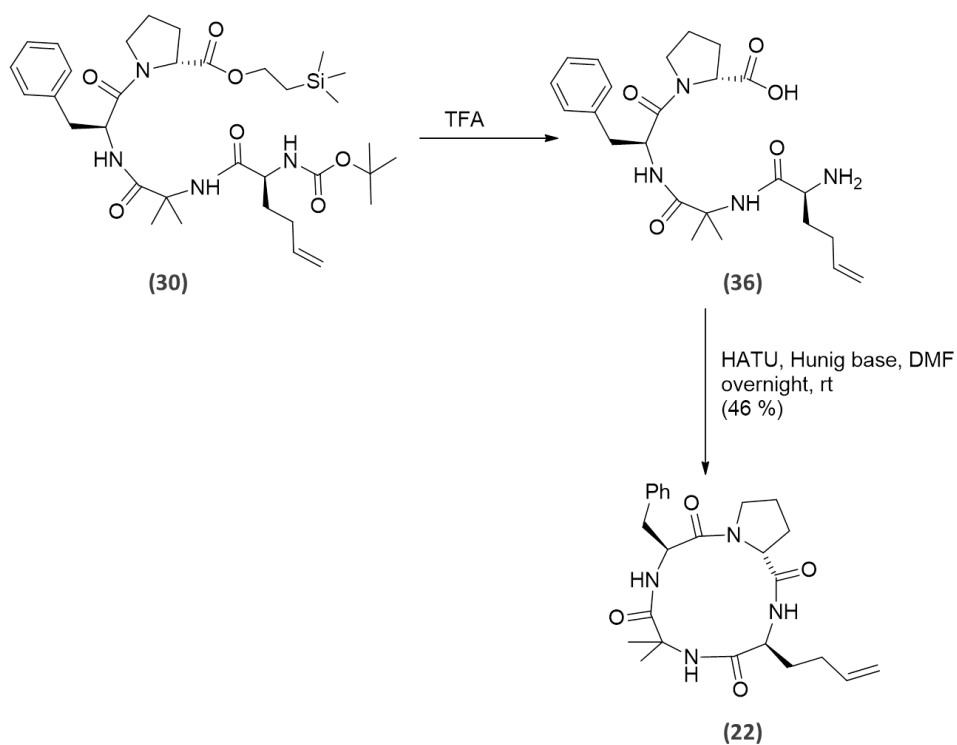
After deprotection of the carboxylic acid of compound **31** and deprotection of the amine of compound **28**, the two amino-acids were coupled to form the desired linear tetrapeptide **30** with a 49 % yield (Scheme 49).



**Scheme 49:** Synthesis of linear tetrapeptide **30**.

**Synthesis of cyclic tetra-cyclopeptide **22**: Cyclisation of compound **30****

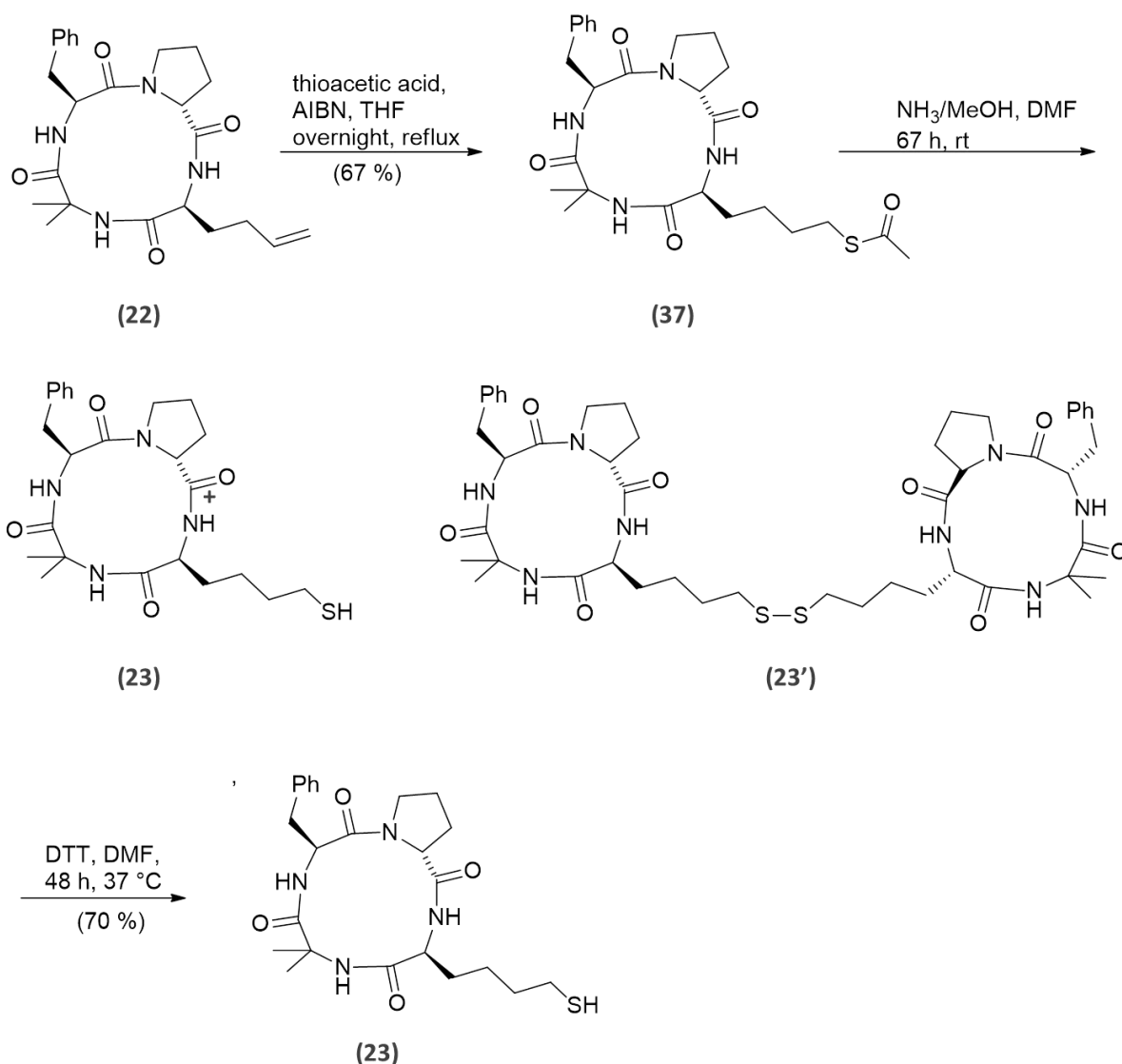
The orthogonal deprotection of the terminal carboxylic acid and amine of compound **30** by TFA allowed to obtain the completely unprotected compound **36**, and a final peptidic coupling afforded the cyclisation of compound **36** to obtain **22** in 46 % yield (Scheme 50).



**Scheme 50:** Synthesis of cyclic tetrapeptide **22**.

### Synthesis of compound 23

Compound **23** was obtained in 3 steps starting from **22** following a described protocol<sup>224</sup>. Functionalization of the terminal olefin into a methyl thioester allowed obtaining **37**. A posterior removal of the acetyl group afforded a mixture of thiol monomer **23** and disulfide dimer **23'**. Reduction by dithiothreitol (DTT) allowed to obtain the desired product **23** (Scheme 51).

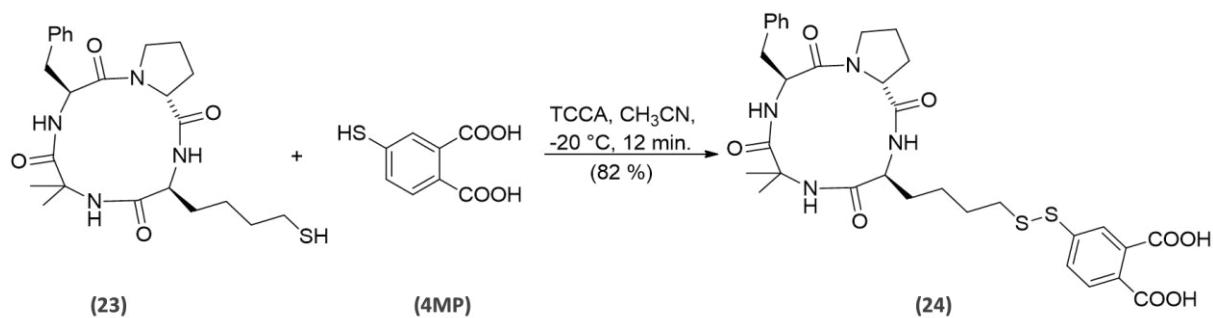


**Scheme 51:** Synthesis of compound **23**.

(ii) Synthesis of compound **24**: coupling of **23** and 4MP

Once the transmembrane carrier obtained and functionalized with a terminal thiol (**23**) it was ready to couple with our molecules. We started by coupling **23** to 4MP.

We performed several essays where the two thiols were incubated in equimolar amounts under different conditions (basic medium, presence of DTT) expecting that just the exposure to air would form both homodisulfides and heterodisulfides. However, we did not observe any formation of the desired product. Thus, we followed a reported procedure by F. Yang<sup>227</sup> to form heterodisulfides using trichloroisocyanuric acid (TCCA) as coupling reagent which allowed us to obtain the desired product **24** in 82 % yield (Scheme 52).



**Scheme 52:** Synthesis of compound **24**.

(iii) *E. coli* MG1655 growth tests with compounds **22** and **24**

Once **24** obtained, *E. coli* MG1655 growth assays were performed in the presence of this molecule (0-200  $\mu$ M) (Figure 59). Compound **22** was also tested as control in order to observe if the tetra-cyclopeptide has an effect by its own on the bacterial growth (Figure 59).

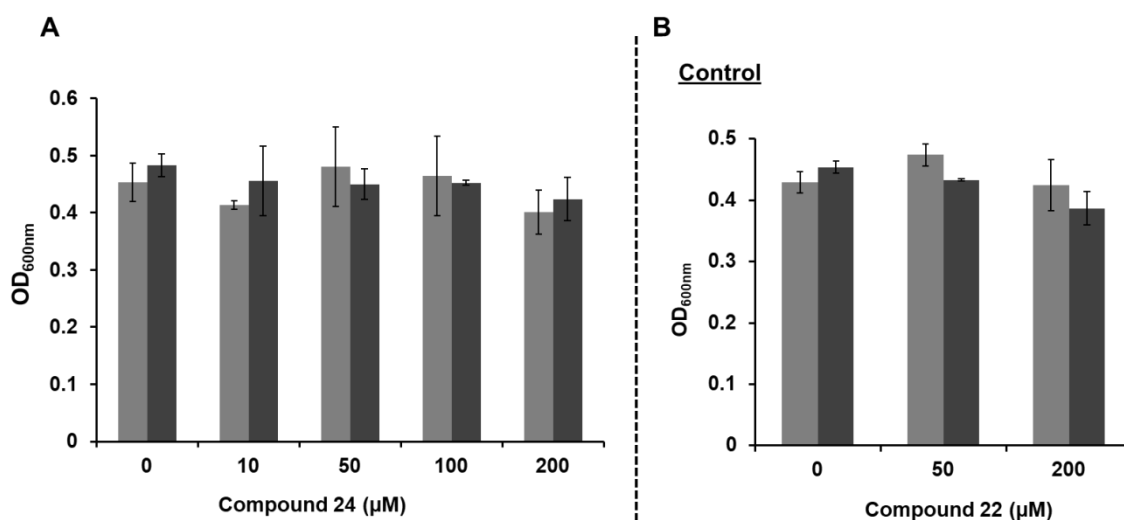


**Figure 59:** *E. coli* MG1655 growth in M9 in the presence of increasing concentrations ( $\mu$ M) of compound **24** (A) and **22** (B) with (dark grey bars) or without (light grey bars) QA (1.4 mg/mL).

We observed that the control **22** does not display an inhibitory effect *in cellulo* on *E. coli* MG1655 strain but unfortunately, **24** does not display any inhibition on bacterial growth either. Once again, it is difficult to conclude about what happens exactly. We don't know if there is no penetration even after assistance with the transmembrane carrier, if there is

penetration but not delivery of the drug due to a lack of the S-S bond cleavage, if there is penetration and 4MP delivery but no inhibitory effect.

### III. Looking for visual penetration evidence

At this point, as explained above, the lack of an *in cellulo* inhibition by our molecules has arisen many questions to which we don't have answers at this stage. We are not able to say if 5MPDC and 4MP penetrate the cell, whether the penetration assistance is working and if it is working, whether the molecules are being released in their active form...

In order to determine whether the tetra-cyclopeptide carrier penetrates *E. coli* bacterial wall (no evidence in the literature yet) we decided to couple it to three fluorescent agents. Little is described about bacterial fluorescence imaging due to the small size of bacteria cells and therefore the difficulty to observe them. Bacteria cells are considerably smaller than eukaryotes, with diameters of 0.1–5.0  $\mu\text{m}$  and 10–100  $\mu\text{m}$ , respectively. Therefore, finding the right conditions for observing fluorescence on bacteria is already a challenge.

The fluorescent agents were chosen based on the size (small), charge (uncharged) and fluorescing strength (Figure 60).

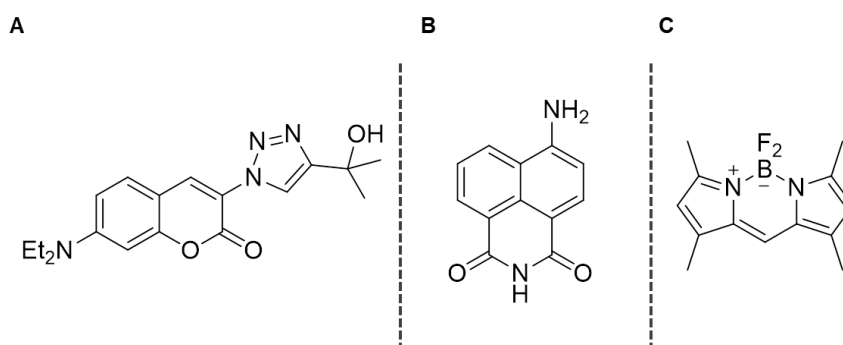


**Figure 60:** A. Coumarin derivative; B. 4-amino-1,8-phthalimide; C. Bodipy.

The idea was to observe an increase of fluorescence inside bacteria from the fluorophores alone to the fluorophores coupled to the tetra-cyclopeptide. This would be indicative of cell penetration of the tetra-cyclopeptide.

The aminocoumarin derivative (**38**) and the resulting molecule after coupling to the transmembrane carrier (**39**) were available in the DPM laboratory from previous work (Figure 61)<sup>183</sup>.

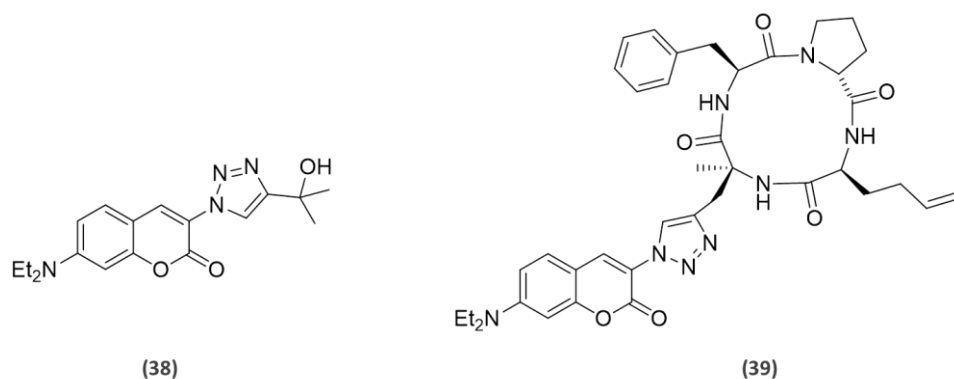


**Figure 61:** A. Coumarin derivative: compound **38**. B. Compound **38** coupled to tetra-cyclopeptide carrier: compound **39**.

The two other fluorophore-cyclopeptide coupled molecules **40** and **41** were synthesized by Leandro Jose Dos Santos (GRAL post-doc) (Figure 62).

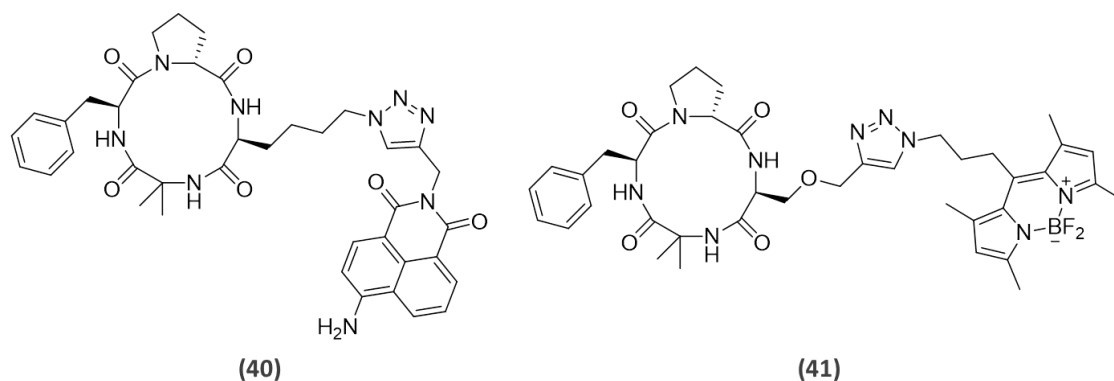


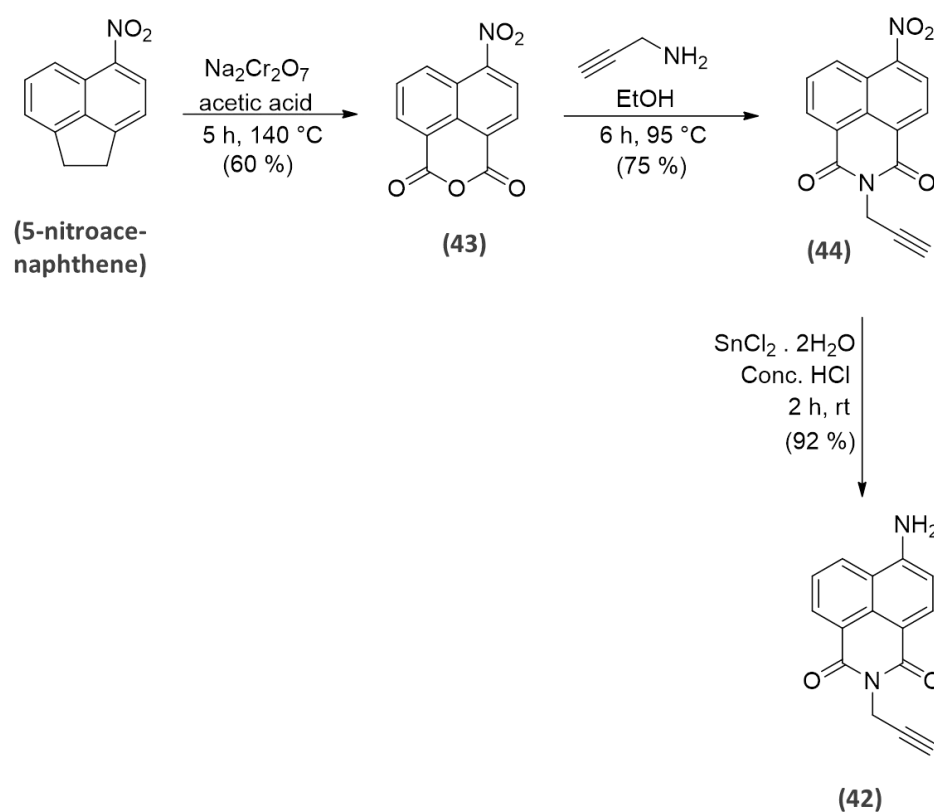
**Figure 62:** 4-amino-1,8-phthalimide coupled to cyclopeptide carrier: compound **40**. Bodipy coupled to cyclopeptide carrier: compound **41**.

### a. Synthesis of compound 40

Compound **40** results from the coupling between the fluorophore and cyclopeptide is described below:

### Synthesis of the fluorophore: Compound 42

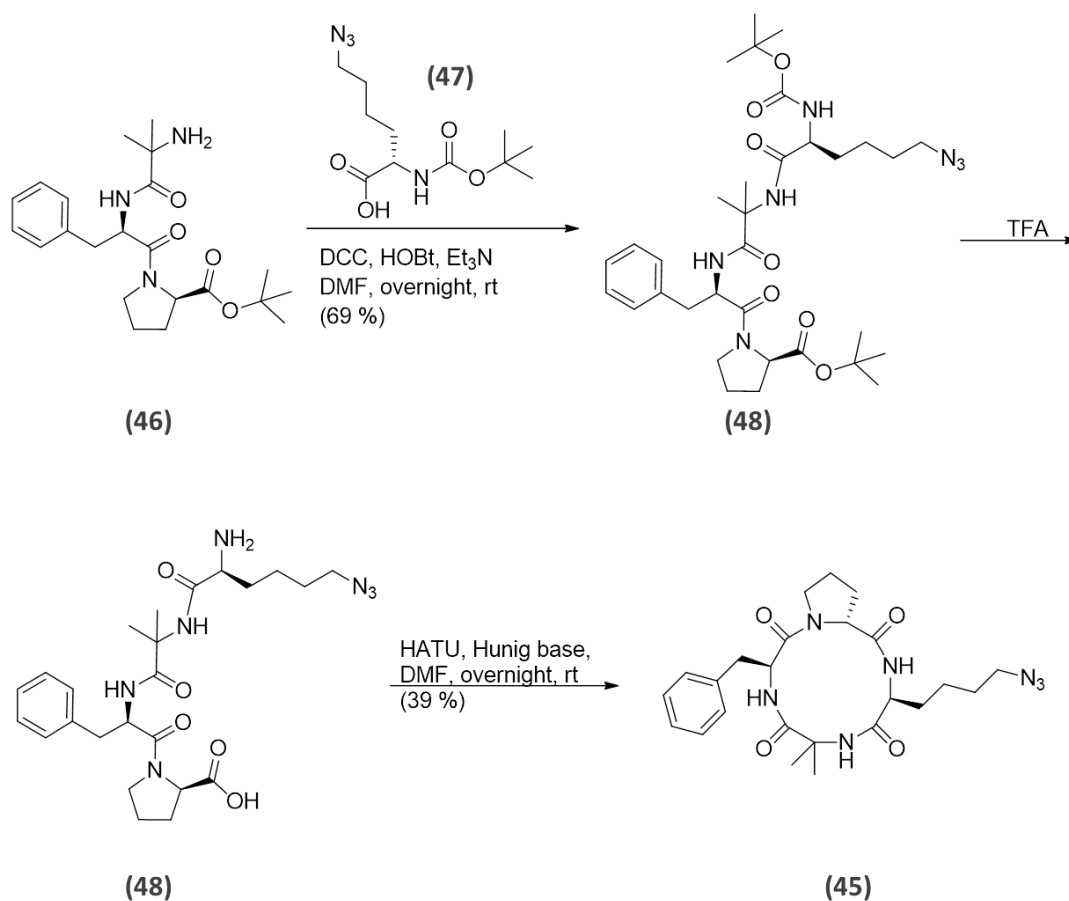
The synthesis of fluorophore **42** with the terminal alkyne was obtained in three steps starting from commercial 5-nitroacenaphthene following a slightly modified procedure with regard to the reported one (Scheme 53)<sup>228,229</sup>. After oxidation of 5-nitroacenaphthene with sodium bichromate to form compound **43**, a condensation with 2-propyne-1-amine yields compound **44** followed by a reduction of NO<sub>2</sub> to NH<sub>2</sub> allows to obtain the desired compound **42**.



**Scheme 53:** Synthesis of fluorophore **42**.

### Synthesis of compound tetra-cyclopeptide: Compound 45

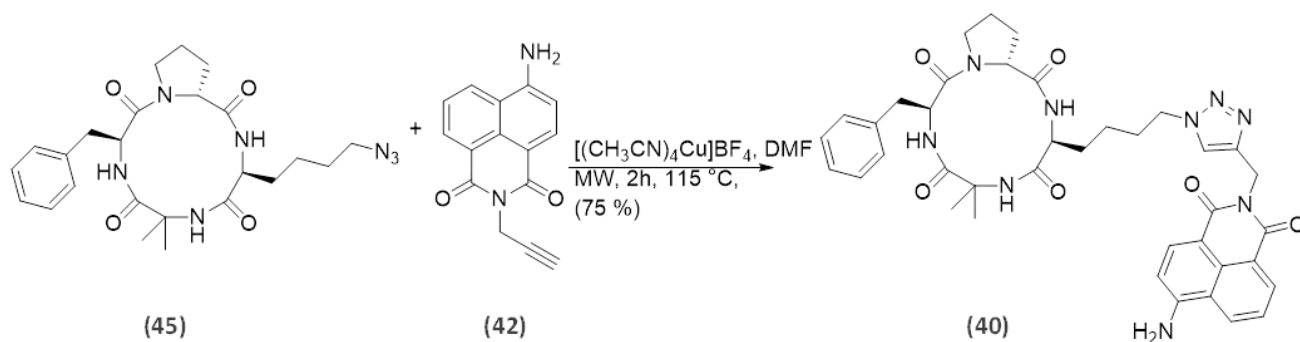
Tripeptide **46** and compound **47** were obtained following reported procedures<sup>230,231</sup>. The coupling of **46** compound with **47** yielded the linear tetra-cyclopeptide **48** which after TFA deprotection of the amine and carboxylic acid (**49**) could be cyclized to obtain the terminal azide functionalized cyclopeptide **45** (Scheme 54).



**Scheme 54:** Synthesis of compound **45**.

**Synthesis of compound 40: Coupling of compounds 42 and 45**

Compounds **42** and **45** were designed with a terminal alkyne and azide respectively, in order to perform the coupling through the Huisgen reaction. Such coupling allowed obtaining the desired molecule **40** with 75 % yield (Scheme 55).



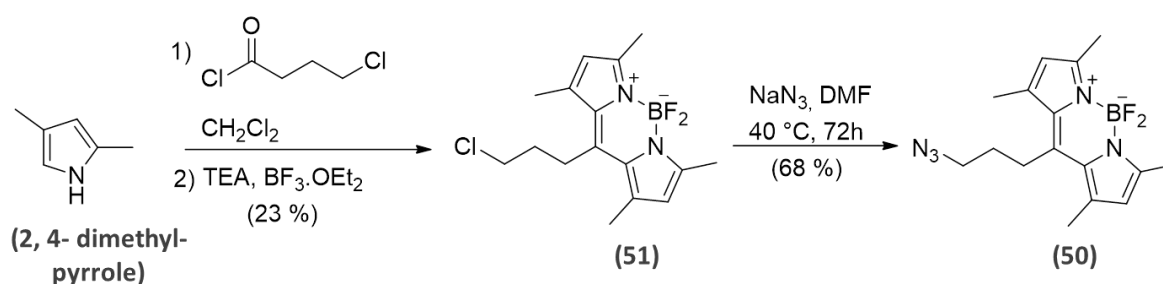
**Scheme 55:** Synthesis of compound **40**.

## b. Synthesis of compound 41

Compound **41** results from the coupling between the fluorophore and cyclopeptide is described below:

### Synthesis of the fluorophore:

Compound **50** was synthesized in two steps according to a reported procedure in literature<sup>232</sup>. A condensation reaction between two pyrrole molecules and a 4-butanoyl

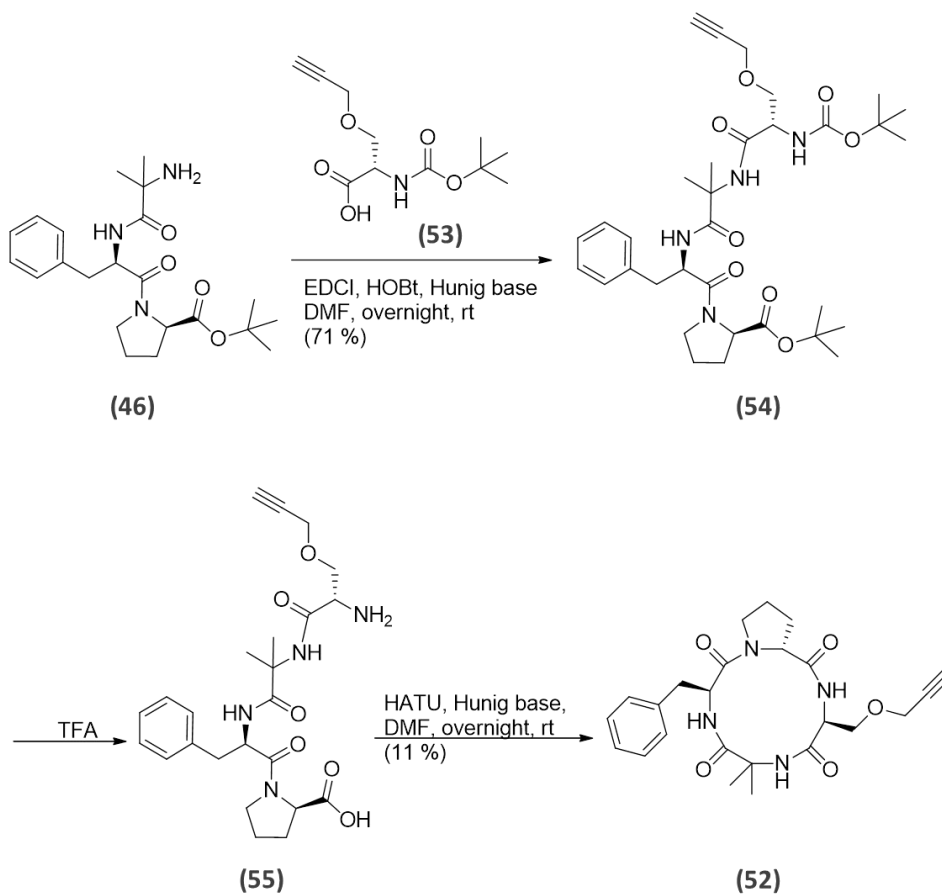


chloride yields chlorinated bodipy **(51)**. A substitution of the chloride by an azide allows the formation of the desired fluorophore **50** (Scheme 56).

**Scheme 56:** Synthesis of compound **50**.

### Synthesis of the tetra-cyclopeptide: compound 52

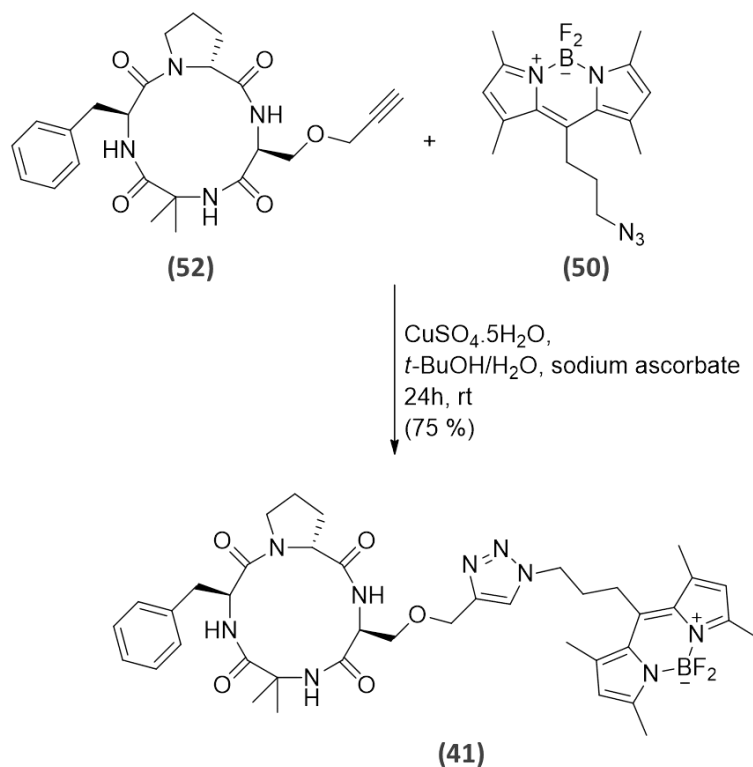
Tripeptide **46** and serine derivative **53** were synthesized following reported procedures<sup>230,233</sup>. Tetrapeptide **54** was obtained by coupling of **46** and **53**. After carboxylic acid and amine deprotection by TFA to yield the unprotected linear tetrapeptide **(55)**, a final cyclisation allowed to obtain the desired tetra-cyclopeptide **52** with 11 % yield (Scheme 57).



**Scheme 57:** Synthesis of compound **52**.

**Synthesis of compound 41: Coupling of compounds 50 and 52**

A Huisgen click reaction allowed the coupling between **50** and **52** to yield the desired compound **41** with a 66 % yield (Scheme 58).



**Scheme 58:** Synthesis of compound **41**.

c. *In cellulo* assays of fluorophores and their cyclopeptide-analogues **38** and **39**; **42** and **40**; **50** and **41**.

We performed *E. coli* bacterial growth assays with the six molecules (fluorophores and their cyclopeptide-coupled analogues) in order to verify that they do not inhibit bacterial growth. The assays were performed at 50  $\mu\text{M}$  of each molecule (Figure 63).

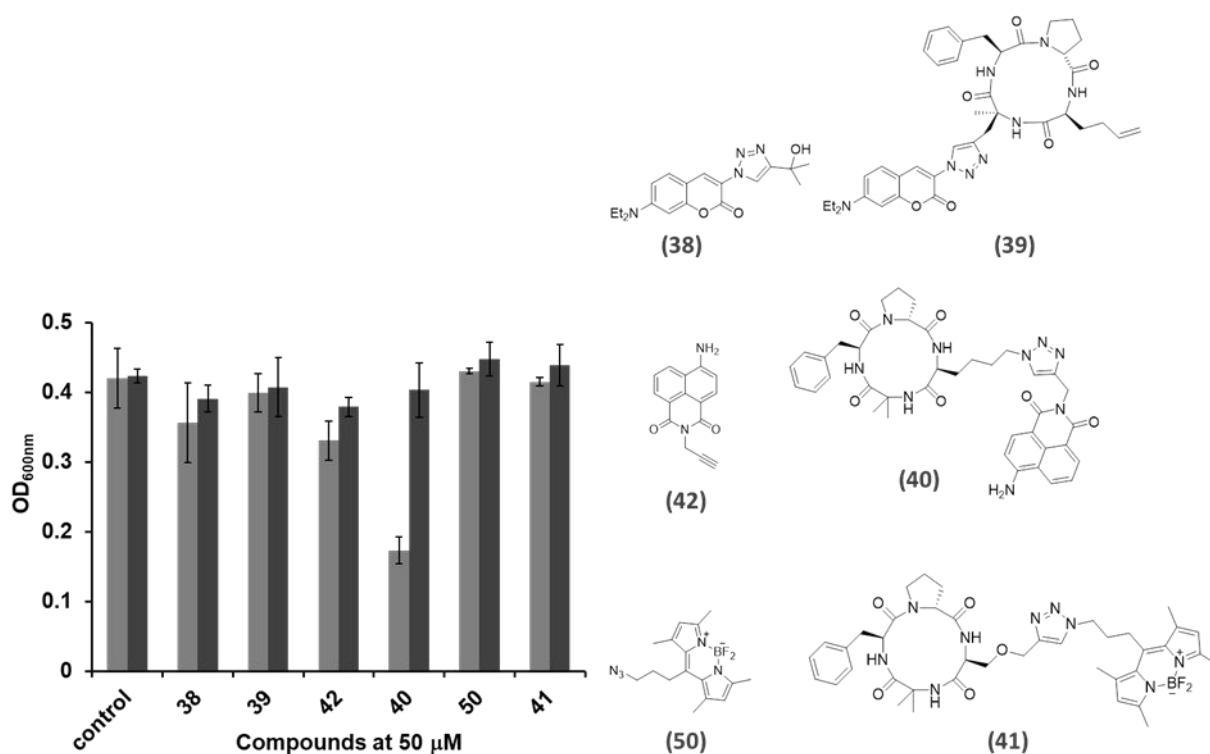


**Figure 63:** *E. coli* MG1655 growth in M9 in the absence (control) and presence of 50 μM of compounds **38**, **39**, **42**, **40**, **50** and **41** with (dark grey bars) or without (light grey bars) QA (1.4 mg/ml).

No inhibition of bacterial growth was observed by any of the molecules except for compound **40** that inhibits around 50 % of the bacterial growth at 50 μM (Figure 63). To have a more detailed look at compound **40** *in cellulo* behavior, additional assays were performed at different concentrations of **40** (0-200 μM) as well as of its analogue **42** (Figure 64).

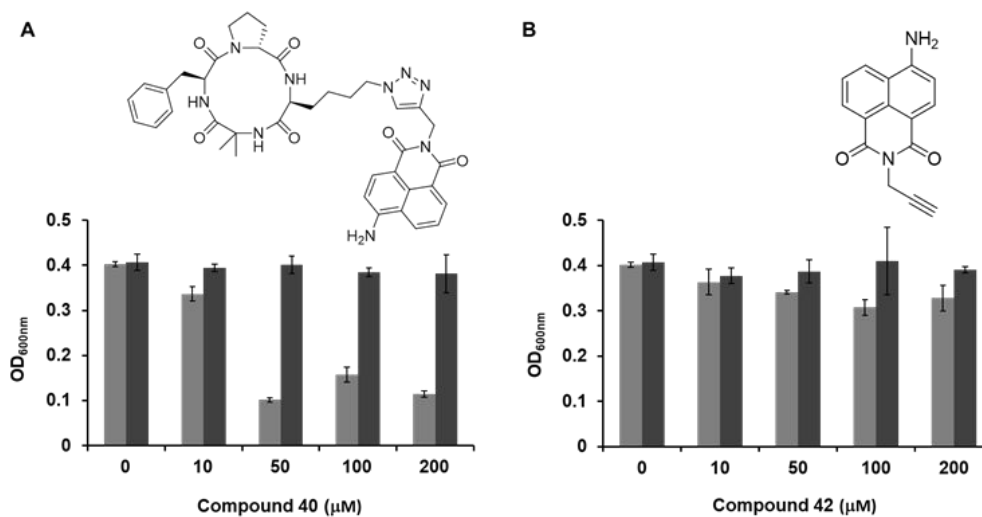


**Figure 64:** *E. coli* MG1655 growth in M9 in the absence (control) and presence of increasing concentrations (0-200  $\mu$ M) of compound **40** (A) and compound **42** (B) with (dark grey bars) or without (light grey bars) QA (1.4 mg/ml).

We confirmed that compound **40** inhibited bacterial growth. A slight inhibition (12 %) was observed at 10  $\mu$ M and it was enhanced at 50  $\mu$ M and above this concentration. Inhibition of 75 % was observed at 200  $\mu$ M. Very surprisingly, the growth inhibition by **40** was reversible by QA, suggesting that such a molecule inhibits the QA pathway, selectively. In contrast, its analogue compound **42** (not coupled to the cyclopeptide), did not inhibit or slightly inhibited the bacterial growth.

These results strongly suggest that compound **40** penetrates *E. coli* cell wall since enzymes on the QA pathway (NadA and NadB) are cytoplasmic. This penetration is likely due to the tetra-cyclopeptide of compound **40** since its analogue lacking the tetra-cyclopeptide part (**42**) does not inhibit the bacterial growth.

#### d. Fluorescence assays *in cellulo*

The six fluorophore compounds were sent to a partner (collaboration with Claire Durmort, IBS) for fluorescence assays. The preliminary tests were performed on gram-positive *Streptococcus pneumoniae*, the bacterial model in this laboratory. We first checked the fluorescing properties on gram-positive bacteria since they are the most permeable (with regard to gram negative bacteria and mycobacteria), to evaluate which chromophore fits best our needs to visualize bacteria.

Bacteria were incubated with the fluorophores in the conditions described in Materials and Methods. Nothing could be seen with the aminocoumarin derivatives **38** and **39** and neither with the phthalimide derivatives **42** and **40**. The images below could be obtained with the bodipy derivatives (Figure 66).

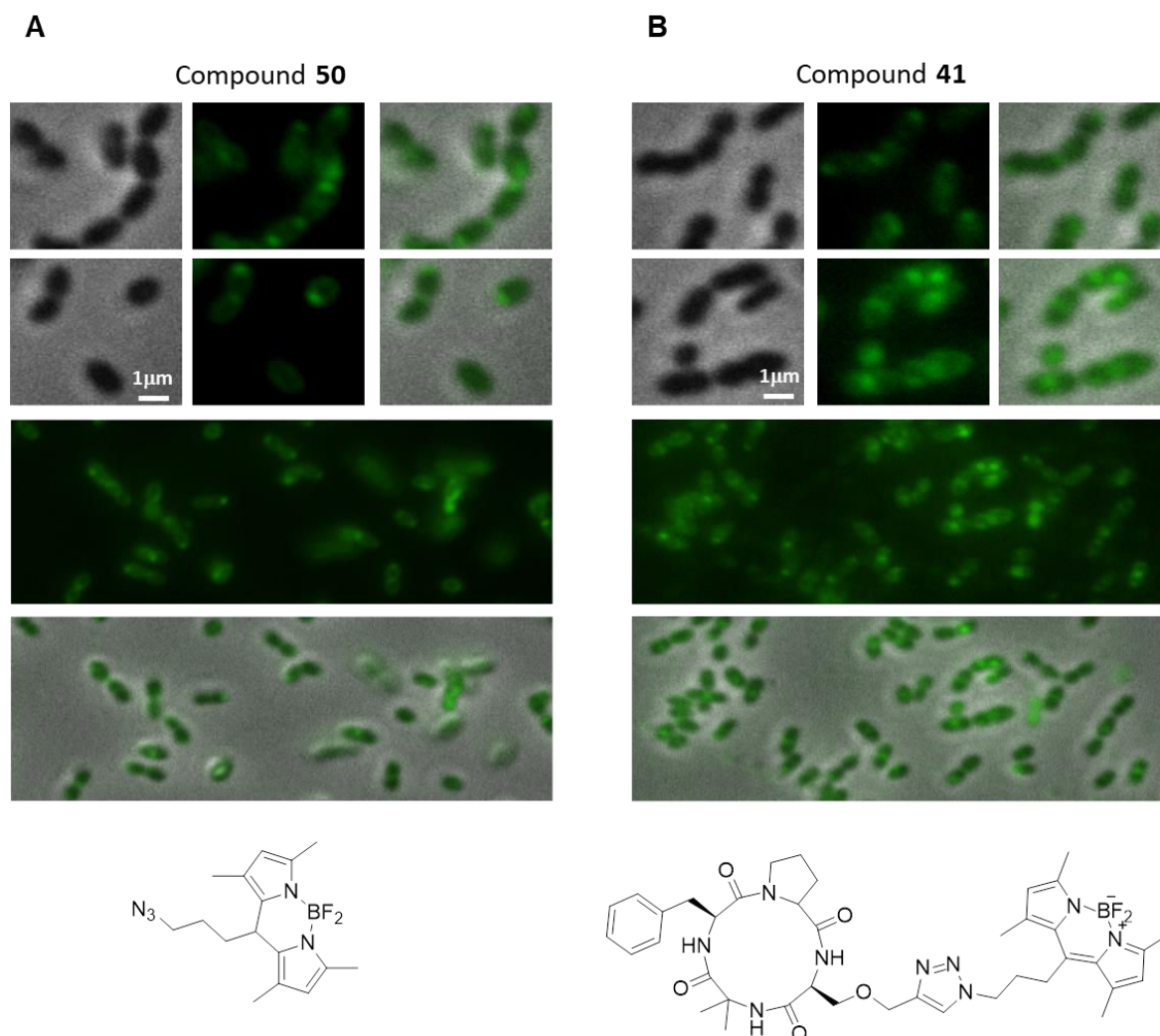


**Figure 66:** Images obtained after 5 min incubation of 50  $\mu$ L bacteria (OD = 15) with 5  $\mu$ L of 20  $\mu$ M compound **50** (A) and 20  $\mu$ M compound **41** (B) at 37° and posterior wash with PBS. Filter: GFP.

Compound **50** is a very apolar fluorophore with high affinity for the cellular membranes. In agreement to this, we observed that the membranes are mainly labelled on the images obtained with both fluorophores **50** and **41**. However, if we take a closer look to the images, we can see that for the case of compound **41**, fluorescence is slightly more intense and diffused inside bacteria, suggesting the cytoplasmic presence of compound **41**.

We have found that bodipy is a fluorophore strong enough to be observed on bacteria but with the drawback of its high affinity for the cell walls. We have to optimize its physical-chemical properties to limit this membrane affinity.

#### IV. DISCUSSION AND CONCLUSION

The four *in vitro* NadA inhibitors studied on the previous chapter were tested *in cellulo*. Two of them, 6MPDC and 5MPzDC showed to inhibit the *E. coli* MG1655 growth. However, this inhibition was not selective of QA pathway. For this reason, 6MPDC and 5MPzDC were no longer considered for further studies. Instead, 5MPDC and 4MP did not show any *in cellulo* activity even at high concentrations (500  $\mu$ M). This was quite disappointing because both molecules display IC<sub>50</sub> values *in vitro* on the range of tens of micromolar.

Based on the fact that 5MPDC and 4MP oxidize easily (disulfides) and form tetracarboxylate molecules as discussed several times in this thesis, we hypothesized that this was likely at the origin of the lack of *in cellulo* inhibition, since such oxidized molecules should hardly penetrate the bacterial wall or not penetrate it at all. To check this hypothesis, we performed three assays: (i) functionalize the carboxylic acids to form non-charged compounds by forming esters, that once inside the cell could be cleaved by esterases releasing the active molecule; (ii) perform the assays under anaerobic conditions to avoid disulfide formation; and (iii) couple the molecules to a tetra-cyclopeptide transmembrane carrier through an *in cellulo* cleavable disulfide bond. Unfortunately, no *in cellulo* inhibition was observed under these three conditions and there were a lot of questions that we could not answer. Thus, we decided to address each question independently.

We started by investigating cellular penetration by the tetra-cyclopeptide. Until now, its ability to permeate cell membranes has only been proved in eukaryotic cells; it does not only penetrate the cell membrane of eukaryotes but it also penetrates their nuclear membrane showing its ability to cross several/different membranes<sup>183</sup>. This justified our choice. Aware that observation of fluorescence in bacteria could be a difficulty due to the small size of these cells, we selected three fluorophores that were coupled to the tetra-cyclopeptide. We were not surprised to find that only Bodipy (**50**) and its tetra-cyclopeptide-

coupled analogue (**41**) were able to be detected in bacteria by confocal microscopy. Even if cell walls are selectively labelled due to the strong affinity of Bodipy, we could observe a slightly more intense fluorescence inside the cell in the case of the cyclopeptide-coupled version of bodipy suggesting a higher concentration of **41** in the bacteria.

Therefore, in this study we have identified a fluorophore (Bodipy) that emit fluorescence strong enough to be detected in bacteria. The next step will be to tune its physical-chemical properties to diminish its affinity for the cell membranes and obtain a more homogeneous labelling of the cytoplasm of bacterial cells to unambiguously prove cell penetration. If we manage to achieve this goal, we will move forward to check if the same effect is observed in gram negative bacteria such as *E. coli*. In the case of penetration, the next step will be to investigate penetration of our molecules 5MPDC and 4MP after coupling to both the transmembrane carrier and Bodipy.

While the fluorophores were sent to our collaborator's for fluorescence assays, we performed *E. coli* MG1655 growth tests in the presence of the six fluorophores in order to control their toxicity. To our surprise, compound **40** displayed a bacterial growth inhibition activity that is specific towards our target QA pathway since the growth is recovered with the addition of exogenous QA. Since QA pathway takes part in the cytoplasm, this suggests a cellular penetration of compound **40**, likely due to the cyclopeptidic part since its fluorescent analogue **42** (without cyclopeptide) did not display any inhibition activity *in cellulo*. Such an unexpected result strongly suggests a penetration by the tetra-cyclopeptide into gram negative *E. coli*. To confirm that the target of compound **40** is the QA pathway, *in vitro* activity/inhibition assays with NadA and NadB will be performed in the next months in the presence of compounds **40** and **42**. If compound **40** inhibits NadA and/or NadB and **42** does not, penetration by the cyclopeptide carrier will be demonstrated and in addition, we will have found a new QA pathway inhibitor, that we will consider as a potential antibacterial against *H. pylori* and *M. leprae*.



# GENERAL CONCLUSION AND PERSPECTIVES

Quinolinate synthase was identified to be an essential enzyme in the NAD biosynthetic pathway for two pathogens, *Helicobacter pylori* and *Mycobacterium leprae*<sup>103,101</sup>. In addition, since NAD biosynthesis differs between prokaryotes and eukaryotes, NadA is an attractive bacterial target for the design of new antibacterials against *Helicobacter pylori* and *Mycobacterium leprae*. At the beginning of my Ph.D, a single quinolinate synthase inhibitor was described, DTHPA<sup>141</sup>. Despite a promising IC<sub>50</sub> value (IC<sub>50</sub> = 10 μM), DTHPA proved to be non-specific *in vitro* and *in cellulose*. In this context, my Ph.D project aimed at designing, synthesizing and testing DTHPA derivatives as specific NadA inhibitors with the aim of finding new antibacterial drugs. It was an ambitious project.

Structure activity study and docking experiments allowed us to design four molecules as potential specific NadA inhibitors. I had to synthesize three of them (6MPDC, 5MPzDC and 5MPDC) that were not commercial nor described in literature. It took me the first Ph.D year to reach this objective. The three syntheses were not completely optimized and the yields considerably low. However, we got sufficient amounts to pursue with enzymatic, spectroscopic and structural studies. If the molecules come to be interesting for a therapeutic application, the synthesis will have to be optimized.

All molecules proved to be NadA inhibitors. Indeed, they all displayed an inhibitory effect on NadA activity with IC<sub>50</sub> values in the range of 10-45 μM (for 10 μM enzyme). A lot of effort was made to characterize the inhibition mechanism of the molecules by using spectroscopic techniques (UV-vis, CD, Mössbauer) with the aim of investigating whether the molecules inhibit NadA as they were designed to inhibit it: by binding in the active site with coordination of the catalytic Fe site of the [4Fe-4S] cluster through their thiol moiety. Despite our effort, this came to be more difficult than expected since none of the used spectroscopic techniques allowed us to unambiguously prove an interaction of the molecules with NadA cluster. Three X-ray structures of *T. maritima* NadA were solved in the presence of three inhibitors (6MPDC, 5MPzDC and 4MP) and allowed to evidence that the molecules interact with the catalytic Fe site of the [4Fe-4S] cluster through their thiol moiety and the carboxylates interact with amino acid residues likely stabilizing the molecules in the active site. We did not evidence a crucial role for the nitrogen of the ring.

The *in vitro* inhibition study was completed by evaluating the specificity of the inhibitors towards NadA using another [4Fe-4S] enzyme, AcnB from *E. coli*, for the reasons

explained on Annex I. Whereas 6MPDC and 5MPzDC inhibited AcnB enzyme at concentrations beyond 10 and 5 equivalents respectively, 5MPDC and 4MP did not inhibit AcnB at all. This part of the Ph.D was ended up with encouraging results, since we had identified two potential specific NadA inhibitors: 4MP and 5MPDC. On the whole, this *in vitro* part took to me roughly a year. The experiments were performed during the second year while working on the syntheses for the *in cellulo* (tetra-cyclopeptide) part and during the third year, at the DPM laboratory.

Concerning the *in cellulo* evaluation of the four NadA inhibitors, we found results in agreement with *in vitro* ones for 6MPDC and 5MPzDC. Indeed, they are not specific inhibitors of *E. coli* QA pathway. For this reason, they were not considered for further studies. To our disappointment, no inhibitory effect was observed with the two most interesting NadA inhibitors, 5MPDC and 4MP. We performed several assays under different conditions with no success. Even the penetration and drug delivery assistance with the coupled tetra-cyclopeptide resulted in no effect.

At this point, we stopped and decided to understand what happens. We have started by looking for penetration evidence of the chosen tetra-cyclopeptide transmembrane carrier and this is still under progress. We have found a fluorophore observable in bacteria which has allowed us to suggest that there is likely some penetration of the tetra-cyclopeptide into bacteria. Still, the properties of the fluorophore have to be tuned for a convenient visualization and unambiguous demonstration of cell penetration by the tetra-cyclopeptide. This is one of the short-term perspectives of the project where a post-doc is already working on (Leandro Jose Dos Santos, GRAL). It is true that this problem of non-penetration has forced us to move a little bit away from our main objective of finding antibacterials that target NadA but we consider it to be necessary. If the lack of *in cellulo* activity of 4MP and 5MPDC comes from a lack of cell penetration into the bacteria, we consider that it is worth to work on this since both molecules are interesting from a NadA inhibition and specificity point of view. Of course, we are aware that it might be risky and we might find negative results concerning the two molecules. Thus, we want to find the best physical-chemical properties of Bodipy fluorophore in order to investigate cell penetration of gram-negative bacteria by the tetra-cyclopeptide transmembrane carrier, for what there is no evidence in literature yet. If we reach this objective and confirm a penetration, we will then investigate

penetration of 4MP and 5MPDC coupled to both the fluorophore and the transmembrane carrier.

As another perspective, we would like to discover other NadA inhibitors. Two approaches are currently used. Using the rational approach that aims at identifying substrate/DTHPA analogues as NadA inhibitors, we have designed a new molecule: (S)-2-((2-mercaptoethyl)amino)succinic acid (Figure 67A). Such molecule contains the desired functions for inhibition (two carboxylates, a nitrogen and a thiol) positioned on the right place in order to interact with active site amino-acids. This molecule is not aromatic nor cyclic as the ones from the family that we have investigated during my thesis (Figure 67B). We would like to investigate whether the flexibility and non-planar geometry might provide better fitting on the active site resulting on a stronger inhibition.

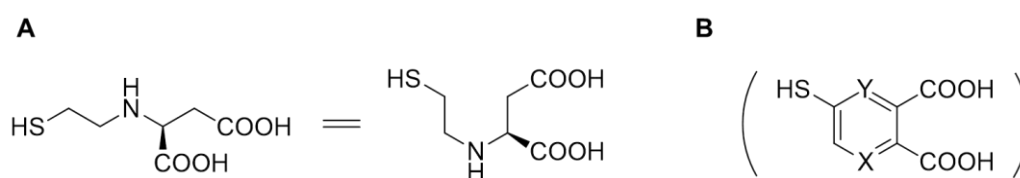
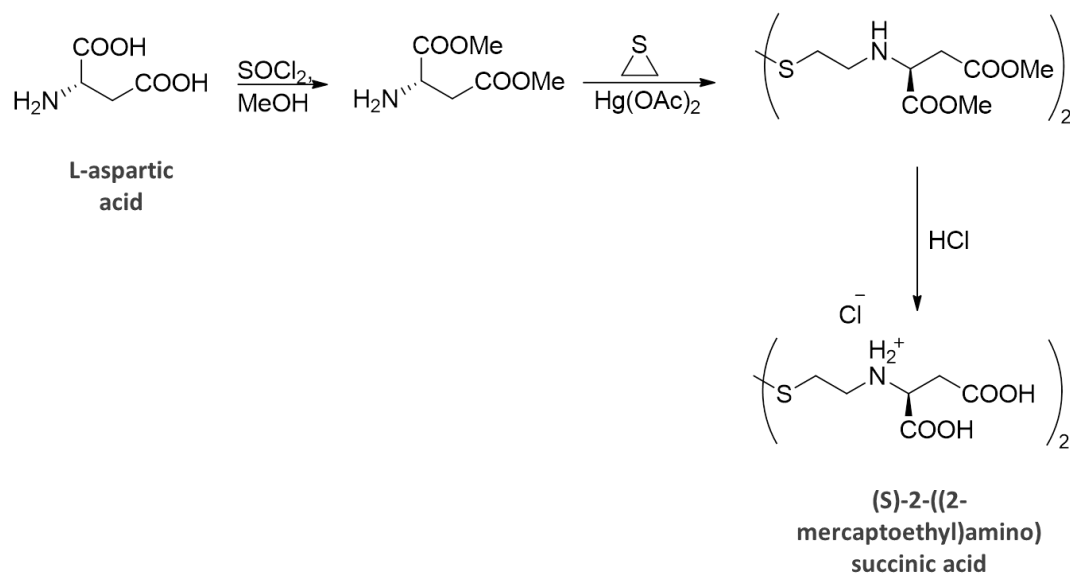


**Figure 67:** **A.** New potential NadA inhibitor: (S)-2-((2-mercaptoethyl)amino)succinic acid. **B.** Family of molecules investigated during my thesis.

A preliminary synthesis of such molecule has already been performed by Olivier Hamelin. The molecule has been obtained as a disulfide dimer starting from L-aspartic acid (Scheme 59). The synthetic pathway has to be well characterized and optimized and then *in vitro* assays will be performed on NadA.



**Scheme 59:** Synthesis of the potential NadA inhibitor (S)-2-((2-mercaptoethyl)amino) succinic acid from L-aspartic acid.

Another way to find new inhibitors is to use a docking approach since we have several X-ray NadA structures solved at a good resolution. We are working with Patricia Amara (IBS, Grenoble) to find new inhibitors *in silico*. This approach consists in docking libraries of molecules on NadA structure (opened form) applying several filters and selecting the best hits. This time, we are focusing on inhibitors that do not target the Fe-S cluster. Some molecules have already been identified and tested *in vitro* but unfortunately no interesting molecules were identified. Another docking will be performed soon using other parameters.

During the last chapter of results when we were looking for a convenient fluorophore to visualize bacteria by confocal microscopy, we found a molecule that inhibited the QA pathway specifically (compound **40**). The molecule needs to be tested *in vitro* on (NadA and NadB). However, the fact of being a specific QA pathway inhibitor (at all tested concentrations, 0-200  $\mu$ M) makes it already a molecule of great interest as antibacterial for *H. pylori* and *M. leprae*.

Finally, we will also use the CMBA High Throughput Screening Platform at BIG (CEA, Grenoble) to find other inhibitors. Two types of assays will be performed. An *in cellulo* one on *E. coli* MG1655 strain and an *in vitro* one using NadA from *T. maritima* whose Fe-S cluster is stable in the enzymatic assay range (30 min).

Every molecule that we consider as good and specific NadA or QA pathway inhibitor coming from whichever approach will be sent to our collaborators (Hilde de Reuse and Stewart Cole, Pasteur Institut) for assays on pathogens.

To summarize, we may consider that the three main objectives of my Ph.D have been fulfilled i) synthesize a new family of NadA inhibitors; ii) study the *in vitro* inhibition and specificity of the inhibitors on NadA; iii) perform *in cellulo* assays on an *E. coli* strain. These objectives pave the way towards new antibacterial agents against *H. pylori* and *M. leprae* but unfortunately we have not been able to reach that stage of the project, since the lack of activity of the inhibitors *in cellulo* slowed down the project. This concerns looking for penetration evidence of 5MPDC and 4MP molecules that we think might not be able to penetrate the cell on their own. However, the collaboration to test the inhibitors with the pathogens is in place and therefore as soon as we obtain positive results, we will send the molecules to test on the pathogens.

It is well known how complex to find new antibacterial agents is and how the lack of antibacterial agents nowadays is related to the very few new antibiotics (due to low rates of success). This was a challenging project with high objectives and even if we could not reach the stage of finding antibacterial agents against *H. pylori* and *M. leprae* yet, we could make progress on it arising interesting perspectives. In addition, the project was very high-versatility demanding. I started the Ph.D only with a chemistry background and no notions in biochemistry. Yet, I have performed some organic synthesis but I have taken in charge the biochemistry part of the project (protein production and purification, *in vitro* enzymatic tests, *in cellulo* assays and perform some spectroscopies (UV-visible, CD) or prepare samples for others (Mössbauer)). It is worth mentioning that the *in vitro* part concerning NadA enzyme was performed using a glove box due to NadA's O<sub>2</sub>-sensitivity which made the study more difficult. Finally, I have to mention that I worked between two laboratories (LCBM and DPM, opposite sides of Grenoble) and three research teams of very different competences (BioCat, biochemistry; BioCE, organic and (bio)inorganic chemistry; MedChem, drug chemistry). I found this very enriching but sometimes hard. Still, I believe on the potential of the project and I worked motivated on it.

# MATERIALS AND METHODS

## I. Biological materials

### a. Bacterial strains

#### *E. coli* BL21(DE3)<sup>258</sup> strain

Genotype: *F ompT gal dcm lon hsdS<sub>B</sub>(r<sub>B</sub><sup>-</sup>m<sub>B</sub><sup>-</sup>)λ(DE3[*lacI lacUV5-T7 gene 1 ind1 sam7 nin5*])*. This strain is commonly used for the overexpression of proteins. It contains mutations at the *lon* and *ompT* genes which encode for proteases. The DE3 chromosomal insertion comes from λ phage and contains the gene that encodes for the T7 RNA polymerase which is dependent of *lacUV5* promoter, inducible by IPTG.

#### *E. coli* MG1655<sup>267</sup> strain

Genotype: *F- λ- ilvG- rfb-50 rph-1*. This is a K-12 wild-type strain, used routinely as control (wild-type) for *in cellulo* complementation tests.

#### *E. coli* MG1655<sup>267</sup> Δ*nadA* strain

Genotype: *F- λ- ilvG- rfb-50 rph-1 ΔnadA*. This strain derives from *E. coli* MG1655 strain. The *nadA* gene has been inactivated by the insertion of a kanamycin resistance cassette, which is maintained by the presence of this antibiotic.

### b. Plasmids

#### pT7-7-*nadA*EcWT

The pT7-7 plasmid contains an ampicillin resistance gene, the pT7 promoter of RNA polymerase of the T7 bacteriophage which is inducible by IPTG, and a multiple cloning site which contains 9 restriction sites that permit the insertion of *Escherichia coli nadA* gene<sup>234</sup>. *E. coli nadA* gene was introduced at the *NdeI* and *HindIII* sites of the pT7-7 vector generating the pT7-7-*nadA*EcWT recombinant plasmid (Carine Rousset thesis).

#### pET-22b-*nadB*Ec

The pET-22b vector contains an ampicillin resistance gene, the T7 promoter of the T7 bacteriophage RNA polymerase which is inducible by IPTG and a multiple cloning site

allowing the insertion of the gene of interest *nadB* (at the *NdeI* and *XhoI* sites) generating the recombinant pET-22b-nadBEc plasmid (Carine Rousset thesis).

### c. Culture media

#### Luria Miller-Broth medium (LB)

This commercial medium (Carl Roth) is used for bacterial cultures in both liquid and solid forms. It contains 10 g/L of tryptic peptone casein, 5 g/L of yeast extracts and 10 g/L of NaCl. The solid form contains 15 g/L agar in addition to the mixture.

#### Minimal medium (M9)

This medium is used when cultures need to be enriched by a labelled atom or molecule,  $^{57}\text{Fe}$  in our case. The composition of this medium consists in 6 g/L of  $\text{Na}_2\text{HPO}_4$ , 3 g/L of  $\text{KH}_2\text{PO}_4$  and 1 g/L of  $\text{NH}_4\text{Cl}$ . At the beginning of the culture the medium is supplemented with 2 mM of  $\text{MgSO}_4$ , 0.4 % of glucose, 10  $\mu\text{M}$  of  $\text{CaCl}_2$ .

## II. Molecular biology methods

### a. Preparation of competent cells

All the steps are performed under strict sterile conditions. In order to make a bacterium competent, it is necessary to weaken its bacterial envelope to make it permeable. Bacteria are first incubated in LB until  $\text{OD}_{600} \approx 0.5$ . After centrifugation at 4°C and 10000 rpm for 10 minutes, pellets are re-suspended in 5 mL of sterile 0.1 M  $\text{CaCl}_2$  and incubated for 30 minutes on ice. The treatment of cells by divalent ions alters the cell membranes structure and creates micropores, which enables the penetration of exogenous DNA. Cells are centrifuged under same conditions as before and re-suspended in 0.7 mL of sterile 0.1 M  $\text{CaCl}_2$ , 10% glycerol. Aliquots of competent cells (100  $\mu\text{L}$ ) are frozen in liquid  $\text{N}_2$  and stored at -80 °C.

### b. Transformation of competent cells

20-50 ng of the plasmid of interest are added to 100  $\mu\text{L}$  of competent cells and the mixture is incubated at 4 °C for 30 min. Then, a thermic shock at 42 °C for 2 min is performed allowing the penetration of the plasmid DNA into the cells. After 5 min on ice, 500  $\mu\text{L}$  of LB

are added and the whole solution is incubated at 37 °C for 2 h, at 700 rpm. After centrifugation and removal of the supernatant, pellets are suspended in 100 µL of fresh LB and spread on two petri dishes (1/10<sup>e</sup> and 9/10<sup>e</sup> dilutions) containing LB-agar and the corresponding antibiotic for the selection of the transformed cells.

### III. Biochemical methods

#### a. Protein overexpression

This protocol is the same for NadA and NadB. One colony of the transformed bacteria is inoculated at 37 °C in 200 mL LB medium containing ampicillin (100 µg/mL). The culture is stirred at 180 rpm overnight. This pre-culture is used to inoculate at 1.5 % a 10 L LB/ampicillin culture. When the optical density at 600 nm reaches 0.5, the protein expression is induced by addition IPTG (final concentration 0.5 mM). After 3 h incubation at 37 °C, bacteria pellets are centrifuged (20 min, 4 °C, 4000 rpm) and pellets washed with buffer A. After centrifugation, bacterial pellets are frozen in liquid nitrogen and stored at -80 °C.

For Mössbauer analysis, production of NadA protein is performed in M9 medium in the presence of <sup>57</sup>Fe (34 µM) which is added right before induction of protein expression by IPTG addition. The <sup>57</sup>Fe solution is prepared by heating off the Fe<sup>0</sup> metal in a 1:1 volume of concentrated nitric acid (70 %) and concentrated hydrochloric acid (37 %).

#### b. Protein extraction

##### (i) Freeze-thaw cycles

This was used for NadA protein and performed under strict anaerobiosis. The bacterial pellets obtained from the culture are thawed and re-suspended in buffer A, containing 1 mM PMSF and 0.6 mg/mL lysozyme. After 45 min incubation inside the glove box at 17 °C, 3 subsequent freeze-thaw cycles are performed: fast freezing of the cells in liquid nitrogen (outside the glove box) and slow thawing at 17°C (inside the glove box). These are necessary for optimal protein extraction.

##### (ii) Sonication

This was used for NadB protein extraction and it was performed under aerobic conditions. The bacterial pellets issued from the culture are thawed and re-suspended in

buffer A containing 1 mM PMSF, 5 mM  $\beta$ -mercaptoethanol and 0.6 mg/mL lysozyme. After 45 min incubation at rt, cells are sonicated by ultrasounds (30 % amplitude) for 20 cycles. Each cycle consists in 15 s of sonication and 10 s of incubation on ice.

Once the cell lysis (sonication or freeze-thaw cycles) is performed, the cell debris are removed by ultracentrifugation (1.5 h, 4 °C, 45000 rpm). The soluble protein extracts are conserved at 4 °C before purification.

### c. Protein purification

*E. coli* NadA protein is purified under anaerobic conditions in order to get an holo form ([4Fe-4S]<sup>2+</sup> containing protein). *E. coli* NadB is purified under aerobic conditions. Both of these proteins possess a 6-Histidine tag at their N-terminus and are purified using the same chromatographic column.

The soluble protein extracts are loaded onto a Nickel-Nitrilotriacetic Acid /Ni-NTA column (Qiagen, 5 mL), that has previously been equilibrated with buffer A. A first washing is performed with 100 mL of buffer A, which is followed by a second washing with 100 mL of buffer A containing 10 mM imidazole. Finally, the protein of interest is eluted by buffer A containing 200 mM imidazole. After collection, the protein is immediately desalted onto NAP-25 desalting column (GE Healthcare) equilibrated with buffer A. The protein fractions are analyzed by SDS-PAGE, concentrated, aliquoted and stored at -80 °C.

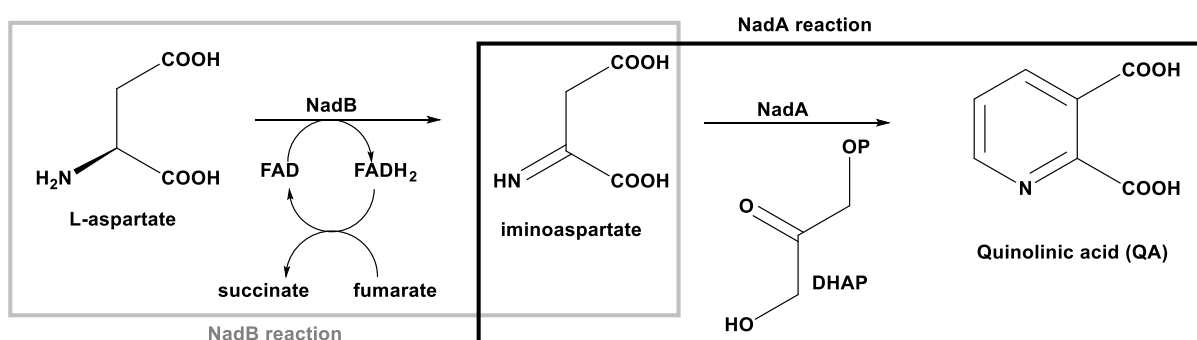
### d. Reconstitution of NadB FAD cofactor

L-aspartate oxidase (NadB) is a FAD-containing enzyme. FAD is lost during purification and it is necessary to load again the protein with this cofactor. This is done by incubation of the purified apoenzyme with 10 equivalents of FAD (Sigma) at rt for 2 h. After incubation, the excess of FAD is removed through a NAP-25 desalting column (GE Healthcare) equilibrated with buffer A. The number of FAD molecules per protein is quantified by measuring the absorbance of the protein at 450 nm ( $\epsilon_{450\text{nm}} = 11300 \text{ M}^{-1} \cdot \text{cm}^{-1}$ ).

### e. Enzymatic activity measurements

(i) *in vitro* NadA activity

**Principle:** This assay is done under anaerobic conditions. NadA catalyzes the condensation of two substrates, Dihydroxyacetone phosphate (DHAP) and iminoaspartate (IA) (Scheme 60). This last one, IA, is very unstable ( $t_{1/2} = 144\text{s}$ ) and therefore IA must be continuously produced *in situ* during the whole reaction time. There are two ways to produce it: enzymatically (through *L*-aspartate and *L*-aspartate oxidase enzyme) or chemically (by the reaction between ammonium sulfate and oxaloacetic acid<sup>117</sup>). During my thesis I have generated IA enzymatically.



**Scheme 60:** *in vitro* NadA activity assay

**Implementation:** NadA (10  $\mu\text{M}$ ) is incubated for 15 min in buffer B at 37 °C. Then, a premix containing DHAP, *L*-Aspartate and fumarate (2 mM, 10 mM and 25 mM respectively, given as final concentrations of the reaction media (100  $\mu\text{L}$ )) are added, and the reaction is incubated for 15 min at 37 °C. The reaction is initiated by addition of NadB (10  $\mu\text{M}$ ). The reaction is quenched after 20 minutes by addition of 0.1 M  $\text{H}_2\text{SO}_4$  (table 10).

For inhibition assays, molecules are added with NadA for 15 min before addition of the premix.

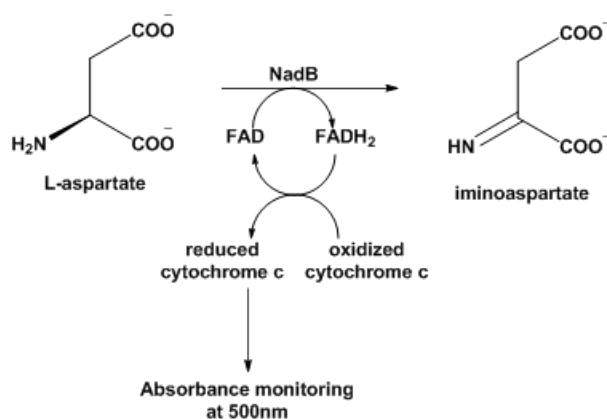
<u>Reactants</u>	<u>Final concentrations</u>
Dihydroxyacetone phosphate (DHAP)	2 mM
<i>L</i> -Aspartate	10 mM
Fumarate	25 mM
NadB	10 $\mu\text{M}$
NadA	10 $\mu\text{M}$
Buffer B	Needed volume to complete 100 $\mu\text{L}$

**Table 10:** *in vitro* NadA activity assay

Samples are centrifuged for 10 min at 12000 rpm. 50  $\mu\text{L}$  of the supernatant are mixed with 50  $\mu\text{L}$  of buffer C. The solution (100  $\mu\text{L}$ ) is put on a HPLC vial for HPLC analysis (see HPLC paragraph for details). The elution is done by a 20-minute linear gradient from 0% to 20% of acetonitrile and a 0.4mL/min flow. Quantification of QA is performed using a calibration curve with known concentrations of commercial QA (Aldrich).

(ii) *in vitro* NadB activity

**Principle:** L-Aspartate oxidase or NadB oxidizes *L*-aspartate to iminoaspartate by using FAD cofactor which is reduced to  $\text{FADH}_2$  during the enzyme reaction. The cofactor is regenerated by reduction of  $\text{O}_2$  to  $\text{H}_2\text{O}_2$  under aerobic conditions or by reduction of fumarate to succinate under anaerobic conditions. For measurement of NadB activity another electron acceptor is used: the cytochrome *c*; a small heme protein. The oxidized form ( $\text{Fe}^{3+}$ ) of cytochrome *c* is colorless whereas the reduced form ( $\text{Fe}^{2+}$ ) is orange, with an absorbance maximum at 550 nm ( $\epsilon_{550\text{nm}} = 22.6 \text{ M}^{-1} \cdot \text{cm}^{-1}$ ). NadB activity is monitored by following the absorbance at 550 nm corresponding to the formation of the reduced cytochrome *c*. The amount of reduced cytochrome *c* is directly proportional to the IA formation (Scheme 61). For one oxidized *L*-Aspartate (one IA produced), one FAD is reduced to  $\text{FADH}_2$  allowing the reduction of two cytochrome *c* molecules. Consequently, the amount of IA produced corresponds to half the quantity of reduced cytochrome *c* (Scheme 61).



**Scheme 61:** *in vitro* NadB activity assay.

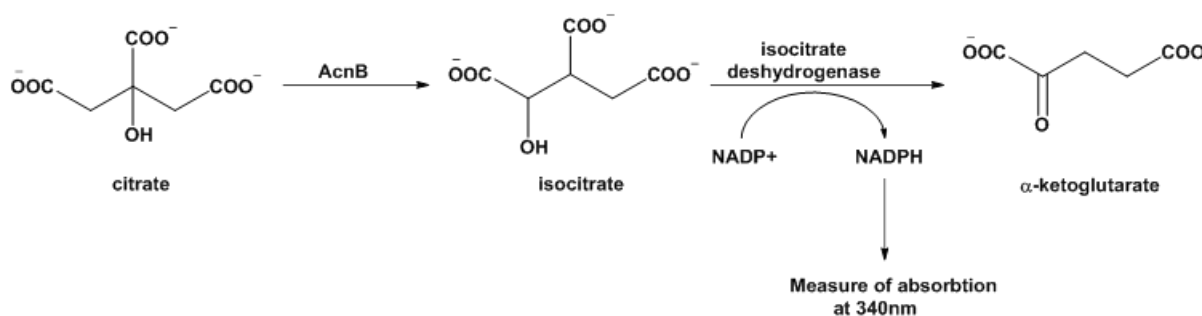
**Implementation:** In a 100  $\mu\text{L}$  quartz cell *L*-aspartate (1 mM) and cytochrome *c* (10  $\mu\text{M}$ ) are mixed in buffer B and the reaction is initiated by the addition of NadB (15  $\mu\text{M}$ ). Absorbance is monitored at 550 nm for 15 min (Table 11).

Reactants	Final concentrations
NadB	15 $\mu$ M
Cytochrome c	10 $\mu$ M
L-aspartate	1 mM
Buffer B	Needed volume to complete 100 $\mu$ L

**Table 11:** *in vitro* NadB activity assay

*(iii) in vitro* AcnB activity

**Principle:** Aconitase B enzyme is a  $[4\text{Fe-4S}]^{2+}$  containing enzyme which catalyzes the interconversion between citrate and isocitrate in the Krebs cycle<sup>235</sup>. Its *in vitro* activity test is performed by a coupled reaction using isocitrate dehydrogenase (IDH) enzyme whose activity is  $\text{NADP}^+$  dependent. Isocitrate dehydrogenase catalyzes the transformation of isocitrate to  $\alpha$ -ketoglutarate and  $\text{NADP}^+$  cofactor is reduced to NADPH during the reaction. NADPH has an absorption at 340 nm ( $\epsilon_{340\text{nm}} = 6220 \text{ mM}^{-1}\cdot\text{cm}^{-1}$ ) and therefore allows to determine the isocitrate transformed by Isocitrate dehydrogenase and therefore the isocitrate formed by AcnB. In other words, the absorbance of NADPH formation is directly proportional to AcnB activity (Scheme 62).



**Scheme 62:** *in vitro* AcnB activity assay

**Implementation:** The test is performed under anaerobic conditions. In a quartz cell (100  $\mu$ L), AcnB (3  $\mu$ M), citrate (25 mM),  $\text{MnCl}_2$  (0.3 mM) and  $\text{NADP}^+$  (0.5 mM) are mixed. The reaction is started by the addition of isocitrate dehydrogenase enzyme (2.8  $\mu$ M). The

absorbance at 340 nm is monitored as a function of time allowing the quantification of NADPH and direct determination of AcnB activity (Table 12).

<u>Reactants</u>	<u>Final concentrations</u>
Aconitase B (AcnB)	3 $\mu$ M
Citrate	25 mM
MnCl <sub>2</sub>	0.3 mM
NADP <sup>+</sup>	0.5 mM
Isocitrate dehydrogenase 8.5mg/mL	2.8 $\mu$ M
Buffer D	Needed volume to complete 100 $\mu$ L

**Table 12:** *in vitro* AcnB activity assay

## f. Biochemical analyses

### (i) Protein quantification using Bradford method

Protein quantification is performed using the Bradford method<sup>236</sup>. The basis of this dosing technique is the color change of Coomassie blue at 595 nm, which is red itself but becomes blue when it is fixed to proteins through their basic residues (lysine, arginine, histidine...) and hydrophobic (tryptophan, phenylalanine...). A calibration curve is performed with known concentrations of Bovin Serum Albumin (BSA, sigma) ( $A_{595nm} = f([BSA])$ ). For this, different amounts of BSA protein at 1 mg/mL (0-10  $\mu$ L) are put in plastic cuvettes and the volume is completed to 10  $\mu$ L with water. 1 mL of a 5-fold diluted solution of Coomassie blue is added. Then, the absorbance is measured at 595 nm. Samples with unknown protein concentrations are prepared on the same way and their concentration is calculated thanks to the calibration curve.

### (ii) Protein quantification using Nanodrop

This technique allows the determination of the concentration of a protein. We measure the protein absorbance at 280 nm and knowing the theoretical molar extinction coefficient ( $\epsilon$ ) of the protein of interest (obtained from Swiss-Prot) the precise protein concentration is calculated. Advantages of this method are its rapidity, the fact that it consumes very little of protein (1  $\mu$ L is enough) and that it is not saturating. The

measurements are made on a UV-visible *Nanodrop 1000 Spectrophotometer* (Thermo scientific) spectrometric device.

### (iii) SDS-PAGE: Electrophoresis

Principle: The name of this technique refers to “Sodium Dodecyl Sulfate-Polyacrylamide Gel Electrophoresis”; an electrophoretic technique based on the differential migration of charged particles within an electric field.

Implementation: Electrophoresis is done under denaturing conditions. Proteins, 5-20 µg, are denatured by heating in a denaturing buffer that consists of 1M Tris-HCl pH=6.8, 10% SDS, 15% glycerol, 2% BPB (Bromophenol blue), 2% β-mercaptoethanol (buffer E).

- SDS is a detergent that acts by disrupting inter and intra-protein interactions, causing the loss of protein conformations leading to their denaturation. This negatively charged detergent allows all proteins to get a similar net negative charge. For this reason, the difference in mobility of the polypeptide chains within the gel can be attributed only to their molecular weight and not their charge.

- β-mercaptoethanol reduces disulfide bridges.

- Blue bromophenol (BPB) is used as a color marker in order to monitor the gel electrophoresis process.

The denatured protein samples are deposited in the wells of a commercial already prepared polyacrylamide gel (Mini-Protean TGX Precast Gels, BIO-RAD). This gel is constituted of a stacking gel (4 % polyacrylamide) and a separation gel (20 % polyacrylamide). The stacking gel allows an homogeneous migration of the proteins that settle down at the top of the separation gel by ensuring that all the proteins from the sample penetrate the second part of the gel simultaneously. At this point, proteins migrate thanks to an electric current (200 V, 150 mA) during 30 minutes. The gel plays the role of a molecular sieve, separating the proteins by their size. The small ones migrate faster than the big ones. The apparent mass of the proteins is evaluated by calibration with known proteins (Roti-Mark Standard 10-150, Roth). The bands corresponding to the proteins on the gel are revealed by a ready to use blue Coomassie protein stain (InstantBlue, Expedeon).

#### (iv) Iron content

Principle: The iron quantitation is performed by a variation of the Fish method<sup>237</sup>. Firstly, a calibration curve must be done.

Calibration curve: The calibration curve is done using a Fe<sup>2+</sup> solution at 500 μM prepared by dissolving Mohr's salt (Aldrich) in water. 1 μL of this solution contains 0.5 nmol of iron (Fe<sup>2+</sup>). Different iron amounts (nmol) are put in different Eppendorf tubes and the volume adjusted to 65 μL with H<sub>2</sub>O, as shown in the following table (Table 13):

<u>Fe<sup>2+</sup> (nmol)</u>	<u>Fe<sup>2+</sup> solution at 500 μM (μL)</u>	<u>water (μL)</u>
0	0	65
2	4	61
4	8	57
6	12	53
8	16	59
10	20	45

**Table 13:** Calibration curve for Fe quantification in proteins.

Then, each Eppendorf is treated on the following way:

- 45 μL of 1M perchloric acid (PCA) are added to the 65 μL solution and the eppendorfs energetically stirred. After 15 minutes at rt, they are centrifuged at 12000 rpm for 5 min. 90 μL of that solution are put in a new clean eppendorf tube and the following is added:
- 72 μL of bathophenanthroline disulfonate at 1.7 mg/mL. This product is an iron chelating agent.
- 36 μL of sodium ascorbate at 38 mg/mL. This product is a reducing agent allowing iron ion to be in Fe<sup>2+</sup> oxidation state.
- 27 μL of a 3 times diluted, saturated ammonium acetate solution (to neutralize the medium).

The solution is vigorously mixed and even though a pink color shows up at the first moment, the reaction medium is left at rt for 30 minutes in order to let the reaction goes until its end. The intensity of the pink color is proportional to the amount of iron present in

the sample. After incubation, the difference in the absorbance at 535-680 nm is measured for each sample. The calibration curve allows to determine the amount of iron per protein (nmol/nmol).

Protein samples: Samples containing a known protein amount (nmols) are prepared in H<sub>2</sub>O in 65 µL final volume. 45 µL of 1 M PCA are added in order to denature the proteins and the samples are energetically mixed. After 15 min incubation at rt, samples are centrifuged at 10000 rpm during 5 min, in order to remove the precipitated protein. 90 µL of the supernatant are taken and treated on the same way as the calibration curve samples. The measure of the absorbance (535-680 nm) allows to determine the iron content of the samples thanks to the calibration curve.

#### (v) Sulfur content

Principle: This technique allows the determination of sulfur content in a protein according to the colorimetric method of Beinert<sup>238</sup>. A calibration curve is also needed.

Calibration curve: The calibration curve is prepared from a Na<sub>2</sub>S solution at 200 µM in water. Samples containing known amounts of sulfide (0 to 10 nmoles) are prepared and the volume adjusted to 100 µL with water, as shown in the following Table 14:

<u>S<sup>2-</sup> (nmol)</u>	<u>Na<sub>2</sub>S solution at 200 µM (µL)</u>	<u>water (µL)</u>
0	0	100
1	5	95
5	25	75
10	50	50
20	100	0

**Table 14:** Calibration curve for S quantification in proteins.

To each eppendorf tube containing 100 µL are added:

- 300 µL of a Zn(OAc)<sub>2</sub> solution at 1 %, immediately followed by the addition of 15 µL of 3 N NaOH. The solution is vigorously stirred. This step avoids the loss of sulfur as H<sub>2</sub>S gas, that is produced by acidification of the medium by Zn(OAc)<sub>2</sub>. The reaction is left at rt for 5 minutes.

- 75  $\mu\text{L}$  of N, N-dimethyl-*p*-phenylenediamine (DMPD) at 0.01 % in 5 N HCl immediately followed by the addition of 16  $\mu\text{L}$  of  $\text{FeCl}_3$  at 23 mM in 1.2 N HCl. The samples are stirred again energetically and left at rt for 30 min. A blue color appears resulting from the formation of methylene blue complex, formed by the reaction of  $\text{S}^{2-}$  anions with DMPD in oxidant medium. The intensity of the blue color is proportional to the sulfide amount within the sample.

- Each tube is centrifuged at 10000 rpm during 5 minutes and then the absorbance measured at 670 nm. The calibration range is obtained by plotting the absorbance as a function of the sulfide amount (nanomole).

Protein samples: As for the calibration curve, defined protein amounts (nmol) are added to water in a final volume of 100  $\mu\text{L}$ . Then, similar treatment as the standard curve is performed except for the addition of DMPD and  $\text{FeCl}_3$  that is performed at 4°C during 3 h. Measurement of the absorbance at 670 nm allows the determination of the sulfur amount present on the protein sample (nmol/nmol).

## IV. Biological methods

### a. Functional complementation tests

Principle: The MG1655 $\Delta$ nadA *E. coli* strain (kana<sup>R</sup>) strain that lacks the *nadA* gene encoding for the quinolinate synthase cannot grow in M9 minimal medium (containing 0.2 % glucose, 200  $\mu\text{M}$   $\text{CaCl}_2$ , 2 mM  $\text{MgSO}_4$ ) without supplementation with quinolinic acid (QA), nicotinic acid (Na) or nicotinamide (Nm).

Implementation: An overnight culture of MG1655 $\Delta$ nadA *E. coli* (10 mL) at 37°C is performed in the presence of kanamycin (25  $\mu\text{g}/\text{mL}$ ). This pre-culture is centrifuged and the bacterial pellets washed five times with 10 mL M9. The bacterial pellet is resuspended in 10 mL of M9 and inoculated at 2 % in M9 medium containing 0.2 % glucose, 200  $\mu\text{M}$   $\text{CaCl}_2$ , 2 mM  $\text{MgCl}_2$ . The bacterial growth is measured at 600 nm after an overnight incubation at 37°C using TECAN (infinite 200) device. Two sets of growth conditions are used, in the absence and in the presence of QA (1.4 mg/mL). As mentioned above, MG1655 $\Delta$ nadA can grow only in the presence of QA.

The growth behavior of the MG1655 $\Delta$ *nadA* *E. coli* strain mimics a situation in which NadA enzyme in a wild-type MG1655 *E. coli* strain is inactivated by an inhibitor. Therefore, if a molecule inhibits a MG1655 *E. coli* strain and the inhibition is reversed by QA (1.4 mg/mL), it is considered as an inhibitor of the QA pathway and so constitutes an interesting molecule.

#### b. *E. coli* MG1655 bacterial growth in the presence of potential inhibitors

The objective of this test is to investigate quinolinate synthase inhibition *in cellulo* (*E. coli* MG1655 strain) in the presence of different molecules that were first shown to inhibit the NadA enzymatic activity *in vitro*. For that, an overnight *E. coli* MG1655 10 mL LB culture (37°C) is centrifuged, the bacterial pellet washed five times with 10 mL M9 and resuspended in 10 mL M9. This pre-culture is used to inoculate (2 %) a 10 mL M9 medium supplemented with 0.2 % glucose, 200  $\mu$ M CaCl<sub>2</sub>, 2 mM MgCl<sub>2</sub>. 300  $\mu$ L of this medium are distributed in the wells of a 96-well plate. The molecule that we want to test for its inhibitory activity is added in the different wells at different concentrations. A duplicate containing QA (8 mM) is performed. After an overnight incubation at 37°C, the bacterial growth is controlled by measuring the absorbance at 600 nm using a TECAN (infinite 200) device. Interesting wells (and therefore molecules) are those where the bacterial growth is inhibited without QA and reversed in the presence of QA.

## V. Spectroscopic, biophysical and analytical methods

### a. Reversed-phase high performance liquid chromatography (HPLC)

Principle: The high performance liquid chromatography (HPLC) is a technique in analytical chemistry used to separate, identify and quantify each component of a mixture. The separation is done according to the polarity of the molecules. The sample to be analyzed is pushed by a solvent (called the mobile phase) through a column which is filled by small sized particles (stationary phase). In order to push the mobile phase through the column with a high flow rate, a high pressure pump is needed. This high flow rate decreases the time of separation of the different compounds comparing to a classical liquid chromatography and the small size on the stationary phase permits a better separation. As a consequence of these two attributes, rapidity and high resolution are obtained, which are the reason for the addition of “high performance” to the name of this liquid chromatography.

In the case of the reversed-phase HPLC (the one I have used), the stationary phase is nonpolar. The column used is a Kinetex 5u C18 100A (Phenomenex), and it consists in a core-shell of silica grafted by 18-carbon alkyl chains, which is apolar. Compounds from the most polar to the least polar are eluted by a polar solvent (mobile phase). By changing the polarity of the mobile phase, the retention time of each compound is modified allowing the elution.

The equipment I have used is an Agilent HP1100 HPLC device that is equipped with an automatic sampler allowing to program of up to 100 injections. Samples to be analyzed are charged onto the column by a robot and through a syringe. A diode array UV detector at the exit of the column allows the detection of the compounds, leading to an HPLC chromatogram which is represented by the absorbance at a chosen wavelength (273 nm) as a function of time. According to our program (Table 15), Quinolinic acid (QA) has a retention time of 8.7 minutes and a characteristic UV-visible spectrum with a well-defined absorption band at 273 nm (Figure 68). A calibration curve plotting the area as a function of commercial QA amounts (10, 20, 30 and 40 nmoles) allows the quantification of QA in our assays.

Time (min)	TFA 0.03 %	Acetonitrile 100 %
0	100	0
17	100	0
37	0	100
47	0	100
57	100	0
77	100	0

**Table 15:** HPLC protocol for QA elution

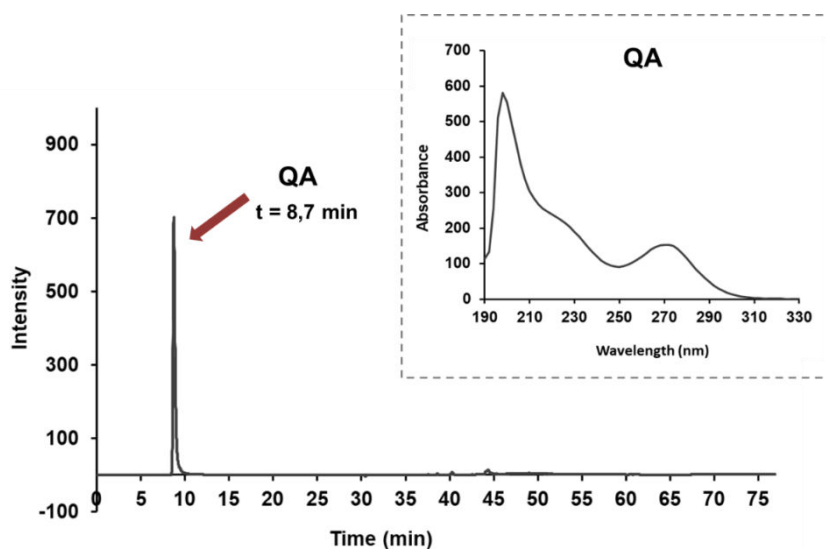


**Figure 68:** QA chromatogram ( $\lambda=273$  nm) and UV-visible spectrum (insert).

## b. UV-visible absorption spectroscopy

Principle: The absorption of a photon by an atom or molecule allows it to move from the ground state  $S_0$  to a higher energy state  $S_1$  by excitation of electrons that move from one orbital to another. The energy of the ultra-violet radiation that is absorbed is equal to the energy difference between the ground state and higher energy states ( $\Delta E = h\nu$ ), where  $h$  is the Planck constant and  $\nu$  the frequency of the photon ( $\nu = c/\lambda$ ,  $\lambda$  corresponds to the wavelength and  $c$  corresponds to the speed of light ( $3.00 \times 10^8$  m/s)). In solution, only low energy transitions are observable, those on the near-UV and visible wavelengths. Each absorption band is characterized by the wavelength at which the absorption reaches its maximum ( $\lambda_{max}$ ) and by its intensity which is given by the molar extinction coefficient ( $\epsilon$ ) at that wavelength. These parameters are related to the concentration thanks to the Beer-Lambert law by the following equation:  $A_\lambda = \epsilon_\lambda \cdot l \cdot [C]$ ; where  $A$  is the absorbance,  $l$  is the optical path length and  $C$  is the concentration of the molecule of interest.

Obtained information: The biological molecules that absorb at the UV-visible energies are those containing conjugated double bonds, aromatic nuclei or those containing a transition metal. The absorption peak observed at 280 nm in protein solutions corresponds to the absorption of the aromatic amino acids of the polypeptide chain, which are tryptophan, tyrosine and phenylalanine. Proteins containing a Fe-S cluster present absorptions between 300 and 550 nm due to a charge transfer band from the ligand to the metal, i.e. from the sulfur to the  $Fe^{3+}$ . This value changes depending on the nature of the Fe-S cluster:  $[2Fe-2S]^{2+}$  clusters display characteristic signatures at 320, 410-420 and 450-460 nm ( $\epsilon_{452nm} = 7 - 10 \text{ mM}^{-1} \cdot \text{cm}^{-1}$ ) and a shoulder at 550 nm for complete cysteinyl coordination and lower values ( $5.3 - 6.3 \text{ mM}^{-1} \cdot \text{cm}^{-1}$ ) for incomplete cysteinyl coordination<sup>239</sup>.  $[4Fe-4S]^{2+}$  clusters display only one signature around 410 nm ( $\epsilon_{410nm} = 9 - 16 \text{ mM}^{-1} \cdot \text{cm}^{-1}$ )<sup>239</sup>. The position of the absorption band maxima as well as their intensity provide information about the Fe-S cluster nature and amount.

Implementation: The absorption spectra are recorded in quartz cells of 1 cm or 1 mm path length depending on the sample concentration. We usually work with the 1 cm optical length cells with volumes between 100-150  $\mu\text{L}$ . In order to have an adequate absorption signal (without reaching saturation), the absorbance should not be higher than 1-1.5. In the case of NadA, this is obtained with protein concentrations around 10  $\mu\text{M}$ . With the samples

for Mössbauer spectroscopy we use the 1 mm cell (200-300  $\mu\text{L}$ ) for protein concentrations around 100-200  $\mu\text{M}$ .

Studies under aerobic conditions are performed with a CARY 50 (Varian) spectrometer and those under anaerobic conditions with a Uvikon XL (Bio-Tek instruments) spectrometer, which is coupled by optic fibers to the quartz cell placed inside the glove box.

### c. Mössbauer spectroscopy

Principle: The Mössbauer spectroscopy is a spectroscopy technique that studies the resonant emission and absorption of  $\gamma$  rays, a type of radiation created by nuclear transitions. It is based on the Mössbauer effect (Figure 69).

When a nucleus undergoes a transition to go from an excited state  $E_E$  to its ground state  $E_G$ , a  $\gamma$  photon is emitted and its energy is equal to the nuclear transition energy minus the recoil energy. However, the Mössbauer effect states that when atoms are held tightly in solid atomic structures, the  $\gamma$  radiation emitted by their nuclei are very close to being recoil-free. This means, that the emitted  $\gamma$  ray has the exact energy that corresponds to the transition energy between the nuclear ground state and the excited state. As a consequence, this photon might be absorbed by an identical nucleus state (which must also be held tightly in solid structure) that will be excited from its ground state  $E_G$  to its excited state  $E_E$ .

$^{57}\text{Fe}$  is by far the most common element studied using this technique and the one we use to study NadA  $[\text{4Fe-4S}]^{2+}$  cluster. For this, the  $\gamma$  ray source is obtained by radioactive disintegration of the isotope  $^{57}\text{Co}$  which is converted to an excited state of  $^{57}\text{Fe}$  ( $^{57}\text{Fe}^*$ ) by electron capture. Within a short period of time of the order of the microsecond,  $^{57}\text{Fe}^*$  comes back to the ground state  $^{57}\text{Fe}$  by emitting a high frequency  $\gamma$  ray.

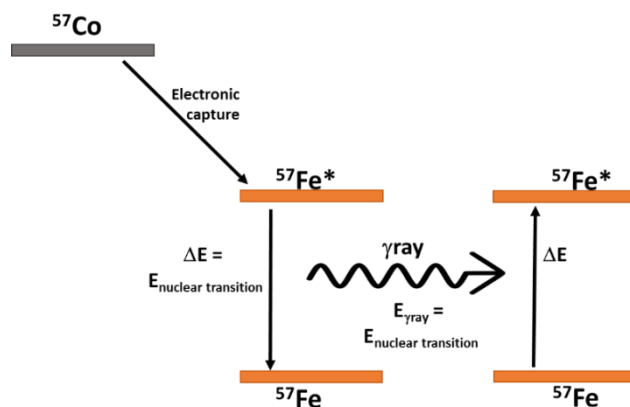


**Figure 69:** Mössbauer effect.

If the nuclei of the sample are on a different environment with regard to those of the source, the environmental electronic modification of the nuclei makes a change on the nuclei energy levels strong enough to not permit the absorption of the  $\gamma$  ray. In order to establish the resonance, the  $\gamma$  ray energy must be modified. This is achieved by moving the source at a relative speed ( $v$ ), with regard to the sample. This allows an appropriate scanning of the  $\gamma$  ray energy spectrum where the sample is likely going to absorb. This is the basis of the Doppler Effect. For this reason, in Mössbauer spectroscopy, energies are expressed in speed units (mm/s). Thus, a Mössbauer spectrum shows the  $\gamma$  ray relative transmission that have gone through the sample (or the  $\gamma$  ray absorbance of the sample) as a function of the relative velocity of the source with regard to the iron atom.

Mössbauer spectroscopy characterizes the  $\gamma$  ray absorption by two different parameters, which correspond to different hyperfine interactions that are caused by perturbations created by the environment of the sample (Figure 70).

***Isomeric shift,  $\delta$  (electric monopole interaction)***

Since the absorbing nucleus environment is different to that of the source, the absorption peak is shifted with regard to the absorption line of the source. This is called the isomeric shift and its unit is mm/s. This shift originates from a hyperfine interaction involving the nucleus and the inner electrons of the atom; the electron charge density at the nucleus. Even though only s orbitals are spherical and incorporate the volume taken up by the nucleus, other electrons may influence the s orbitals' electron density, such as the oxidation

state of the iron and its chemical environment. For this reason, this parameter provides information about the oxidation state, the covalence degree and the nature of the ligands of the iron atom, ( $^{57}\text{Fe}$ ).

### **Quadrupole splitting, $\Delta_{EQ}$ (electric quadrupole interaction)**

On the one hand, the asymmetry of the charge distribution around the nucleus creates an electric field gradient. On the other hand, when the spin state of the nucleus is  $|>1/2|$  it possesses an electric quadrupole moment,  $Q$ . The interaction of these two is called the quadrupole interaction and leads to a splitting of the excited state. The energy separation between those substrates is the quadrupole splitting parameter and it is expressed in mm/s. It provides information about site symmetry and the arrangement of charges around the iron nucleus.

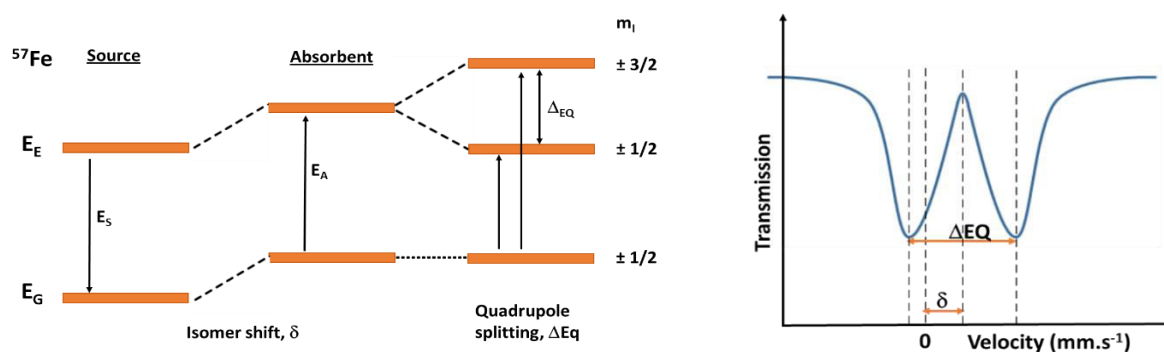


**Figure 70:** Chemical shift ( $\delta$ ) and quadrupole splitting ( $\Delta_{EQ}$ ) of the nuclear energy levels and corresponding Mössbauer spectrum.

The volume of a Mössbauer cup is 400  $\mu\text{L}$  and the concentration of the protein is adjusted depending on its iron content. In order to have a nice Mössbauer spectrum, the  $^{57}\text{Fe}$  concentration should be between 500  $\mu\text{M}$  and 1 mM.

### **d. Circular dichroism**

Principle: Circular dichroism is an absorption spectroscopy in the ultraviolet region that is used in biology to obtain information about macromolecules in solution. These macromolecules must be optically active, in other words, they must be chiral and absorb differently depending on the polarization of the light (dextrorotary and levorotary). This

technique is very used for the study of protein secondary structures, since proteins are chiral macromolecules.

Obtained information: By measuring the absorption difference of a protein when exposed to two types of polarized light, many information can be obtained, especially concerning its secondary structure. It allows to estimate the proportion of a protein that is in the alpha-helix conformation, the beta-sheet conformation ( $\beta$ -I or  $\beta$ -II) or just disordered (Figure 71).

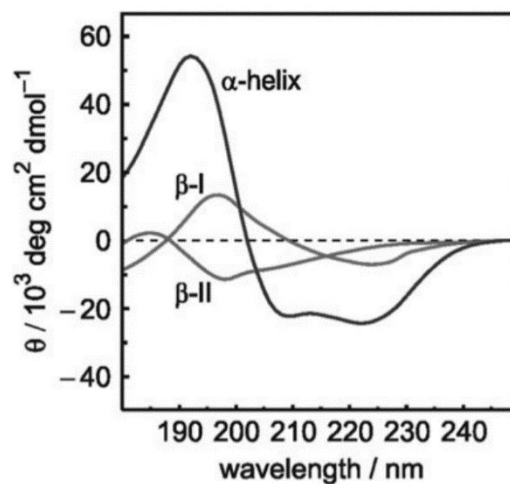


**Figure 71:** Characteristic CD spectra of secondary structure elements ( $\beta$ -I,  $\beta$ -II,  $\alpha$ -helix). The vertical axis shows intensity as the mean residue ellipticity,  $\theta^{240}$ .

CD is a qualitative technique, very useful especially for studying changes in the secondary structure of a protein as a function of temperature or concentration of exogenous ligands (proteins, metals, inhibitors...). It is a fast and non-destructive technique that does not consume a lot of protein.

In our case, CD was used in order to investigate the interaction of inhibitors with NadA protein. The advantage of this technique with regard to UV-visible spectroscopy is that one detects only what is interacting with the protein, regardless of what is remaining in solution (excess of inhibitor...).

Implementation: Spectra are recorded with a JASCO J-1500 circular dichroism spectrometer in a 3 mL quartz cell of 1 cm optical path length. The protein concentration is around 10  $\mu$ M in order to have a good signal. The volume is completed with buffer D. The

samples are prepared in the glove box, the cell firmly closed with a septum and parafilm and only taken out of the glove box at the moment of the measurement, in order to avoid any exposure to O<sub>2</sub>.

## VI. Protein crystallization and X-Ray structures

### a. Crystallization

All experiments were performed under anaerobic conditions with the *TmNadA*\*Y21F variant, starting from a stock solution with a protein concentration of 65 mg/mL in 50 mM KCl and 100 mM Tris HCl buffer at pH 8.0. The three protein-ligand complexes were prepared as follows.

#### i. 4MP (4-mercaptopyridine-2,3-dicarboxylic acid) complex.

The protein stock solution was diluted inside a glove box to 20 mg/mL in 50 mM KCl and 125 mM Tris HCl at pH 7.2. A volume of 50 µL of this solution was incubated overnight at 20 °C with 0.8 µL of 75 mM 4MP in 25 mM Tris HCl at pH 8.0, providing a 1:2 protein to ligand ratio. Hanging drops were prepared by mixing one µL of the complex solution with the same volume of a reservoir solution consisting of 26 % PEG33500, 100 mM NaCl, 200 mM Na<sub>2</sub>HPO<sub>4</sub> and 100 mM MES at pH 6.7 and equilibrated against 1 mL of the latter by vapor diffusion. A plate-shaped brown crystal grew after three weeks in one of these drops. This crystal was transferred to a cryo-protectant solution prepared with 40 % PEG33500, 100 mM HEPES pH 7.0, 200 mM Na<sub>2</sub>HPO<sub>4</sub> and 100 mM NaCl, and was flash-cooled anaerobically using liquid propane and immediately stored in liquid nitrogen, as previously described<sup>241</sup>.

#### ii. 6MPDC (6-mercaptopyridine-2,3-dicarboxylic acid) complex.

The protein stock solution was diluted inside a glove box to 20 mg/mL by Microcon-10 kDa dialysis in 10 mM Tris HCl pH 8.0. Next 45 µL of this solution was incubated overnight at 20 °C with 1.3 µL of 50 mM 6MPDC in 10 mM KCl and 50 mM HEPES pH 7.1, giving a 1: 2.6 protein to ligand ratio. One µL of the complex solution was mixed with 1 µL of a solution of 26 % PEG33500, 1 % dioxane, 200 mM Na<sub>2</sub>HPO<sub>4</sub> and 100 mM HEPES at pH 7.3 and the resulting hanging drop was equilibrated with 1 mL of the latter reservoir solution. Brown plate-shaped crystals obtained after 2 days were transferred to a cryo-protectant solution of 34% PEG33500, 1 % dioxane, 200 mM Na<sub>2</sub>HPO<sub>4</sub> and 100 mM HEPES at pH 7.5, flash-cooled and stored as described above for the 4MP complex.

iii. 5MPDC (5-mercaptopyridine-2,3-dicarboxylic acid) complex.

The protein solution was first diluted inside a glove box to 32 mg/mL as described for 6MPDC. 50  $\mu$ L of this solution was incubated overnight at 20 °C with 22  $\mu$ L of 7.5 mM 5MPDC in 25 mM Tris HCl pH 8.0 and 9.25  $\mu$ L of 50 mM KCl and 10 mM Tris HCl pH 8.0, to give a 1:3:5 protein to ligand ratio. One  $\mu$ L of the complex solution was next mixed with 1  $\mu$ L of a reservoir solution of 28 % PEG33500, 100 mM NaCl, 200 mM Na<sub>2</sub>HPO<sub>4</sub> and 100 mM CHES pH 9.3. The resulting hanging drop was equilibrated in the vapor phase with 1 mL of the reservoir solution and crystalline brown plates were obtained after 10 days. These were transferred to a cryo-protectant solution of 34 % PEG33500, 100 mM NaCl, 200 mM Na<sub>2</sub>HPO<sub>4</sub> and 100 mM CHES at pH 9.3 and flash-cooled and stored as described above for the complexes with 4MP and 5MPDC.

iv. TmNadA\*-QA Complex (5MPDC-derived)

First, 50  $\mu$ L of a 44.6 mg mL<sup>-1</sup> protein solution in 50 mM KCl, 100 mM Tris HCl pH 8.0 were incubated anaerobically overnight at 20 °C after the addition of 27  $\mu$ L 7.5 mM 5MPDC in 25 mM Tris HCl pH 8.0 and 23  $\mu$ L of a solution containing 50 mM KCl and 125 mM Tris HCl pH 7.2. One  $\mu$ L of the resulting solution, containing 22.3 mg mL<sup>-1</sup> protein, was initially mixed with 1  $\mu$ L of a solution containing 22 % PEG3350, 200 mM Na<sub>2</sub>HPO<sub>4</sub> in 100 mM CHES pH 9.1. Prior to mixing the latter solution was left to sit in order to deposit some precipitated Na<sub>2</sub>HPO<sub>4</sub>. After 37 days, the crystallization drop was transferred to a well containing 1 mL of a solution that before phosphate precipitation contained 34 % PEG3350, 200 mM Na<sub>2</sub>HPO<sub>4</sub> in 100 mM CHES pH 9.1. Twelve days later, the drop was again transferred to a well containing 1 mL of a solution composed of 36 % PEG3350, 200 mM Na<sub>2</sub>HPO<sub>4</sub> in 100 mM CHES pH 9.1 before phosphate precipitation. Several brown crystals were observed in the transferred drop 105 days later. A fragment of one of these crystals was transferred to a cryoprotecting solution composed of 40 % PEG3350, 200 mM Na<sub>2</sub>HPO<sub>4</sub> in 100 mM CHES pH 9.5 and flash-cooled using liquid propane inside the glovebox.

**b. X-Ray Structure Determination.**

X-ray diffraction data were collected at beam lines ID29 and ID30B of the European Synchrotron Radiation Facility in Grenoble, France (Table 16 and 17), using the program *MXCuBe*<sup>242</sup>. After indexation, integration and initial scaling with the *XDS* package<sup>243</sup>, the data were submitted to a final scaling and merging step with *AIMLESS*<sup>244</sup> of the *CCP4* package<sup>245</sup>.

Structures were solved by molecular replacement with *PHASER*<sup>246</sup> using the *TmNadA*\*-citrate complex<sup>138</sup> (pdb code 5F35) as the starting model. Manual model corrections were performed with *COOT*<sup>247</sup>. *REFMAC5*<sup>248</sup> was used to refine individual atomic positions and isotropic temperature factors along with TLS parameters of the three NadA domains and its cluster binding region for the 6MPDC and 5MPDC complexes, whereas the same program was used to refine atomic positions and anisotropic temperature factors for the 4MP complex. Dictionary files needed for the refinement of the three ligands were built as described previously for reaction intermediate **W**<sup>138</sup>. Refinement statistics are included in Table 16. All the programs mentioned above, except *MXCuBe*, were provided by SBGrid<sup>249</sup>.

Complex	4MP	6MPDC	5MPDC
pH	pH 7.0	pH 7.3	pH 9.3
<b>Data collection</b>			
ESRF beamline	ID29	ID30B	ID30B
Wavelength (Å)	1.07438	0.97625	1.00394
Space group	P2 <sub>1</sub>	P2 <sub>1</sub>	P2 <sub>1</sub>
Cell: a, b, c (Å)	55.7, 48.4, 60.6	55.5, 48.7, 60.5	55.3, 48.5, 60.5
Cell: β(°)	107.66	106.9	107.1
Resolution (Å)	46.8-1.60	46.4-1.80	37.2-2.10
high resolution shell*:	(1.66-1.60)	(1.86-1.80)	(2.17-2.10)
anisotropy along <b>a</b> , <b>b</b> and <b>c</b> (Å)	1.60 1.60 1.76	1.80 1.86 1.97	2.56 2.10 2.10
Measured reflections	176966 (18269)	92266 (8344)	34884 (3403)
Unique reflections	40160 (3936)	27322 (2615)	16840 (1658)
Redundancy	4.4 (4.6)	3.4 (3.2)	2.1 (2.1)
Completeness (%)	98.7 (99.5)	95.4 (93.7)	94.9 (96.6)
R <sub>merge</sub> (%)	7.6 (129.8)	8.8 (140.8)	10.3 (76.5)
CC <sub>1/2</sub>	0.997 (0.314)	0.995 (0.288)	0.983 (0.392)
<I/σ <sub>I</sub> >	8.7 (1.0)	7.2 (0.8)	4.9 (0.9)
<b>Refinement</b>			
Resolution (Å)	46.8-1.64	46.5-1.90	37.2-2.10
Used reflections	35415	22114	16006
R <sub>work</sub> (%)	15.7	19.1	21.0
Reflections for R <sub>free</sub>	1845	1167	826
R <sub>free</sub> (%)	20.6	22.1	24.3
Number of atoms	2704	2635	2557
Average B-factor (Å <sup>2</sup> )	34.1	37.1	46.2
R.m.s. deviations			
Bond lengths (Å)	0.010	0.012	0.012
Bond angles (°)	1.4	1.5	1.5

\* the high resolution shell is given in parenthesis for all values

**Table 16:** X-ray data and refinement statistics for *TmNadA*\*-Y21F crystals.

<b>TmNadA* 5MPDC-derived QAcomplex</b>	
<b>Data collection</b>	
ESRF beamline	ID30A3
Wavelength (Å)	0.96770
Space group	P2 <sub>1</sub>
Cell: a (Å)	55.4
b (Å)	49.31
c (Å)	61.90
α (deg)	90
β (deg)	107.21
γ (deg)	90
Resolution (Å)	47.0-2.30
(high-resolution shell)	(2.38-2.30)
Measured reflections	77646 (8006)
Unique reflections	14259 (1412)
Redundancy	5.4 (5.7)
Completeness (%)	99.1 (99.7)
Rmerge (%)	12.0 (157.4)
CC1/2	0.996 (0.375)
<I/σI>	8.9 (1.0)
<b>Refinement</b>	
Resolution (Å)	47.0-2.30
Used reflections	13514
R <sub>work</sub> (%)	20.2
Reflections for R <sub>free</sub>	720
R <sub>free</sub> (%)	22.1
Number of atoms	2468
Average B-factor (Å <sup>2</sup> )	55.1
Bond lengths (Å)	0.011
Bond angles (deg)	1.4

\* the high resolution shell is given in parenthesis for all values

**Table 17:** X-ray data and refinement statistics for *TmNadA\**-5MPDC-derived QA crystals.

## VII. QA Production by 5MPDC and NadA in Solution.

*TmNadA\** (430 μM) was mixed with 3.5 mol equiv of 5MPDC in 125 mM Tris, 50 mM KCl pH 8.0 buffer. After an overnight incubation, 100 mM CHES pH 9.5 crystallization buffer was added to a 1:1 ratio (v/v) to the *TmNadA\**-5MPDC solution. Formation of QA was monitored by HPLC by withdrawing 20 μL from this reaction mixture daily for the first 2 days and every 5 days until the 35th day. At that time, 2 μL of 2 M H<sub>2</sub>SO<sub>4</sub> was added to the withdrawn 20 μL in order to stop the reaction. Then, samples were diluted by the addition of 80 μL of 0.03% trifluoroacetic acid, pH 2.4 buffer and centrifuged at 13000 rpm for 15 min to

remove all insoluble materials. The supernatant (80  $\mu$ L) was then injected to a HPLC system. QA formation was detected and quantified as previously described. A control experiment with 5MPDC but without TmNadA\*, was carried out in parallel and a sample from this solution was analyzed by HPLC at day 35.

## VIII. Confocal microscopy

Fluorescence was observed on an Olympus BX61 microscope equipped with a UPFLN 100 O-2PH/1.3 objective and a QImaging Retiga-SRV 1394 cooled charge-coupled-device camera. Images were acquired using the Volocity software (PerkinElmer). 50  $\mu$ L of bacteria concentrated to OD=15 were incubated in the presence of 5  $\mu$ L of the molecule of interest (20  $\mu$ M) during 5 min at 37 °C. Bacteria were observed after 3 washes with PBS (3x1 mL). Observation filter GFP, acquisition time 500 ms to 1 s.

---

## IX. Buffers

**Buffer A:** 100 mM Tris-HCl, pH 8, 50 mM NaCl

**Buffer B:** 50 mM Hepes-Na, pH 7.5, 100 mM KCl

**Buffer C:** 0.03 % TFA, pH 2.4

**Buffer D:** 50 mM Tris-HCl, pH 7.5

**Buffer E** (denaturation buffer): 1 M Tris-HCl, pH 6.8, 10% SDS, 15% glycerol, 2 % BPB, 2 %  $\beta$ -mercaptoethanol

## X. Chemistry experimental section

### a. Products and solvents

The products used come from Sigma-Aldrich, Fluka, Oribase Pharma, Life Chemicals and Chem space and were used without any purification. The solvents were not distilled before use, except for DMSO, which was distilled and dried with CaH<sub>2</sub>.

## b. Analytic devices

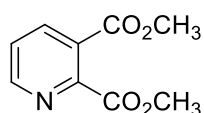
**NMR spectra** were recorded on a Bruker Avance 300 MHz, Bruker Avance 400 MHz or Bruker Avance 500 MHz at 298 K and processed with Bruker TopSpin software. The chemical shifts  $\delta$  are reported in parts per million (ppm).  $^1\text{H}$ - and  $^{13}\text{C}$ -NMR shifts are referenced according to the applied deuterated solvent as internal standard (Eurisotop). Coupling constants  $J$  are presented as absolute values in Hz. For the characterization of the NMR signals, the following abbreviations are used: s= singlet, d= doublet, t, triplet, q= quartet, m= multiplet, dd= doublets of doublets, ddd= doublet of doublets of doublets, bs= broad signal). Attributions were given using 2D spectra.

**ESI-MS** values are given as  $m/z$ . Mass spectrometric measurements were performed on a LXQ-linear ion trap (Thermo Scientific, San Jose, CA, USA), equipped with an electrospray source in a aqueous or aqueous/acetone mixture. Electrospray full scan spectra in the range  $m/z$  50-2000 amu, were obtained by infusion through fused silica tubing at 2-10  $\mu\text{L}\cdot\text{min}^{-1}$ . The LXQ calibration was achieved according to the standard calibration procedure from the manufacturer (mixture of caffeine/MRFA and Ultramark 1621). The temperature of the heated capillary of the LXQ was set to the range 150-200 °C, the ion spray voltage was in the range 1-3kV. The experimental isotopic profile was compared in each case to the theoretical one. The spectra were performed in SCIB/INAC/CEA-Grenoble in collaboration with Colette Lebrun.

## c. Synthesis of NadA inhibitors

### i. 6MPDC: 6- mercaptopyridine- 2, 3-dicarboxylic acid

Pyridine- 2, 3- dicarboxylic acid dimethyl ester[1]<sup>190</sup>

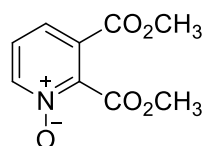


To a suspension of pyridine- 2, 3- dicarboxylic acid (10.02 g, 59.96 mmol) in MeOH (50 mL) at 0 °C, concentrated  $\text{H}_2\text{SO}_4$  (4.0 mL, 74.95 mmol) was added. The mixture was refluxed for 24 h and then cooled to rt. After evaporation of the solvent, the remaining residue was treated with a saturated solution of  $\text{NaHCO}_3$  until pH 8 followed by four

extractions with EtOAc. The combined organic phases were dried with MgSO<sub>4</sub> then concentrated under reduced pressure. The resulting oily residue was washed several times with Et<sub>2</sub>O to yield the desired product as a white shiny powder (9.13 g, 78 %).

**RMN <sup>1</sup>H (300 MHz, CDCl<sub>3</sub>):** δ (ppm) 8.76 (dd, *J* = 4.80, 1.6 Hz, 1H), 8.17 (dd, *J* = 7.9, 1.6 Hz, 1H), 7.49 (dd, *J* = 7.9, 4.8 Hz, 1H), 4.00 (s, 3H), 3.93 (s, 3H). **RMN <sup>13</sup>C (75 MHz, CDCl<sub>3</sub>):** δ (ppm) 166.5 (C), 165.8 (C), 151.8 (CH), 150.7 (C), 137.5 (CH), 126.5 (C), 124.9 (CH), 53.1 (CH<sub>3</sub>), 52.9 (CH<sub>3</sub>). **ESI-MS: m/z calcd for [C<sub>9</sub>H<sub>9</sub>NO<sub>4</sub>+H<sup>+</sup>]<sup>+</sup>:** 196.1; **found:** 195.9.

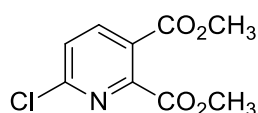
Pyridine- 2, 3- dicarboxylic acid dimethyl ester N-oxide [2]<sup>190</sup>



To a solution of pyridine- 2, 3-dicarboxylic acid dimethyl ester (9.03 g, 46.26 mmol) in chloroform (130 mL), *m*-CPBA (31.94 g, 185.07 mmol) was added. The reaction mixture was refluxed for 24 h, cooled to rt and the resulting insoluble benzoic acid was filtered off. The filtrate was treated with a saturated solution of NaHCO<sub>3</sub> until pH 8 then extracted 3 times with CH<sub>2</sub>Cl<sub>2</sub>. The combined organic phase was washed with brine, dried with MgSO<sub>4</sub> and concentrated *in vacuo*. Solubilization of the residue in a minimum of CH<sub>2</sub>Cl<sub>2</sub> and precipitation of the product by addition of the resulting solution into a large volume of Et<sub>2</sub>O cooled at -20 °C afforded the desired product (4.98 g, 51 %) as a pale yellow solid pure enough to be used without further purification. However, the product can be purified for characterization by recrystallization in a CH<sub>2</sub>Cl<sub>2</sub>/Et<sub>2</sub>O 1:1 mixture.

**RMN <sup>1</sup>H (300 MHz, CDCl<sub>3</sub>):** δ (ppm) 8.35 (dd, *J* = 6.6, 1.2 Hz, 1H), 7.86 (dd, *J* = 8.1, 1.2 Hz, 1H), 7.38 (dd, *J* = 8.1, 6.6 Hz, 1H), 4.05 (s, 3H), 3.93 (s, 3H). **RMN <sup>13</sup>C (75 MHz, CDCl<sub>3</sub>):** δ (ppm) 162.4 (C), 161.6 (C), 143.9 (C), 142.6 (CH), 127.2 (C), 126.4 (CH), 125.8 (CH), 53.5 (CH<sub>3</sub>), 53.4 (CH<sub>3</sub>). **ESI-MS: m/z calcd for [C<sub>9</sub>H<sub>9</sub>NO<sub>5</sub>+H<sup>+</sup>]<sup>+</sup>:** 212.1; **found:** 212.0.

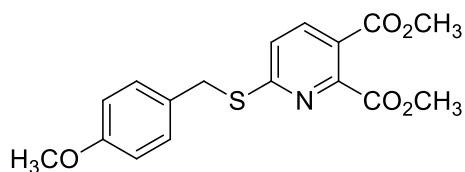
6-chloropyridine- 2, 3- dicarboxylic acid dimethyl ester [3]<sup>190</sup>



A solution of pyridine- 2, 3- dicarboxylic acid dimethyl ester N-oxide (4.88 g, 23.11 mmol) was refluxed in phosphorus (V) oxychloride (20 mL) for 8 h. After cooling to rt the solution was cautiously added to an ice-water mixture and the product was further extracted three times with EtOAc. The combined organics were washed with brine, dried with MgSO<sub>4</sub>. After evaporation of the solvent, the residue was purified by silica gel column chromatography (20 % EtOAc in Et<sub>2</sub>O) to yield the desired product as a yellow oil (3.70 g, 16.11 mmol, 70 %).

**RMN <sup>1</sup>H (300 MHz, CDCl<sub>3</sub>):** δ (ppm) 8.17 (d, J = 8.3 Hz, 1H), 7.52 (d, J = 8.3 Hz, 1H), 4.00 (s, 3H), 3.94 (s, 3H). **RMN <sup>13</sup>C (75 MHz, CDCl<sub>3</sub>):** δ (ppm) 165.4 (C), 164.6 (C), 154.2 (C), 151.7 (C), 140.3 (CH), 125.7 (CH), 124.3 (C), 53.2 (CH<sub>3</sub>), 53.1 (CH<sub>3</sub>). **ESI-MS: calcd for [C<sub>9</sub>H<sub>8</sub>ClNO<sub>4</sub>+H<sup>+</sup>]<sup>+</sup>:** 230.0; **found:** 229.9.

6- ((4- methoxybenzyl)thio) pyridine- 2, 3- dicarboxylic acid dimethyl ester [4]

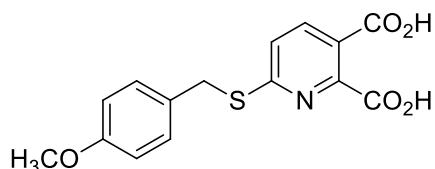


To a solution of triethylamine (4.12 mL, 29.6 mmol) in MeOH (90 mL) previously deoxygenated by argon bubbling for 10 min, α-methoxytoluenethiol (4.12 mL, 29.6 mmol) and 6-chloropyridine- 2, 3-dicarboxylic acid dimethyl ester (3.40 g, 14.8 mmol) were added. The mixture was then refluxed for three days then diluted with water and extracted three times with EtOAc. The organic layers were combined, washed with brine, dried over MgSO<sub>4</sub> and the solvent was evaporated. The obtained residue was purified by column chromatography (2 % MeOH in CH<sub>2</sub>Cl<sub>2</sub>) to afford the tittle compound as a white yellowish powder (7.78 g, 53 %).

**RMN <sup>1</sup>H (300.12 MHz, CDCl<sub>3</sub>):** δ (ppm) 8.00 (d, J = 8.4 Hz, 1H), 7.34 (d, J = 8.7 Hz, 2H), 7.25 (d, J = 8.4 Hz, 1H), 6.84 (d, J = 8.7 Hz, 2H), 4.44 (s, 2H), 4.03 (s, 3H), 3.91 (s, 3H), 3.80 (s, 3H). **RMN <sup>13</sup>C (75 MHz, CDCl<sub>3</sub>):** δ (ppm) 167.1 (C), 165.1 (C), 164.2 (C), 158.9 (C), 152.0 (C), 137.0

(CH), 130.3 (2 CH), 129.0 (C), 122.3 (CH), 119.8 (C), 114.0 (2 CH), 55.3 (CH<sub>3</sub>), 52.9 (CH<sub>3</sub>), 52.6 (CH<sub>3</sub>), 34.1 (CH<sub>2</sub>). **MS-ESI: calcd for [C<sub>17</sub>H<sub>17</sub>NO<sub>5</sub>S+H<sup>+</sup>]<sup>+</sup>: 348.1; found: 348.0.**

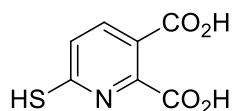
#### Synthesis of 6-((4-methoxybenzyl)thio)pyridine-2,3-dicarboxylic acid [5]



To a solution of 6-((4-methoxybenzyl)thio)pyridine-2,3-dicarboxylic acid dimethyl ester (2,56 g, 7,37 mmol) in Et<sub>2</sub>O (14 mL), an aqueous solution of 5 M NaOH (14 mL) was added. The mixture was refluxed for 24 h then cooled to rt. After acidification of the solution until pH 2 by dropwise addition of concentrated HCl, the product was extracted three times with EtOAc. The combined organic layers were dried with MgSO<sub>4</sub> then evaporated. The resulting residue was washed several times with acetone to afford the tittle compound as a white solid (2.21 g, 94 %).

**RMN <sup>1</sup>H (300MHz, acetone-d<sub>6</sub>):** δ (ppm) 8.12 (d, *J* = 8.5 Hz, 1H), 7.46 (d, *J* = 8.5 Hz, 1H), 7.41 (d, *J* = 8.5 Hz, 2H), 6.86 (d, *J* = 8.5 Hz, 2H), 4.47 (s, 2H), 3.77 (s, 3H). **RMN <sup>13</sup>C (75 MHz, acetone-d<sub>6</sub>):** δ (ppm) 166.7 (C), 165.2 (C), 163.2 (C), 159.1 (C), 152.6 (C), 137.8 (CH), 130.3 (2 CH), 129.3 (C), 122.1 (CH), 120.5 (C), 113.8 (2 CH), 54.6 (OCH<sub>3</sub>), 33.3 (CH<sub>2</sub>). **MS-ESI: calcd for [C<sub>15</sub>H<sub>13</sub>NO<sub>5</sub>S-H<sup>+</sup>]<sup>-</sup>: 318.0; found: 317.9, calcd for [C<sub>15</sub>H<sub>13</sub>NO<sub>5</sub>S-H<sup>+</sup>-CO<sub>2</sub>]<sup>-</sup>: 274.1; found: 273.9, calcd for [C<sub>15</sub>H<sub>13</sub>NO<sub>5</sub>S-H<sup>+</sup>-2CO<sub>2</sub>]<sup>-</sup>: 230.1; found: 229.9.**

#### Synthesis of 6-mercaptopyridine-2,3-dicarboxylic acid [6]<sup>205</sup>



A mixture of 6-((4-methoxybenzyl)thio)-pyridine-2,3-dicarboxylic acid (2.00 g, 6,33 mmol) and anisole (40,56 mL) was cooled to -5°C in a water-ice-NaCl bath. Then, trifluoroacetic acid (200 mL) and mercury (II) acetate (2.07 g, 6,52 mmol) were added. The

reaction mixture was stirred for 1 h at -5 °C and then concentrated under reduced pressure to afford an orange oil. The product was precipitated as a white solid by addition of a 1:1 water-Et<sub>2</sub>O mixture to the residue. After filtration and drying under vacuum, the resulting solid was allowed to react with sodium borohydride (0,48 g, 12,66 mmol) in MeOH (150 mL) for 72 h. After that, the resulting mixture was cooled to 0 °C then cautiously quenched by slow addition of concentrated HCl until pH= 2-3. After dilution with water, the product was extracted three times with EtOAc. The organics were combined, dried with MgSO<sub>4</sub>, and concentrated to the fifth. The title compound was obtained by precipitation in a large volume of hexane (250 mg, 1.27 mmol, 20 %).

**RMN <sup>1</sup>H (300MHz, acetone-d<sub>6</sub>):** δ (ppm) 7.89 (dd, *J* = 8.5, 4.5 Hz, 1H), 7.41 (dd, *J* = 8.5, 4.5 Hz, 1H). **RMN <sup>13</sup>C (75 MHz, acetone-d<sub>6</sub>):** δ (ppm) 170.9 (C), 165.2 (C), 165.1 (C), 149.5 (C), 138.1 (CH), 126.5 (CH), 119.5 (C). **HRMS: calc for [C<sub>7</sub>H<sub>5</sub>NO<sub>4</sub>S-H<sup>+</sup>]:** 197.9866; **found:** 197.9868.

ii. 5MPzDC: 5- mercaptopyrazine- 2, 3- dicarboxylic acid

5-chloropyrazine- 2, 3- dicarboxylic acid dimethyl ester [8]



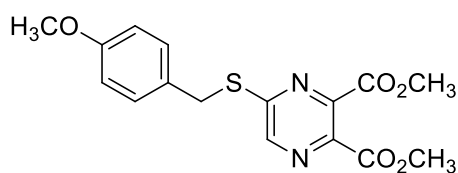
To a refluxed solution of 2-chloroquinoxaline (5.00 g, 30.4 mmol) in H<sub>2</sub>O (250 mL), a solution of KMnO<sub>4</sub> (24.00 g, 151.9 mmol) in H<sub>2</sub>O (250 mL) was added dropwise within 2 h. After that, the mixture was refluxed for an additional hour and then cooled to 60 °C to filtrate off the MnO<sub>2</sub> over Celite which was rinsed twice with hot water (2 x 80 mL). The filtrate was concentrated to about 80 mL and then acidified with concentrated HCl until pH 0, then the solvent evaporated. The crude product was engaged in the next step without further purification<sup>187</sup>.

To a solution of 5-chloropyrazine-2, 3-dicarboxylic acid issued from the previous step in MeOH (13 mL) cooled at 0 °C, concentrated H<sub>2</sub>SO<sub>4</sub> (1.00 mL, 18,7 mmol) was added

dropwise within 5 minutes. The resulting mixture was heated at 50 °C for 2 h and stirred at rt for additional 3 h. After concentration under reduced pressure, the resulting residue was basified with saturated aqueous NaHCO<sub>3</sub> until pH ≈ 8 and extracted 3 times with EtOAc. The combined organic fractions were dried with Na<sub>2</sub>SO<sub>4</sub> concentrated *in vacuo* and the residue purified by silica gel column chromatography (2 % MeOH in CH<sub>2</sub>Cl<sub>2</sub>) affording the desired compound (2.44 g, 35 % over two steps) as a brown solid.

**RMN <sup>1</sup>H (300 MHz, CDCl<sub>3</sub>):** δ (ppm) 8.77 (1H), 4.05 (s, 6H). **RMN <sup>13</sup>C (75MHz, CDCl<sub>3</sub>):** δ (ppm) 163.8 (C), 163.6 (C), 150.5 (C), 145.6 (CH), 145.0 (C), 141.9 (C), 53.7 (CH<sub>3</sub>), 53.6 (CH<sub>3</sub>). **MS-ESI:** calcd for [C<sub>7</sub>H<sub>4</sub>ClN<sub>2</sub>O<sub>3</sub>+H<sup>+</sup>]<sup>+</sup>: 200.0; **found:** 198.9; calcd for [C<sub>8</sub>H<sub>7</sub>ClN<sub>2</sub>O<sub>4</sub>+H<sup>+</sup>]<sup>+</sup>: 231.0 ; **found:** 230.9 .

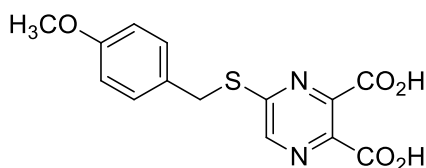
#### Synthesis of 5-((4-methoxybenzyl)thio)pyrazine-2,3-dicarboxylic acid dimethyl ester [9]



A solution of 5-chloropyrazine-2,3-dicarboxylic acid dimethyl ester (2,28 g, 9,92 mmol) in MeOH (70 mL) was deoxygenated by argon bubbling for 10 min. Then, triethylamine (1,38 mL, 9,92 mmol) and 4-methoxy- $\alpha$ -toluenethiol (1,38 mL, 9,92 mmol) were added and the resulting solution was heated at 50 °C for 30 min under argon atmosphere. After dilution with water, the product was extracted three times with EtOAc. The organics were combined, dried with anhydrous Na<sub>2</sub>SO<sub>4</sub> and the solvent was evaporated under reduced pressure. The obtained residue was purified by silica gel column chromatography (5 % MeOH in CH<sub>2</sub>Cl<sub>2</sub>) to afford the tittle compound (3.35 g, 97 %) as a yellow oil.

**RMN <sup>1</sup>H (300 MHz, CDCl<sub>3</sub>):** δ (ppm) 8.49 (s, 1H), 7.32 (d, *J* = 8.0 Hz, 2H), 6.83 (d, *J* = 8.0 Hz, 2H), 4.04 (s, 3H), 3.98 (s, 3H), 3.78 (s, 3H). **RMN <sup>13</sup>C (75 MHz, CDCl<sub>3</sub>):** δ (ppm) 165.5 (C), 164.4 (C), 160.5 (C), 159.2 (C), 146.5 (C), 143.4 (CH), 136.4 (C), 130.4 (2 CH), 127.9 (C), 114.1 (2 CH), 55.2 (CH<sub>3</sub>), 53.2 (CH<sub>3</sub>), 53.2 (CH<sub>3</sub>), 33.9 (CH<sub>2</sub>). **ESI-MS:** calcd for [C<sub>16</sub>H<sub>16</sub>N<sub>2</sub>O<sub>5</sub>S+H<sup>+</sup>]<sup>+</sup>: 349.1; **found:** 348.9.

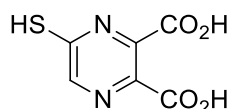
### 5-((4-methoxybenzyl)thio)pyrazine-2,3-dicarboxylic acid [10]



To a solution of 5-((4-methoxybenzyl)thio)pyrazine-2,3-dicarboxylic acid dimethyl ester (0,575 g 1.65 mmol) in Et<sub>2</sub>O (3.00 mL), a 5 M aqueous solution of NaOH (3.00 mL) was added. The mixture was refluxed for 24 h then acidified to pH 2 by dropwise addition of concentrated HCl. After that, the solution was extracted three times with EtOAc and the combined organic layers were dried with anhydrous Na<sub>2</sub>SO<sub>4</sub> and concentrated *in vacuo*. From the residue, the product was extracted with acetone and the resulting solution dried with anhydrous Na<sub>2</sub>SO<sub>4</sub>, then concentrated under vacuum to give the tittle compound (0.448 g, 85 %) as a dark orange oil.

**RMN <sup>1</sup>H (300 MHz, acetone-d<sub>6</sub>):** δ (ppm) 8.68 (s, 1H), 7.46 (d, *J* = 7.2 Hz, 2H), 6.89 (d, *J* = 7.2 Hz, 2H), 4.54 (s, 2H), 3.79 (s, 3H). **RMN <sup>13</sup>C (75 MHz, acetone-d<sub>6</sub>):** δ (ppm) 165.1 (C), 164.5 (C), 159.6 (C), 159.3 (C), 145.8 (C), 143.2 (CH), 137.8 (C), 130.5 (2 CH), 128.6 (C), 113.9 (2 CH), 54.6 (CH<sub>3</sub>), 33.1 (CH<sub>2</sub>). **MS-ESI: calcd for [C<sub>14</sub>H<sub>12</sub>N<sub>2</sub>O<sub>5</sub>S-H<sup>+</sup>]:** 319.0; found: 318.9.

### Synthesis of 5-mercaptopyrazine-2,3-dicarboxylic acid [11]<sup>205</sup>



To a mixture of 5-((4-methoxybenzyl)thio)pyrazine-2,3-dicarboxylic acid (0.448 g, 1.4 mmol) and anisole (9 mL) cooled to -5° C, trifluoroacetic acid (90 mL) and mercury (II) acetate (0.535 g, 1.68 mmol) were added. The reaction mixture was stirred for 1 h at -5 °C. The mixture was concentrated under vacuum to afford an orange oil. Addition of a 1:1 mixture of water- Et<sub>2</sub>O (150 mL) resulted in the precipitation of a part of the product. The

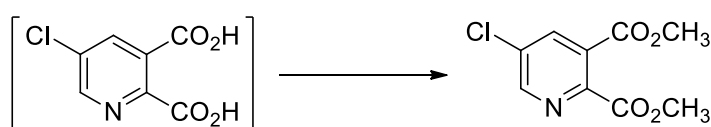
precipitated solid and the water phase were put together and the resulting suspension was concentrated *in vacuo*.

The recovered solid was allowed to react with sodium borohydride (0.106 g, 2.8 mmol) in refluxed MeOH (80 mL) for 72 h. After cooling to 0 °C, the resulting mixture was then hydrolyzed by slow addition of concentrated HCl until pH ≈ 2-3. MeOH was then evaporated. The resulting residue was taken up in water and the product extracted 3-4 times with EtOAc. The combined organics layers were concentrated to the fifth and the desired product was precipitated by addition of the concentrated solution into a large volume of hexane. The resulting residue was taken up in acetone and H<sub>2</sub>S was bubbled at rt for 2 h. After filtration through Celite, the filtrate was concentrated *in vacuo* to give the desired compound. Finally, due to a slow degradation of the product, it was stored at -80 °C (0.155 g, 55 %).

**RMN <sup>1</sup>H (300 MHz, acetone-d<sub>6</sub>):** δ (ppm) 8.74 (s, 1H). **RMN <sup>13</sup>C (75 MHz, acetone-d<sub>6</sub>):** δ (ppm) 176.4 (2C), 164.2 (C), 161.5 (C), 157.3 (CH), 136.7 (C). **HRMS: calcd for [C<sub>6</sub>H<sub>4</sub>N<sub>2</sub>O<sub>4</sub>S-H<sup>+</sup>]** : 198.9819; **found:** 198.9821.

iii. 5MPDC: 5- mercaptopyridine- 2, 3- dicarboxylic acid

5-chloropyridine -2, 3- dicarboxylic acid dimethyl ester [13]

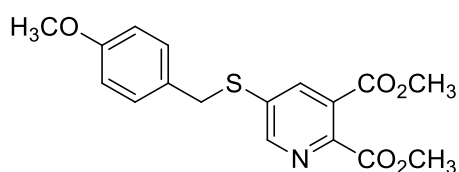


5-Chloropyridine-2, 3-dicarboxylic acid (1.67 g) was synthesized using a reported procedure starting from 3-chloroquinoline (3.50 g, 21.4 mmol)<sup>187</sup>. The crude product was engaged in the next step without further purification. To a solution of the obtained 5-chloropyridine -2, 3- dicarboxylic acid in MeOH (7 mL) at 0 °C, H<sub>2</sub>SO<sub>4</sub> (0.47 mL, 8.81 mmol) was added dropwise within 5 min. The resulting mixture was refluxed for 24 h until completion. After concentration *in vacuo*, the resulting residue was basified with saturated aqueous NaHCO<sub>3</sub> until pH ≈ 8 and the product extracted three times with EtOAc. The combined organic fractions were dried with Na<sub>2</sub>SO<sub>4</sub> and concentrated under reduced

pressure. The resulting residue was purified by silica gel column chromatography (2 % MeOH in CH<sub>2</sub>Cl<sub>2</sub>) to afford 1.16 g (24 % over two steps) of the desired product as a white powder.

**RMN <sup>1</sup>H (300 MHz, CDCl<sub>3</sub>):** δ (ppm) 8.73 (d, *J* = 2.4 Hz, 1H), 8.15 (d, *J* = 2.4 Hz, 1H), 4.02 (s, 3H), 3.97 (s, 3H). **RMN <sup>13</sup>C (75MHz, CDCl<sub>3</sub>):** δ (ppm) 165.7 (C), 164.7 (C), 150.6 (CH), 148.1 (C), 137.01 (CH), 133.8 (C), 127.9 (C), 53.2 (2 CH<sub>3</sub>). **MS-ESI: calcd for [C<sub>9</sub>H<sub>8</sub>ClNO<sub>4</sub>+H<sup>+</sup>]<sup>+</sup>: 230.0; found: 230.2.**

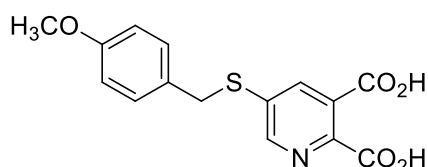
5-((4-methoxybenzyl)thio)pyridine-2,3-dicarboxylic acid dimethyl ester [14]



A solution of dimethyl-5-chloropyridine-2,3-dicarboxylate (1.15 g, 5.01 mmol) in anhydrous DMSO (25 mL) was deoxygenated by argon bubbling for 10 min. Then, Cs<sub>2</sub>CO<sub>3</sub> (1.80 g, 5.51 mmol) and 4-methoxy- $\alpha$ -toluenethiol (0.73 mL, 5.26 mmol) were added and the resulting solution was stirred at rt under argon atmosphere for 48 h. The reaction mixture was quenched by addition of water (25 mL) and extracted three times with Et<sub>2</sub>O. The organic layers were combined, dried across MgSO<sub>4</sub> and the solvent evaporated. The obtained residue was purified by silica gel column chromatography (5 % MeOH in CH<sub>2</sub>Cl<sub>2</sub>) to afford 1.06 g (57 %) of the desired product as a pale yellow powder.

**RMN <sup>1</sup>H (300 MHz, CDCl<sub>3</sub>):** δ (ppm) 8.55 (s, 1H), 7.89 (s, 1H), 7.23 (d, *J* = 8.4 Hz, 2H), 6.84 (d, *J* = 8.4 Hz, 2H) 4.16 (s, 2H), 3.97 (s, 3H), 3.92 (s, 3H), 3.79 (s, 3H). **RMN <sup>13</sup>C (75MHz, CDCl<sub>3</sub>):** δ (ppm) 165.9 (C), 163.0 (C), 159.3 (C), 150.3 (CH), 146.2 (C), 137.4 (C), 136.3 (CH), 130.0 (2 CH), 127.5 (C), 127.3 (C), 114.3 (2 CH), 55.3 (CH<sub>3</sub>), 53.1 (CH<sub>3</sub>), 53.0 (CH<sub>3</sub>), 37.3 (CH<sub>2</sub>). **MS-ESI: calcd for [C<sub>17</sub>H<sub>17</sub>NO<sub>5</sub>S+H<sup>+</sup>]<sup>+</sup> : 348.1; found: 348.1.**

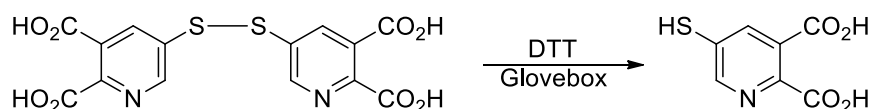
5-((4 methoxybenzyl)thio)pyridine-2,3-dicarboxylic acid [15]



To a solution of 5-((4-methoxybenzyl)thio)pyridine-2,3-dicarboxylic acid dimethyl ester (0.90 g, 2.59 mmol) in Et<sub>2</sub>O (4.5 mL), a 5M aqueous solution of NaOH (3.2 mL) was added. The mixture was refluxed for 24 h then acidified to pH≈ 2 by dropwise addition of concentrated HCl solution. The resulting mixture was extracted three times with EtOAc and the combined organic layers dried with Na<sub>2</sub>SO<sub>4</sub> and concentrated *in vacuo*. Reextraction of the product from the resulting residue with acetone, drying with Na<sub>2</sub>SO<sub>4</sub> and evaporation of the solvent under reduce pressure afforded 0.55g (62 %) of the title compound as a yellow powder.

**RMN <sup>1</sup>H (300 MHz, acetone-d<sub>6</sub>):** δ (ppm) 8.62 (s, 1H), 8.13 (s, 1H), 7.36 (d, *J* = 8.3 Hz, 2H), 6.89 (d, *J* = 8.3 Hz, 2H), 4.40 (s, 2H), 3.77 (s, 3H). **RMN <sup>13</sup>C (75MHz, acetone-d<sub>6</sub>):** δ (ppm) 165.6 (C), 165.5 (C), 159.3 (C), 149.2 (C), 146.3 (C), 137.5 (CH), 136.4 (C), 130.2 (2 CH), 128.0 (C), 127.8 (CH), 114.0 (2 CH), 54.6 (CH<sub>3</sub>), 36.1 (CH<sub>2</sub>). **MS-ESI: calcd for [C<sub>15</sub>H<sub>13</sub>NO<sub>5</sub>S-H<sup>+</sup>]:** 318.1; **found:** 317.9.

#### 5-mercaptopyridine-2, 3-dicarboxylic acid [17]



To a mixture of 5-((4 methoxybenzyl)thio)pyridine-2,3-dicarboxylic acid (0.472 g, 1.48 mmol) and anisole (9.5 mL, 87.27 mmol) cooled to -5 °C, trifluoroacetic acid (95 mL) and mercury (II) acetate (0.49 g, 1.53 mmol) were added. The reaction mixture was stirred for 1 h at -5 °C then concentrated under vacuum to afford an orange oil. Addition of a 1:1 mixture of water-Et<sub>2</sub>O (150 mL) resulted in the precipitation of a part of the product. The precipitated solid and the water phase were mixed together and the resulting suspension was concentrated *in vacuo* and taken up in MeOH (40 mL). Then, hydrogen sulfide was bubbled into the MeOH solution for 2 h. The black suspension was filtered through celite with MeOH, and the obtained filtrate was concentrated *in vacuo* and purified by C<sub>18</sub> column chromatography to afford 0.053 g (9 %) of the title compound as a disulfide dimer (**16**).

**RMN <sup>1</sup>H (300 MHz, 1M TRIS-D2O, pH 7.5):** δ (ppm) 8.55 (s, 1H), 8.16 (s, 1H). **RMN <sup>13</sup>C (75MHz, acetone-d6):** δ (ppm) 165.9 (C), 165.0 (C), 150.2 (C), 149.8 (CH), 136.8 (CH), 135.0 (C), 127.2 (C). **MS-ESI: calcd for [C<sub>14</sub>H<sub>8</sub>N<sub>2</sub>O<sub>8</sub>S<sub>2</sub>-H<sup>+</sup>]:** 395.0; **found** 395.0 (88), **calcd for [C<sub>14</sub>H<sub>8</sub>N<sub>2</sub>O<sub>8</sub>S<sub>2</sub>-2H<sup>+</sup>]<sup>2-</sup>:** 197.2; **found:** 197.2 (100).

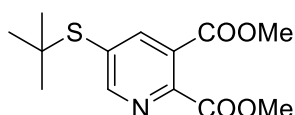
Due to the fast oxidation of the title compound when exposed to air, the compound was stored as a dimer and reduced in glove box just before use with 1 equivalent of DTT as reducing agent. It permitted to obtain the desired monomeric form in a quantitative manner.

**RMN <sup>1</sup>H (300 MHz, 1M TRIS-D2O, pH 7.5):** δ (ppm) 8.29 (s, 1H), 7.73 (s, 1H). **MS-ESI: calcd for [C<sub>7</sub>H<sub>4</sub>NO<sub>4</sub>S-H<sup>+</sup>]:** 198.0; **found** 198.2.

(i) Alternative synthesis of 5MPDC: 5- mercaptopyridine- 2, 3- dicarboxylic acid

All of the steps until the obtaining of dimethyl-5-chloropyridine-2,3-dicarboxylate were performed as described on the above synthesis of 5MPDC. Only the last two steps are different:

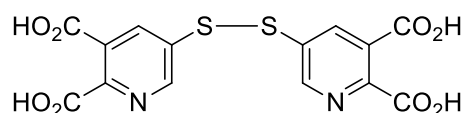
Dimethyl 5-(tert-butylthio)pyridine-2,3-dicarboxylate [18]



A stirred solution of sodium 2-methyl-2-propanethiolate (0.1 g, 0.565 mmol) in dry DMF (5 mL) was flushed several times with Ar. To this solution, dimethyl-5-chloropyridine-2,3-dicarboxylate (0.07 g, 0.435 mmol) was added and the resulting mixture was stirred at rt overnight under strict Ar atmosphere. After evaporation of the solvent, the resulting residue was taken up in a Et<sub>2</sub>O-H<sub>2</sub>O mixture (1:1) and extracted several times with the same solvent. The combined extracts were dried across MgSO<sub>4</sub> and the solvent evaporated. The resulting residue was purified by silica gel column chromatography (0.5 % MeOH in CH<sub>2</sub>Cl<sub>2</sub>) to yield 53 mg of the title compound as a white powder (43 %).

**RMN <sup>1</sup>H (300 MHz, CDCl<sub>3</sub>):** δ (ppm) 8.82 (d, *J* = 1.3 Hz, 1H), 8.27 (d, *J* = 1.3 Hz, 1H), 4.00 (s, 3H), 3.94 (s, 3H), 1.32 (s, 9H). **RMN <sup>13</sup>C (75MHz, CDCl<sub>3</sub>):** δ (ppm) 166.3 (C), 165.4 (C), 158.1 (CH), 150.6 (C), 145.0 (CH), 132.7 (C), 126.4 (C), 53.2 (OCH<sub>3</sub>), 53.1 (OCH<sub>3</sub>), 47.7 (C), 31.2 (3CH<sub>3</sub>). **HRMS: calcd for [C<sub>13</sub>H<sub>17</sub>NO<sub>4</sub>S+H]<sup>+</sup>:** 284.0956; **found:** 284.0951.

5-mercaptopyridine-2, 3-dicarboxylic acid [16]

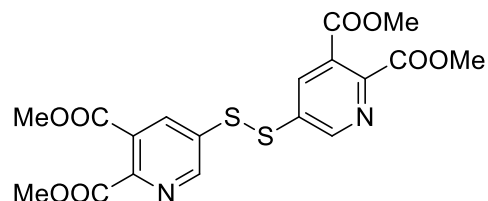


Compound **18** (0.027 g, 0.106 mmol) was dissolved in concentrated HCl and the solution was put in reflux for three days. Evaporation of the solvent and purification by reversed phase C-18 column chromatography yielded the desired product as a pale yellow disulfide dimer at 71 % (15 mg).

Spectroscopic data were identical to the ones described above for the same molecule.

d. Synthesis of molecules for *in cellulo* assays

Tetramethyl 5,5'-disulfanediyldis(pyridine-2,3-dicarboxylate) [19]

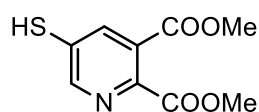


To a solution of 4,4'-disulfanediyldiphthalic acid (0.03 g, 0.076 mmol) in MeOH (3 mL) at 0 °C, concentrated H<sub>2</sub>SO<sub>4</sub> (0.1 mL mL, 1.88 mmol) was added. The mixture was refluxed for 24 h. After evaporation of the solvent, the remaining residue was treated with a saturated solution of NaHCO<sub>3</sub> until pH 8 followed by several extractions with EtOAc. The combined organic phases were dried with MgSO<sub>4</sub> then concentrated under reduced pressure. The title compound was obtained after purification of the obtained residue by

silica gel column chromatography (0.5 % MeOH in CH<sub>2</sub>Cl<sub>2</sub>) as a yellow oil and 44 % of yield (0.015 g, 0.033 mmol).

**RMN <sup>1</sup>H (300 MHz, CDCl<sub>3</sub>):** δ (ppm) 8.82 (d, *J* = 2.6 Hz, 2H), 8.24 (d, *J* = 2.6 Hz, 2H), 4.00 (s, 6H), 3.95 (s, 6H). **RMN <sup>13</sup>C (75MHz, CDCl<sub>3</sub>):** δ (ppm) 165.7 (2C), 164.9 (2C), 150.1 (2CH), 149.2 (2C), 136.5 (2CH), 135.2 (2C), 127.3 (2C), 53.2 (4CH<sub>3</sub>). **HRMS-ESI: calcd for [C<sub>18</sub>H<sub>16</sub>N<sub>2</sub>O<sub>8</sub>S<sub>2</sub>+H<sup>+</sup>]<sup>+</sup>:** 453.0426; **found:** 453.0421.

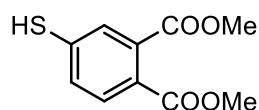
#### Dimethyl 5-mercaptopyridine-2,3-dicarboxylate [20]



To a solution of compound **19** (0.015 g, 0.033 mmol) in CH<sub>2</sub>Cl<sub>2</sub>, DTT (0.005 mg, 0.033 mmol) was added. After evaporation of the solvent, compound **19** was used for tests without any further purification.

**RMN <sup>1</sup>H (300 MHz, CDCl<sub>3</sub>):** δ (ppm) 8.60 (d, 2.3 Hz, H), 7.98 (d, 2.3 Hz, H), 4.00 (s, 3H), 3.95 (s, 3H).

#### Dimethyl 4-mercaptophthalate [21]

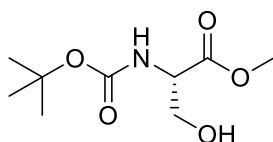


To a suspension of 4-mercaptophthalic acid (4MP) (68 mg, 34.0 mmol) in MeOH (4 mL) at rt was added concentrated H<sub>2</sub>SO<sub>4</sub> (0.022 mL, 0.43 mmol). The mixture was refluxed for 24 h and then cooled to rt. After evaporation of the solvent, the remaining residue was treated with a solution of 4 % NaHCO<sub>3</sub> until pH 8 followed by three extractions with EtOAc (3 × 5 mL). The combined organic phases were dried with MgSO<sub>4</sub> then concentrated under reduce pressure to afforded the product pure enough to be used (60 mg, about 80 % of

purity). When the product was purified by flash chromatography (silica gel, 10 % EtOAc in cyclohexane), the corresponding product **21** was obtained (27 mg, 35 %) as an oil.

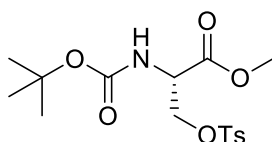
**<sup>1</sup>H NMR (400 MHz, CDCl<sub>3</sub>):**  $\delta$  (ppm) 7.66 (d,  $J$  = 8.1 Hz, 1H), 7.50 (d,  $J$  = 2.0 Hz, 1H), 7.37 (dd,  $J$  = 2 Hz,  $J$  = 8.1 Hz, 1H), 3.90 (s, 3H), 3.88 (s, 3H), 3.65 (s, 1H). **<sup>13</sup>C NMR (100 MHz, CDCl<sub>3</sub>):**  $\delta$  (ppm) 168.1 (C), 167.2 (C), 137.4 (C), 134.0 (C), 130.5 (CH), 130.2 (CH), 128.4 (C), 128.0 (C), 53.0 (CH<sub>3</sub>), 52.8 (CH<sub>3</sub>). **HRMS-ESI: calcd for [C<sub>10</sub>H<sub>10</sub>O<sub>4</sub>S -H<sup>+</sup>]: 225.0227; found: 225.0220.**

Methyl N-(*tert*-butoxycarbonyl)-L-serinate [32]<sup>250</sup>



To a solution of Boc<sub>2</sub>O (24.8 g, 113.63 mmol) in CH<sub>3</sub>CN (220 mL) was added L-serine methyl ester hydrochloride (17.7 g, 113.77 mmol) and Et<sub>3</sub>N (48 mL, 344.38 mmol). The reaction mixture was allowed to stir for 6 h at rt. After the reaction was completed, CH<sub>2</sub>Cl<sub>2</sub> (200 mL) was added and the mixture was washed with 1N HCl and aqueous NaHCO<sub>3</sub>. The organic layer was dried over MgSO<sub>4</sub>, filtered and concentrated to give the title compound as colorless oil in 59% yield (14.8 g, 67.51 mmol). Spectroscopic data were identical to those reported in literature.

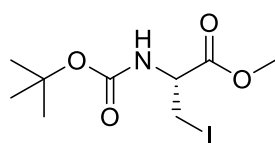
Methyl N-(*tert*-butoxycarbonyl)-O-tosyl-L-serinate [33]<sup>250</sup>



Compound **32** (14.8 g, 67.51 mmol) in anhydrous CH<sub>2</sub>Cl<sub>2</sub> (140 mL) was cooled at 0 °C before adding 4-DMAP (0.4 g, 3.25 mmol), Me<sub>3</sub>N.HCl (0.62 g, 6.53 mmol) and *p*-TsCl (12.43 g, 65.20 mmol). A solution of Et<sub>3</sub>N (9.6 mL, 68.94 mmol) dissolved in anhydrous CH<sub>2</sub>Cl<sub>2</sub> (20 mL) was added dropwise and the reaction was stirred for 2 h at 0°C. After the reaction was

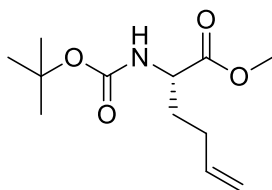
completed, small pieces of ice and 1N HCl (34 mL) were added and the mixture was extracted with CH<sub>2</sub>Cl<sub>2</sub>. The organic layer was washed with brine, dried over MgSO<sub>4</sub>, filtered and concentrated. The crude product obtained was dissolved in Et<sub>2</sub>O, filtered and concentrated. The residue was recrystallized in cyclohexane to give the title compound as white solid in 77 % yield (19.51 g, 52.25 mmol). Spectroscopic data were identical to those reported in literature.

Methyl (*R*)-2-((*tert*-butoxycarbonyl)amino)-3-iodopropanoate [34]<sup>250</sup>



Compound **33** (21.17 g, 56.69 mmol) was dissolved in anhydrous acetone (130 mL) and the reaction flask was wrapped with aluminium foil before the addition of NaI (10.13 g, 67.58 mmol). The reaction mixture was stirred for 48 h at rt before a second portion of NaI (2.53g, 16.87 mmol) was added. After 24 h of stirring, the reaction was completed. The mixture was filtered and the solid obtained was washed with acetone till it turns white. The filtrate was concentrated to give an oil that was dissolved again in Et<sub>2</sub>O. The resulting solution was washed with a saturated aqueous solution of Na<sub>2</sub>S<sub>2</sub>O<sub>3</sub>. The organic layer was washed with brine, dried over MgSO<sub>4</sub>, filtered and concentrated to give an oil that crystallized in cyclohexane to give **34** as white solid in 58% yield (10.9 g, 33.12 mmol). Spectroscopic data were identical to those reported in literature.

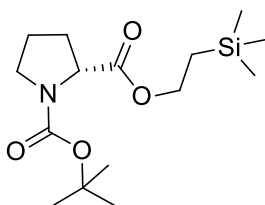
(+)-(2*S*)-*tert*-Butyl 1-(methoxycarbonyl)hex-4-enylcarbamate [31]<sup>224</sup>



A suspension of zinc powder (5.42 g, 82.74 mmol) in dry DMF (64 mL) was degased under argon for 10 min. The rest of the protocol was performed under strict Ar atmosphere

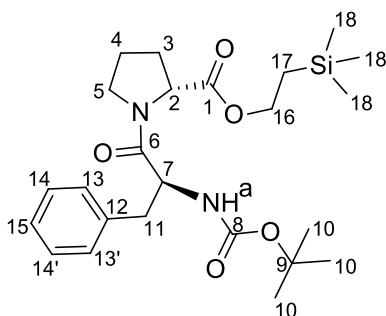
conditions. To the degassed Zn suspension 1,2-dibromoethane (0.36 mL, 4.14 mmol) was injected. The mixture was stirred for 30 min at rt. Then, TMSCl (0.11 mL, 0.83 mmol) was injected and the solution was stirred at 60°C for 40 min. A solution of **34** (4.54 g, 13.79 mmol) in anhydrous DMF (14 mL) was added dropwise and the solution was stirred for 30 min at 60°C. Then, the solution was brought to -55 °C and a mixture of LiCl (1.29 g, 30.34 mmol) and CuCN (1.36 g, 15.17 mmol) in DMF (14 mL) were injected. The reaction mixture was allowed to react at -55 °C for 15 min and then warmed up 0 °C for 15 min. The solution was cooled again at -55 °C and allyl bromide (1.52 mL, 17.93 mmol) was injected dropwise. After 15 min, the mixture was warmed up to 0 °C and then stirred for 2.5 h at this temperature. The unreacted zinc was removed by celite filtration and the filtrate was quenched with a saturated aqueous NH<sub>4</sub>Cl solution. The product was extracted with EtOAc and the combined organic layer were washed with brine, dried over MgSO<sub>4</sub> and concentrated. The obtained residue was purified by silica gel column chromatography (EtOAc/cyclohexane, 5:95) to give the title compound as a colorless oil in 69 % yield (2.32 g, 9.54 mmol). Spectroscopic data were identical those reported in literature.

N-Boc-(*R*)-Proline-(2-trimethylsilylethyl)ester [27]<sup>226</sup>



To a solution of commercial N-Boc-D-Proline (6.97 g, 32.38 mmol) in anhydrous CH<sub>2</sub>Cl<sub>2</sub> (160 mL) cooled to 0 °C, EDCI (6.83 g, 35.62 mmol) and DMAP (0.36 g, 2.95 mmol) were added. After dropwise addition of 2-(trimethylsilyl) ethanol (4.64 mL, 32.38 mmol), the reaction mixture was allowed to warm to rt and stir overnight. The solvent was evaporated and the residue was dissolved in EtOAc (250 mL). The solution was washed with 10% HCl (100 mL), saturated NaHCO<sub>3</sub>, and brine and dried over MgSO<sub>4</sub>. The solvent was evaporated and the resulting residue was purified by distillation with a Kugelrohr at 150 °C and 1.2 mbar to yield the desired product at 78 % (8.00 g, 25.36 mmol) as a colorless oil. Spectroscopic data were identical to those reported in literature.

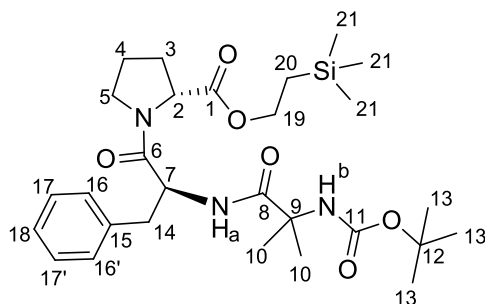
(R)-2-(trimethylsilyl)ethyl-1-((S)-2-((tert-butoxycarbonyl)amino)-3-phenylpropanoyl)pyrrolidine-2-carboxylate [25]



To compound **27** (4.35 g, 13.81 mmol) was added 4 M HCl in dioxane (57 mL) and the mixture was stirred for 2.5 h at rt. The solvent was evaporated and the residue was dried in high vacuum (oil pump) for 3 h. The resulting N-deprotected amino acid was dissolved in anhydrous CH<sub>2</sub>Cl<sub>2</sub> and to this Boc-L-phenylalanine was added. The mixture put at 0 °C and EDCI (3.71 g, 19.33 mmol), HOBT (2.96 g, 19.33 mmol) and Hünig base (9.6 mL, 55.26 mmol) were added on the described order. The mixture was stirred at 0 °C for 30 min and then the mixture was allowed to stir at rt overnight. The reaction mixture was then washed three times with 10 % citric acid (3 x 10 mL) and then with 4 % NaHCO<sub>3</sub>. The whole was dried with MgSO<sub>4</sub> and the solvent evaporated. The resulting mixture was purified by silica gel column chromatography (EtOAc/Cyclohexane, 15:85) to obtain the title compound as a colorless oil with 57 % of yield (3.67 g, 7.94 mmol).

**<sup>1</sup>H NMR (400 MHz, CDCl<sub>3</sub>):**  $\delta$  (ppm) 7.28-7.16 (m, 5H, H13, H13', H14, H14', H15), 5.36 (d, J = 8.5 Hz, 1H, NH<sub>a</sub>), 4.63-4.58 (m, 1H, H7), 4.24-4.22 (m, 1H, H2), 4.18-4.14 (m, 2H, H16), 3.50-3.46 (m, 1H, H5a), 3.04-3.00 (m, 1H, H11a), 2.92-2.87 (m, 1H, H11b), 2.62-2.58 (m, 1H, H5b), 1.93-1.81 (m, 3H, H3a, H3b, H4a), 1.48-1.52 (m, 1H, H4b), 1.40 (s, 9H, 9xH10), 0.98-0.94 (m, 1H, H17), 0.003 (s, 9H, 9xH18). **<sup>13</sup>C NMR (100 MHz, CDCl<sub>3</sub>):**  $\delta$  (ppm) 172.1, 170.3 (2C, C1, C6), 156.4 (1C, C8), 136.7 (1C, C12), 129.7, 128.5 (4CH, C13, C13', C14, C14'), 126.4 (1CH, C15), 79.7 (1C, C9), 63.6 (1CH<sub>2</sub>, C16), 59.1 (1CH, C2), 53.7 (1CH, C7), 46.9 (1CH<sub>2</sub>, C5), 40.6, 29.1, 28.5, 24.6, 17.5 (4CH<sub>2</sub>, 3CH<sub>3</sub>, C17, 3XC10, 11, C4, C3), -1.3 (3CH<sub>3</sub>, 3XC18). **HRMS-ESI: calcd for [C<sub>24</sub>H<sub>38</sub>N<sub>2</sub>O<sub>5</sub>Si+H<sup>+</sup>]: 463.2628; found: 463.2626.**

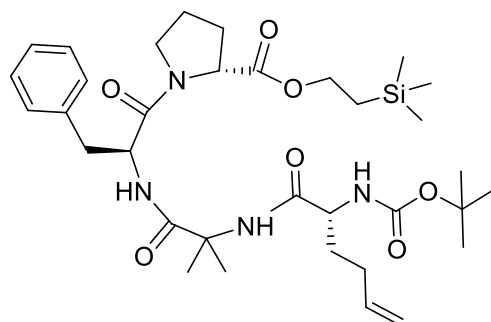
(R)-2-(trimethylsilyl)ethyl-1-((S)-2-(2-((tert-butoxycarbonyl)amino)-2-methylpropanamido)-3-phenylpropanoyl)pyrrolidine-2-carboxylate [28]



To compound **25** (1.96 g, 4.24 mmol), 4 M HCl in dioxane (20 mL) were added and the mixture was stirred at rt for 2.5 h. The solvent was evaporated and the resulting N-deprotected amino acid was dried under high vacuum (oil pump) for 3h. The residue was dissolved in anhydrous CH<sub>2</sub>Cl<sub>2</sub> (40 mL) and to this, 2-(tert-butoxycarbonylamino)-isobutyric acid (0.86 g, 4.24 mmol) was added. After cooling down the mixture at 0 °C, EDCI (1.14 g, 5.94 mmol), HOBT (0.91 g, 5.94 mmol) and Hünig base (2.95 mL, 16.96 mmol) were added on the described order. The mixture was allowed to react at 0 °C for 30 min and then at rt overnight. The mixture was washed twice with citric acid (40 mL) and 4 % NaHCO<sub>3</sub>, dried with MgSO<sub>4</sub> and the solvent evaporated. The resulting residue was purified by silica gel column chromatography (EtOAc/cyclohexane, 1:3) to yield the title compound as white crystals at 60 % yield (1.39 g, 2.54 mmol).

**<sup>1</sup>H NMR (400 MHz, CDCl<sub>3</sub>):**  $\delta$  (ppm) 7.27-7.16 (m, 5H, H13, H14, H14', H15, H15'), 6.85-6.93 (m, 1H, NHa), 5.93 (s, 1H, NHb), 4.93-4.87 (m, 1H, H7), 4.27-4.24 (m, 1H, H2), 4.16-4.07 (m, 2H, 2xH19), 3.41-3.60 (m, 1H, H5a), 3.10-3.06 (m, 1H, H14a), 2.86-2.92 (m, 1H, H14b), 2.60-2.56 (m, 1H, H5b), 1.84-1.78 (m, 3H, H3a, H3b, H4a), 1.70-1.44 (m, 16H, 6xH10, 9xH13, H4b), 0.97-0.93 (2H, 2xH20), 0.03 (s, 9H, 9xH21). **<sup>13</sup>C NMR (100 MHz, CDCl<sub>3</sub>):**  $\delta$  (ppm) 174.0, 171.7, 169.8 (3C, C1, C6, C8), 154.2 (1C, C11), 136.5, 129.6, 128.4, 126.9 (1C, 5CH, C15, C16, C16', C17, C17', C18), 79.90 (1C, C12), 63.4 (1C, C19), 58.9, 52.6, 52.2, 46.8 (2CH<sub>2</sub>, 2CH, C2, C5, C7, C9), 28.9, 28.1, 27.2, 24.3, 17.3, 14.2 (5CH<sub>3</sub>, 4CH<sub>2</sub>, C3, C4, 2xC10, 3xC13, C14, C20), -1.3 (3CH<sub>3</sub>, 3xC21). **HRMS-ESI: calcd for [C<sub>28</sub>H<sub>45</sub>N<sub>3</sub>O<sub>6</sub>Si+H<sup>+</sup>]:** 548.3156; **found:** 548.3164.

(R)-2-(Trimethylsilyl)ethyl-1-((6R,12S)-12-benzyl-6-(but-3-en-1-yl)-2,2,9,9-tetramethyl-4,7,10-trioxo-3-oxa-5,8,11-triazatridecan-13-oyl)pyrrolidine-2-carboxylate [30]



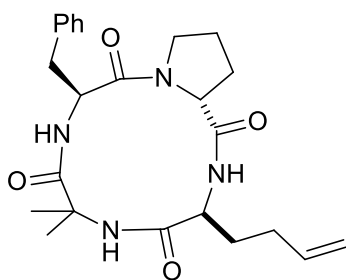
To compound **28** (1.2 g, 2.19 mmol) was added 4 M HCl in dioxane (10 mL) and the mixture was allowed to react for 2.5 h. The solvent was evaporated and the N-deprotected amino acid was dried under high vacuum (oil pump) for 3 h.

To a solution of LiOH (0.19 g, 7.77 mmol) in water (7.3 mL), a solution of compound **31** (0.53 g, 2.19 mmol) in THF (7.3 mL) was added and then MeOH (1.2 mL). The mixture was allowed to react at rt for 3 h and then acidified with 5 % H<sub>3</sub>PO<sub>4</sub> until pH 3. The mixture was extracted with EtOAc, dried over MgSO<sub>4</sub> and the solvent evaporated to yield the carboxylic acid-deprotected amino acid.

After solubilization of each deprotected amino acid in 10 mL CH<sub>2</sub>Cl<sub>2</sub> each, the mixture was cooled to 0 °C. To this, EDCI (0.59 g, 3.07 mmol), HOBt (0.47 g, 3.07 mmol) and Hünig base (1.53 mL, 8.76 mmol) were added in strict order and the mixture was stirred at 0°C for 30 min. Then, the resulting mixture was allowed to stir at rt overnight. After evaporation of the solvent, the residue was taken up in EtOAc and washed four times with citric acid (4x20 mL), with 4 % NaHCO<sub>3</sub> (2x20 mL), dried across MgSO<sub>4</sub> and evaporated. The crude product was purified through silica gel column chromatography (EtOAc/cyclohexane, 50:50) to yield the title compound as a white solid in 49 % yield (0.7 g, 1.06 mmol).

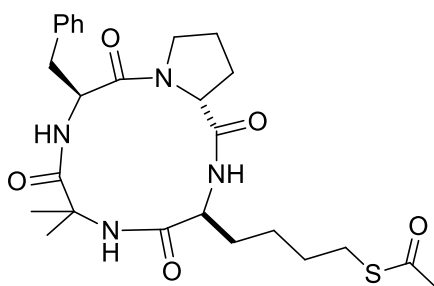
**HRMS-ESI: calcd for [C<sub>34</sub>H<sub>54</sub>N<sub>4</sub>O<sub>7</sub>Si+H<sup>+</sup>]: 659.3840; found: 659.3834**

(3S,9S,14aR)-9-benzyl-3-(but-3-en-1-yl)-6,6-dimethyldecahydropyrrolo[1,2-a][1,4,7,10]tetraazacyclododecine-1,4,7,10-tetraone [22]<sup>224</sup>



Compound **30** (0.61 g, 0.93 mmol), TFA (5 mL) were added under ice-cooling. The mixture was stirred for 30 min at 0 °C and then at rt for 5.5 h. The solvent was evaporated to give the tetrapeptide trifluoroacetic acid. The product was triturated with dry Et<sub>2</sub>O to obtain a precipitate and the Et<sub>2</sub>O was removed *in vacuo*. The residue was dried under high vacuum (oil pump) overnight. The obtained white powder was dissolved in anhydrous DMF and then HATU (0.47 g, 1.23 mmol) and Hünig base (0.64 mL, 3.7 mmol) were added in 5 equal additions, separated by 30 min under vigorous stirring. The reaction mixture was stirred at rt overnight. The solvent was evaporated and the remaining product taken up in EtOAc, washed with citric acid three times (40 mL each), twice with 4 % NaHCO<sub>3</sub>, dried across MgSO<sub>4</sub> and evaporated. The obtained residue was purified by silica gel column chromatography (MeOH/CH<sub>2</sub>Cl<sub>2</sub>, 1:99) to yield the desired compound as a white solid at 46 % yield (185 mg, 0.42 mmol). Spectroscopic data were identical those reported in literature.

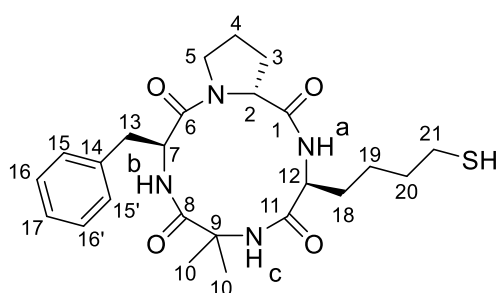
S-(4-(((3*S*,9*S*,14*aR*)-9-benzyl-6,6-dimethyl-1,4,7,10-tetraoxotetradecahydropyrrolo[1,2-a][1,4,7,10]tetraazacyclododecin-3-yl)butyl) ethanethioate [37]



Compound **22** (0.08 g, 0.18 mmol) was dissolved in THF (25 mL) and thioacetic acid (0.1 mL, 1.45 mmol) was added. The resulting mixture was refluxed for 1 h under argon atmosphere. Then, AIBN (0.003 g, 0.018 mmol) was added, and the mixture was allowed to

react at strong reflux overnight. Additional thioacetic acid (0.1 mL, 1.45 mmol) and AIBN (0.003 g, 0.018 mmol) allowed the completion of the reaction. The solvent was evaporated and the residue purified by silica gel column chromatography (MeOH/CH<sub>2</sub>Cl<sub>2</sub>) to yield 67 % yield (0.061 g, 0.12 mmol) of the title compound as a colorless oil. Spectroscopic data were identical to those reported in literature.

(-)-(3*S*,9*S*,14*a**R*)-9-benzyl-3-(4-mercaptobutyl)-6,6-dimethyldecahydropyrrolo[1,2-*a*][1,4,7,10]tetraazacyclododecine-1,4,7,10-tetraone [23]

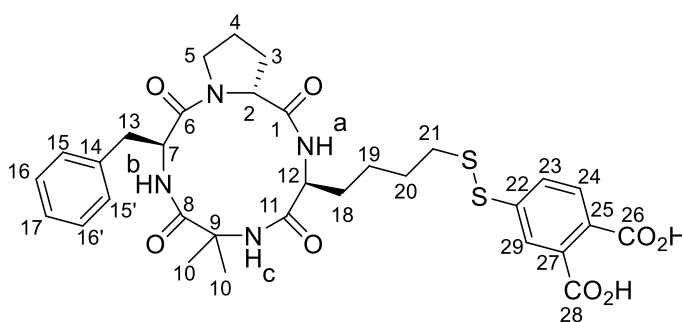


The thioester cyclopeptide **37** (33 mg, 0.064 mmol) was dissolved in DMF (1.1 mL), and NH<sub>3</sub>/MeOH (0.64 mL of 7 N solution) was added. The mixture was kept at rt under Ar for 67 h. The solvent was evaporated *in vacuo*. The crude product was dissolved in DMF (1.5 mL) then dithiotreitol (200 mg, 1.28 mmol) was added, and the mixture was kept at 37°C under Ar for 48 h. DMF was evaporated *in vacuo*, and the product was extracted with EtOAc and washed with water. After evaporation, the crude product was purified using column chromatography (alumina, 99.75:0.25 CH<sub>2</sub>Cl<sub>2</sub>/MeOH) to give the desired product **23** with 70 % yield (21 mg) as a colorless film.

**<sup>1</sup>H NMR (400 MHz, CDCl<sub>3</sub>):**  $\delta$  (ppm) 7.49 (d, *J* = 10.2 Hz, 1H, NH<sub>b</sub>), 7.29-7.20 (m, 5H, H15, H15', H16, H16', H17), 7.12 (d, *J* = 10.1 Hz, 1H, NH<sub>a</sub>), 5.93 (s, 1H, NH<sub>c</sub>), 5.20-5.13 (m, 1H, H7), 4.67-4.65 (m, 1H, H2), 4.22-4.16 (m, 1H, H12), 3.89-3.83 (m, 1H, H5a), 3.29-3.19 (m, 2H, H5b, H13a), 2.95 (dd, *J* = 13.5 Hz, *J* = 5.6 Hz, 1H, H13b), 2.53 (q, *J* = 7.2 Hz, 2H, 2×H21), 2.33-2.31 (m, 1H, H3a), 2.21-2.16 (m, 1H, H4a), 1.84-1.63 (m, 9H, H3b, H4b, 3×H10, 2×H18, 2×H20), 1.46-1.34 (m, 5H, 2×H19, 3×H10). **<sup>13</sup>C NMR (100 MHz, CDCl<sub>3</sub>):**  $\delta$  (ppm) 175.8, 174.5,

173.0, 172.1 (4×C, C1, C6, C8, C11), 137.3 (C, C14), 129.3, 128.8 (4×CH, C15, C15', C16, C16'), 126.9 (CH, C17), 59.0 (C, C9), 58.0 (CH, C2), 54.5 (CH, C12), 53.7 (CH, C7), 47.2 (CH<sub>2</sub>, C5), 36.0 (CH<sub>2</sub>, C13), 33.7, 28.7, 26.7, 25.2, 25.0, 24.9, 24.5, 23.8 (8 carbons, C3, C4, 2×C10, C18, C19, C20, C21). **HRMS-ESI: calcd for [C<sub>24</sub>H<sub>34</sub>N<sub>4</sub>O<sub>4</sub>S-H<sup>+</sup>]: 473.2228; Found: 473.2218.**

(-)-(S)-4-((4-((3*S*,9*S*,14*a**R*)-9-Benzyl-6,6-dimethyl-1,4,7,10-tetra-oxotetra-decahydropyrrolo[1,2-*a*][1,4,7,10]tetra-azacyclododecin-3-yl)butyl)disulfanyl)phthalic acid  
**[24]**<sup>227</sup>



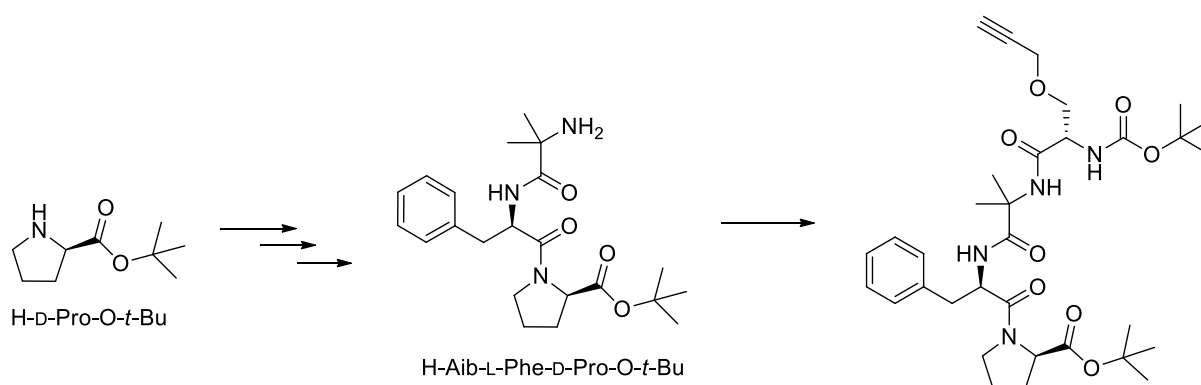
Solution 1: 4MP (2.6 mg, 0.013 mmol) in 0.1 mL acetonitrile at -20 °C. Solution 2: TCCA (1.0 mg, 0.0043 mmol) in 0.65 mL acetonitrile at -20 °C. Solution 3: compound **23** (6.2 mg, 0.013 mmol) in 0.1 mL acetonitrile at -20 °C.

To a stirred solution 1 was added a *solution 2*, the mixture turned yellow. After 35 min, solution 3 was added quickly to the mixture. The reaction was kept stirring for 12 min and neutralized with 28 % ammonia. The mixture turned white. The solution was evaporated under reduced pressure and the crude solid was purified by flash silica gel column chromatography using 10 % MeOH in CH<sub>2</sub>Cl<sub>2</sub> to afford the title compound as a white pasty solid, 7.1 mg, 82 %.

**<sup>1</sup>H NMR (500 MHz, DMSO-d<sub>6</sub>):** δ (ppm) 9.11-9.09 (m, 1H, NH<sub>a</sub>), 8.50-8.10 (br, COOH, H<sub>29</sub>), 7.89-7.86 (m, 1H, NH<sub>b</sub>), 7.71-7.64 (m, 3H, NH<sub>c</sub>, H<sub>23</sub>, H<sub>24</sub>), 7.43 (d, *J* = 7.4 Hz, 2H, H<sub>15</sub>, H<sub>15'</sub>), 7.27-7.17 (m, 3H H<sub>16</sub>, H<sub>16'</sub>, H<sub>17</sub>), 5.27 (d, *J* = 7.9 Hz, 1H, H<sub>2</sub>), 4.70-4.65 (m, 1H, H<sub>7</sub>), 3.90-3.85 (m, 1H, H<sub>12</sub>), 3.60-3.30 (overlapping signal, 2H, 2×H<sub>5</sub>), 3.20-3.11 (m, 1H, H<sub>13a</sub>), 2.94 (dd, *J* = 13.7 Hz, *J* = 3.9 Hz, 1H, H<sub>13b</sub>), 2.85-2.82 (m, 2H, 2×H<sub>21</sub>), 2.26-2.21 (m, 1H, H<sub>3a</sub>), 2.01-1.99 (m, 1H, H<sub>3b</sub>), 1.86-1.66 (m, 6H, 2×H<sub>4</sub>, 2×H<sub>18</sub>, 2×H<sub>20</sub>), 1.47-1.40 (m, 4H, H<sub>19a</sub>,

3×H10), 1.27-1.24 (m, 1H, H19b), 1.04 (m, 3H, 3×H10). <sup>13</sup>C NMR (125 MHz, DMSO-d<sub>6</sub>): δ (ppm) 175.8, 175.8, 174.7, 172.9, 169.8, 169.7 (6×C, C1, C6, C8, C11, C26, C28), 152.2 (C, C22), 138.5 (C, C14), 138.4 (C, C2), 137.3 (CH, C8), 130.0, 129.1, 127.3 (3×CH, C23, C24, C29), 130.2, 128.9 (4×CH, C15, C15', C16, C16'), 127.2 (CH, C17), 59.9 (C, C9), 58.9, 58.6, 53.7 (3×CH, C2, C7, C12), 48.8 (CH<sub>2</sub>, C5), 33.1, 29.6, 28.7, 28.3, 28.2, 25.6, 25.6, 25.3, 21.4 (9 carbons, C3, C4, 2×C10, C13, C18, C19, C20, C21). HRMS-ESI: calcd for [C<sub>32</sub>H<sub>37</sub>N<sub>4</sub>O<sub>4</sub>S<sub>2</sub>-H<sup>+</sup>]<sup>+</sup>: 669.2058; found: 669.2040.

*tert*-Butyl (2-((*S*)-2-((*tert*-butoxycarbonyl)amino)-3-(prop-2-yn-1-yloxy)propanamido)-2-methylpropanoyl)-D-phenylalanyl-D-prolinate [54]

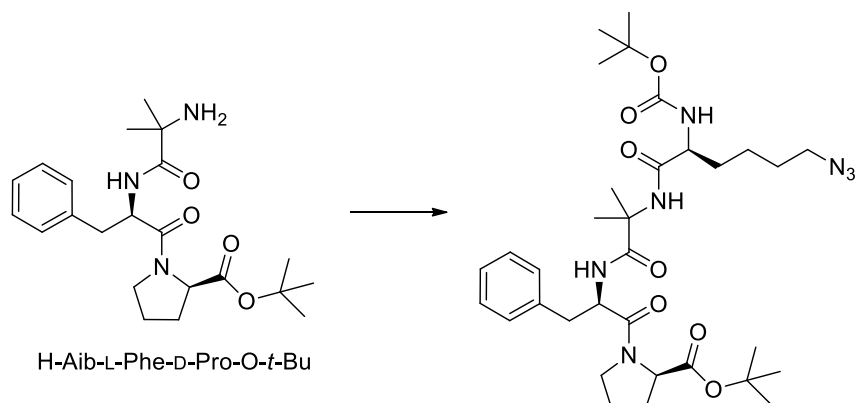


The tripeptide H-Aib-L-Phe-D-Pro-O-*t*-Bu was synthesized according to literature<sup>230</sup>.

The *N*-(*tert*-butoxycarbonyl)-*O*-(prop-2-yn-1-yl)-L-serine was synthesized according to literature<sup>233</sup>. The solution of tripeptide H-Aib-L-Phe-D-Pro-O-*t*-Bu (970 mg, 2.39 mmol) and *N*-(*tert*-butoxycarbonyl)-*O*-(prop-2-yn-1-yl)-L-serine (480 mg, 2.00 mmol) in dry DMF (6 mL) at 0 °C were added EDCI (540 mg, 2.80 mmol), HOBT·H<sub>2</sub>O (380 mg, 4.00 mmol), and Hünig base (1.4 mL), and the mixture was stirred at 0 °C for 30 min and then at rt overnight (18 h). DMF was evaporated, and the residue was diluted with EtOAc and washed with 10 % citric acid, 4 % NaHCO<sub>3</sub>, and brine. The organic phase was dried (MgSO<sub>4</sub>) and evaporated. The residue was purified by flash chromatography (silica gel, 1:1 cyclohexane/EtOAc) to give the corresponding tetrapeptide 54 as a white foam in 71 % yield (860 mg).

HRMS-ESI: calcd for [C<sub>33</sub>H<sub>48</sub>N<sub>4</sub>O<sub>8</sub>+H<sup>+</sup>]<sup>+</sup>: 629.3545; Found: 629.3535.

*tert*-Butyl-(2-((*S*)-6-azido-2-((*tert*-butoxycarbonyl)amino)hexanamido)-2-methylpropanoyl)-*D*-phenylalanyl-*D*-prolinate [48]



The tripeptide H-Aib-L-Phe-D-Pro-O-*t*-Bu was synthesized according to literature<sup>230</sup>.

The *N*-(*tert*-butoxycarbonyl)-*O*-(prop-2-yn-1-yl)-*L*-serine was synthesized according to literature<sup>233</sup>.

To a solution of tripeptide H-Aib-L-Phe-D-Pro-O-*t*-Bu (3.22 g, 8.00 mmol) and *N*<sup>2</sup>-(*tert*-butoxycarbonyl)-*N*<sup>6</sup>-diazo-*L*-lysine (2.82 g, 10.36 mmol) in dry DMF (20 mL) at 0 °C were added HOBt·H<sub>2</sub>O (1.24 g, 9.18 mmol), DCC (2.00 g, 9.69 mmol), and triethylamine (1.2 mL), and the mixture was stirred at 0 °C for 30 min and then at rt overnight (18 h). DMF was evaporated, and the residue was diluted with EtOAc and washed with 10 % citric acid, 4 % NaHCO<sub>3</sub>, and brine. The organic phase was dried over MgSO<sub>4</sub> and evaporated. The residue was purified by flash chromatography (silica gel, 2% MeOH in CH<sub>2</sub>Cl<sub>2</sub>) to give the corresponding tetrapeptide **48** as a white foam in 69 % yield (3.63 g).

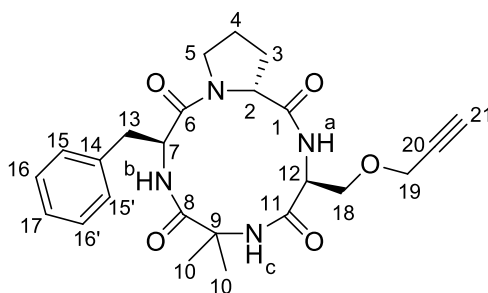
**HRMS-ESI: calcd for [C<sub>33</sub>H<sub>51</sub>N<sub>7</sub>O<sub>7</sub>+H<sup>+</sup>]<sup>+</sup>: 658.3923; Found: 658.3911.**

### General procedure: cyclopeptide synthesis

The corresponding tetrapeptide was dissolved in TFA at 0 °C and stirred for 3 h at this temperature. After evaporation, the product was precipitated in dry Et<sub>2</sub>O to give the unprotected product after filtration which was dried overnight under vacuum. The tetrapeptide trifluoroacetic acid, HATU, and Hünig base were added in five aliquots with a time interval of 30 min under vigorous stirring in DMF. Then the reaction mixture was stirred for 18 h at rt. The DMF was evaporated, and EtOAc was added. After washing with a solution

of 10 % citric acid followed by 4 % NaHCO<sub>3</sub>, the organic phase was dried over MgSO<sub>4</sub> and evaporated. After flash chromatography (silica gel) the cyclic tetrapeptide was isolated.

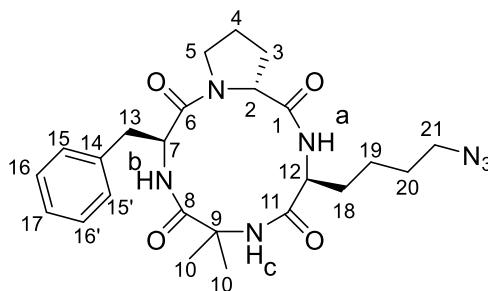
(-)-(3*S*,9*S*,14*aR*)-9-benzyl-6,6-dimethyl-3-((prop-2-yn-1-yloxy)methyl)decahydropyrrolo[1,2-*a*][1,4,7,10]tetraazacyclododecine-1,4,7,10-tetraone [52]



See general procedure for the cyclopeptide synthesis. TFA (3.8 mL), tetrapeptide **54** (770 mg, 1.25 mmol), HATU (570 mg, 1.5 mmol), and Huning base (520 mg, 4.0 mmol in DMF (125 mL). The product was purified by flash silica gel column chromatography using 1:1 cyclohexane/EtOAc to afford the cyclopeptide **52** in 11 % yield (60 mg) as a white pasty foam.

**<sup>1</sup>H NMR (400 MHz, CDCl<sub>3</sub>):**  $\delta$  (ppm) 7.31-7.18 (m, 7H, NH<sub>a</sub>, NH<sub>b</sub>, H15, H15', H16, H16', H17), 6.14 (s, 1H, NH<sub>c</sub>), 5.16-5.10 (m, 1H, H7), 4.71-4.69 (m, 1H, H2), 4.56-4.50 (m, 1H, H12), 4.25 (dd, *J* = 15.9 Hz, *J* = 2.4 Hz, 1H, H19a), 4.16 (dd, *J* = 15.9 Hz, *J* = 2.4 Hz, 1H, H19b), 3.90-3.85 (m, 1H, H18a), 3.84-3.80 (m, 1H, H5a), 3.72 (dd, *J* = 9.5 Hz, *J* = 5.8 Hz, 1H, H18b), 3.28-3.22 (m, 1H, H13a), 3.17-3.11 (m, 1H, H5b), 2.98-2.93 (m, 1H, H13b), 2.35-2.31 (m, 1H, H3a), 2.22-2.13 (m, 1H, H4a), 1.93 (bs, 1H, H21), 1.81-1.66 (m, 5H, H3b, H4b, 3×H10), 1.36 (s, 3H, 3×H10). **<sup>13</sup>C NMR (100 MHz, CDCl<sub>3</sub>):**  $\delta$  (ppm) 175.6, 173.3, 172.8, 172.2 (4×C, C1, C6, C8, C11), 137.1 (C, C14), 129.2, 128.8 (4×CH, C15, C15', C16, C16'), 127.0 (CH, C17), 79.2 (C, C20), 75.5 (CH, C21), 67.3 (CH<sub>2</sub>, C18), 59.0 (C, C9), 58.9 (C, C19), 58.0 (CH, C2), 53.9 (CH, C12), 53.8 (CH, C7), 47.1 (CH<sub>2</sub>, C5), 36.4 (CH<sub>2</sub>, C13), 25.0, 24.9 (2×CH<sub>2</sub>, C3, C4), 26.2, 24.0 (2×CH<sub>3</sub>, 2×C10). **HRMS-ESI: calcd for [C<sub>24</sub>H<sub>30</sub>N<sub>4</sub>O<sub>5</sub>+H<sup>+</sup>]<sup>+</sup>: 455.2289; Found: 455.2285.**

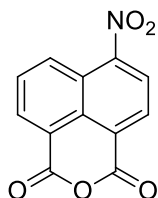
(-)-(3*S*,9*S*,14*aR*)-3-(4-Azidobutyl)-9-benzyl-6,6-dimethyldecahydropyrrolo[1,2-*a*][1,4,7,10]tetraazacyclododecine-1,4,7,10-tetraone [45]



See general procedure for the cyclopeptide synthesis: TFA (7 mL), tetrapeptide **48** (1.65 g, 2.50 mmol), HATU (1.14 g, 3.00 mmol), and Hünig base (1.4 mL, 8.04 mmol) in DMF (250 mL). Purified by flash silica gel column chromatography using 1.5 % MeOH in CH<sub>2</sub>Cl<sub>2</sub> to afford the desired product **45** (475 mg, 39 %) as a white solid.

**<sup>1</sup>H NMR (400 MHz, CDCl<sub>3</sub>):**  $\delta$  (ppm) 7.50 (d,  $J = 10.2$  Hz, 1H, NH<sub>b</sub>), 7.29-7.20 (m, 5H, H15, H15', H16, H16', H17), 7.15 (d,  $J = 10.3$  Hz, 1H, NH<sub>a</sub>), 5.98 (s, 1H, NH<sub>c</sub>), 5.20-5.13 (m, 1H, H7), 4.68-4.66 (m, 1H, H2), 4.25-4.19 (m, 1H, H12), 3.89-3.83 (m, 1H, H5a), 3.30-3.21 (m, 4H, H5b, H13a, 2×H21), 2.95 (dd,  $J = 10$  Hz,  $J = 5.9$  Hz, 1H, H13b), 2.33-2.30 (m, 1H, H3a), 2.18-2.16 (m, 1H, H4a), 1.85-1.72 (m, 6H, H3b, H4b, 3×H10, H18a), 1.70-1.58 (m, 3H, H18b, 2×H20) 1.45-1.34 (m, 5H, 2×H19, 3×H10). **<sup>13</sup>C NMR (100 MHz, CDCl<sub>3</sub>):**  $\delta$  (ppm) 175.7, 174.3, 173.0, 172.0 (4×C, C1, C6, C8, C11), 137.2 (C, C14), 129.2, 128.8 (4×CH, C15, C15', C16, C16'), 126.9 (CH, C17), 59.0 (C, C9), 57.9 (CH, C2), 54.4 (CH, C12), 53.6 (CH, C7), 51.3 (CH<sub>2</sub>, C21), 47.16 (CH<sub>2</sub>, C5), 36.0 (CH<sub>2</sub>, C13), 28.7, 28.7, 24.9, 25.2, 23.0 (5×C, C3, C4, C18, C19, C20), 26.6, 23.7 (2×CH<sub>3</sub>, 2×C10). **HRMS-ESI: calcd for [C<sub>24</sub>H<sub>33</sub>N<sub>7</sub>O<sub>4</sub>+H<sup>+</sup>]<sup>+</sup>: 484.2672; Found: 484.2663.**

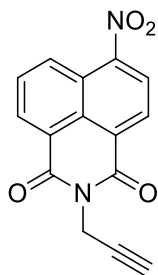
4-Nitro-1,8-naphthalic anhydride [43]<sup>228</sup>



To a stirred solution of sodium bichromate (3.73 g, 12.50 mmol) in acetic acid (8.3 mL) was added 5-nitroacenaphthene (1.00 g, 5.00 mmol) in acetic acid (8.3 mL). After 5 h at 140 °C, the reaction mixture was diluted with water (100 mL) at 0 °C, then the precipitate

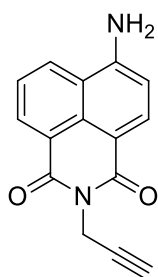
was removed by filtration and the solid was washed with water until the aqueous phase was neutral. The residue was dried *in vacuo* to afford the desired product **43** (72 mg, 60 %) as an orange solid pure enough to be used without further purification. The  $^1\text{H}$  and  $^{13}\text{C}$  NMR data were in agreement with literature values.

*N*-propargyl-4-nitro-1,8-naphthalimide [44]<sup>229</sup>



2-Propyn-1-amine (130 mg, 2.31 mmol) was quickly added to a cloudy solution of 4-nitro-1,8-naphthalic anhydride **43** (510 mg, 2.10 mmol) in EtOH (13 mL). After 6 h at 90-95 °C under Ar, the reaction was allowed to cool to rt and filtered off, washed with cold EtOH (7 mL). The residue was dried *in vacuo* to afford the desired product **44** (440 mg, 75 %) as a brown powder pure enough to be used without further purification. The  $^1\text{H}$  and  $^{13}\text{C}$  NMR data were in agreement with the literature values.

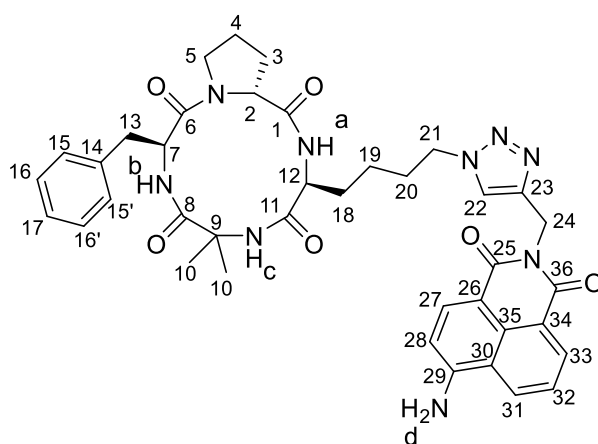
*N*-propargyl-4-amino-1,8-naphthalimide [42]<sup>229</sup>



A solution of  $\text{SnCl}_2 \cdot 2\text{H}_2\text{O}$  (2.60 g, 10.22 mmol) in concentrated HCl (4 mL) was carefully added dropwise (10 min) to a stirred suspension of *N*-propargyl-4-nitro-1,8-naphthalimide **44** (41 mg, 1.46 mmol) in EtOH (16 mL). The mixture was stirred for 2 h at rt and quenched with an aqueous solution containing 10 %  $\text{NaHCO}_3$  (60 mL). The mixture was filtered and the collected solid was rinsed twice with  $\text{CH}_2\text{Cl}_2$  (280 mL) and dried off *in vacuo*.

The residue was diluted in a solution 10 % MeOH in EtOAc and filtered through a pad of Celite. The solvent was removed *in vacuo* and the desired product **42** was obtained (250 mg, 92 %) as an orange powder. The  $^1\text{H}$  and  $^{13}\text{C}$  NMR data were in agreement with the literature values.

(-)-(3*S*,9*S*,14*aR*)-3-(4-(4-((6-Amino-1,3-dioxo-1*H*-benzo[*de*]isoquinolin-2(3*H*)-yl)methyl)-1*H*-1,2,3-triazol-1-yl)butyl)-9-benzyl-6,6-dimethyldecahydropyrrolo[1,2-*a*][1,4,7,10]tetraazacyclododecine-1,4,7,10-tetraone [40]<sup>229</sup>

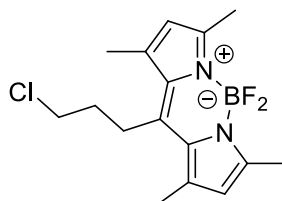


The cyclopeptide **45** (44 mg, 0.092 mmol) and tetrakis(acetonitrile)copper(I) tetrafluoroborate ( $[(\text{CH}_3\text{CN})_4\text{Cu}]\text{BF}_4$ ) (4.4 mg, 0.014 mmol) were added to a solution of *N*-propargyl-4-amino-1,8-naphthalimide **42** (41 mg, 0.16 mmol) in DMF (1.2 mL) in a microwave vial. The mixture was stirred for 2 h at 115 °C in a microwave reactor. The solvent was removed under reduced pressure and the residue dissolved in a mixture of MeOH/ $\text{CH}_2\text{Cl}_2$  (1:2, 1 mL). The residue was filtered through a bed of Celite and the filtrate was concentrated under reduced pressure and purified by flash chromatography (silica gel, 2 % MeOH in  $\text{CH}_2\text{Cl}_2$ ) to give the corresponding product **40** as an orange oil (50 mg, 75 %).

$^1\text{H}$  NMR (500 MHz,  $\text{CDCl}_3$ ):  $\delta$  (ppm) 8.49 (d,  $J = 7.3$  Hz, 1H, H33 ), 8.26 (d,  $J = 8.2$  Hz, 1H, H27), 8.02 (d,  $J = 7.8$  Hz, 1H, H31), 7.65 (s, 1H, H22), 7.50-7.45 (m, 2H, H32, NH<sub>b</sub>), 7.29-7.26 and 7.22-7.20 (m, 5H, H15, H15', H16, H16', H17), 7.12 (d,  $J = 10.3$  Hz, 1H, NH<sub>a</sub>), 6.70 (d,  $J = 8.2$  Hz, 1H, H28), 6.01 (s, 1H, NH<sub>c</sub>), 5.47 (s, 1H, H24a), 5.29 (s, 1H, H24b), 5.18-5.13 (m, 1H, H7), 4.65-4.64 (m, 1H, H2), 4.33-4.30 (m, 2H, 2×H21), 4.18-4.13 (m, 1H, H12), 3.87-3.82 (m, 1H,

H5a), 3.28-3.18 (m, 2H, H5b, H13a), 2.94 (dd,  $J = 13.5$  Hz,  $J = 5.7$  Hz, 1H, H13b), 2.32-2.28 (m, 1H, H3a), 2.18-2.13 (m, 1H, H4a), 1.94-1.88 (m, 2H, 2×H20), 1.83-1.64 (m, 7H, H3b, H4b, 3×H10, 2×H18), 1.36-1.26 (m, 5H, 2×H19, 3×H10).  $^{13}\text{C}$  NMR (125 MHz,  $\text{CDCl}_3$ ):  $\delta$  (ppm) 175.8, 174.3, 173.0, 172.1 (4×C, C1, C6, C8, C11), 164.6, 163.9 (2×C, C25, C36), 150.1, 144.4 (2×C, C23, C29), 137.3 (C, C14), 134.2, 131.8 (2×CH, C27, C33), 130.0 (C, C35), 129.3, 128.8 (4×CH, C15, C15', C16, C16'), 127.6, 127.0, 124.9, 123.21 (4×CH, C17, C22, C31, C32), 120.1, 122.9 (2×C, C30, C34), 111.4 (C, C26), 109.6 (C, C28), 59.1 (C, C9), 58.0 (CH, C2), 54.3 (CH, C12), 53.7 (CH, C7), 50.0 ( $\text{CH}_2$ , C21), 47.2 ( $\text{CH}_2$ , C5), 36.0 ( $\text{CH}_2$ , C13), 35.2 ( $\text{CH}_2$ , C24), 30.0, 28.5, 25.2, 25.0, 22.7 (5×C, C3, C4, C18, C19, C20), 26.6, 23.7 (2× $\text{CH}_3$ , 2×C10). HRMS-ESI: calcd for  $[\text{C}_{39}\text{H}_{43}\text{N}_9\text{O}_6+\text{H}^+]^+$ : 734.3409; Found: 734.3390.

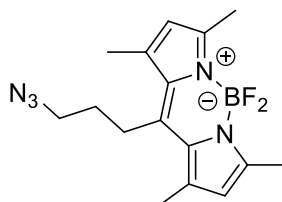
10-(3-Chloropropyl)-5,5-difluoro-1,3,7,9-tetramethyl-5H-4 $\lambda^4$ ,5 $\lambda^4$ -dipyrrolo[1,2-c:2',1'-f][1,3,2]diazaborinine [51]<sup>232</sup>



2,4-Dimethylpyrrole (1.80 g, 19.00 mmol) was added to a solution of 4-chlorobutanoyl chloride (1.23 g, 8.80 mmol) in  $\text{CH}_2\text{Cl}_2$  (20 mL) over 13 min at 0 °C. The reaction was stirred at 0 °C for 30 min, then warmed up to 20 °C and stirred vigorously for an additional 30 min. Then triethylamine (2.63 g, 26.00 mmol) was added in small portions at 0 °C for 13 min and the mixture was stirred at 20 °C for 20 min.  $\text{BF}_3\cdot\text{OEt}_2$  (5.41 g, 44.00 mmol) was then added in portions for 18 min and the mixture was stirred at 20 °C for 23 h. The reaction was quenched with careful addition of  $\text{H}_2\text{O}$  (20 mL) and the mixture was stirred vigorously for 15 min. The aqueous layer was extracted with  $\text{CH}_2\text{Cl}_2$  (3 × 10 mL). The organic layers were combined and washed with  $\text{H}_2\text{O}$  (2 × 10 mL) and brine (10 mL). The organic layer was dried over  $\text{MgSO}_4$ , filtered, and the solvent was removed under reduced pressure. The brown powder was dissolved in small amount of  $\text{CH}_2\text{Cl}_2$  and filtered through a short plug of silica. The solvent was removed under reduced pressure and the remaining powder was

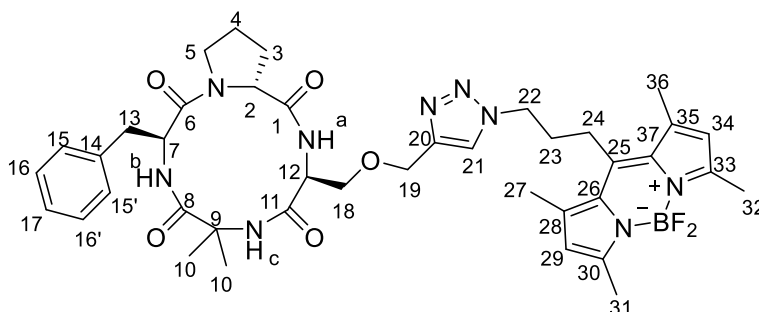
recrystallized from EtOAc to afford the desired product **51** (660 mg, 23 %) as an orange solid. The  $^1\text{H}$  and  $^{13}\text{C}$  NMR data were in agreement with the literature values.

10-(3-Azidopropyl)-5,5-difluoro-1,3,7,9-tetramethyl-5H-4 $\lambda^4$ ,5 $\lambda^4$ -dipyrrolo[1,2-c:2',1'-f][1,3,2]diazaborinine [50]<sup>232</sup>



Sodium azide (100 mg, 1.54 mmol) was added to a solution of **51** (250 mg, 0.76 mmol) in DMF (15 mL). The mixture was stirred at 40 °C for 72 h. Water (20 mL) was then added and the suspension was extracted with EtOAc (3 × 20 mL). The organic layers were washed with H<sub>2</sub>O (2 × 20 mL) and brine (20 mL). The organic layer was dried over MgSO<sub>4</sub>, filtered, and the solvent was removed under reduced pressure to afford the desired product **50** (170 mg, 68 %) as an orange solid. The  $^1\text{H}$  and  $^{13}\text{C}$  NMR data were in agreement with the literature values.

(-)-(3*S*,9*S*,14*a**R*)-9-Benzyl-3-(((1-(3-(5,5-difluoro-1,3,7,9-tetramethyl-5H-4 $\lambda^4$ ,5 $\lambda^4$ -dipyrrolo[1,2-c:2',1'-f][1,3,2]diazaborinin-10-yl)propyl)-1*H*-1,2,3-triazol-4-yl)methoxy)methyl)-6,6-dimethyldecahydropyrrolo[1,2-*a*][1,4,7,10]tetraazacyclododecine-



1,4,7,10-tetraone [41]

To a mixture of **50** (18 mg, 0.054 mmol) and alkyne cyclopeptide **52** (20.6 mg, 0.045 mmol) in 1 mL of *tert*-butanol (1 mL) and H<sub>2</sub>O (1 mL), were added CuSO<sub>4</sub>·5H<sub>2</sub>O (2.2 mg, 0.009 mmol) and sodium ascorbate (3.6 mg, 0.018 mmol). The mixture was stirred for 24 h at rt. The organic layer was diluted with CH<sub>2</sub>Cl<sub>2</sub>, and washed with water. The organic phase was dried over anhydrous MgSO<sub>4</sub> and filtered. The crude mixture was concentrated and purified by flash silica gel column chromatography using EtOAc to afford the product **41** (21 mg, 66 %) as an orange oil.

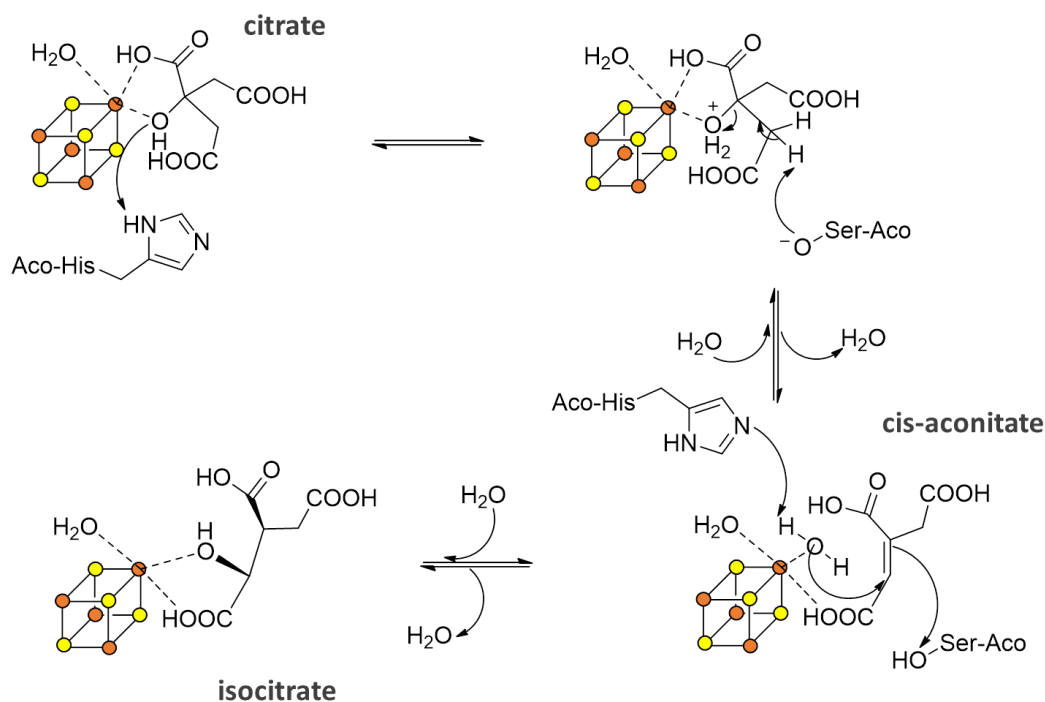
**<sup>1</sup>H NMR (500 MHz, CDCl<sub>3</sub>):**  $\delta$  (ppm) 7.61 (s, 1H, H<sub>21</sub>), 7.32 (d, *J* = 10.5 Hz, 1H, NH<sub>a</sub>), 7.28-7.19 (m, 6H, NH<sub>b</sub>, H<sub>15</sub>, H<sub>15'</sub>, H<sub>16</sub>, H<sub>16'</sub>, H<sub>17</sub>), 6.37 (s, 1H, NH<sub>c</sub>), 6.04 (s, 2H, H<sub>29</sub>, H<sub>34</sub>), 5.13-5.80 (m, 1H, H<sub>7</sub>), 4.75-4.66 (m, 3H, H<sub>2</sub>, 2×H<sub>19</sub>), 4.55-4.49 (m, 3H, H<sub>12</sub>, 2×H<sub>22</sub>), 3.88-3.86 (m, 1H, H<sub>18a</sub>), 3.82-3.77 (m, 1H, H<sub>5a</sub>), 3.67 (dd, *J* = 9.5 Hz, *J* = 5.2 Hz, 1H, H<sub>18b</sub>), 3.22-3.18 (m, 1H, H<sub>13a</sub>), 3.13-3.08 (m, 1H, H<sub>5b</sub>), 3.05-3.01 (m, 2H, 2×H<sub>24</sub>), 2.94 (dd, *J* = 13.4 Hz, *J* = 5.6 Hz, 1H, H<sub>13b</sub>), 2.50 (s, 6H, 3×H<sub>31</sub>, 3×H<sub>32</sub>), 2.34-2.30 (m, 1H, H<sub>3a</sub>), 2.24-2.19 (m, 8H, 2×H<sub>23</sub>, 3×H<sub>27</sub>, 3×H<sub>36</sub>), 2.19-2.12 (m, 1H, H<sub>4a</sub>), 1.76-1.70 (m, 5H, H<sub>3b</sub>, H<sub>4b</sub>, 3×H<sub>10</sub>), 1.37 (s, 3H, 3×H<sub>10</sub>). **<sup>13</sup>C NMR (125 MHz, CDCl<sub>3</sub>):**  $\delta$  (ppm) 175.6, 173.4, 172.8, 172.3 (4×C, C<sub>1</sub>, C<sub>6</sub>, C<sub>8</sub>, C<sub>11</sub>), 154.8 (2×C, C<sub>30</sub>, C<sub>33</sub>), 145.1 (2×C, C<sub>28</sub>, C<sub>35</sub>), 143.7 (C, C<sub>20</sub>), 140.3 (C, C<sub>25</sub>), 137.1 (C, C<sub>14</sub>), 131.5 (2×C, C<sub>26</sub>, C<sub>37</sub>), 129.2, 128.8 (4×CH, C<sub>15</sub>, C<sub>15'</sub>, C<sub>16</sub>, C<sub>16'</sub>), 127.0 (CH, C<sub>17</sub>), 123.0, 122.2 (3×CH, C<sub>21</sub>, C<sub>29</sub>, C<sub>34</sub>), 67.8, 65.0 (2×CH<sub>2</sub>, C<sub>18</sub>, C<sub>9</sub>), 58.8 (C, C<sub>9</sub>), 58.1 (CH, C<sub>2</sub>), 54.0 (CH, C<sub>12</sub>), 53.9 (CH, C<sub>7</sub>), 50.4 (CH<sub>2</sub>, C<sub>22</sub>), 47.1 (CH<sub>2</sub>, C<sub>5</sub>), 36.5 (CH<sub>2</sub>, C<sub>13</sub>), 32.3 (CH<sub>2</sub>, C<sub>24</sub>), 25.9 (CH<sub>3</sub>, C<sub>10</sub>), 25.7 (CH<sub>2</sub>, C<sub>23</sub>), 24.9, 24.9 (2×CH<sub>2</sub>, C<sub>3</sub>, C<sub>4</sub>), 24.2 (CH<sub>3</sub>, C<sub>10</sub>), 16.4 (2×CH<sub>3</sub>, C<sub>31</sub>, C<sub>32</sub>), 14.7 (2×CH<sub>3</sub>, C<sub>27</sub>, C<sub>36</sub>). **HRMS-ESI: calcd for [C<sub>40</sub>H<sub>50</sub>BF<sub>2</sub>N<sub>9</sub>O<sub>5</sub>+H]<sup>+</sup>: 786.4069; Found: 786.4061.**



# ANNEXES

## I. ANNEX I: Aconitase B enzyme (AcnB)

Aconitase B (AcnB) is [4Fe-4S] bacterial enzyme that catalyzes the interconversion of citrate to isocitrate via cis-aconitate during the [Krebs](#) cycle. It is the functional homologue of mitochondrial aconitase<sup>251</sup>. Few biochemical and spectroscopic characterizations were performed on AcnB from *E. coli*<sup>251</sup>. Only a structure of the apo-AcnB from *E. coli* exists in literature<sup>252</sup>. However, its mammalian homologue was largely investigated biochemically, spectroscopically and structurally<sup>253,254,134</sup>). This allowed to demonstrate that aconitase contains an essential non-redox [4Fe-4S]<sup>2+</sup> cluster<sup>130</sup>. Three Fe atoms from its cluster are coordinated by conserved cysteines, the fourth iron being coordinated by a non-protein ligand, an exchangeable ligand (water molecule)<sup>255</sup>. This iron coordinated by an exchangeable ligand is the catalytic site where the enzymatic reaction occurs. It plays a Lewis acid role by catalyzing the hydration/dehydration reaction of aconitase once the substrate is coordinated. The general mechanism for aconitase is represented below (Scheme 63)<sup>256</sup>.



**Scheme 63:** Proposed Aconitase enzyme mechanism, adapted from “Takusagawa’s note”<sup>257</sup>.

Therefore, we can consider that AcnB enzyme displays many similarities with NadA.

- It is a dehydratase.

- It has a catalytic  $[4\text{Fe-4S}]^{2+}$  cluster.
- Three of the irons of its cluster are coordinated by three strictly conserved cysteines and the fourth iron site is an accessible iron site, coordinated by water molecules in the resting state and by substrate and the water molecule during catalysis. The iron site plays a Lewis acid role during catalysis.

For all these resemblances with quinolinate synthase, AcnB was the enzyme we have chosen to perform the *in vitro* specificity tests of the different NadA inhibitors.

## II. ANNEX II: NadA, a highly structurally conserved enzyme in different organisms

### a. Sequence alignment of NadA from different organisms

```

SP|P11458|NADA_ECOLI      -----YPF-PPKPTPLSIDEKAYYREKIKRLLKERNAMVVAHYTDPPEIQQLAEETG--- 62
SP|Q9X1X7|NADA_THEMA     -----MVEIILKLLKKEKGYIILAHNYQIPELQDIA----- 30
SP|O25910|NADA_HELPY     -----MP-----TD-NDLKAAILE--LLRDLDVLLVAHFYQKDEIVELA----- 36
SP|Q49622|NADA_MYCLE     -----AGITDSPVGYAGVDGDEQWATEIRRLTRLRGATVLAHNYQLPAIQDIA----- 66
SP|P9WJK1|NADA_MYCTU     -----ADITNTPLGYGGVDGDERWAAEIRRLAHLRGATVLAHNYQLPAIQDVA----- 63
SP|P65498|NADA_MYCBO     -----ADITNTPLGYGGVDGDERWAAEIRRLAHLRGATVLAHNYQLPAIQDVA----- 63
SP|O57767|NADA_PYRHO     -----MDLVEEILRLKEERNAIILAHNYQLPEVQDIA----- 32
SP|Q9V2R2|NADA_PYRAB     -----MDIVEEILKKEERNAVILAHNYQLPEVQDIA----- 32
SP|Q8TZL3|NADA_PYRFU     -----MEKVEELKKEIERLKKERNAIILAHNYQLPEVQDVA----- 36
SP|Q9KWZ1|NADA_BACSU     -----MPESYKELSR-KDMETRVAAIKKKFGSRLFIPGHYQKDEVIQFA----- 57
SP|Q817V8|NADA_BACCR     -----LPERYYTMST-EDMEKRVREIKEKMGKMLFIPGHYQKDEVVQFS----- 57
SP|C3P9B5|NADA_BACAA     -----LPERYYTMST-EDMEKRVREIKEKMGETLFIIPGHYQKDEVVQFS----- 57
SP|Q8XNE3|NADA_CLOPE     -----MDIRDEILKLLKKEKGAIIILAHYQIPEIQEIA----- 32
SP|Q9I4W9|NADA_PSEAE     -----HLA-AKQPRVLSEQESAHEHRAAIAELKAQNAVLAHYCDPVIQALAEETG--- 63
SP|Q1JRP2|NADA_PSEPF     -----HLD-AKQPKPLTAEAEAYRSAIAELKAQDAVLAHVAHFYCDPIIQALAEETG--- 63
SP|Q5SJM4|NADA_THET8     -----MGRMRGEALAQEVLRLKREERNAVILAHSYQLPEVQEVA----- 38
SP|Q1CFN2|NADA_YERPN     -----YPF-PARPVPLDTNEKAFYREKIKTLKQRDAVLAHYYTDPPEIQALAEETG--- 62
SP|Q66D87|NADA_YERPS     -----YPF-PARPVPLDTNEKAFYREKIKTLKQRDAVLAHYYTDPPEIQALAEETG--- 62
SP|A1JRP2|NADA_YERE8     -----YPF-PARPVPLDQKAFYREKIKTLKQRDAVLAHYYTDPPEIQALAEETG--- 62
SP|Q93CP9|NADA_SHIFL     -----YPF-PPKPTPLSIDEKAYYREKIKRLLKERNAMVVAHYTDPPEIQQLAEETG--- 62
SP|Q32IH8|NADA_SHIDS     -----YPF-PPKPTPLSIDEKAYYREKIKRLLKERNAMVVAHYTDPPEIQQLAEETG--- 62
SP|Q9KR14|NADA_VIBCH     -----YPF-PPKPIPLRDEEKQAYIAEIKQLLIEKDAVLAHYYTDPPEIQALAEETG--- 62
SP|Q7MJ90|NADA_VIBVY     -----YPF-PPKPIPLTQDEKAAYIASIKQLLKEKDAVLAHYYTDPPEIQALAEETG--- 62
SP|O67730|NADA_AQUAE     -----VQLALKEEKELTKKEIKELQKEVRRLAKEKNAVILAHYYQRPEVQDIA----- 49
SP|Q9FGS4|NADA_ARATH     GIEAKGSFAQAQAKYLFP--EESRVEELVNVLKEKKIGVVAHFYMDPEVQGVLTAAQKHW 298
                                : . * * : .

SP|P11458|NADA_ECOLI     --GCISDSLEMARFGA---KHPASTLLVAGVRFMGETAKILSPEK-----TIL-MPTLQA 111
SP|Q9X1X7|NADA_THEMA     --DFVGDSDLQARKAM---ELSEKKILFLGVDFMAELVKILNPKD-----KVI-VPDRSA 79
SP|O25910|NADA_HELPY     --HYTGDSLELAKIAS---QSDKNLIVFCGVHFMGESVKALAFDK-----QVI-MPK-LS 84
SP|Q49622|NADA_MYCLE     --DYVGDSDLALSRIA---EVPEETIVFCGVHFMMAETAKILSPNK-----TVL-IPDQRA 115
SP|P9WJK1|NADA_MYCTU     --DHVGDSDLALSRVAA---EAPEDTIVFCGVHFMMAETAKILSPHK-----TVL-IPDQRA 112
SP|P65498|NADA_MYCBO     --DHVGDSDLALSRVAA---EAPEDTIVFCGVHFMMAETAKILSPHK-----TVL-IPDQRA 112
SP|O57767|NADA_PYRHO     --DFIGDSLELARRAT---RVDADVIVFAGVDFMAETAKILNPKD-----VVL-IPSREA 81
SP|Q9V2R2|NADA_PYRAB     --DFIGDSLELARKAT---KVDADVIVFAGVDFMAETAKILNPKD-----TVL-LPSREA 81
SP|Q8TZL3|NADA_PYRFU     --DFVGDSDLQARKAT---KVDADVIVFAGVDFMAETAKILNPKD-----IVL-IPNKRA 85
SP|Q9KWZ1|NADA_BACSU     --DQTGDSLQQAQVAE---KNKEADYIVFCGVHFMMAETADMLTSEQ-----QTVVLPDMRA 108
SP|Q817V8|NADA_BACCR     --DAVGDSDLQQAQVAA---SNKDASYIVFCGVHFMMAETADMLTDD-----QVVLPDMRA 108
SP|C3P9B5|NADA_BACAA     --DAAGDSLQQAQVAA---SNKEAYIVFCGVHFMMAETADMLTDE-----QVVLPDMRA 108
SP|Q8XNE3|NADA_CLOPE     --DYVGDSSYLSKIAK---DCEENIIVFCGVKFMMAESAKILSPEK-----TVI-LPVMEA 81
SP|Q9I4W9|NADA_PSEAE     --GCVSDSLEMARFGN---QHPAQTVVVAGVRFMGETAKILNPEK-----RVL-MPTLEA 112
SP|Q3K7X0|NADA_PSEPF     --GCVSDSLEMARFGN---AHPAKTVVVAGVRFMGETAKILNPEK-----RVL-MPTLEA 112
SP|Q5SJM4|NADA_THET8     --DFVGDSDLGLAQVA---RTRPEETIVFCGVHFMMAETAAILNPEK-----TVL-LPDLA 87
SP|Q1CFN2|NADA_YERPN     --GCVADSLEMARFGN---NHPASTLLVAGVRFMGETAKILNPEK-----KVL-MPTLNA 111
SP|Q66D87|NADA_YERPS     --GCVADSLEMARFGN---NHPASTLLVAGVRFMGETAKILNPEK-----KVL-MPTLNA 111
SP|A1JRP2|NADA_YERE8     --GCVADSLEMARFGN---NHPASTLLVAGVRFMGETAKILNPEK-----QVL-MPTLNA 111
SP|Q93CP9|NADA_SHIFL     --GCISDSLEMARFGA---KHPASTLLVAGVRFMGETAKILSPEK-----TIL-MPTLQV 111
SP|Q32IH8|NADA_SHIDS     --GCISDSLEMARFGA---KHPASTLLVAGVRFMGETAKILSPEK-----TIL-MPTLQA 111
SP|Q9KR14|NADA_VIBCH     --GFVGDSDLMAKFGN---RYPATTLIIAGVRFMGESAKILTPEK-----RIL-MPTLEA 111
SP|Q7MJ90|NADA_VIBVY     --GFVGDSDLMAKFGN---RHPAGTLIIAGVRFMGESAKILTPEK-----RIL-MPTLEA 111
SP|O67730|NADA_AQUAE     --DFVGDSDLARKAS---QTDADIVFCGVRFMCETAKIVNPEK-----KVL-HPNPES 98
SP|Q9FGS4|NADA_ARATH     PHISISDSLVMAADSAVTMAKAGCFITVVLGVDFMSENVRALDQAGFEKVGVRMSDETI 358
                                . ** :: . : . ** * * . : .

SP|P11458|NADA_ECOLI     ECSDLGCPVEEFNA-FCDA---H-PDRTVVVYANTSAAVKARA-----DWVVTSSIAVE 161
SP|Q9X1X7|NADA_THEMA     TCPMANRLTPEIIRE-YREK---F-PDAPVVLYVNSTSECKTLA-----DVICTSANAVE 129
SP|O25910|NADA_HELPY     CCSMARMIDSHYYDRSVHLLKCEGVKEFYPIITYINSNAEVKAKVAK-DDGVVCTSRNASK 143
SP|Q49622|NADA_MYCLE     GCSLADSIPTDELCA-WKDE---H-PGAAVVSYVNTTAEVKALT-----DICCTSSNAVD 165
SP|P9WJK1|NADA_MYCTU     GCSLADSIPTDELRA-WKDE---H-PGAVVVSYVNTTAAVKALT-----DICCTSSNAVD 162
SP|P65498|NADA_MYCBO     GCSLADSIPTDELRA-WKDE---H-PGAVVVSYVNTTAAVKALT-----DICCTSSNAVD 162
SP|O57767|NADA_PYRHO     TCAMANMLKVEHILE-AKRK---Y-PNAPVVLYVNSTAEAKAYA-----DVTVTSANAVE 131
SP|Q9V2R2|NADA_PYRAB     TCAMANMLKVEHIIIE-AKRK---Y-PNAPVVLYVNSTAETKAYA-----DVTVTSANAVK 131
SP|Q8TZL3|NADA_PYRFU     TCAMANMLKVKHILE-AKCK---Y-PNAPVVLYVNSTAETKAYA-----DVTVTSANAVD 135
SP|Q9KWZ1|NADA_BACSU     GCSMADMDMQQTNRWKKLQHFIDTIIPLTYVNSTAEIKAFVGK-HGGATVTSNAKK 167

```

SP|Q817V8|NADA\_BACCR GCSMADMADIEQTERAWKELTKLFGDTMIPLTYVNSTAAIKAFCCGR-NGGATVTSSNAKQ 167  
SP|C3P9B5|NADA\_BACAA GCSMADMADIEQTERAWHEELTKLFGDTMIPLTYVNSTAAIKAFCCGR-NGGATVTSSNAKQ 167  
SP|Q8XNE3|NADA\_CLOPE GCVADMADIEEGLAK-LKEE---H-PNAAKVVVYINSSTEVKALS-----DVCCTSSNAEN 131  
SP|Q9I4W9|NADA\_PSEAE TCSDLGCPVDEFSA-FCDQ---H-PERTVVVYANTSAAVKARA-----DWVVTSSCAVE 162  
SP|Q3K7X0|NADA\_PSEFF TCSDLGCPVDEFSA-FCDQ---H-PERTVVVYANTSAAVKARA-----DWVVTSSCALE 162  
SP|Q5SJM4|NADA\_THET8 GCSSLADSIREDVLA-WKAK---H-PDGIVVAYVNTKAEVKALA-----DVCVTSANAVE 137  
SP|Q1CFN2|NADA\_YERPN ECSDLGCPVDEFTA-FCDS---H-PDRTVVVYANTSAAVKAKA-----DWVVTSSIAVE 161  
SP|Q66D87|NADA\_YERPS ECSDLGCPVDEFTA-FCDS---H-PDRTVVVYANTSAAVKAKA-----DWVVTSSIAVE 161  
SP|A1JRP2|NADA\_YERE8 ECSDLGCPDEFSA-FCDS---H-PDRTVVVYANTSAAVKARA-----DWVVTSSIAVE 161  
SP|Q93CP9|NADA\_SHIFL ECSDLGCPVEEFNA-FYDA---H-PDRTVVVYANTSAAVKARA-----DWVVTSSIAVE 161  
SP|Q32IH8|NADA\_SHIDS ECSDLGCPVEEFNA-FCDA---H-PDHTVVVYANTSAAVKARA-----DWVVTSSIAVE 161  
SP|Q9KR14|NADA\_VIBCH ECSDLGCPADKfte-FCDA---H-PDHTVVVYANTSAAVKARA-----DWVVTSSIALE 161  
SP|Q7MJ90|NADA\_VIBVY ECSDLGCPADKfte-FCDA---H-PDHTVVVYANTSAAVKARA-----DWVVTSSIALE 161  
SP|O67730|NADA\_AQUAE GCPMADMITAKQVRE-LREK---H-PDAEFVAYINTTADVKAEV-----DICVTSANAPK 148  
SP|Q9FGS4|NADA\_ARATH GCSLADAASAPAYLN-YLEAASRS-PPSLHVVYINTSLETKAFHELVPTICTSSNVVQ 416  
\* : : \* \* . \* : \*\* .

SP|P11458|NADA\_ECOLI LIDHLDSL--GEKI I WAPDKHLGRYVQKQTGGD-----I 193  
SP|Q9X1X7|NADA\_THEMEA VVKKLD---SSVVFPGPDRNLGEYVAEKTGKK-----V 159  
SP|O25910|NADA\_HELPY IFNHALKQ--NKKIFFLPDKCLGENLALENGLKS---AILGA-----NSQEEIKNA 189  
SP|Q49622|NADA\_MYCLE VVESIDP---SREVLFCPDQFLGAHVRRVTGRK-----N 196  
SP|P9WJK1|NADA\_MYCTU VVASIDP---DREVLFCPDQFLGAHVRRVTGRK-----N 193  
SP|P65498|NADA\_MYCBO VVASIDP---DREVLFCPDQFLGAHVRRVTGRK-----N 193  
SP|O57767|NADA\_PYRHO VVKKLD---SDVVFPGPKNLAHYVAKMTGKK-----I 161  
SP|Q9V2R2|NADA\_PYRAB IVSKLD---ADVVFPGPKNLAHYVAKMTGKK-----V 161  
SP|Q8T2L3|NADA\_PYRFU IIRKLD---SDVVFPGPKNLAHYVAKVTGKT-----I 161  
SP|Q9KWZ1|NADA\_BACSU VLEWAFTQ--KKRILFLPDQHLGRNTAYDLGIAL---EDMAVWDPMKDELVAESGHTNV 225  
SP|Q817V8|NADA\_BACCR MVSWAFTQ--KERLVFLPDQHLGRNTAYDLGIPL---DKMAVWDPHTDSLEYDGDIEEI 221  
SP|C3P9B5|NADA\_BACAA MVSWAFTQ--KERLVFLPDQHLGRNTAYDLGIPL---DKMAVWDPHTDSLEYDGDIEEI 221  
SP|Q8XNE3|NADA\_CLOPE IINNLE---EKEIIFLPDRNLGSYIQEKTDPK-----K 161  
SP|Q9I4W9|NADA\_PSEAE IVEHLMDN--GEPILWAPDQHLGRYI QRETGAD-----M 194  
SP|Q3K7X0|NADA\_PSEFF IVESLKN--GETI IWGPDKHLGTYIQRQTGAD-----M 194  
SP|Q5SJM4|NADA\_THET8 VVSRLPQ---DRPIYFVPMDFLGAHVAVRTGRR----- 167  
SP|Q1CFN2|NADA\_YERPN LIEHLDSL--GEKI I WAPDRHLGSYVQKKSAD-----V 193  
SP|Q66D87|NADA\_YERPS LIEHLDSL--GEKI I WAPDRHLGSYVQKKSAD-----V 193  
SP|A1JRP2|NADA\_YERE8 LIEHLDSL--GEKI I WAPDRHLGNVYQKRSAD-----V 193  
SP|Q93CP9|NADA\_SHIFL LIDHLDSL--GEKI I WAPDKHLGRYVQKQTGGD-----I 193  
SP|Q32IH8|NADA\_SHIDS LIDHLDSL--GEKI I WAPDKHLGRYVQKQTGAD-----I 193  
SP|Q9KR14|NADA\_VIBCH IVEHLDE--GKPI IWGPDRLGAYIAKKTGAD-----M 193  
SP|Q7MJ90|NADA\_VIBVY IVEHLDAE--DKPI IWGPDRLGSIYANKTGAD-----M 193  
SP|O67730|NADA\_AQUAE IIKKLE---AKKIVFLPDQALGNVWAKQVPEK-----E 178  
SP|Q9FGS4|NADA\_ARATH TILQAFQMPELTVWYGPDSYMGANIVKLFQQMTLMTNNEIANIHPK-HSLDSIKSLLPR 475  
. : : \* \* .

SP|P11458|NADA\_ECOLI --LCWQGACIVHDEFKQALTRLQEEYPDAAILVHPESPQAVVDMA-----DAV 240  
SP|Q9X1X7|NADA\_THEMEA ITIPENGHCVPVHQ-FNAESIDAVRKKYPDARKVIVHPECCKPVRDKA-----DYV 207  
SP|O25910|NADA\_HELPY DVVYNGFCSVHQFLKLEIDIEFYRQKYPDILIAVHPECEPSSVVSNA-----DFS 238  
SP|Q49622|NADA\_MYCLE V-YVWMEGCHVHAGINGDELVDQARANPDALFVHPECGCATSALYLAGEGAFPPDRVKI 255  
SP|P9WJK1|NADA\_MYCTU L-HVWAGECHVHAGINGDELADQARAHPDALFVHPECGCATSALYLAGEGAFPAERVKI 252  
SP|P65498|NADA\_MYCBO L-HVWAGECHVHAGINGDELADQARAHPDALFVHPECGCATSALYLAGEGAFPAERVKI 252  
SP|O57767|NADA\_PYRHO IPVPSKGHCYVHQKFTLDDVERAKKLLHFNALMIHPECIPEVQEKA-----DII 210  
SP|Q9V2R2|NADA\_PYRAB IPVPPNGHCYVHQKFTIEDVERAKKLLHFNALMIHPECIPEVQEKA-----DII 210  
SP|Q8T2L3|NADA\_PYRFU IPIPEGHCYVHKKFTIEDVERAKKLLHFNALMIHPECNPEVQEHA-----DII 214  
SP|Q9KWZ1|NADA\_BACSU KVILWKGHCYVHEKFTTKNIHDMRERDPDIQIVHPECSHEVVTL-----DDN 270  
SP|Q817V8|NADA\_BACCR QVILWKGHCYVHQKFTVKNIESVRKNHSDMMNIIVHPECCYEVVAAS-----DYA 270  
SP|C3P9B5|NADA\_BACAA QVILWKGHCYVHQKFTVKNIESVRKNHSDMMNIIVHPECCYEVVAAS-----DYA 270  
SP|Q8XNE3|NADA\_CLOPE F-ILWNGFCIVHEAIQKEEILRLKSEHEGILTVAHPECSKEIRDIS-----DFI 209  
SP|Q9I4W9|NADA\_PSEAE --LLWDGACIVHEEFKAKQLEDKALYPDAAILVHPESPESVVALA-----DAV 241  
SP|Q3K7X0|NADA\_PSEFF --LLWDGACIVHEEFKSKQLEDKALYPDAAILVHPESPESVVALA-----DAV 241  
SP|Q5SJM4|NADA\_THET8 L-DLFPGECHVHAGIREEHLKALLEAHPGAEFLIHPCEGCGSGCLYLKPD-----AKM 219  
SP|Q1CFN2|NADA\_YERPN --LCWQGACIVHDEFKQALARMKALYPDAAVLVHPESPQAVVDMA-----DAV 240  
SP|Q66D87|NADA\_YERPS --LCWQGACIVHDEFKQALARMKALYPDAAVLVHPESPQAVVDMA-----DAV 240  
SP|A1JRP2|NADA\_YERE8 --LCWKGACIVHDEFKQALAQMKALHPDAAVLVHPESPQAVVDMA-----DAV 240  
SP|Q93CP9|NADA\_SHIFL --LCWQGACIVHDEFKQALTRLQEEYPDAAILVHPESPQAVVDMA-----DAV 240  
SP|Q32IH8|NADA\_SHIDS --LCWQGACIVHDEFKQALTRLQEEYLDAAILVHPESPQAVVDMA-----DAV 240  
SP|Q9KR14|NADA\_VIBCH --LLWQGEVCHVHDEFADALRKMALYPDAAILVHPESPASVVELA-----DAV 240  
SP|Q7MJ90|NADA\_VIBVY --LLWQGEVCHVHDEFADALRKMALYPDAAILVHPESPASVVELA-----DAV 240  
SP|P9WJK1|NADA\_AQUAE F-I IWKGFPCPHFETYKELEKLEMYPDARKAVHPECHPRVIELA-----DFV 226  
SP|Q9FGS4|NADA\_ARATH LHYFQEGTCIVHHLFGHEVVERIKYMYCDAFLTAHLEVPGEFMFLAMEAK--KREMGVV 532  
\* \* \* : . : \* \*

SP|P11458|NADA\_ECOLI GSTSQLIAAAKTL-----PHQRLIVATDRGIFYKMQQAVPD----- 276  
SP|Q9X1X7|NADA\_THEMEA GSTGQMEKIPEKD-----PSRIFVIGTEIGMIHKLKPKFPD----- 243  
SP|O25910|NADA\_HELPY GSTSQIIEFVEKL-----SPNQKVAIGTESHLVNRLLKAKRHH----- 275  
SP|Q49622|NADA\_MYCLE LSTGGMLTAARQT-----QYRKILVATEVGMQLYQLRRAAPE----- 291  
SP|P9WJK1|NADA\_MYCTU LSTGGMLEAAHTT-----RARQVLVATEVGMQLYQLRRAAPE----- 288  
SP|P65498|NADA\_MYCBO LSTGGMLEAAHTT-----RARQVLVATEVGMQLYQLRRAAPE----- 288

SP|O57767|NADA\_PYRHO ASTGGMIKRACE-----WDEWVVFTEREMVYRLRKLYPQ----- 244  
 SP|Q9V2R2|NADA\_PYRAB VSTGGMIKNACL-----HDEWVVFTEREMVYRLKLYPE----- 244  
 SP|Q8TZL3|NADA\_PYRFU VSTGGMIRRACE-----WDEWVVFTEREMVYRLSKLYPN----- 248  
 SP|Q9KWZ1|NADA\_BACSU GSTKYIIDTINQA-----PAGSKWAIGTEMNLVQRIIHEHPD----- 307  
 SP|Q817V8|NADA\_BACCR GSTKYIIDMIESA-----PPGSKWAIGTEMNLVNRIIQQHPD----- 307  
 SP|C3P9B5|NADA\_BACAA GSTKYIIDMIESA-----PSGSKWAIGTEMNLVNRIIQQHPD----- 307  
 SP|Q8XNE3|NADA\_CLOPE GSTSEIINFVNNS-----SNKKFIIITEEGVLHQLRKNNGEE----- 245  
 SP|Q9I4W9|NADA\_PSEAE GSTSqliKAAQTL-----PNKTFIVATDRGIFYKMQQLCPD----- 277  
 SP|Q3K7X0|NADA\_PSEPF GSTSqliIAAAQSL-----PNKTLIVATDRGIFYKMQQLCPD----- 277  
 SP|Q5SJM4|NADA\_THET8 LSTEGMVRYAKGA-----EAREFVVATEVGIHLRLKKEAPE----- 255  
 SP|Q1CFN2|NADA\_YERPN GSTSqliQAATL-----PQKTLIVATDRGIFYKMQQACPD----- 276  
 SP|Q66D87|NADA\_YERPS GSTSqliQAATL-----PQKTLIVATDRGIFYKMQQACPD----- 276  
 SP|A1JRP2|NADA\_YERE8 GSTSqliMAAKTL-----PQKTLIVATDRGIFYKMQQACPD----- 276  
 SP|Q93CP9|NADA\_SHIFL GSTSqliIAAAKAL-----PHQLRIVATDRGIFYKMQQAVPD----- 276  
 SP|Q32IH8|NADA\_SHIDS GSTSqliIAAATL-----PHQWLIVATDRGIFYKMQQAVPD----- 276  
 SP|Q9KR14|NADA\_VIBCH GSTSqliKAAKTL-----PQQKMIVATDKGIFFKMQQMVPE----- 276  
 SP|Q7MJ90|NADA\_VIBVY GSTSqliKAAKEL-----PQQKMIVATDKGIFFKMQQLVPE----- 276  
 SP|O67730|NADA\_AQUAE GSTSqliKYATSV-----DAKRVIIVTEVGLKYTLEKINPN----- 262  
 SP|Q9FGS4|NADA\_ARATH GSTQNILDFIKQKVQEAVDNRVDDHLQFVLGTESGMVTSIVAVIRSLGSSANSKLVVEV 592  
 \*\* : : \* : :

SP|P11458|NADA\_ECOLI -----KELLEAPTAGEGA---TCRSCAHCPPWAMNGLQAIA 309  
 SP|Q9X1X7|NADA\_THEMA -----REFVPL-EM-----AVCVNMKNTLENTL 266  
 SP|O25910|NADA\_HELPY -----QNTFILSSTL-----ALCPTMNETTLKDLF 300  
 SP|Q49622|NADA\_MYCLE -----IDFRAVNR-----ASCKYMKMITPGALL 315  
 SP|P9WJK1|NADA\_MYCTU -----VDFRAVNR-----ASCKYMKMITPAALL 312  
 SP|P65498|NADA\_MYCBO -----VDFRAVNR-----ASCKYMKMITPAALL 312  
 SP|O57767|NADA\_PYRHO -----KKFYPAED-----AFCIGMKAITLKNIY 268  
 SP|Q9V2R2|NADA\_PYRAB -----KKFYPAED-----AICIGMKAITLKHIY 268  
 SP|Q8TZL3|NADA\_PYRFU -----KKFYPAED-----AVCVGMKAITLQHVY 272  
 SP|Q9KWZ1|NADA\_BACSU -----KQIESLNPDM-----CPCLTMNRIDLPHLL 332  
 SP|Q817V8|NADA\_BACCR -----KEIVSLNPFM-----CPCLTMNRIDLPHLL 332  
 SP|C3P9B5|NADA\_BACAA -----KEIVSLNPFM-----CPCLTMNRIDLPHLL 332  
 SP|Q8XNE3|NADA\_CLOPE -----KEYFIIPYK-----MVCRNMKMTTLKDLY 269  
 SP|Q9I4W9|NADA\_PSEAE -----KDFIEAPTAGNGA---ACRSCAHCPPWAMNTLERTL 310  
 SP|Q3K7X0|NADA\_PSEPF -----KVFIEAPTAGNGA---ACRSCAHCPPWAMNTLERTL 310  
 SP|Q5SJM4|NADA\_THET8 -----KAFFPVKPD-----AVCEYMKRITLEKVY 279  
 SP|Q1CFN2|NADA\_YERPN -----KELFEAPTAGEGA---TCRSCAHCPPWAMNGLRAIA 309  
 SP|Q66D87|NADA\_YERPS -----KELFEAPTAGEGA---TCRSCAHCPPWAMNGLRAIA 309  
 SP|A1JRP2|NADA\_YERE8 -----KELFEAPTAGEGA---TCRSCAHCPPWAMNGLKAIA 309  
 SP|Q93CP9|NADA\_SHIFL -----KELLEAPTAGEGA---TCRSCAHCPPWAMNDLQAIA 309  
 SP|Q32IH8|NADA\_SHIDS -----KELLEAPTAGEGA---TCRSCAHCPPWAMNGLQAIA 309  
 SP|Q9KR14|NADA\_VIBCH -----KELIEAPTAGAGA---TCRSCAHCPPWAMNGLQAIA 309  
 SP|Q7MJ90|NADA\_VIBVY -----KELIEAPTAGAGA---TCRSCAHCPPWAMNGLKAIE 309  
 SP|O67730|NADA\_AQUAE -----KEYIFPQSMN-----YCGTVYCCTMKGITLPKVY 291  
 SP|Q9FGS4|NADA\_ARATH VFPVSSDSMTKTSSDSSNSIKVGDVALPVVPGVAGGEGCSIHGGCASCOPYMKMNSLSL 652  
 \* \*

SP|P11458|NADA\_ECOLI EALEQ---EGSNHEVHVDERL-----RERALVPLNRMLDFAATLRG----- 347  
 SP|Q9X1X7|NADA\_THEMA HALQT---ES---FEVILPKEV-----IEKAKKPIRLRMFELMG----- 298  
 SP|O25910|NADA\_HELPY EVLKAYKNHRAYNTIELKDEV-----ARLAKLALTKMMELS----- 336  
 SP|Q49622|NADA\_MYCLE RCLVE---GT---DEVHVDSEI-----AAAGRRSVQRMIEIIGLPGGGE----- 352  
 SP|P9WJK1|NADA\_MYCTU RCLVE---GA---DEVHVDPGI-----AASGRRSVQRMIEIIGHPGGGE----- 349  
 SP|P65498|NADA\_MYCBO RCLVE---GA---DEVHVDPGI-----AASGRRSVQRMIEIIGHPGGGE----- 349  
 SP|O57767|NADA\_PYRHO ESLKD---MK---YKVEVPPEI-----ARKARKAIERMLEMSK----- 300  
 SP|Q9V2R2|NADA\_PYRAB ESLRD---MK---YKVEVPRDI-----AEKARRAIERMLEMS----- 299  
 SP|Q8TZL3|NADA\_PYRFU ESLRD---MK---YEVTVPEEI-----AEKARKAIERMLEMS----- 303  
 SP|Q9KWZ1|NADA\_BACSU WSLEQIEKGEPSGVIKVPKAI-----QEDALLALNRMLSIT----- 368  
 SP|Q817V8|NADA\_BACCR WALETIERGEEINVISVDKQV-----TAEAVLALNRMLERV----- 368  
 SP|C3P9B5|NADA\_BACAA WALETIERGEEINVISVDKQV-----TEEAVLALNRMLERV----- 368  
 SP|Q8XNE3|NADA\_CLOPE ESLLK---ME---NKIEIDEDL-----RLKAYNSLKNMHKLG----- 301  
 SP|Q9I4W9|NADA\_PSEAE ACLRE---GS---GEIFVDPAL-----IPRAVRPLKRLDFTQAARLRQA---GNA- 352  
 SP|Q3K7X0|NADA\_PSEPF KCLKE---GS---NEIFVDPAL-----IPQAIRPLKRLDFTQAARMKLA---GNA- 352  
 SP|Q5SJM4|NADA\_THET8 LSLKE---MR---HVVRVPEEV-----AGRARRALEAMVAVG----- 310  
 SP|Q1CFN2|NADA\_YERPN EGLEQ---GGGMHEIHVDEEL-----RQQALIPLNRLMDFANQLKLVK---GNA- 353  
 SP|Q66D87|NADA\_YERPS EGLEQ---GGVMHEIHVDEEL-----RQQALIPLNRLMDFANQLKLVK---GNA- 353  
 SP|A1JRP2|NADA\_YERE8 EGLEQ---GGVMHEIHVDEQL-----RQQALIPLNRLMDFANELKLVK---GNA- 353  
 SP|Q93CP9|NADA\_SHIFL EALEQ---EGSNHEVHVDERL-----RERALVPLNRMLDFAATLRG----- 347  
 SP|Q32IH8|NADA\_SHIDS EALEQ---EGSNHEVHVDERL-----RERALVPLNRMLDFAATLRG----- 347  
 SP|Q9KR14|NADA\_VIBCH QALRE---GGKQHEIFVDEAL-----RVKSLIPLNRLMDFAEQLNLKVK---GNA- 353  
 SP|Q7MJ90|NADA\_VIBVY TALRE---GGEQHEIFVDEAL-----RVKSLIPLNRLMDFAEKLNMQVK---GNV- 353  
 SP|O67730|NADA\_AQUAE ETLKN---EI---NEVTLPKDI-----IERARRPIERMLELS----- 322  
 SP|Q9FGS4|NADA\_ARATH KVCHKLPLDENYVGGFIAERFKRQTPQKGLIADVGCPEILHMRHFQANKELPKLVHQLV 712  
 : . : \*

**Figure 72:** Sequence alignment of NadA protein from different organisms. (\*) indicates fully conserved amino-acid residues; (:) indicates amino-acids with strong physical-chemical properties ;(.) indicates amino-acids with weak properties. (ECOLI: *Escherichia coli*; THEMA: *Thermotoga maritima*; HELPY: *Helicobacter pylori*; MYCLE: *Mycobacterium leprae*; MYCTU: *Mycobacterium tuberculosis*, MYCBO: *Mycobacterium Bovis*; PYRHO: *Pyrococcus Horikoshii*; PYRAB: *Pyrococcus abyssi*; PYRFU: *Pyrococcus furiosus*; BACSU: *Bacillus subtilis*; BACCR: *Bacillus cereus*; BACAA: *Bacillus anthracis*; CLOPE: *Clostridium perfringens*; PSEAE: *Pseudomonas aeruginosa*; PSEPF: *Pseudomonas fluorescens*; THET8: *Thermus thermophiles*; YERP: *Yersinia pestis*; YERPS: *Yersinia pseudotuberculosis*; YERE8: *Yersinia enterocolitica*; SHIFL: *Shigella flexneri*; SHIDS: *Shigella dysenteriae*; VIBCH: *Vibrio cholera*; VIBVY: *Vibrio vulnificus*; AQUAE: *Aquifex aeolicus*; ARATH: *Arabidopsis thaliana*.)

In the sequence alignment are included NadA from the targeted pathogens *H. pylori* and *M. leprae*; *E. coli* NadA (that we used in our *in vitro* studies); *T. maritima* NadA (that we used for crystallographic studies); and NadA from *P. horikoshii* (included for comparison, since it is the only structure of NadA available in the literature apart from that of *T. maritima* NadA). The % of sequence identity and % of sequence similarity in comparison to NadA *E. coli* are indicated below in Table 18. All these data show that NadA is a highly conserved protein from one organism to another.

ORGANISM	NUMBER OF RESIDUES	% OF SEQUENCE IDENTITY WITH <i>E. coli</i>	% OF SEQUENCE SIMILARITY WITH <i>E. coli</i>
<i>E. coli</i>	347	100	100
<i>H. pylori</i>	336	29	47
<i>M. leprae</i>	352	33	51
<i>T. maritima</i>	298	33	55
<i>P. horikoshii</i>	300	35	56

**Table 18:** Sequence identity (%) and sequence similarity (%) of NadA from different organisms in comparison with *E. coli* NadA (Blast program).

Structural homologies (especially the presence of the tunnel that connects the catalytic [4Fe-4S] with the surface) are also visible by superposition of the two structures of NadA which are available in the literature, NadA from *T. maritima* and *P. horikoshii* (Figure 73)<sup>131,214</sup>. Note that *E. coli* NadA has 100% of structure homology with *T. maritima* and *P. furiosus* NadA (Phyre program).

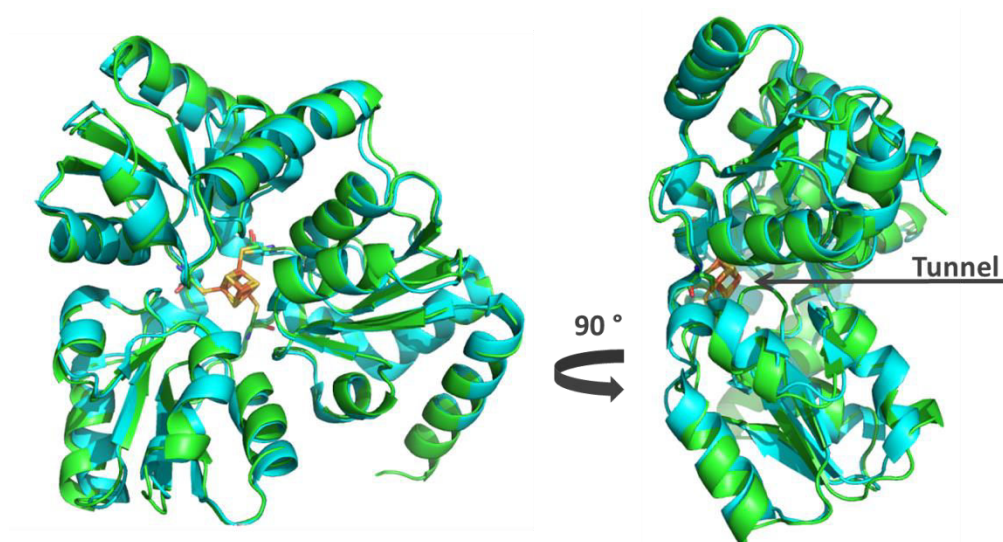


**Figure 73:** Superposed structures of *T. maritima* NadA (green, PDB: 4P3X) and *P. horikoshii* NadA (blue, PDB: 5KTM).

If we look from the entrance of the tunnel towards the cluster (Figure 73, left), we observe that the two structures are highly superimposable and we can identify the three domains of the protein described in the introduction. If the structures superposition is turned 90° (Figure 73, right), the tunnel is visible in both proteins. We can also easily identify the concave and convex side of the protein described during introduction.

# BIBLIOGRAPHY

1. Harden, A. & Young, W. The alcoholic ferment of yeast-juice. Part II.—The coferment of yeast-juice. *Proc. R. Soc. London. Ser. B, Contain. Pap. a Biol. Character* **78**, 369–375 (1906).
2. Von Euler, H. Fermentation of sugars and fermentative enzymes. *Nobel Lect. Nobel Found.* (1930).
3. Warburg, O. & Christian, W. Pyridin, der wasserstoffübertragende Bestandteil von Gärungsfermenten. *Helv. Chim. Acta* **19**, E79–E88 (1936).
4. Kornberg, A. The Participation of Inorganic Pyrophosphate in The Reversible Enzymatic Synthesis of Diphosphopyridine Nucleotide. *J. Biol. Chem.* **176**, 1475–1476 (1948).
5. Preiss, J. & Handler, P. Biosynthesis of Diphosphopyridine Nucleotide: I. Identification of Intermediates. *J. Biol. Chem.* **233**, 488–492 (1958).
6. Berger, F., Ramírez-Hernández, M. H. & Ziegler, M. The new life of a centenarian: signalling functions of NAD(P). *Trends Biochem. Sci.* **29**, 111–118 (2018).
7. Cantó, C., Menzies, K. & Auwerx, J. NAD(+) metabolism and the control of energy homeostasis - a balancing act between mitochondria and the nucleus. *Cell Metab.* **22**, 31–53 (2015).
8. Pollak, N., Dölle, C. & Ziegler, M. The power to reduce: pyridine nucleotides – small molecules with a multitude of functions. *Biochem. J.* **402**, 205 LP-218 (2007).
9. Dagley, S. The chemical reactions of living cells: Being a Review Essay of Biochemistry. The Chemical Reactions Living Cells by David E. Metzler. Pp 1168. Academic Press, London, New York and San Francisco. 1977. \$24.95 or £17.75. Now also available in an Internatio. *Biochem. Educ.* **6**, 51–52 (1978).
10. Lin, S.-J. & Guarente, L. Nicotinamide adenine dinucleotide, a metabolic regulator of transcription, longevity and disease. *Curr. Opin. Cell Biol.* **15**, 241–246 (2003).
11. ADAMS, M. J. *et al.* Structure of Lactate Dehydrogenase at 2.8 Å Resolution. *Nature* **227**, 1098 (1970).
12. Israel, H. Proteopedia: Rossmann fold: A beta-alpha-beta fold at dinucleotide binding sites. *Biochem. Mol. Biol. Educ.* **43**, 206–209 (2015).
13. Rich, P. R. The molecular machinery of Keilin's respiratory chain. *Biochem. Soc. Trans.* **31**, 1095–1105 (2003).
14. Freitag, A. & Bock, E. Energy conservation in Nitrobacter. *FEMS Microbiol. Lett.* **66**, 157–162 (1990).
15. Starkenburg, S. R. *et al.* Genome Sequence of the Chemolithoautotrophic Nitrite-Oxidizing Bacterium Nitrobacter winogradskyi Nb-255. *Appl. Environ. Microbiol.* **72**, 2050–2063 (2006).
16. Nicholls, D. & Ferguson, S. *Bioenergetics 3rd edition.* (2002).
17. Johansson, T. *et al.* X-ray Structure of Domain I of the Proton-pumping Membrane Protein Transhydrogenase from Escherichia coli. *J. Mol. Biol.* **352**, 299–312 (2005).
18. Diefenbach, J. & Bürkle, A. Poly-ADP-ribosylation in health and disease. *Cell. Mol. Life Sci. C.* **62**, 721–730 (2005).
19. Alexander, B. Poly(ADP-ribose). The most elaborate metabolite of NAD+. *FEBS J.* **272**,

- 4576–4589 (2005).
20. Mathias, Z. New functions of a long-known molecule. *Eur. J. Biochem.* **267**, 1550–1564 (2001).
  21. Sauve, A. A. Sirtuin chemical mechanisms. *Biochim. Biophys. Acta - Proteins Proteomics* **1804**, 1591–1603 (2010).
  22. Hoff, K. G., Avalos, J. L., Sens, K. & Wolberger, C. Insights into the Sirtuin Mechanism from Ternary Complexes Containing NAD<sup>+</sup> and Acetylated Peptide. *Structure* **14**, 1231–1240 (2006).
  23. Guarente, L. Sir2 links chromatin silencing, metabolism, and aging. *Genes Dev.* **14**, 1021–1026 (2000).
  24. Imai, S. & Guarente, L. Ten years of NAD-dependent SIR2 family deacetylases: implications for metabolic diseases. *Trends Pharmacol. Sci.* **31**, 212–220 (2010).
  25. Sauve, A. A., Wolberger, C., Schramm, V. L. & Boeke, J. D. The Biochemistry of Sirtuins. *Annu. Rev. Biochem.* **75**, 435–465 (2006).
  26. Schär, P., Herrmann, G., Daly, G. & Lindahl, T. A newly identified DNA ligase of *Saccharomyces cerevisiae* involved in RAD52-independent repair of DNA double-strandbreaks. *Genes Dev.* **11**, 1912–1924 (1997).
  27. Wilkinson, A., Day, J. & Bowater, R. Bacterial DNA ligases. *Mol. Microbiol.* **40**, 1241–1248 (2001).
  28. Sauve, A. A. NAD<sup>+</sup> and Vitamin B: From Metabolism to Therapies. *J. Pharmacol. Exp. Ther.* **324**, 883 LP-893 (2008).
  29. Pittelli, M. *et al.* Pharmacological Effects of Exogenous NAD on Mitochondrial Bioenergetics, DNA Repair, and Apoptosis. *Mol. Pharmacol.* **80**, 1136 LP-1146 (2011).
  30. VanLinden, M. R. *et al.* Subcellular Distribution of NAD(+) between Cytosol and Mitochondria Determines the Metabolic Profile of Human Cells. *J. Biol. Chem.* **290**, 27644–27659 (2015).
  31. C., A. C. *et al.* Differences among cell types in NAD<sup>+</sup> compartmentalization: A comparison of neurons, astrocytes, and cardiac myocytes. *J. Neurosci. Res.* **85**, 3378–3385 (2007).
  32. Osterman, A. L. & Begley, T. P. A subsystems-based approach to the identification of drug targets in bacterial pathogens BT - Systems Biological Approaches in Infectious Diseases. in (eds. Boshoff, H. I. & Barry, C. E.) 131–170 (Birkhäuser Basel, 2007).
  33. Nasu, S., Wicks, F. D. & Gholson, R. K. L-Aspartate oxidase, a newly discovered enzyme of *Escherichia coli*, is the B protein of quinolinate synthetase. *J. Biol. Chem.* **257**, 626–632 (1982).
  34. Wicks, F. D., Sakakibara, S. & Gholson, R. K. Evidence for an intermediate in quinolinate biosynthesis in *Escherichia coli*. *J. Bacteriol.* **136**, 136–141 (1978).
  35. Gabriella, T. *et al.* L-Aspartate Oxidase from *Escherichia coli*. II. Interaction with C4 dicarboxylic acids and identification of a novel L-aspartate: fumarate oxidoreductase activity. *Eur. J. Biochem.* **239**, 427–433 (2004).
  36. Marinoni, I. *et al.* Characterization of l-aspartate oxidase and quinolinate synthase from *Bacillus subtilis*. *FEBS J.* **275**, 5090–5107 (2008).
  37. Yang, Z. *et al.* Aspartate Dehydrogenase, a Novel Enzyme Identified from Structural and Functional Studies of TM1643. *J. Biol. Chem.* **278**, 8804–8808 (2003).
  38. Ollagnier-de Choudens, S., Loiseau, L., Sanakis, Y., Barras, F. & Fontecave, M.

- Quinolinate synthetase, an iron–sulfur enzyme in NAD biosynthesis. *FEBS Lett.* **579**, 3737–3743 (2005).
39. Cicchillo, R. M. *et al.* Escherichia coli Quinolinate Synthetase Does Indeed Harbor a [4Fe-4S] Cluster. *J. Am. Chem. Soc.* **127**, 7310–7311 (2005).
  40. Bhatia, R. & Calvo, K. C. The Sequencing, Expression, Purification, and Steady-State Kinetic Analysis of Quinolinate Phosphoribosyl Transferase from Escherichia coli. *Arch. Biochem. Biophys.* **325**, 270–278 (1996).
  41. C., F. A., C., Z. W. & Robert, S. Quinolinic Acid Phosphoribosyltransferase in Rat Brain. *J. Neurochem.* **44**, 446–454 (1985).
  42. Kurnasov, O. *et al.* NAD Biosynthesis: Identification of tryptophan to quinolinate pathway in bacteria. *Chem. Biol.* **10**, 1195–1204 (2003).
  43. Thackray, S. J., Mowat, C. G. & Chapman, S. K. Exploring the mechanism of tryptophan 2,3-dioxygenase. *Biochem. Soc. Trans.* **36**, 1120 LP-1123 (2008).
  44. Pabarcus, M. K. & Casida, J. E. Kynurenine formamidase: determination of primary structure and modeling-based prediction of tertiary structure and catalytic triad. Portions of this paper were presented at the Fifteenth Symposium of The Protein Society (FASEB), Philadelphia, PA, USA, July. *Biochim. Biophys. Acta - Protein Struct. Mol. Enzymol.* **1596**, 201–211 (2002).
  45. Han, Q., Beerntsen, B. T. & Li, J. The tryptophan oxidation pathway in mosquitoes with emphasis on xanthurenic acid biosynthesis. *J. Insect Physiol.* **53**, 254–263 (2007).
  46. Sandra, M. *et al.* The Pseudomonas siderophore quinolobactin is synthesized from xanthurenic acid, an intermediate of the kynurenine pathway. *Mol. Microbiol.* **52**, 371–384 (2004).
  47. Phillips, R. S. Structure and mechanism of kynureninase. *Arch. Biochem. Biophys.* **544**, 69–74 (2014).
  48. Zhang, Y., Colabroy, K. L., Begley, T. P. & Ealick, S. E. Structural Studies on 3-Hydroxyanthranilate-3,4-dioxygenase: The Catalytic Mechanism of a Complex Oxidation Involved in NAD Biosynthesis. *Biochemistry* **44**, 7632–7643 (2005).
  49. Colabroy, K. L. & Begley, T. P. The Pyridine Ring of NAD Is Formed by a Nonenzymatic Pericyclic Reaction. *J. Am. Chem. Soc.* **127**, 840–841 (2005).
  50. Zhang, Y. *et al.* Crystal Structure and Mechanism of Tryptophan 2,3-Dioxygenase, a Heme Enzyme Involved in Tryptophan Catabolism and in Quinolinate Biosynthesis. *Biochemistry* **46**, 145–155 (2007).
  51. Sugimoto, H. *et al.* Crystal structure of human indoleamine 2,3-dioxygenase: Catalytic mechanism of O(2) incorporation by a heme-containing dioxygenase. *Proc. Natl. Acad. Sci. U. S. A.* **103**, 2611–2616 (2006).
  52. Han, Q., Robinson, H. & Li, J. Biochemical identification and crystal structure of kynurenine formamidase from Drosophila melanogaster. *Biochem. J.* **446**, 253 LP-260 (2012).
  53. Saito, Y., Hayaishi, O. & Rothberg, S. Studies on Oxygenases: Enzymatic formation 3-hydroxy-L-kinurenine from L-kynurenine. *J. Biol. Chem.* **229**, 921–934 (1957).
  54. Lima, S., Khristoforov, R., Momany, C. & Phillips, R. S. Crystal Structure of Homo sapiens Kynureninase. *Biochemistry* **46**, 2735–2744 (2007).
  55. Magni, G., Amici, A., Emanuelli, M., Orsomando, G. & Ruggieri, N. R. and S. Structure and Function of Nicotinamide Mononucleotide Adenylyltransferase. *Current Medicinal*

- Chemistry* **11**, 873–885 (2004).
56. Manfred, S. *et al.* Characterization of recombinant human nicotinamide mononucleotide adenylyl transferase (NMNAT), a nuclear enzyme essential for NAD synthesis. *FEBS Lett.* **492**, 95–100 (2001).
  57. Symersky, J., Devedjiev, Y., Moore, K., Brouillette, C. & DeLucas, L. NH<sub>3</sub>-dependent NAD<sup>+</sup> synthetase from *Bacillus subtilis* at 1 Å resolution. *Acta Crystallogr. Sect. D* **58**, 1138–1146 (2002).
  58. Allibert, P., Willison, J. C. & Vignais, P. M. Complementation of nitrogen-regulatory (ntr-like) mutations in *Rhodobacter capsulatus* by an *Escherichia coli* gene: cloning and sequencing of the gene and characterization of the gene product. *J. Bacteriol.* **169**, 260–271 (1987).
  59. Nessi, C., Albertini, A. M., Speranza, M. L. & Galizzi, A. The outB Gene of *Bacillus subtilis* Codes for NAD Synthetase. *J. Biol. Chem.* **270**, 6181–6185 (1995).
  60. Bu, K. G. *et al.* Crystal structure of NH<sub>3</sub>-dependent NAD<sup>+</sup> synthetase from *Helicobacter pylori*. *Proteins Struct. Funct. Bioinforma.* **58**, 985–988 (2005).
  61. Zerez, C. R., Wong, M. D. & Tanaka, K. R. Partial purification and properties of nicotinamide adenine dinucleotide synthetase from human erythrocytes: evidence that enzyme activity is a sensitive indicator of lead exposure. *Blood* **75**, 1576 LP-1582 (1990).
  62. Bellinzoni, M. *et al.* Glutamine amidotransferase activity of NAD<sup>+</sup> synthetase from *Mycobacterium tuberculosis* depends on an amino-terminal nitrilase domain. *Res. Microbiol.* **156**, 173–177 (2005).
  63. Bieganowski, P., Pace, H. C. & Brenner, C. Eukaryotic NAD<sup>+</sup> Synthetase Qns1 Contains an Essential, Obligate Intramolecular Thiol Glutamine Amidotransferase Domain Related to Nitrilase. *J. Biol. Chem.* **278**, 33049–33055 (2003).
  64. Wojcik, M., Seidle, H. F., Bieganowski, P. & Brenner, C. Glutamine-dependent NAD<sup>+</sup> Synthetase: How a two-domain, three-substrate enzyme avoids waste. *J. Biol. Chem.* **281**, 33395–33402 (2006).
  65. Magni, G. & Raffaelli, G. O. and N. Structural and Functional Properties of NAD Kinase, a Key Enzyme in NADP Biosynthesis. *Mini-Reviews in Medicinal Chemistry* **6**, 739–746 (2006).
  66. Garavaglia, S., Galizzi, A. & Rizzi, M. Allosteric Regulation of *Bacillus subtilis* NAD Kinase by Quinolinic Acid. *J. Bacteriol.* **185**, 4844–4850 (2003).
  67. Shigeyuki, K., Shigetaru, M., Takako, M., Wataru, H. & Kousaku, M. Molecular characterization of *Escherichia coli* NAD kinase. *Eur. J. Biochem.* **268**, 4359–4365 (2001).
  68. Garavaglia, S., Raffaelli, N., Finaurini, L., Magni, G. & Rizzi, M. A Novel Fold Revealed by *Mycobacterium tuberculosis* NAD Kinase, a Key Allosteric Enzyme in NADP Biosynthesis. *J. Biol. Chem.* **279**, 40980–40986 (2004).
  69. Cheng, W. & Roth, J. R. Evidence for two NAD kinases in *Salmonella typhimurium*. *J. Bacteriol.* **176**, 4260–4268 (1994).
  70. Jicai, B., Honghai, W. & Jianping, X. Comparative genomics of NAD(P) biosynthesis and novel antibiotic drug targets. *J. Cell. Physiol.* **226**, 331–340 (2010).
  71. Belenky, P., Bogan, K. L. & Brenner, C. NAD<sup>+</sup> metabolism in health and disease. *Trends Biochem. Sci.* **32**, 12–19 (2018).

72. Belenky, P., Stebbins, R., Bogan, K. L., Evans, C. R. & Brenner, C. Nrt1 and Tna1-Independent Export of NAD<sup>+</sup> Precursor Vitamins Promotes NAD<sup>+</sup> Homeostasis and Allows Engineering of Vitamin Production. *PLoS One* **6**, e19710 (2011).
73. Grose, J. H. *et al.* Assimilation of Nicotinamide Mononucleotide Requires Periplasmic AphA Phosphatase in *Salmonella enterica*. *J. Bacteriol.* **187**, 4521–4530 (2005).
74. Llorente, B. & Dujon, B. Transcriptional regulation of the *Saccharomyces cerevisiae* DAL5 gene family and identification of the high affinity nicotinic acid permease TNA1 (YGR260w). *FEBS Lett.* **475**, 237–241 (2000).
75. Zhu, N., Olivera, B. M. & Roth, J. R. Genetic characterization of the *pnuC* gene, which encodes a component of the nicotinamide mononucleotide transport system in *Salmonella typhimurium*. *J. Bacteriol.* **171**, 4402–4409 (1989).
76. Frothingham, R., Meeker-O’Connell, W. A., Talbot, E. A., George, J. W. & Kreuzer, K. N. Identification, cloning, and expression of the *Escherichia coli* pyrazinamidase and nicotinamidase gene, *pncA*. *Antimicrob. Agents Chemother.* **40**, 1426–1431 (1996).
77. Seiner, D. R., Hegde, S. S. & Blanchard, J. S. Kinetics and Inhibition of Nicotinamidase from *Mycobacterium tuberculosis*. *Biochemistry* **49**, 9613–9619 (2010).
78. Du, X. *et al.* Crystal Structure and Mechanism of Catalysis of a Pyrazinamidase from *Pyrococcus horikoshii*. *Biochemistry* **40**, 14166–14172 (2001).
79. Gross, J., Rajavel, M., Segura, E. & Grubmeyer, C. Energy Coupling in *Salmonella typhimurium* Nicotinic Acid Phosphoribosyltransferase: Identification of His-219 as Site of Phosphorylation. *Biochemistry* **35**, 3917–3924 (1996).
80. Grose, J. H., Bergthorsson, U. & Roth, J. R. Regulation of NAD Synthesis by the Trifunctional NadR Protein of *Salmonella enterica*. *J. Bacteriol.* **187**, 2774–2782 (2005).
81. Raffaelli, N. *et al.* The *Escherichia coli* NadR Regulator Is Endowed with Nicotinamide Mononucleotide Adenylyltransferase Activity. *J. Bacteriol.* **181**, 5509–5511 (1999).
82. Kurnasov, O. V *et al.* Ribosylnicotinamide Kinase Domain of NadR Protein: Identification and Implications in NAD Biosynthesis. *J. Bacteriol.* **184**, 6906–6917 (2002).
83. Gazzaniga, F., Stebbins, R., Chang, S. Z., McPeck, M. A. & Brenner, C. Microbial NAD Metabolism: Lessons from Comparative Genomics. *Microbiol. Mol. Biol. Rev.* **73**, 529–541 (2009).
84. Herbert, M. *et al.* Nicotinamide Ribosyl Uptake Mutants in *Haemophilus influenzae*. *Infect. Immun.* **71**, 5398–5401 (2003).
85. Sorci, L. *et al.* Nicotinamide mononucleotide synthetase is the key enzyme for an alternative route of NAD biosynthesis in *Francisella tularensis*. *Proc. Natl. Acad. Sci. U. S. A.* **106**, 3083–3088 (2009).
86. Biao, M., Shih-Jung, P., L., Z. M. & P., C. B. Assimilation of NAD<sup>+</sup> precursors in *Candida glabrata*. *Mol. Microbiol.* **66**, 14–25 (2007).
87. Belenky, P., Christensen, K. C., Gazzaniga, F., Pletnev, A. A. & Brenner, C. Nicotinamide Riboside and Nicotinic Acid Riboside Salvage in Fungi and Mammals: Quantitative Basis For Urh1 And Purine Nucleoside Phosphorylase Function In NAD<sup>+</sup> Metabolism. *J. Biol. Chem.* **284**, 158–164 (2009).
88. Belenky, P. *et al.* Nicotinamide Riboside Promotes Sir2 Silencing and Extends Lifespan via Nrk and Urh1/Pnp1/Meu1 Pathways to NAD<sup>+</sup>. *Cell* **129**, 473–484 (2007).
89. Andreoli, A. J., Okita, T. W., Bloom, R. & Grover, T. A. The pyridine nucleotide cycle: Presence of a nicotinamide mononucleotide-specific glycohydrolase in *Escherichiacoli*.

- Biochem. Biophys. Res. Commun.* **49**, 264–269 (1972).
90. Gerdes, S. Y. *et al.* Comparative Genomics of NAD Biosynthesis in Cyanobacteria. *J. Bacteriol.* **188**, 3012–3023 (2006).
  91. Martin, P. R., Shea, R. J. & Mulks, M. H. Identification of a Plasmid-Encoded Gene from *Haemophilus ducreyi* Which Confers NAD Independence. *J. Bacteriol.* **183**, 1168–1174 (2001).
  92. Miller, E. S. *et al.* Complete Genome Sequence of the Broad-Host-Range Vibriophage KVP40: Comparative Genomics of a T4-Related Bacteriophage. *J. Bacteriol.* **185**, 5220–5233 (2003).
  93. Raffaelli, N. *et al.* Identification of a novel human nicotinamide mononucleotide adenylyltransferase. *Biochem. Biophys. Res. Commun.* **297**, 835–840 (2002).
  94. Penfound, T. & Foster, J. W. NAD-Dependent DNA-Binding Activity of the Bifunctional NadR Regulator of *Salmonella typhimurium*. *J. Bacteriol.* **181**, 648–655 (1999).
  95. Rossolillo, P., Marinoni, I., Galli, E., Colosimo, A. & Albertini, A. M. YrxA Is the Transcriptional Regulator That Represses De Novo NAD Biosynthesis in *Bacillus subtilis*. *J. Bacteriol.* **187**, 7155–7160 (2005).
  96. Rodionov, D. A. *et al.* Transcriptional regulation of NAD metabolism in bacteria: genomic reconstruction of NiaR (YrxA) regulon. *Nucleic Acids Res.* **36**, 2032–2046 (2008).
  97. Dobrzanska, M., Szurmak, B., Wyslouch-Cieszynska, A. & Kraszewska, E. Cloning and Characterization of the First Member of the Nudix Family from *Arabidopsis thaliana*. *J. Biol. Chem.* **277**, 50482–50486 (2002).
  98. Rodionov, D. A. *et al.* Transcriptional regulation of NAD metabolism in bacteria: NrtR family of Nudix-related regulators. *Nucleic Acids Res.* **36**, 2047–2059 (2008).
  99. Velu, S. E. *et al.* Antibacterial Nicotinamide Adenine Dinucleotide Synthetase Inhibitors: Amide- and Ether-Linked Tethered Dimers with  $\alpha$ -Amino Acid End Groups. *J. Med. Chem.* **50**, 2612–2621 (2007).
  100. Poncet-Montange, G., Assairi, L., Arold, S., Pochet, S. & Labesse, G. NAD Kinases Use Substrate-assisted Catalysis for Specific Recognition of NAD. *J. Biol. Chem.* **282**, 33925–33934 (2007).
  101. Gerdes, S. Y. *et al.* From Genetic Footprinting to Antimicrobial Drug Targets: Examples in Cofactor Biosynthetic Pathways. *J. Bacteriol.* **184**, 4555–4572 (2002).
  102. Sorci, L. *et al.* Targeting NAD biosynthesis in bacterial pathogens. Structure-based development of inhibitors of nicotinate mononucleotide adenylyltransferase NadD. *Chem. Biol.* **16**, 849–861 (2009).
  103. Salama, N. R., Shepherd, B. & Falkow, S. Global Transposon Mutagenesis and Essential Gene Analysis of *Helicobacter pylori*. *J. Bacteriol.* **186**, 7926–7935 (2004).
  104. Jayaram, H. N., Grusch, M., Cooney, D. A. & Krupitza, G. Consequences of IMP dehydrogenase inhibition, and its relationship to cancer and apoptosis. *Curr. Med. Chem.* **6**, 561–574 (1999).
  105. Bieganski, P. & Brenner, C. Discoveries of Nicotinamide Riboside as a Nutrient and Conserved NRK Genes Establish a Preiss-Handler Independent Route to NAD<sup>+</sup> in Fungi and Humans. *Cell* **117**, 495–502 (2004).
  106. Guarente, L. Sirtuins as potential targets for metabolic syndrome. *Nature* **444**, 868 (2006).

107. Howitz, K. T. *et al.* Small molecule activators of sirtuins extend *Saccharomyces cerevisiae* lifespan. *Nature* **425**, 191 (2003).
108. Yanofsky, C. The absence of a tryptophan-niacin relationship in *Escherichia coli* and *Bacillus subtilis*. *J. Bacteriol.* **68**, 577–584 (1954).
109. Andreoli, A. J., Ikeda, M., Nishizuka, Y. & Hayaishi, O. Quinolinic acid: A precursor to nicotinamide adenine dinucleotide in *Escherichiacoli*. *Biochem. Biophys. Res. Commun.* **12**, 92–97 (1963).
110. Dickinson, E. S. & Sundaram, T. K. Chromosomal Location of a Gene Defining Nicotinamide Deamidase in *Escherichia coli*. *J. Bacteriol.* **101**, 1090–1091 (1970).
111. Tritz, G. J. & Chandler, J. L. Recognition of a Gene Involved in the Regulation of Nicotinamide Adenine Dinucleotide Biosynthesis. *J. Bacteriol.* **114**, 128–136 (1973).
112. Tritz, G. J., Matney, T. S. & Gholson, R. K. Mapping of the *nadB* Locus Adjacent to a Previously Undescribed Purine Locus in *Escherichia coli* K-12. *J. Bacteriol.* **102**, 377–381 (1970).
113. Ogasawara, N., Chandler, J. L. R., Gholson, R. K., Rosser, R. J. & Andreoli, A. J. Biosynthesis of quinolinic acid in a cell-free system. *Biochim. Biophys. Acta - Gen. Subj.* **141**, 199–201 (1967).
114. Chandler, J. L. R., Gholson, R. K. & Scott, T. A. Studies on the de novo biosynthesis of NAD in *Escherichia coli* I. Labelling patterns from precursors. *Biochim. Biophys. Acta - Gen. Subj.* **222**, 523–526 (1970).
115. Suzuki, N., Carlson, J., Griffith, G. & Gholson, R. K. Studies on the De novo biosynthesis of NAD in *Escherichia coli* V. properties of the quinolinic acid synthetase system. *Biochim. Biophys. Acta - Gen. Subj.* **304**, 309–315 (1973).
116. Wicks, F. D., Sakakibara, S., Gholson, R. K. & Scott, T. A. The mode of condensation of aspartic acid and dihydroxyacetone phosphate in quinolinate synthesis in *escherichia coli*. *Biochim. Biophys. Acta - Gen. Subj.* **500**, 213–216 (1977).
117. Nasu, S. & Gholson, R. K. Replacement of the B protein requirement of the *E. coli* quinolinate synthetase system by chemically-generated iminoaspartate. *Biochem. Biophys. Res. Commun.* **101**, 533–539 (1981).
118. Covès, J., Lebrun, C., Gervasi, G., Dalbon, P. & Fontecave, M. Overexpression of the FAD-binding domain of the sulphite reductase flavoprotein component from *Escherichia coli* and its inhibition by iodonium diphenyl chloride. *Biochem. J.* **342**, 465 LP-472 (1999).
119. Michele, M. *et al.* L-Aspartate Oxidase from *Escherichia coli*. I. Characterization of coenzyme binding and product inhibition. *Eur. J. Biochem.* **239**, 418–426 (1996).
120. Ralf, F. *et al.* Molecular biology of pyridine nucleotide biosynthesis in *Escherichia coli*. *Eur. J. Biochem.* **175**, 221–228 (2018).
121. Gardner, P. R. & Fridovich, I. Quinolinate synthetase: The oxygen-sensitive site of de novo NAD(P)<sup>+</sup> biosynthesis. *Arch. Biochem. Biophys.* **284**, 106–111 (1991).
122. Ceciliani, F. *et al.* Cloning, Overexpression, and Purification of *Escherichia coli* Quinolinate Synthetase. *Protein Expr. Purif.* **18**, 64–70 (2000).
123. Sakuraba, H., Tsuge, H., Yoneda, K., Katunuma, N. & Ohshima, T. Crystal Structure of the NAD Biosynthetic Enzyme Quinolinate Synthase. *J. Biol. Chem.* **280**, 26645–26648 (2005).
124. Saunders, A. H. *et al.* Characterization of Quinolinate Synthases from *Escherichia coli*,

- Mycobacterium tuberculosis, and Pyrococcus horikoshii Indicates That [4Fe-4S] Clusters Are Common Cofactors throughout This Class of Enzymes. *Biochemistry* **47**, 10999–11012 (2008).
125. M., N. M. U. *et al.* Characterization of Arabidopsis thaliana SufE2 and SufE3: Functions In Chloroplast Iron-Sulfur Cluster Assembly And NAD Synthesis. *J. Biol. Chem.* **282**, 18254–18264 (2007).
  126. Rousset, C. Etude structurale et fonctionnelle de la quinolinate synthase: une protéine fer-soufre cible d'agents antibactériens. (2009).
  127. Soriano, E. V *et al.* Active-site models for complexes of quinolinate synthase with substrates and intermediates. *Acta Crystallogr. Sect. D Biol. Crystallogr.* **69**, 1685–1696 (2013).
  128. Brown, O. R., Yein, F., Boehme, D., Foudin, L. & Cheng Shu Song. Oxygen poisoning of NAD biosynthesis: A proposed site of cellular oxygen toxicity. *Biochem. Biophys. Res. Commun.* **91**, 982–990 (1979).
  129. Brown, O. R. & Song, C.-S. Pyridine nucleotide coenzyme biosynthesis: A cellular site of oxygen toxicity. *Biochem. Biophys. Res. Commun.* **93**, 172–178 (1980).
  130. Flint, D. H. & Allen, R. M. Iron–Sulfur Proteins with Nonredox Functions. *Chem. Rev.* **96**, 2315–2334 (1996).
  131. Cherrier, M. V *et al.* The Crystal Structure of Fe<sub>4</sub>S<sub>4</sub> Quinolinate Synthase Unravels an Enzymatic Dehydration Mechanism That Uses Tyrosine and a Hydrolase-Type Triad. *J. Am. Chem. Soc.* **136**, 5253–5256 (2014).
  132. Weixue, W. & Eric, O. Bioorganometallic Chemistry with IspG and IspH: Structure, Function, and Inhibition of the [Fe<sub>4</sub>S<sub>4</sub>] Proteins Involved in Isoprenoid Biosynthesis. *Angew. Chemie Int. Ed.* **53**, 4294–4310 (2014).
  133. Zhang, Y. *et al.* Diphthamide biosynthesis requires an organic radical generated by an iron–sulphur enzyme. *Nature* **465**, 891 (2010).
  134. Robbins, A. H. & Stout, C. D. Structure of activated aconitase: formation of the [4Fe-4S] cluster in the crystal. *Proc. Natl. Acad. Sci.* **86**, 3639 LP-3643 (1989).
  135. Chen, J. & Tritz, G. J. Detection of precursors of quinolinic acid in Escherichia coli. *Microbios* **16**, 207–218 (1976).
  136. Begley, T. P., Kinsland, C., Mehl, R. A., Osterman, A. & Dorrestein, P. B. T.-V. & H. The biosynthesis of nicotinamide adenine dinucleotides in bacteria. in *Cofactor Biosynthesis* **61**, 103–119 (Academic Press, 2001).
  137. Reichmann, D., Couté, Y. & Ollagnier de Choudens, S. Dual Activity of Quinolinate Synthase: Triose Phosphate Isomerase and Dehydration Activities Play Together To Form Quinolinate. *Biochemistry* **54**, 6443–6446 (2015).
  138. Volbeda, A. *et al.* Crystal Structures of Quinolinate Synthase in Complex with a Substrate Analogue, the Condensation Intermediate, and Substrate-Derived Product. *J. Am. Chem. Soc.* **138**, 11802–11809 (2016).
  139. Volbeda, A. *et al.* Crystallographic Trapping of Reaction Intermediates in Quinolinic Acid Synthesis by NadA. *ACS Chem. Biol.* **13**, 1209–1217 (2018).
  140. Fenwick, M. K. & Ealick, S. E. Crystal Structures of the Iron–Sulfur Cluster-Dependent Quinolinate Synthase in Complex with Dihydroxyacetone Phosphate, Iminoaspartate Analogues, and Quinolinate. *Biochemistry* **55**, 4135–4139 (2016).
  141. Chan, A. *et al.* Studies of Inhibitor Binding to the [4Fe-4S] Cluster of Quinolinate

- Synthase. *Angew. Chemie Int. Ed.* **51**, 7711–7714 (2012).
142. Ciurli, S. *et al.* Subsite-differentiated analogs of native iron sulfide [4Fe-4S]<sub>2</sub><sup>+</sup> clusters: preparation of clusters with five- and six-coordinate subsites and modulation of redox potentials and charge distributions. *J. Am. Chem. Soc.* **112**, 2654–2664 (1990).
  143. Sengupta, S., Chattopadhyay, M. K. & Grossart, H.-P. The multifaceted roles of antibiotics and antibiotic resistance in nature. *Front. Microbiol.* **4**, 47 (2013).
  144. Abraham, E. P. & Chain, E. An Enzyme from Bacteria able to Destroy Penicillin. *Nature* **146**, 837 (1940).
  145. Wright, G. D. Q&A: Antibiotic resistance: where does it come from and what can we do about it? *BMC Biol.* **8**, 123 (2010).
  146. de Kraker, M. E. A., Stewardson, A. J. & Harbarth, S. Will 10 Million People Die a Year due to Antimicrobial Resistance by 2050? *PLOS Med.* **13**, e1002184 (2016).
  147. Willyard, C. The drug-resistant bacteria that pose the greatest health threats. *Nature* **543**, (2017).
  148. Brown, L., Wolf, J. M., Prados-Rosales, R. & Casadevall, A. Brown, L., Wolf, J. M., Prados-Rosales, R., & Casadevall, A. (2015). Through the wall: extracellular vesicles in Gram-positive bacteria, mycobacteria and fungi. *Nature Reviews. Microbiology*, 13(10), 620–630. <https://doi.org/10.1038/nrmicro3480>Through the . *Nat. Rev. Microbiol.* **13**, 620–630 (2015).
  149. Chatterjee, D. The mycobacterial cell wall: structure, biosynthesis and sites of drug action. *Curr. Opin. Chem. Biol.* **1**, 579–588 (1997).
  150. Brown, L., Wolf, J. M., Prados-Rosales, R. & Casadevall, A. Through the wall: extracellular vesicles in Gram-positive bacteria, mycobacteria and fungi. *Nat. Rev. Microbiol.* **13**, 620 (2015).
  151. Silver, L. L. Challenges of Antibacterial Discovery. *Clin. Microbiol. Rev.* **24**, 71–109 (2011).
  152. Singh, S. B. & Barrett, J. F. Empirical antibacterial drug discovery—Foundation in natural products. *Biochem. Pharmacol.* **71**, 1006–1015 (2006).
  153. Fischbach, M. A. & Walsh, C. T. Antibiotics for Emerging Pathogens. *Science (80-. )*. **325**, 1089–1093 (2009).
  154. Yang, J.-C., Lu, C.-W. & Lin, C.-J. Treatment of Helicobacter pylori infection: Current status and future concepts. *World J. Gastroenterol.* **20**, 5283–5293 (2014).
  155. Sachs, G., Scott, D. R. & Wen, Y. Gastric Infection by Helicobacter pylori. *Curr. Gastroenterol. Rep.* **13**, 540–546 (2011).
  156. Borody, T. J. *et al.* Recurrence of duodenal ulcer and Campylobacter pylori infection after eradication. *Med. J. Aust.* **151**, 431–435 (1989).
  157. Alsolaiman, M. M., Bakis, G., Nazeer, T., MacDermott, R. P. & Balint, J. A. Five years of complete remission of gastric diffuse large B cell lymphoma after eradication of Helicobacter pylori infection. *Gut* **52**, 507 LP-509 (2003).
  158. Forman, D. *et al.* Association between infection with Helicobacter pylori and risk of gastric cancer: evidence from a prospective investigation. *BMJ Br. Med. J.* **302**, 1302–1305 (1991).
  159. Hum., I. M. E. C. R. *Anonymous Live flukes and Helicobacter pylori. IARC Working Group on the Evaluation of Carcinogenic Risks to Humans.* (1994).
  160. Bazzoli, F. *et al.* Short-term low-dose triple therapy for the eradication of Helicobacter

- pylori. *Eur. J. Gastroenterol. Hepatol.* **6**, 773–778 (1994).
161. Mégraud, F. & Lamouliatte, H. Review article: the treatment of refractory *Helicobacter pylori* infection. *Aliment. Pharmacol. Ther.* **17**, 1333–1343 (2003).
  162. Cammarota, G. *et al.* Efficacy of two one-week rabeprazole/levofloxacin-based triple therapies for *Helicobacter pylori* infection. *Aliment. Pharmacol. Ther.* **14**, 1339–1343 (2001).
  163. Lu, H., Zhang, W. & Graham, D. Y. Bismuth-containing quadruple therapy for *Helicobacter pylori*: Lessons from China. *Eur. J. Gastroenterol. Hepatol.* **25**, 10.1097/MEG.0b013e3283633b57 (2013).
  164. Jenks, P. J. & Edwards, D. I. Metronidazole resistance in *Helicobacter pylori*. *Int. J. Antimicrob. Agents* **19**, 1–7 (2002).
  165. Alves, L. *et al.* *Mycobacterium leprae* infection of human Schwann cells depends on selective host kinases and pathogen-modulated endocytic pathways. *FEMS Microbiol. Lett.* **238**, 429–437 (2006).
  166. Balamayooran, G., Pena, M., Sharma, R. & Truman, R. W. The armadillo as an animal model and reservoir host for *Mycobacterium leprae*. *Clin. Dermatol.* **33**, 108–115 (2015).
  167. Gelber, R. . & Grosset, J. The chemotherapy of leprosy: an interpretive history. *Lepr Rev* 221–240 (2012).
  168. Smith, C. S. *et al.* Multidrug therapy for leprosy: a game changer on the path to elimination. *Lancet Infect. Dis.* **17**, e293–e297 (2017).
  169. Honore, N. & Cole, S. T. Molecular basis of rifampin resistance in *Mycobacterium leprae*. *Antimicrob. Agents Chemother.* **37**, 414–418 (1993).
  170. Cipolla, L., Polissi, A., Airoldi, C., Galliani, P. & Nicotra, P. S. and F. The Kdo Biosynthetic Pathway Toward OM Biogenesis as Target in Antibacterial Drug Design and Development. *Current Drug Discovery Technologies* **6**, 19–33 (2009).
  171. Fair, R. J. & Tor, Y. Antibiotics and Bacterial Resistance in the 21st Century. *Perspect. Medicin. Chem.* **6**, 25–64 (2014).
  172. Yang, N. J. & Hinner, M. J. Getting Across the Cell Membrane: An Overview for Small Molecules, Peptides, and Proteins. *Methods Mol. Biol.* 1266, 29–53 (2015).
  173. Park, J. *The Cell: A Molecular Approach*, Second Edition. *Yale J. Biol. Med.* **74**, 361 (2001).
  174. Letoha, T. *et al.* Membrane translocation of penetratin and its derivatives in different cell lines. *J. Mol. Recognit.* **16**, 272–279 (2003).
  175. Wadia, J. S., Stan, R. V & Dowdy, S. F. Transducible TAT-HA fusogenic peptide enhances escape of TAT-fusion proteins after lipid raft macropinocytosis. *Nat. Med.* **10**, 310 (2004).
  176. Mislin, G. L. A. & Schalk, I. J. Siderophore-dependent iron uptake systems as gates for antibiotic Trojan horse strategies against *Pseudomonas aeruginosa*. *Metallomics* **6**, 408–420 (2014).
  177. Möllmann, U., Heinisch, L., Bauernfeind, A., Köhler, T. & Ankel-Fuchs, D. Siderophores as drug delivery agents: application of the ‘Trojan Horse’ strategy. *BioMetals* **22**, 615–624 (2009).
  178. Chopra, I. Molecular mechanisms involved in the transport of antibiotics into bacteria. *Parasitology* **96** Suppl, S25–44 (1988).

179. Ahlbach, C. L. *et al.* Beyond cyclosporine A: conformation-dependent passive membrane permeabilities of cyclic peptide natural products. *Future Med. Chem.* **7**, 2121–2130 (2015).
180. Mori, H. *et al.* FR235222, a fungal metabolite, is a novel immunosuppressant that inhibits mammalian histone deacetylase (HDAC). I. Taxonomy, fermentation, isolation and biological activities. *J. Antibiot. (Tokyo)*. **56**, 72–79 (2003).
181. Weerasinghe, S. V. W., Estiu, G., Wiest, O. & Pflum, M. K. H. Residues in the 11 Å Channel of Histone Deacetylase 1 Promote Catalytic Activity: Implications for Designing Isoform-Selective Histone Deacetylase Inhibitors. *J. Med. Chem.* **51**, 5542–5551 (2008).
182. Weerasinghe, S. V. W., Estiu, G., Wiest, O. & Pflum, M. K. H. Residues in the 11 Å Channel of Histone Deacetylase 1 Promote Catalytic Activity: Implications for Designing Isoform-Selective Histone Deacetylase Inhibitors. *J. Med. Chem.* **51**, 5542–5551 (2008).
183. Francisco Hilário, F. *et al.* Synthesis of an Uncharged Tetra-cyclopeptide Acting as a Transmembrane Carrier: Enhanced Cellular and Nuclear Uptake. *Org. Lett.* **19**, 612–615 (2017).
184. Ferreira, S. Z. *et al.* Synthesis of a New Peptide–Coumarin Conjugate: A Potential Agent against Cryptococcosis. *ACS Med. Chem. Lett.* **6**, 271–275 (2015).
185. Sivakumar, K. *et al.* A Fluorogenic 1,3-Dipolar Cycloaddition Reaction of 3-Azidocoumarins and Acetylenes. *Org. Lett.* **6**, 4603–4606 (2004).
186. Guo, H. *et al.* Pseudoxyllallemycins A–F, Cyclic Tetrapeptides with Rare Allenyl Modifications Isolated from *Pseudoxyllaria* sp. X802: A Competitor of Fungus-Growing Termite Cultivars. *Org. Lett.* **18**, 3338–3341 (2016).
187. Obafemi, C. A. & Pfeleiderer, W. Permanganate Oxidation of Quinoxaline and Its Derivatives. *Helv. Chim. Acta* **77**, 1549–1556 (1994).
188. Laurent, B. *et al.* A Total Synthesis of Subarine, a Marine Alkaloid Related to the Pyridoacridine Family. *European J. Org. Chem.* 1891–1893 (2004).
189. Moshe Gavish, Jehuda Arie Veenman, Alex Shterenberg, I. M. Derivatives, pharmaceutical compositions and methods of use thereof. (2006).
190. Luigi Piero Stasi, L., Claudio Rovati, R. & Artusi, Fabrizio Colace, Stefano Mandelli, L. P. Chemical compounds. (2014).
191. Hosangadi, B. D. & Dave, R. H. An efficient general method for esterification of aromatic carboxylic acids. *Tetrahedron Lett.* **37**, 6375–6378 (1996).
192. Klingsberg, E. The Chemistry of Heterocyclic Compounds-Pyridine and Its Derivatives. (2009).
193. Londregan, A. T., Jennings, S. & Wei, L. Mild Addition of Nucleophiles to Pyridine-N-Oxides. *Org. Lett.* **13**, 1840–1843 (2011).
194. Varma, R. S. & Naicker, K. P. The Urea–Hydrogen Peroxide Complex: Solid-State Oxidative Protocols for Hydroxylated Aldehydes and Ketones (Dakin Reaction), Nitriles, Sulfides, and Nitrogen Heterocycles. *Org. Lett.* **1**, 189–192 (1999).
195. McKillop, A. & Kemp, D. Further functional group oxidations using sodium perborate. *Tetrahedron* **45**, 3299–3306 (1989).
196. Jain, S. L., Joseph, J. K. & Sain, B. Rhenium-Catalyzed Highly Efficient Oxidations of Tertiary Nitrogen -Compounds to N-Oxides Using Sodium Percarbonate as Oxygen Source. *Synlett*, 2661–2663 (2006).
197. Ueki, M., Honda, M., Kazama, Y. & Katoh, T. A New Method for the Preparation of 3-

- Nitro-2-pyridinesulfonyl Chloride and One-Pot Syntheses of N( $\alpha$ )-tert-butoxycarbonyl-S-3-nitro-2-pyridinesulfonyl Derivatives of Cysteine and D-Penicillamine. *Synthesis (Stuttg)*. 21–22 (1994).
198. Wu, S. C. *et al.* Discovery of 3-hydroxy-4-cyano-isoquinolines as novel, potent, and selective inhibitors of human 11 $\beta$ -hydroxydehydrogenase 1 (11 $\beta$ -HSD1). *Bioorg. Med. Chem. Lett.* **21**, 6693–6698 (2011).
  199. Ha, T.-H. *et al.* TRPV1 antagonist with high analgesic efficacy: 2-Thio pyridine C-region analogues of 2-(3-fluoro-4-methylsulfonylaminophenyl)propanamides. *Bioorg. Med. Chem.* **21**, 6657–6664 (2013).
  200. Avery, M. A. Protective Groups in Organic Synthesis. Third Edition By Theodora W. Greene and Peter G. M. Wuts. John Wiley & Sons, New York. 1999. xxi + 779 pp. 16 × 24 cm. ISBN 0-471-16019-9. \$84.95. *J. Med. Chem.* **42**, 5285 (1999).
  201. Ong, C. J. Herbicidal emulsifiable concentrate compositions of imidazolinone herbicides. (1993).
  202. Heathcock, C. H. & Ratcliffe, R. Stereoselective total synthesis of the guaiazulenic sesquiterpenoids  $\alpha$ -bulnesene and bulnesol. *J. Am. Chem. Soc.* **93**, 1746–1757 (1971).
  203. Kolpin, A. *et al.* Quantitative Differences in Sulfur Poisoning Phenomena over Ruthenium and Palladium: An Attempt To Deconvolute Geometric and Electronic Poisoning Effects Using Model Catalysts. *ACS Catal.* **7**, 592–605 (2017).
  204. Gui, B. *et al.* Tackling poison and leach: catalysis by dangling thiol–palladium functions within a porous metal–organic solid. *Chem. Commun.* **51**, 6917–6920 (2015).
  205. Holler, T. P., Ruan, F., Spaltenstein, A. & Hopkins, P. B. Total synthesis of marine mercaptohistidines: ovolthiols A, B, and C. *J. Org. Chem.* **54**, 4570–4575 (1989).
  206. John Wiley & Sons. The Chemistry of Heterocyclic Compounds - The Pyrazines. (2009).
  207. Taylor, A. W. & Dean, D. K. A new synthesis of thioflavones. *Tetrahedron Lett.* **29**, 1845–1848 (1988).
  208. Xu, H.-J., Zhao, X.-Y., Deng, J., Fu, Y. & Feng, Y.-S. Efficient C–S cross coupling catalyzed by Cu<sub>2</sub>O. *Tetrahedron Lett.* **50**, 434–437 (2009).
  209. Parchment, O. G., Burton, N. A., Hillier, I. H. & Vincent, M. A. Predictions of tautomeric equilibria in 2-hydroxypyridine and pyridine-2-thiol: correlation effects and possible discrepancies with experiment. *J. Chem. Soc. Perkin Trans. 2* 861–863 (1993). doi:10.1039/P29930000861
  210. Maltese, M. Reductive Demercuration in Deprotection of Trityl Thioethers, Trityl Amines, and Trityl Ethers. *J. Org. Chem.* **66**, 7615–7625 (2001).
  211. Janssen, F. J. *et al.* Comprehensive Analysis of Structure–Activity Relationships of  $\alpha$ -Ketoheterocycles as sn-1-Diacylglycerol Lipase  $\alpha$  Inhibitors. *J. Med. Chem.* **58**, 9742–9753 (2015).
  212. Krinsky, J. L., Arnold, J. & Bergman, R. G. Platinum Group Thiophenoxyimine Complexes: Syntheses and Crystallographic/Computational Studies. *Organometallics* **26**, 897–909 (2007).
  213. Lundt, B. F., Johansen, N. L., Vølund, A. & Markussen, J. Removal of t-butyl and t-butoxycarbonyl protecting groups with trifluoroacetic acid. *Int. J. Pept. Protein Res.* **12**, 258–268 (2018).
  214. Esakova, O. A. *et al.* Structure of Quinolinate Synthase from *Pyrococcus horikoshii* in

- the Presence of Its Product, Quinolinic Acid. *J. Am. Chem. Soc.* **138**, 7224–7227 (2016).
215. Krebs, C., Broderick, W. E., Henshaw, T. F., Broderick, J. B. & Huynh, B. H. Coordination of Adenosylmethionine to a Unique Iron Site of the [4Fe-4S] of Pyruvate Formate-Lyase Activating Enzyme: A Mössbauer Spectroscopic Study. *J. Am. Chem. Soc.* **124**, 912–913 (2002).
216. Lanz, N. D. & Booker, S. J. Auxiliary iron–sulfur cofactors in radical SAM enzymes. *Biochim. Biophys. Acta - Mol. Cell Res.* 1853, 1316–1334 (2015).
217. Curtis, M. D. & Druker, S. H. Homolytic C–S Bond Scission in the Desulfurization of Aromatic and Aliphatic Thiols Mediated by a Mo/Co/S Cluster: Mechanistic Aspects Relevant to HDS Catalysis. *J. Am. Chem. Soc.* **119**, 1027–1036 (1997).
218. Perez, C., Daniel, K. B. & Cohen, S. M. Evaluating Prodrug Strategies for Esterase-Triggered Release of Alcohols. *ChemMedChem* **8**, 1662–1667 (2013).
219. Müller, C. E., Daniel, P. T., Holzschuh, J. & Roth, H. J. Lipophilic disulfide prodrugs — syntheses and disulfide bond cleavage. *Int. J. Pharm.* **57**, 41–47 (1989).
220. Caldarelli, S. A. *et al.* Disulfide Prodrugs of Albitiazolium (T3/SAR97276): Synthesis and Biological Activities. *J. Med. Chem.* **55**, 4619–4628 (2012).
221. Vrudhula, V. M., MacMaster, J. F., Li, Z., Kerr, D. E. & Senter, P. D. Reductively activated disulfide prodrugs of paclitaxel. *Bioorg. Med. Chem. Lett.* **12**, 3591–3594 (2002).
222. Edwards, P. R. & Ewing, W. H. Identification of enterobacteriaceae. *Identif. Enterobact.* (1962).
223. Partridge, J. D., Scott, C., Tang, Y., Poole, R. K. & Green, J. Escherichia coli Transcriptome Dynamics during the Transition from Anaerobic to Aerobic Conditions. *J. Biol. Chem.* 281, 27806–27815 (2006).
224. Traoré, M. *et al.* Flexible Synthesis and Evaluation of Diverse Anti-Apicomplexa Cyclic Peptides. *J. Org. Chem.* **78**, 3655–3675 (2013).
225. Jornada, D. H. *et al.* The prodrug approach: a successful tool for improving drug solubility. *Molecules* **21**, 42 (2015).
226. Lassen, K. M. & Joullié, M. M. Total Synthesis of Lys3 Tamandarin M: A Potential Affinity Ligand. *Org. Lett.* **12**, 5306–5309 (2010).
227. Yang, F., Wang, W., Li, K., Zhao, W. & Dong, X. Efficient one-pot construction of unsymmetrical disulfide bonds with TCCA. *Tetrahedron Lett.* **58**, 218–222 (2017).
228. Dong, M., Wang, Y.-W. & Peng, Y. Highly Selective Ratiometric Fluorescent Sensing for Hg<sup>2+</sup> and Au<sup>3+</sup>, Respectively, in Aqueous Media. *Org. Lett.* **12**, 5310–5313 (2010).
229. Calatrava-Pérez, E. *et al.* Glycosidase activated release of fluorescent 1,8-naphthalimide probes for tumor cell imaging from glycosylated ‘pro-probes’. *Chem. Commun.* **52**, 13086–13089 (2016).
230. Nishino, N. *et al.* Chlamydocin–hydroxamic acid analogues as histone deacetylase inhibitors. *Bioorg. Med. Chem.* **12**, 5777–5784 (2004).
231. Yang, R., Bi, X., Li, F., Cao, Y. & Liu, C.-F. Native chemical ubiquitination using a genetically incorporated azidonorleucine. *Chem. Commun.* **50**, 7971–7974 (2014).
232. Kamkaew, A. & Burgess, K. Double-Targeting Using a TrkC Ligand Conjugated to Dipyrrrometheneboron Difluoride (BODIPY) Based Photodynamic Therapy (PDT) Agent. *J. Med. Chem.* **56**, 7608–7614 (2013).
233. Dupuis, S. N. *et al.* Synthetic diversification of natural products: Semi-synthesis and evaluation of triazole jadomycins. *Chem. Sci.* **3**, 1640–1644 (2012).

234. Tabor, S. & Richardson, C. C. A bacteriophage T7 RNA polymerase/promoter system for controlled exclusive expression of specific genes. *Proc. Natl. Acad. Sci.* **82**, 1074 (1985).
235. Engelking, L. R. Tricarboxylic Acid (TCA) Cycle BT - Textbook of Veterinary Physiological Chemistry (Third Edition). in 208–213 (Academic Press, 2015). doi:https://doi.org/10.1016/B978-0-12-391909-0.50034-7
236. Bradford, M. M. A rapid and sensitive method for the quantitation of microgram quantities of protein utilizing the principle of protein-dye binding. *Anal. Biochem.* **72**, 248–254 (1976).
237. fish, W. W. [27] Rapid colorimetric micromethod for the quantitation of complexed iron in biological samples. in *Methods in Enzymology* **158**, 357–364 (Academic Press, 1988).
238. Beinert, H. Semi-micro methods for analysis of labile sulfide and of labile sulfide plus sulfane sulfur in unusually stable iron-sulfur proteins. *Anal. Biochem.* **131**, 373–378 (1983).
239. Ollagnier de Choudens, S. & Barras, F. *Methods in enzymology. Fe-S Cluster Enzymes Part A - Genetic, Biochemical, and Biophysical Methods for Studying Fe-S Proteins and Their Assembly.* (2017).
240. Bulheller, B. M., Rodger, A. & Hirst, J. D. Circular and linear dichroism of proteins. *Phys. Chem. Chem. Phys.* **9**, 2020–2035 (2007).
241. Vernède, X. & Fontecilla-Camps, J. C. A method to stabilize reduced and/or gas-treated protein crystals by flash-cooling under a controlled atmosphere. **32**, 505–509 (1999).
242. Gabadinho, J. *et al.* MxCuBE: a synchrotron beamline control environment customized for macromolecular crystallography experiments. *J. Synchrotron Radiat.* **17**, 700–707 (2010).
243. Kabsch, W. XDS. *Acta Crystallogr. Sect. D Biol. Crystallogr.* **66**, 125–132 (2010).
244. Evans, P. R. & Murshudov, G. N. How good are my data and what is the resolution? *Acta Crystallogr. Sect. D* **69**, 1204–1214 (2013).
245. Winn, M. D. *et al.* Overview of the CCP4 suite and current developments. *Acta Crystallogr. Sect. D* **67**, 235–242 (2011).
246. McCoy, A. J. *et al.* Phaser crystallographic software. *J. Appl. Crystallogr.* **40**, 658–674 (2007).
247. Emsley, P., Lohkamp, B., Scott, W. G. & Cowtan, K. Features and development of Coot. *Acta Crystallogr. Sect. D* **66**, 486–501 (2010).
248. Murshudov, G. N. *et al.* REFMAC5 for the refinement of macromolecular crystal structures. *Acta Crystallogr. Sect. D* **67**, 355–367 (2011).
249. Morin, A. *et al.* Collaboration gets the most out of software. *Elife* **2**, e01456 (2013).
250. Jackson, R. F. W. & Perez-Gonzalez, M. Synthesis of N-(tert-Butoxycarbonyl)- $\beta$ -Iodoalanine Methyl Ester: A Useful Building Block in the Synthesis of Nonnatural  $\alpha$ -Amino Acids via Palladium Catalyzed Cross Coupling Reactions: (l-Alanine, N-[(1, 1-dimethylethoxy) carbonyl]-3-iodo-, methyl ester). *Org. Synth.* **81**, 77–88 (2003).
251. Jordan, P. A., Tang, Y., Bradbury, A. J., Thomson, A. J. & Guest, J. R. Biochemical and spectroscopic characterization of *Escherichia coli* aconitases (AcnA and AcnB). *Biochem. J.* **344**, 739 LP-746 (1999).
252. Williams, C. H. *et al.* *E. coli* aconitase B structure reveals a HEAT-like domain with implications for protein–protein recognition. *Nat. Struct. Biol.* **9**, 447 (2002).

253. Kent, T. A. *et al.* Mössbauer studies of aconitase. Substrate and inhibitor binding, reaction intermediates, and hyperfine interactions of reduced 3Fe and 4Fe clusters. *J. Biol. Chem.* **260**, 6871–6881 (1985).
254. Surerus, K. K., Kennedy, M. C., Beinert, H. & Münck, E. Mössbauer study of the inactive Fe<sub>3</sub>S<sub>4</sub> and Fe<sub>3</sub>Se<sub>4</sub> and the active Fe<sub>4</sub>Se<sub>4</sub> forms of beef heart aconitase. *Proc. Natl. Acad. Sci.* **86**, 9846 LP-9850 (1989).
255. Werst, M. M., Kennedy, M. C., Houseman, A. L., Beinert, H. & Hoffman, B. M. Characterization of the [4Fe-4S]<sup>+</sup> cluster at the active site of aconitase by <sup>57</sup>Fe, <sup>33</sup>S, and <sup>14</sup>N electron nuclear double resonance spectroscopy. *Biochemistry* **29**, 10533–10540 (1990).
256. Rose, I. A. & O'Connell, E. L. Mechanism of Aconitase Action: I. The Hydrogen Transfer Reaction. *J. Biol. Chem.* **242**, 1870–1879 (1967).
257. F, T. Takusagawa's note. Chapter 16 'the cytric acid cycle'. (2012).

# PUBLICATIONS



# Crystallographic Trapping of Reaction Intermediates in Quinolinic Acid Synthesis by NadA

Anne Volbeda,<sup>†</sup> Jaione Saez Cabodevilla,<sup>‡,§</sup> Claudine Darnault,<sup>†</sup> Océane Gigarel,<sup>†</sup> Thi-Hong-Lien Han,<sup>‡</sup> Oriane Renoux,<sup>†</sup> Olivier Hamelin,<sup>γ</sup> Sandrine Ollagnier-de-Choudens,<sup>‡</sup> Patricia Amara,<sup>†</sup> and Juan C. Fontecilla-Camps<sup>\*,†,⊕</sup>

<sup>†</sup>Univ. Grenoble Alpes, CEA, CNRS, IBS, Metalloproteins Unit, F-38000 Grenoble, France

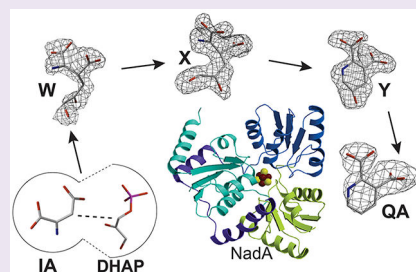
<sup>‡</sup>Univ. Grenoble Alpes, CNRS, CEA, Laboratoire de Chimie et Biologie des Métaux, BioCat, 38000, Grenoble, France

<sup>§</sup>Univ. Grenoble Alpes, CNRS, ICMG FR 2607, Département de Pharmacochimie Moléculaire, F-38041, Grenoble, France

<sup>γ</sup>Univ. Grenoble Alpes, CNRS, CEA, Laboratoire de Chimie et Biologie des Métaux, BioCE, 38000, Grenoble, France

## Supporting Information

**ABSTRACT:** NadA is a multifunctional enzyme that condenses dihydroxyacetone phosphate (DHAP) with iminoaspartate (IA) to generate quinolinic acid (QA), the universal precursor of the nicotinamide adenine dinucleotide (NAD(P)) cofactor. Using X-ray crystallography, we have (i) characterized two of the reaction intermediates of QA synthesis using a “pH-shift” approach and a slowly reacting *Thermotoga maritima* NadA variant and (ii) observed the QA product, resulting from the degradation of an intermediate analogue, bound close to the entrance of a long tunnel leading to the solvent medium. We have also used molecular docking to propose a condensation mechanism between DHAP and IA based on two previously published *Pyrococcus horikoshii* NadA structures. The combination of reported data and our new results provide a structure-based complete catalytic sequence of QA synthesis by NadA.



The synthesis of the essential nicotinamide adenine dinucleotide (NAD(P)) cofactor by all organisms uses quinolinic acid (QA) as its main precursor.<sup>1</sup> The QA-derived nicotinamide fragment of NAD(P) is the site of hydride transfer of the cofactor, a fundamental process in many central redox pathways such as the Krebs and Calvin cycles and glycolysis.<sup>2</sup> The first step in the de novo II pathway, used by most prokaryotes to synthesize QA, is the production of iminoaspartate (IA) from L-Asp.<sup>3</sup> In *Escherichia coli* (*Ec*), IA is produced by the L-Asp oxidase NadB, whereas in *Thermotoga maritima* (*Tm*), this substrate is made by an aspartate dehydrogenase called either NadB-II or NadX.<sup>4</sup> IA can also be produced by combining oxaloacetate with ammonium ions, to be used by NadA in in vitro experiments.<sup>5</sup> Although IA is synthesized differently in *E. coli* and *T. maritima*, in both microorganisms the remaining reactions leading to QA synthesis are catalyzed by the same enzyme, the quinolinate synthase NadA.<sup>4,6,7</sup> The enzyme has three homologous domains and appears to be extensively multifunctional (Scheme 1).<sup>8,9</sup> Indeed, QA synthesis involves (i) the generation of the nucleophilic C3 atom of IA;<sup>3,10</sup> (ii) the attack of this nucleophile to dihydroxyacetone phosphate (DHAP)—a triose phosphate sugar produced by the glycolytic pathway—resulting in the condensed intermediate W; (iii) the keto-aldo isomerization of W to form X; (iv) a first dehydration reaction upon formation of a Schiff base and cyclization of the intermediate X to generate Y; and (v) a second dehydration, reminiscent of the reaction catalyzed by aconitase,<sup>11</sup> to yield QA. Like aconitase,

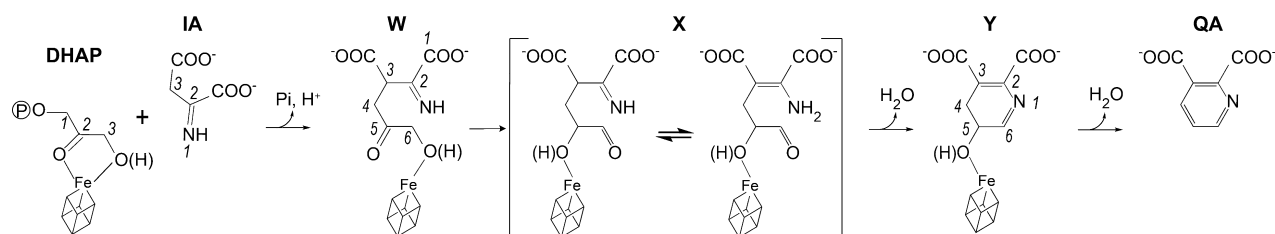
NadA uses three cysteine ligands to bind a [4Fe-4S] cluster, leaving an iron ion with a coordination site available for Lewis-type chemistry.<sup>12</sup> As shown by Mössbauer spectroscopy, this unique iron ion can interact with the thiolate groups of the QA analogue and NadA inhibitor 4,5-dithiohydroxyphthalic acid.<sup>13</sup>

In 2014, we reported the first crystal structure of a [4Fe-4S] cluster-containing NadA enzyme, the one from *T. maritima*.<sup>12</sup> We showed then that the unique iron from the [4Fe-4S] cluster is found at the end of a long tunnel that connects this metal ion with the molecular surface.<sup>12</sup> More recently, the structural aspects of QA synthesis has been the subject of intense scrutiny. Thus, crystal structures have been communicated by Fenwick and Ealick for the wild type (wt) *Pyrococcus horikoshii* (*Ph*)NadA complexes with three similar IA analogues and DHAP<sup>14</sup> and by us for the *Tm*NadA-K219R/Y107F-W intermediate and the *Tm*NadA-K219R/Y107F phosphoglycolohydroxamate (PGH) complex;<sup>15</sup> PGH is a DHAP-like molecule and a triose phosphate isomerase (TIM) inhibitor. In addition, three very similar structures of cluster-bound QA in NadA complexes have also been recently determined, one of them by us.<sup>14–16</sup> We will abbreviate “*Tm*NadA-K219R” to “*Tm*NadA\*” because it is functionally equivalent to the wt enzyme.

Received: December 25, 2017

Accepted: April 11, 2018

Published: April 11, 2018

Scheme 1. Mechanism of QA Synthesis by NadA<sup>a</sup>

<sup>a</sup>This mechanism is based on the X and Y complexes (this study) and previous propositions (see text). Atoms are numbered according to IUPAC rules. W: 2-imino, 3-carboxy, 5-oxo, 6-hydroxy hexanoic acid, X: 2-(2-hydroxy-3-oxopropyl)-3-iminosuccinic acid or 2-amino-3-(2-hydroxy-3-oxopropyl)maleic acid, Y: 5-hydroxy-4,5-dihydropyridine-2,3-dicarboxylic acid (these names correspond to the protonated states).

Table 1. X-ray Data and Refinement Statistics

crystal	1	2	3	4
	<i>TmNadA</i> *-Y21F XY-complex	<i>TmNadA</i> * SMPDC-derived QA-complex	<i>TmNadA</i> *-Y21F phthalate-complex	<i>TmNadA</i> *-Y21F PGH-complex
	Data Collection			
ESRF beamline	ID30A3	ID30A3	ID23-1	ID30B
wavelength (Å)	0.96770	0.96770	0.97242	1.00000
space group	P2 <sub>1</sub>	P2 <sub>1</sub>	P1	C2
cell: <i>a</i> (Å)	55.50	55.44	49.14	102.97
<i>b</i> (Å)	48.95	49.31	52.16	49.17
<i>c</i> (Å)	61.25	61.90	58.95	69.39
$\alpha$ (deg)	90	90	103.82	90
$\beta$ (deg)	107.27	107.21	90.63	107.79
$\gamma$ (deg)	90	90	90.37	90
resolution (Å)	37.5–1.50	47.0–2.30	49.1–2.00	44.0–2.00
(high-resolution shell)	(1.55–1.50)	(2.38–2.30)	(2.07–2.00)	(2.07–2.00)
measured reflections	217368 (21491)	77646 (8006)	82582 (8437)	72297 (6484)
unique reflections	49728 (4844)	14259 (1412)	34665 (3465)	22406 (2193)
redundancy	4.4 (4.4)	5.4 (5.7)	2.4 (2.4)	3.2 (3.0)
completeness (%)	98.8 (99.3)	99.1 (99.7)	90.2 (91.9)	99.3 (99.1)
Rmerge (%)	4.0 (78.3)	12.0 (157.4)	5.0 (24.1)	8.0 (79.6)
CC1/2	0.998 (0.719)	0.996 (0.375)	0.996 (0.898)	0.996 (0.469)
$\langle I/\sigma I \rangle$	16.8 (1.7)	8.9 (1.0)	12.1 (3.2)	10.2 (1.4)
	Refinement			
resolution (Å)	37.5–1.50	47.0–2.30	43.4–2.00	39.2–2.00
used reflections	47225	13514	32832	21244
$R_{\text{work}}$ (%)	13.7	20.2	19.0	19.2
reflections for $R_{\text{free}}$	2499	720	1831	1156
$R_{\text{free}}$ (%)	17.9	22.1	23.4	24.1
number of atoms	2813	2468	5934	2662
average B-factor (Å <sup>2</sup> )	27.2	55.1	31.3	37.0
rms deviations				
bond lengths (Å)	0.011	0.011	0.011	0.011
bond angles (deg)	1.5	1.4	1.4	1.5

Here we report the crystal structures of complexes of the *TmNadA*\*Y21F variant with (i) the substrate-derived products X and Y (Scheme 1) at 1.5 Å resolution, (ii) PGH at 2.0 Å resolution, (iii) the QA analogue phthalate at 2.0 Å resolution, and (iv) of *TmNadA*\* with a differently bound QA derived from 5-mercaptopyridine-2,3-dicarboxylic acid (SMPDC) at 2.3 Å resolution (Table 1). We also discuss the structure of *TmNadA*\* with citrate bound in two conformations, which combined with a series of docking experiments may explain an unexpected result concerning our previously published W complex.<sup>15</sup> In addition, and based on the *PhNadA*-citrate complex,<sup>14</sup> we have carried out another series of docking experiments that generate a plausible model for *NadA*-bound IA and DHAP substrates correctly poised to initiate the

condensation reaction that generates W. Taken together, our results provide a structure-based sequence for all the catalytic steps of QA synthesis by *NadA*.

## RESULTS AND DISCUSSION

**Trapping Experiments and the Orientation of the W Intermediate.** We already showed in our previous crystallographic analysis<sup>15</sup> that a 20 mg mL<sup>-1</sup> solution of the slowly reacting *TmNadA*\*Y21F variant can, after several days, produce QA from DHAP and IA, the latter being obtained from oxaloacetate and ammonium ions.<sup>5</sup> Here an equivalent solution was incubated 36 h in the glovebox at pH 7.5, a value that is close to optimal for *NadA* activity.<sup>17</sup> Next, the protein solution was mixed with our standard crystallization solution to a final

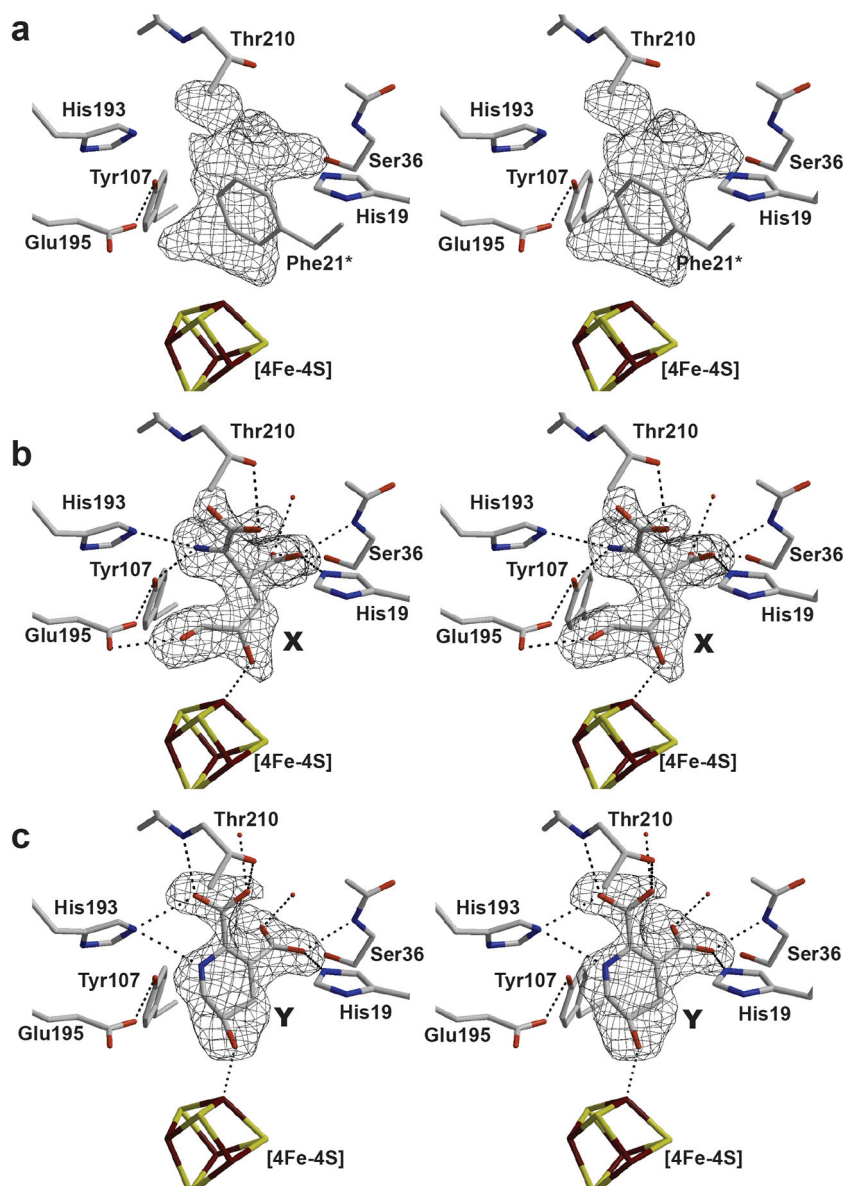


**Figure 1.** X and Y reaction intermediates. (a) Stereo image of the electron density ( $F_{\text{obs}} - F_{\text{calc}}$ ) omit map calculated with diffraction data at 1.5 Å resolution from a crystal grown from a *TmNadA*\*Y21F protein solution first incubated with DHAP, oxaloacetate and ammonium sulfate for 36 h at pH 7.5 and then set at pH 7.1 during the crystallization experiment (the “pH-shift” trapping experiment; see text). This electron density has been modeled as a combination of the X and Y intermediates (40% each) and solvent (20%). The mutation of Tyr21 is indicated by a \*. (b) Stereo image of the X intermediate in a partial electron density ( $F_{\text{obs}} - F_{\text{calc}}$ ) omit map calculated after adding a 40% occupied Y intermediate and four 20% occupied water molecules to the calculated phases and structure factors. c. Stereo pair of the Y intermediate in an equivalent ( $F_{\text{obs}} - F_{\text{calc}}$ ) omit map obtained after adding instead 40% X and 20% occupied water to the model phases and structure factors. The modeled X, Y and water molecules (not shown) fully explain the original map in a. All omit maps were contoured at  $3.5\sigma$ .

pH of 7.1 where wt *NadA* displays very little activity<sup>17</sup> (and its *TmNadA*\*Y21F variant should be even less efficient). An omit ( $F_{\text{obs}} - F_{\text{calc}}$ ) electron density map calculated using X-ray data from a crystal grown under these “pH-shifted” intermediate trapping conditions<sup>17</sup> and refined model phases displayed a significant electron density peak at the active site (Figure 1a). Examination of the shape and size of this peak suggested that it corresponds to a mixture of different species. Indeed, by adjusting their relative occupancies, it was possible to build the X and Y intermediates (Scheme 1) into partial omit electron density maps with a remarkably good match (Figure 1b,c and Methods).

Our comparison of the previously obtained *TmNadA*\*Y107F-W intermediate<sup>15</sup> with X (Figure 1b) indicates that the former binds in an approximately 180°-rotated position relative to the latter (Supplementary Figure 1). This likely explains why catalysis stops at W in the *TmNadA*\*Y107F variant. However, in both cases, IA and DHAP must be productively positioned for the condensation reaction to occur because, as indicated by the comparison of the shape and chirality of the imino forms of W and X (Supplementary Figure 1), the rotated stereochemically correct W intermediate is also obtained with *TmNadA*\*Y107F. Alternative positions for the W condensation reaction product would be consistent with our observation of citrate bound to *TmNadA*\* in two conforma-

tions related by an approximate  $140^\circ$  rotation axis (Supplementary Figure 2).<sup>15</sup> We also note that in wt *PhNadA*, DHAP binds in an orientation that is consistent with X<sup>14</sup> and, consequently, rotated relative to our previously reported W.<sup>15</sup> Although we have not been able to crystallize DHAP complexes with *TmNadA*\*Y107F and *TmNadA*\*Y21F to verify the different relative orientations of the substrate molecule, we observe this rotation effect in the crystal structures of the two variants in complex with PGH (Supplementary Figure 3).

Taken together, these observations indicate that the *NadA* active site can lodge the same molecule in different orientations and that in the Y107F variant W binds in an unproductive configuration. In order to try and elucidate the origin of the Y107F phenotype, we have used PGH and DHAP to perform a series of docking experiments and structural analyses in the closed form of *NadA* (see Methods for details). The results may be interpreted as follows: (i) in the wt *PhNadA* and *TmNadA*\*Y21F variant the  $-OH$  group of Tyr107 (Tyr109 in *PhNadA*) forms an H-bond with the “proximal” carbonyl O atom from the carboxylate group of Glu195 (Glu198 in *PhNadA*). The other, “distal” O atom, is protonated and in the *PhNadA*-DHAP structure it interacts with the terminal iron-bound O of the substrate (Supplementary Figure 4a).<sup>14</sup> Because in the *TmNadA*\*Y107F variant this  $-OH$  group is missing, docking results indicate that in this case it is the proximal O that should be protonated (Supplementary Figure 4b and Methods). We conclude that in the Y107F variant, the loss of the partial positive charge from the  $-OH$  group switches the binding affinity of the carboxylate group of Glu195 from the terminal O (Supplementary Figures 3a and 4a) to the carbonyl O of the substrate (Supplementary Figure 4b). In addition, in the *TmNadA*\*Y107F-PGH structure (Supplementary Figure 3b), the rotated iron-bound terminal O also interacts with Asn109, which requires the conformational change of Phe58 also observed in the closed *TmNadA*\*Y107F-W (Supplementary Figure 1), *TmNadA*\*-citrate (Supplementary Figure 2) and *PhNadA*-citrate and -maleate structures (PDB codes SKTS and SKTR, respectively).<sup>14</sup> Based on the rotated W structure, we mistakenly postulated that Tyr21 was involved in the last dehydration reaction.<sup>15</sup> In the productive W model, Tyr21 still has acid/base properties except that its postulated role is in the first dehydration reaction with the deprotonation of the Schiff base and the protonation of the O atom that will become the leaving water molecule upon cyclization (Supplementary Scheme 1).

The unproductive binding of the condensation product in the *TmNadA*\*Y107F-W structure induces a partially closed form of *NadA*. In this structure, the  $-OH$  group of Ser36 forms an H-bond with the N atom of W. This H-bond may help keeping *TmNadA*\*-Y107F in its partially closed form because Ser36 is located at the N-terminal end of a helix that significantly shifts positions between open and closed structures.<sup>12,15</sup> Conversely, the active *TmNadA*\*Y21F-X/Y structure is in its open form like in ligand-free *TmNadA*\*.<sup>12</sup> In this structure, the main chain N of Ser36 interacts with one of the carboxylate groups in both ligands. Because the only difference between W and X is the keto-aldo isomerization (Scheme 1) it seems reasonable to conclude that the partially closed form in the *TmNadA*\*Y107F-W complex is also the consequence of the mutation. To test this hypothesis, we have also docked W in open *TmNadA*\* and found that, indeed, it preferentially adopts a conformation similar to the one observed for X (Supplementary Figure 5).

**New QA Binding Mode in *NadA*.** Another surprising result was obtained when, as part of our ongoing efforts to characterize intermediate analogue binding to *NadA*, we solved the structure of *TmNadA*\* cocrystallized with SMPDC. Indeed, in this structure we could clearly see QA bound in a position completely different from the one previously observed.<sup>14–16</sup> In addition, the amide fragment of Asn109 was missing and the [4Fe-4S] cluster appeared to be partially disrupted (Figure 2a).

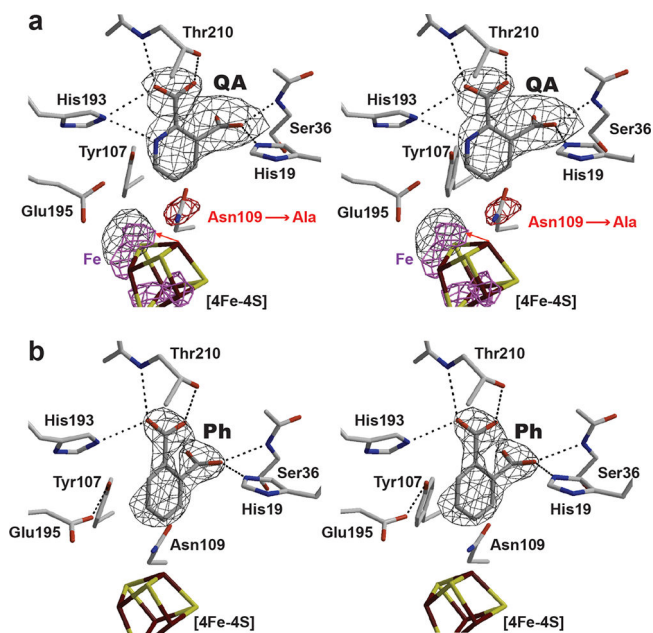


**Figure 2.** (a) *NadA*-QA structure from SMPDC. Electron density ( $F_{\text{obs}} - F_{\text{calc}}$ ) omit map in the crystal structure of the *TmNadA*\*-SMPDC-derived QA complex. The positive black mesh at the top of the figure has been modeled as QA, whereas the one at the bottom, and based on a coinciding peak in the anomalous scattering difference map (shown as a pink mesh), is thought to correspond to a Fe ion displaced from the [4Fe-4S] cluster. The negative red mesh in the center of the figure indicates the missing amide group of Asn109 (see text). The omit, the  $F_o - F_c$  around Asn109 and the  $\Delta_{\text{anom}}$  maps were contoured at  $3.3\sigma$ ,  $-3.3\sigma$ , and  $4\sigma$ , respectively. (b) Electron density ( $F_{\text{obs}} - F_{\text{calc}}$ ) omit map in the crystal structure of the *TmNadA*\*Y21F-phthalate complex. The QA analogue binds the enzyme as the reaction product does. The omit map is contoured at  $4\sigma$ .

A plausible explanation for the desulfurization reaction that must have generated QA from SMPDC would be the homolytic cleavage of the SMPDC's S–C bond followed by H atom abstraction from the amide group of Asn109 by the nascent QA radical (Supplementary Scheme 2). The resulting radical amide group will rearrange causing the cleavage of the Asn109 C $\beta$ -C $\gamma$  bond and the release of isocyanate. Finally, the generated Ala109 radical will abstract an H atom from a component of the solution. Conversely, the thiyl radical probably oxidizes the [4Fe-4S] cluster causing its observed changes that, however, cannot be unambiguously modeled. An example of the homolytic cleavage of an aromatic C–S bond while bound to a sulfur–metal cluster is given by Curtiss & Druker.<sup>18</sup>

The new QA position makes catalytic sense because the final reaction product now points at the tunnel that leads to the solvent medium<sup>12</sup> and coincides with the equivalent fragment in Y (Figures 1c and 2a). Although the desulfurization of SMPDC and the dehydration of Y are not chemically related reactions both involve the loss of a ring substituent to produce

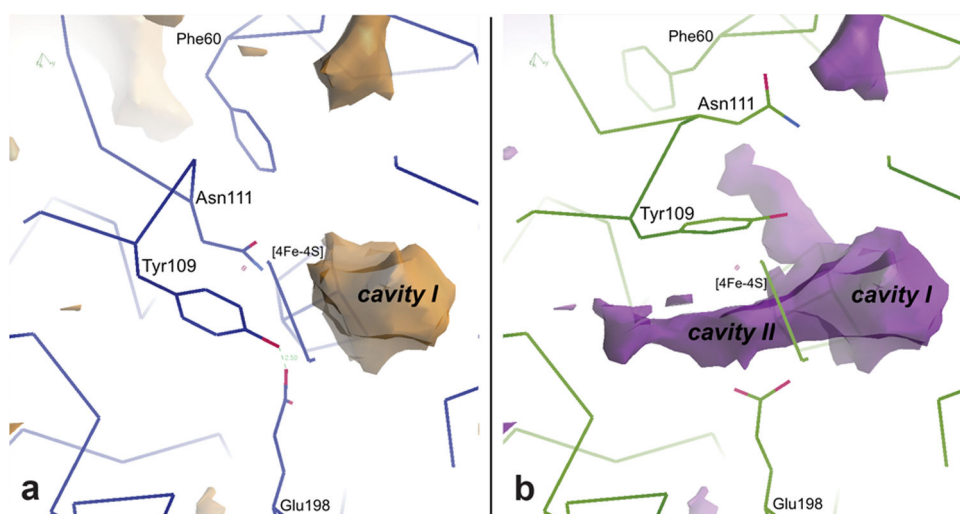


**Figure 3.** Active site cavities in NadA. (a) Active site cavity I in structure A (60%) of citraconate-bound *PhNadA* (with ligand and structural water molecules removed).<sup>14</sup> (b) Active site cavities I and II in structure B (40%) of citraconate-bound *PhNadA* (with ligand and structural water molecules removed). The probe radius used to contour the cavity maps is 0.9 Å.

QA. We have also detected the slow synthesis of QA from SMPDC and *TmNadA*\* in the crystallization buffer (see [Methods](#)). For the first 25 days we observed no peak on the HPLC chromatogram at 12.8 min, indicative of QA (dashed line in [Supplementary Figure 6a](#)). Conversely, at day 35 there was a small peak at 12.8 min (black line in [Supplementary Figure 6a](#)), which UV–visible spectrum matched that of authentic QA ([Supplementary Figure 6b](#)). After quantitation, the QA concentration corresponded to 1/100 of the NadA concentration and 1/330 of the initial SMPDC equivalents. The control experiment without NadA did not produce any QA after 35 days (gray line in [Supplementary Figure 6a](#) and [Supporting Information](#)). This result from the reaction between NadA and SMPDC in solution agrees well with our observation, after five months, of QA in a crystal of *TmNadA*\* initially complexed with SMPDC ([Figure 2a](#)). The functional relevance of this new QA position is also supported by the crystal structure of a *TmNadA*\*Y21F-phthalate complex where this QA analogue occupies the same position as the NadA reaction product and establishes the same interactions with the protein, with only one exception due to the missing N atom in the phthalate ring ([Figure 2b](#)).

The previously observed QA position<sup>15</sup> bound as a bidentate ligand to the [4Fe-4S] cluster in a closed form of NadA was puzzling because it provided no clues for the release of the reaction product from the enzyme. Based on our new result, we believe that that binding does not belong in the catalytic sequence; instead it is an *in vitro* artifact caused by either an excess of added QA or crystal packing effects.<sup>14–16</sup>

**Condensation Reaction of DHAP with IA.** Next, we turned our attention to the first reaction, which involves the condensation of DHAP with IA ([Scheme 1](#)). According to previous work, the phosphate group of DHAP (and PGH<sup>15</sup>) and the carboxylate groups of the IA analogues malate, citraconate, itaconate, and maleate bind to the same site in NadA.<sup>14</sup> Furthermore, X, Y, and the QA reported here, as well as W,<sup>15</sup> also bind to that site with their two carboxylate groups. This precludes the simultaneous binding of DHAP and IA there and suggests that either (i) at least one of these two binding modes is artificial, (ii) the condensation reaction does not take place at the identified active site of NadA, or (iii) their

binding to the same site is sequential. We already have discussed possibilities (ii) and (iii).<sup>15</sup> A new element to be considered in this respect is the observation by Fenwick and Ealick that in the *PhNadA* citraconate and maleate complexes about 40% of the protein molecules in the crystal (structure B) have alternative positions for residues Tyr109, Asn111 and Phe60 (Tyr107, Asn109 and Phe58 in *Tm*).<sup>14</sup> The concerted movement of these three residues generates a cavity (cavity II in [Figure 3b](#)) that in the reported structures is occupied by three water molecules. The position and shape of that cavity, next to the DHAP binding site (cavity I in [Figure 3](#)), and its rather unusual generation by the concerted movement of three buried residues suggests that it could serve to bind IA productively. Indeed, after removal of the three waters, it was possible to dock IA with its reactive C3 atom<sup>3,10</sup> oriented toward, and not far from, the C1 atom of DHAP ([Figure 4](#) and [Supplementary Figure 7](#)).

It is now possible to postulate an initial sequence where IA, synthesized by NadB (or NadX), binds to the site where citraconate and maleate bind ([Supplementary Figure 8](#)), possibly facilitating and/or stabilizing the concerted conformational shift of Tyr107, Asn109, and Phe58, which then

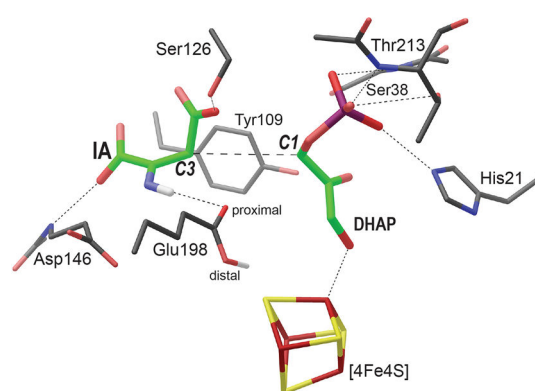


**Figure 4.** Structure B of *PhNadA* with docked DHAP and IA in cavities I and II ([Figure 3b](#)), respectively (see [Methods](#) for details). In this configuration, the distance between the atoms C1 (DHAP) and C3 (IA) is 4.4 Å.

generates cavity II. In the next step, IA is displaced to cavity II by the arrival of DHAP that occupies cavity I with higher affinity (due to its additional interaction with the [4Fe-4S] cluster relative to IA binding) in a productive position that differs from the one observed in the *PhNadA*-DHAP complex (Figure 4 and Supplementary Figure 7);<sup>14</sup> both substrates are now well poised to form a pentavalent transition state. The condensation reaction ends when the C1–O bond of DHAP is broken, being replaced by a C1–C3 bond thus forming **W** while concomitantly phosphate leaves the active site through the long protein channel.<sup>12</sup> During this process the nascent **W** intermediate rearranges occupying either the productive orientation equivalent to the one observed for **X** in its complex with *TmNadA*\*Y21F—and mimicked by DHAP in its complex with *PhNadA*<sup>14</sup>—or the unproductive one found in the *TmNadA*\*Y107F-**W** complex, which is imitated by our *TmNadA*\*Y107F-PGH complex.<sup>15</sup> Based on the docking experiments reported above, we believe that these orientations depend, at least partially, on which of the carboxylate O atoms of Glu195 (Glu198 in *PhNadA*) is protonated. This protonation should differ in the wt enzyme and Y107F variant. We have tried to cocrystallize different combinations of citraconate, IA, DHAP, and PGH with *TmNadA*, in order to get a structure where the two cavities are occupied, but have not yet succeeded. In the future, we will consider the possibility of synthesizing a transition-state analogue that could occupy both cavities and will prepare new site-directed variants to test this hypothesis. For the time being, docking experiments performed to explore its validity indicate that the proposed reaction is clearly plausible (Figure 4).

## CONCLUSIONS

We first note that although in our previously published structure **W** was not bound in a productive orientation, it was the correct intermediate species. More importantly, here we present a series of significant results that allow us to describe fully the structural aspects of QA synthesis by *NadA*. A rather convincing model for the condensation of IA and DHAP is based on cavity II, which is generated by the concerted shift of residues Tyr109, Asn111, and Phe60 in 40% in the *PhNadA* citraconate and maleate complex structures.<sup>14</sup> The presence of this cavity explains why both substrates can sequentially bind to the same site at the top of cavity I. Indeed, this site may represent an entry point for the unstable IA before it is displaced to cavity II by DHAP. It also provides a plausible model for the condensation reaction because the phosphate group of DHAP is properly positioned to leave through the protein tunnel. Next in the catalytic sequence, our trapping experiment yielded the key structures of **X** and **Y**. In addition, we were able to solve the structure of an intermediate analogue-derived **QA** bound to *TmNadA*\* in an orientation that favors its release from the active site and is likely to represent the physiologically relevant one. This is also supported by the *TmNadA*\*Y21F with phthalate. Taken together, our results provide a complete structure-based description of QA synthesis by *NadA*.

## METHODS

### Purification and Chemical Reconstitution of *NadA* Proteins.

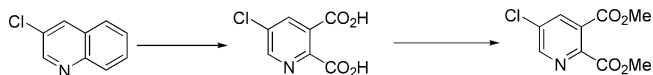
Expression and purification of *TmNadA*\* and the *TmNadA*\*Y21F variant were performed as in ref 15. Briefly, BL21DE3 *E. coli* cells were grown aerobically at 37 °C in LB medium containing 100 μg/mL ampicillin. Expression was induced with 0.5 mM Isopropyl 1-thio-β-d-

galactopyranoside (Eurogentec) and cultures were shaken for 4 h. Purification of proteins was performed using an affinity Ni-NTA column. After extensive washing with 100 mM Tris-HCl, 500 mM NaCl, 10 mM imidazole pH 8 buffer, *TmNadA*\*, and *TmNadA*\*Y21F were eluted with the above buffer containing 0.2 M imidazole. Imidazole was removed using a desalting PD-25 column (Pharmacia).

Chemical reconstitution was performed anaerobically as described in ref 15. Briefly, purified *TmNadA*\* proteins (150 μM) were incubated with 5 mM DTT for 15 min. Then, 6 mol equiv of L-cysteine with catalytic amount of IscS cysteine desulfurase (1.5 μM) and 6 mol equiv ferrous iron ((NH<sub>4</sub>)<sub>2</sub>Fe(SO<sub>4</sub>)<sub>2</sub>) were added. After a 5 h incubation, proteins were heated for 30 min at 65 °C in the presence of 50 mM DTT. Monomeric [4Fe-4S]-*TmNadA*\* proteins were obtained after Superdex-75 chromatography and concentrated to 20 mg mL<sup>-1</sup>.

### 5MPDC Synthesis. 1. 5-Chloropyridine-2,3-dicarboxylic Acid Dimethyl Ester.

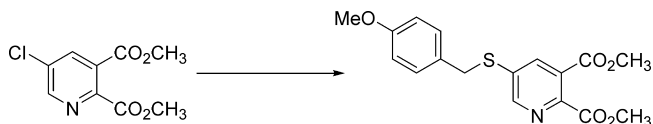
5-Chloropyridine-2,3-dicarboxylic acid (1.67 g) was



synthesized using a reported procedure<sup>19</sup> starting from 3-chloroquinoline (3.50 g, 21.4 mmol). The crude product was engaged in the next step without further purification. To a solution of the obtained 5-chloropyridine-2,3-dicarboxylic acid in methanol (7 mL) at 0 °C, H<sub>2</sub>SO<sub>4</sub> (0.47 mL, 8.81 mmol) was added dropwise within 5 min. The resulting mixture was refluxed for 24 h until completion (monitored by TLC (2% methanol in CH<sub>2</sub>Cl<sub>2</sub>)). After concentration in vacuo, the resulting residue was basified with saturated aqueous sodium bicarbonate to pH ≈ 8, and the product was extracted three times with ethyl acetate. The combined organic fractions were dried with sodium sulfate and concentrated under reduced pressure. The resulting residue was purified by silica gel column chromatography (2% methanol in CH<sub>2</sub>Cl<sub>2</sub>) to afford 1.16g (24% over two steps) of the desired product as a white powder. <sup>1</sup>H NMR (300 MHz, CDCl<sub>3</sub>), δ 8.73 (d, *J* = 2.4 Hz, 1H), 8.15 (d, *J* = 2.4 Hz, 1H), 4.02 (s, 3H), 3.97 (s, 3H). <sup>13</sup>C NMR (75 MHz, CDCl<sub>3</sub>), δ 165.7 (C), 164.7 (C), 150.6 (CH), 148.1 (C), 137.01 (CH), 133.8 (C), 127.9 (C), 53.2 (2 CH<sub>3</sub>). MS-ESI: calculated *m/z* for [C<sub>9</sub>H<sub>8</sub>ClNO<sub>4</sub>+H<sup>+</sup>]<sup>+</sup>, 230.0; found, 230.2.

### 2. 5-((4-Methoxybenzyl)thio)pyridine-2,3-dicarboxylic Acid Dimethyl Ester.

A solution of dimethyl-5-chloropyridine-2,3-dicarbox-



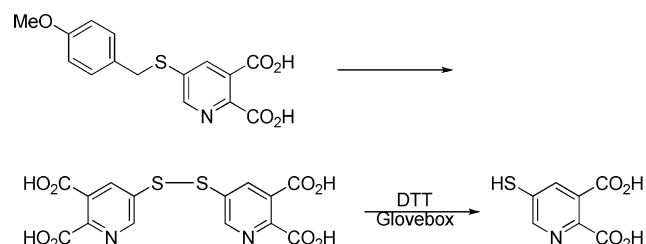
ylate (1.15 g, 5.01 mmol) in anhydrous dimethyl sulfoxide (DMSO; 25 mL) was deoxygenated by argon bubbling for 10 min. Then, Cs<sub>2</sub>CO<sub>3</sub> (1.80 g, 5.51 mmol) and 4-methoxy-*α*-toluenethiol (0.73 mL, 5.26 mmol) were added, and the resulting solution was stirred at RT under an argon atmosphere for 48 h (monitored by TLC (2% methanol in CH<sub>2</sub>Cl<sub>2</sub>)). The reaction mixture was quenched by addition of water (25 mL) and extracted three times with diethyl ether (Et<sub>2</sub>O). The organic layers were combined, dried across magnesium sulfate, and the solvent evaporated. The obtained residue was purified by silica gel column chromatography (5% methanol in CH<sub>2</sub>Cl<sub>2</sub>) to afford 1.06 g (57%) of the desired product as a pale yellow powder. <sup>1</sup>H NMR (300 MHz, CDCl<sub>3</sub>), δ 8.55 (s, 1H), 7.89 (s, 1H), 7.23 (d, *J* = 8.4 Hz, 2H), 6.84 (d, *J* = 8.4 Hz, 2H), 4.16 (s, 2H), 3.97 (s, 3H), 3.92 (s, 3H), 3.79 (s, 3H). <sup>13</sup>C NMR (75 MHz, CDCl<sub>3</sub>), δ 165.9 (C), 163.0 (C), 159.3 (C), 150.3 (CH), 146.2 (C), 137.4 (C), 136.3 (CH), 130.0 (2 CH), 127.5 (C), 127.3 (C), 114.3 (2 CH), 55.3 (CH<sub>3</sub>), 53.1 (CH<sub>3</sub>), 53.0 (CH<sub>3</sub>), 37.3 (CH<sub>2</sub>). ESI-MS: calculated *m/z* for [C<sub>17</sub>H<sub>17</sub>NO<sub>5</sub>S+H<sup>+</sup>]<sup>+</sup>, 348.1; found, 348.1.

3. Dimethyl 5-((4-Methoxybenzyl)thio)pyridine-2,3-dicarboxylic Acid. To a solution of 5-((4-methoxybenzyl)thio)pyridine-2,3-dicarboxylic acid dimethyl ester (0.90 g, 2.59 mmol) in diethyl ether (4.5 mL), a 5 M aqueous solution of NaOH (3.2 mL) was added. The mixture was refluxed for 24 h and then acidified to pH ≈ 2 by



dropwise addition of a concentrated HCl solution. The resulting mixture was extracted three times with ethyl acetate, and the combined organic layers were dried with  $\text{Na}_2\text{SO}_4$  and concentrated in vacuo. Reextraction of the product from the resulting residue with acetone, drying with sodium sulfate, and evaporation of the solvent under reduce pressure afforded 0.55g (62%) of the title compound as a yellow powder.  $^1\text{H}$  NMR (300 MHz, acetone- $d_6$ ),  $\delta$  8.62 (s, 1H), 8.13 (s, 1H), 7.36 (d,  $J$  = 8.3 Hz, 2H), 6.89 (d,  $J$  = 8.3 Hz, 2H), 4.40 (s, 2H), 3.77 (s, 3H).  $^{13}\text{C}$  NMR (75 MHz, acetone- $d_6$ ),  $\delta$  165.6 (C), 165.5 (C), 159.3 (C), 149.2 (C), 146.3 (C), 137.5 (CH), 136.4 (C), 130.2 (2 CH), 128.0 (C), 127.8 (CH), 114.0 (2 CH), 54.6 (CH<sub>3</sub>), 36.1 (CH<sub>2</sub>). ESI-MS: calculated  $m/z$  for  $[\text{C}_{15}\text{H}_{13}\text{NO}_5\text{S}-\text{H}^+]^-$ , 318.1; found, 317.9.

**4. 5-Mercaptopyridine-2,3-dicarboxylic Acid.** To a mixture of 5-((4-methoxybenzyl)thio)pyridine-2,3-dicarboxylic acid (0.472 g, 1.48



mmol) and anisole (9.5 mL, 87.27 mmol) and cooled to  $-5^\circ\text{C}$ , trifluoroacetic acid (95 mL) and mercury(II) acetate (0.49 g, 1.53 mmol) were added.<sup>20</sup> The reaction mixture was stirred for 1 h at  $-5^\circ\text{C}$  and then concentrated in vacuo to afford an orange oil. Addition of a 1:1 mixture of water- $\text{Et}_2\text{O}$  (150 mL) resulted in the precipitation of a part of the product. The precipitated solid and the water phase were mixed together, and the resulting suspension was concentrated in vacuo and taken up in methanol (40 mL). Next, the methanolic solution was bubbled with hydrogen sulfide for 2 h. The black suspension was filtered through Celite with methanol, and the obtained filtrate was concentrated in vacuo and purified by  $\text{C}_{18}$  column chromatography to afford 0.053 g (9%) of the title compound as a disulfide dimer.  $^1\text{H}$  NMR (300 MHz, acetone- $d_6$ ),  $\delta$  8.48 (d,  $J$  = 2.4 Hz, 1H), 8.94 (d,  $J$  = 2.4 Hz, 1H).  $^1\text{H}$  NMR (300 MHz, 1 M Tris- $\text{D}_2\text{O}$ , pH = 7.5)  $\delta$  8.55 (s, 1H), 8.16 (s, 1H).  $^{13}\text{C}$  NMR (75 MHz, acetone- $d_6$ ),  $\delta$  165.9 (C), 165.0 (C), 150.2 (C), 149.8 (CH), 136.8 (CH), 135.0 (C), 127.2 (C). ESI-MS: calculated  $m/z$  for  $[\text{C}_{14}\text{H}_8\text{N}_2\text{O}_8\text{S}_2-\text{H}^+]^-$ , 395.0; found, 395.0 (88); calculated  $m/z$  for  $[\text{C}_{14}\text{H}_8\text{N}_2\text{O}_8\text{S}_2-2\text{H}^+]^{2-}$ , 197.2; found, 197.2 (100).

Because of the fast oxidation of the title compound when exposed to air, it was stored as a dimer and reduced in the glovebox just before further use with 1 equiv of DTT as reducing agent. This procedure permitted to obtain the desired monomeric form in a quantitative manner.  $^1\text{H}$  NMR (300 MHz, 1 M Tris- $\text{D}_2\text{O}$ , pH = 7.5),  $\delta$  8.29 (s, 1H), 7.73 (s, 1H).  $^{13}\text{C}$  NMR (75 MHz),  $\delta$ . ESI-MS: calculated  $m/z$  for  $[\text{C}_7\text{H}_4\text{NO}_4\text{S}-\text{H}^+]^-$ , 198.0; found, 198.2 (100).

**Crystallization Conditions. *TmNadA*\*Y21F-PGH Complex.** First, 100  $\mu\text{L}$  of a 20 mg  $\text{mL}^{-1}$  protein solution in 50 mM KCl, 10 mM Tris HCl pH 8.0 were incubated anaerobically overnight with 7  $\mu\text{L}$  20 mM PGH in water at  $20^\circ\text{C}$ . One microliter of this solution was mixed with the same volume of a 24% w/v PEG3350, 200 mM  $\text{Na}_2\text{HPO}_4$ , 100 mM Tris base pH 8.5 crystallization solution on a siliconized coverslip. The resulting drop was then equilibrated in the vapor phase against 1 mL of the crystallization solution at  $20^\circ\text{C}$ . A brown crystalline plate was obtained after 3 days. The crystal was subsequently transferred to a cryo-protecting solution composed of 40% PEG3350, 200 mM  $\text{Na}_2\text{HPO}_4$  in 100 mM Tris base pH 8.4 buffer, and it was flash-cooled using liquid propane inside the glovebox as previously described.<sup>21</sup>

***TmNadA*\*Y21F-X/Y Complex.** Initially, 50  $\mu\text{L}$  of a 20 mg  $\text{mL}^{-1}$  protein solution in 50 mM KCl, 125 mM Tris HCl pH 7.5 were incubated anaerobically 36 h at  $20^\circ\text{C}$  after the addition of 0.5  $\mu\text{L}$  of 0.5 M  $(\text{NH}_4)_2\text{SO}_4$ , 1  $\mu\text{L}$  of 0.5 M oxaloacetic acid, and 2  $\mu\text{L}$  of 50 mM DHAP. One microliter of this solution was then mixed with the same volume of a 21% PEG3350, 200 mM NaF 100 mM Bis Tris propane pH 7.1 crystallization solution and set up as indicated in the previous paragraph. Several brown crystals appeared in the drop after 9 days. One of these crystals was transferred to a cryo-protecting solution composed of 28% PEG3350, 200 mM NaF, 20% glycerol in 100 mM Bis Tris propane buffer pH 7.1 and flash-cooled using liquid ethane inside the glovebox.

***TmNadA*\*5MPDC Complex.** First, 50  $\mu\text{L}$  of a 44.6 mg  $\text{mL}^{-1}$  protein solution in 50 mM KCl, 100 mM Tris HCl pH 8.0 were incubated anaerobically overnight at  $20^\circ\text{C}$  after the addition of 27  $\mu\text{L}$  7.5 mM 5MPDC in 25 mM Tris HCl pH 8.0 and 23  $\mu\text{L}$  of a solution containing 50 mM KCl and 125 mM Tris HCl pH 7.2. One  $\mu\text{L}$  of the resulting solution, containing 22.3 mg  $\text{mL}^{-1}$  protein, was initially mixed with 1  $\mu\text{L}$  of a solution containing 22% PEG3350, 200 mM  $\text{Na}_2\text{HPO}_4$  in 100 mM CHES pH 9.1. Prior to mixing the latter solution was left to sit in order to deposit some precipitated  $\text{Na}_2\text{HPO}_4$ . After 37 days, the crystallization drop was transferred to a well containing 1 mL of a solution that before phosphate precipitation contained 34% PEG3350, 200 mM  $\text{Na}_2\text{HPO}_4$  in 100 mM CHES pH 9.1. Twelve days later, the drop was again transferred to a well containing 1 mL of a solution composed of 36% PEG3350, 200 mM  $\text{Na}_2\text{HPO}_4$  in 100 mM CHES pH 9.1 before phosphate precipitation. Several brown crystals were observed in the transferred drop 105 days later. A fragment of one of these crystals was transferred to a cryo-protecting solution composed of 40% PEG3350, 200 mM  $\text{Na}_2\text{HPO}_4$  in 100 mM CHES pH 9.5 and flash-cooled using liquid propane inside the glovebox.

***TmNadA*\*Y21F-Phthalate Complex.** In the initial step, 100  $\mu\text{L}$  of a 20 mg  $\text{mL}^{-1}$  protein solution in 50 mM KCl, 125 mM Tris HCl pH 7.2 were incubated anaerobically overnight with 2.4  $\mu\text{L}$  50 mM Phthalate in 50 mM Hepes pH 7.0 at  $20^\circ\text{C}$ . One microliter of this solution was mixed with the same volume of a 26% w/v PEG3350, 200 mM  $\text{Na}_2\text{HPO}_4$ , 100 mM Hepes pH 7.8 crystallization solution on a siliconized coverslip. The resulting drop was then equilibrated in the vapor phase against 1 mL of the crystallization solution at  $20^\circ\text{C}$ . A brown crystalline plate was obtained after 3 days. The crystal was subsequently transferred to a cryo-protecting solution composed of 40% PEG3350, 200 mM  $\text{Na}_2\text{HPO}_4$  in 100 mM Hepes pH 7.8 buffer, and flash-cooled using liquid propane inside the glovebox as previously described.

**X-ray Structure Determination.** All diffraction data (Table 1) were collected on a Pilatus detector, using the program MXCuBe<sup>22</sup> at beamlines ID30A3, ID30B, and ID23-1 of the European Synchrotron Radiation Facility in Grenoble, France. Data indexing, integration and initial scaling was performed with the XDS package,<sup>23</sup> followed by a final scaling and merging step with AIMLESS<sup>24</sup> of the CCP4 package.<sup>25</sup> Structures were solved by molecular replacement with the PHASER program<sup>26</sup> using previously published *TmNadA* structures.<sup>12,15</sup> The obtained models were refined with REFMACS.<sup>27</sup> The resolution of the Y21F-XY model was good enough to refine individual anisotropic B-factors. For the three other models, isotropic B-factors were refined along with TLS parameters.<sup>27</sup>

Local manual model corrections were performed with COOT.<sup>28</sup> Except for MXCuBe, the programs mentioned above were compiled by SBrGrid.<sup>29</sup>

A series of 1.5 Å resolution ( $F_{\text{obs}} - F_{\text{calc}}$ ) omit maps were used to resolve the mixture of reaction intermediates observed in crystal 1, which resulted from the pH shift experiment described in the main text. The first omit map (Figure 1a) was calculated after removing all atoms inside cavity I (Figure 3a) from the protein model. This map showed a continuous electron density leading to the unique Fe ion of the [4Fe-4S] cluster that could be assigned to a partially occupied intermediate Y. After including this in the atomic model with an occupation of 40%, the next omit map revealed clear electron density for the X intermediate, which was also included at 40% occupation.

Different relative occupations of X and Y resulted in worse refinement statistics. Remaining features in the following ( $F_{\text{obs}} - F_{\text{calc}}$ ) map could be satisfactorily explained by four water molecules at H-bonding distances from each other, with an occupation of 20% each. Including these waters with 40% X and 0% Y or 40% Y and 0% X improved the quality of the respective omit maps for Y and X, allowing to obtain well-defined structures for their bound forms (Figure 1b,c). Dictionary files needed for the refinement of the X and Y intermediates were developed in the same way as previously described for intermediate W.<sup>15</sup> Because their structures are very similar, replacing 40% of X by 40% of properly rotated W in the protein model gave the same refinement statistics, with a final  $R_{\text{free}}$  of 17.9% (Table 1). The assignment to X is based on the observed binding mode to the cluster (an alkoxide oxygen ligand at C5 should be preferred over a carbonyl one, see also Scheme 1), combined with the presence of Y (the next intermediate in the catalytic mechanism) and our previous finding that the Y21F variant is able to produce QA.<sup>15</sup>

Unexpectedly, the crystal structure of the complex of *TmNadA*\* with SMPDC revealed that the QA product can be obtained from the latter molecule. Refinement of the structure revealed the cleavage of the C $\beta$ -C $\gamma$  bond of Asn109 (Figure 2a). In addition, a large electron density peak next to the [4Fe-4S] cluster coinciding with one of the highest peaks in the anomalous difference map (Figure 2a) indicated a significant movement of the unique Fe ion of the cluster (Fe3 in the PDB file). Because of the limited 2.3 Å resolution of the diffraction data and possible disorder, we were not able to resolve the new cluster structure, which could also be part of a mixture of different forms. The observed structural changes are compatible with the formation of reactive radical species during the production of QA from SMPDC (Supplementary Scheme 2). Examination of the data obtained for the phthalate complex indicated that the crystal contained a mixture of open and closed *NadA* conformations, which were modeled starting from previous PDB depositions 4P3X<sup>12</sup> and 5F33,<sup>15</sup> respectively. Their occupations were manually refined to 59% and 41%, respectively, which gave the lowest  $R_{\text{free}}$  factor. The phthalate molecule binds to the open form (Figure 2b) in almost the same way as the QA product obtained from SMPDC. Finally, the 2.0 Å resolution omit electron density of PGH in complex with *TmNadA*\*-Y21F (Supplementary Figure 3a) could be explained by a mixture of 70% PGH and 30% phosphate from the crystallization mixture, the position of the latter coinciding with the phosphate moiety of PGH. The four crystal structures are deposited in the Protein Data Bank (PDB). Their refinement statistics are given in Table 1.

Figures 1 and 2 and Supplementary Figure 3a were prepared with *BOBSCRIPT*,<sup>30</sup> and Supplementary Figures 1, 2, and 3b with *MOLSCRIPT*.<sup>31</sup> All these figures were rendered with *Raster3D*.<sup>32</sup> Figure 3 and Supplementary Figure 7 were prepared with *COOT*,<sup>28</sup> using the *CAVENV* program of the CCP4 package<sup>25</sup> to calculate the protein cavities.

**QA Production by SMPDC and *NadA* in Solution.** *TmNadA*\* (430  $\mu\text{M}$ ) was mixed with 3.5 mol equiv of SMPDC in 125 mM Tris, 50 mM KCl pH 8.0 buffer. After an overnight incubation, 100 mM CHES pH 9.5 crystallization buffer was added to a 1:1 ratio (v/v) to the *TmNadA*\*-SMPDC solution. Formation of QA was monitored by HPLC by withdrawing 20  $\mu\text{L}$  from this reaction mixture daily for the first 2 days and every 5 days until the 35th day. At that time, 2  $\mu\text{L}$  of 2 M  $\text{H}_2\text{SO}_4$  was added to the withdrawn 20  $\mu\text{L}$  in order to stop the reaction. Then, samples were diluted by the addition of 80  $\mu\text{L}$  of 0.03% trifluoroacetic acid, pH 2.4 buffer and centrifuged at 13000 rpm for 15 min to remove all insoluble materials. The supernatant (80  $\mu\text{L}$ ) was then injected to a HPLC system (Agilent 1100, column HPLC Kinetex reversed-phase 5u C18 100A, 250  $\times$  4.6 mm). QA formation was detected and quantified as previously described.<sup>13</sup> A control experiment with SMPDC but without *TmNadA*\*, was carried out in parallel and a sample from this solution was analyzed by HPLC at day 35 (Supplementary Figure 6a).

**Molecular Docking.** All calculations were performed with the Schrödinger suite.<sup>33</sup> The used X-ray structures from citraconate-containing *PhNadA*<sup>14</sup> (B structure from PDB code SKTS and Figure 4), DHAP-containing *PhNadA*<sup>14</sup> (PDB code SKTN, Supplementary

Figure 4a) and PGH-containing *TmNadA*\*-Y107F<sup>15</sup> (PDB code 5F33, Supplementary Figure 4b) correspond to the closed form of the protein. The ligand-free, open form of *TmNadA*\* was also used<sup>12</sup> (PDB code 4P3X and Supplementary Figure 5a). Hydrogen atoms were added to the models and protonation states were assigned using the standard protein preparation protocol within the Schrödinger suite. The positions of the built hydrogen atoms were then optimized, and water molecules present in the X-ray model were removed. A special attention was paid to the protonation state of Glu195 (Glu198 in *PhNadA*) that was set to be either deprotonated or protonated on the distal or proximal oxygen atom relative to *PhNadA* Tyr109 (Figure 4). A receptor docking grid was defined by the ligand position for the three closed forms of *NadA* and by the water molecules filling the cavity in the case of the open form; ligands and water molecules were removed. The DHAP, PGH, and W molecules were prepared using the Ligprep program and then docked using the Glide program with the standard (SP) and the extra precision (XP) docking procedures. The docked poses were then compared to the available X-ray models. Next, IA was first docked in the B structure of the citraconate-containing *PhNadA* in a grid centered at the citraconate position (without the ligand); in these conditions IA binds as citraconate except that the amino group of the former is opposite to the methyl group of the latter (Supplementary Figure 8). To try and investigate the first condensation reaction between IA and DHAP (Scheme 1), we performed a multiple ligand docking procedure using Glide.<sup>34</sup> IA was docked in a grid defined by the three water molecules present in cavity II (Figure 3b) while keeping citraconate present in cavity I. Analyzing the IA docked poses, we found only one family where the C3 atom involved in the condensation reaction (see main text) points toward cavity I (Figure 4). We then used this IA-containing model to generate a grid defined by the citraconate position and we docked DHAP. The DHAP docked pose shown in Figure 4 is the most suitable one we found for condensation, that is, with the C1 atom from DHAP and the C3 atom from IA at a distance of 4.4 Å. Further rearrangements, such as substrate displacements and the change from a closed to an open form of *NadA* will be necessary for the reaction to proceed (see main text).

Figure 4 and Supplementary Figures 4, 5, and 8 were prepared with Maestro from Schrödinger.<sup>33</sup>

## ■ ASSOCIATED CONTENT

### 📄 Supporting Information

The Supporting Information is available free of charge on the ACS Publications website at DOI: 10.1021/acscchembio.7b01104.

Additional X-ray structure superpositions, docking experiments, solution experiment, and schemes for the role of Y21 and QA formation (PDF)

## ■ AUTHOR INFORMATION

### Corresponding Author

\*E-mail: [juan.fontecilla@ibs.fr](mailto:juan.fontecilla@ibs.fr).

### ORCID

Juan C. Fontecilla-Camps: 0000-0002-3901-1378

### Notes

The authors declare no competing financial interest.

The atomic coordinates and structure factors have been deposited to the PDB (ID code 6F48, 6F4D, 6F4L, and 6G74)

## ■ ACKNOWLEDGMENTS

We thank the CEA and the CNRS for institutional support. We also thank the Agence Nationale pour la Recherche for contract ANR-16-CE18-0026 (NADIN). S.O.d.C. also acknowledges partial financial support from the ARCANÉ Labex (ANR-11-LABX-0003-01) and GRAL Labex (ANR-10-LABEX-04 GRAL

Labex, Grenoble Alliance for Integrated Structural Cell Biology). Part of this work used the platforms of the Grenoble Instruct center (ISBG; UMS 3518 CNRS-CEA-UJF-EMBL) with support from FRISBI (ANR-10-INSB-05-02) and GRAL (ANR-10-LABX-49-01) within the Grenoble Partnership for Structural Biology (PSB). We appreciate the help from the staff of the ESRF beamlines (Grenoble) with X-ray data collection and of the computing facility provided by the Commissariat à l'Énergie Atomique et aux Énergies Alternatives (CEA/DRF/GIPSI), Saclay.

## REFERENCES

- (1) Foster, J. W., and Moat, A. G. (1980) Nicotinamide adenine dinucleotide biosynthesis and pyridine nucleotide cycle metabolism in microbial systems. *Microbiol. Rev.* *44*, 83–105.
- (2) Pollak, N., Dölle, C., and Ziegler, M. (2007) The power to reduce: pyridine nucleotides – small molecules with a multitude of functions. *Biochem. J.* *402*, 205–218.
- (3) Nasu, S., Wicks, F. D., and Gholson, R. K. (1982) L-Aspartate oxidase, a newly discovered enzyme of *Escherichia coli*, is the B protein of quinolinate synthetase. *J. Biol. Chem.* *257*, 626–632.
- (4) Yang, Z., Savchenko, A., Yakunin, A., Zhang, R., Edwards, A., Arrowsmith, C., and Tong, L. (2003) Aspartate dehydrogenase, a novel enzyme identified from structural and functional studies of TM1643. *J. Biol. Chem.* *278*, 8804–8808.
- (5) Nasu, S., and Gholson, R. K. (1981) Replacement of the B protein requirement of the *E. coli* quinolinate synthetase system by chemically-generated iminoaspartate. *Biochem. Biophys. Res. Commun.* *101*, 533–539.
- (6) Nasu, S., Wicks, F. D., Sakakibara, S., and Gholson, R. K. (1978) Synthesis of quinolinate from D-aspartate in the mammalian liver-*Escherichia coli* quinolinate synthetase system. *Biochem. Biophys. Res. Commun.* *84*, 928–935.
- (7) Begley, T. P., Kinsland, C., Mehl, R. A., Osterman, A., and Dorrestein, P. (2001) The biosynthesis of nicotinamide adenine dinucleotides in bacteria. *Vitam. Horm.* *61*, 103–119.
- (8) Ollagnier-de Choudens, S., Loiseau, L., Sanakis, Y., Barras, F., and Fontecave, M. (2005) Quinolinate synthetase, an iron-sulfur enzyme in NAD biosynthesis. *FEBS Lett.* *579*, 3737–3743.
- (9) Cicchillo, R. M., Tu, L., Stromberg, J. A., Hoffart, L. M., Krebs, C., and Booker, S. J. (2005) *Escherichia coli* quinolinate synthetase does indeed harbor a [4Fe-4S] cluster. *J. Am. Chem. Soc.* *127*, 7310–7311.
- (10) Flint, D. H., and Allen, R. M. (1996) Iron-sulfur proteins with nonredox functions. *Chem. Rev.* *96*, 2315–2334.
- (11) Beinert, H., Kennedy, M. C., and Stout, C. D. (1996) Aconitase as iron-sulfur protein, enzyme, and iron-regulatory protein. *Chem. Rev.* *96*, 2335–2374.
- (12) Cherrier, M. V., Chan, A., Darnault, C., Reichmann, D., Amara, P., Ollagnier de Choudens, S., and Fontecilla-Camps, J. C. (2014) The crystal structure of Fe<sub>4</sub>S<sub>4</sub> quinolinate synthase unravels an enzymatic dehydration mechanism that uses tyrosine and a hydrolase-type triad. *J. Am. Chem. Soc.* *136*, 5253–5256.
- (13) Chan, A., Clemancey, M., Mouesca, J.-M., Amara, P., Hamelin, O., Latour, J.-M., and Ollagnier de Choudens, S. (2012) Studies of inhibitor binding to the [4Fe-4S] cluster of quinolinate synthase. *Angew. Chem., Int. Ed.* *51*, 7711–7714.
- (14) Fenwick, M. K., and Ealick, S. E. (2016) Crystal structures of the iron-sulfur cluster-dependent quinolinate synthase in complex with dihydroxyacetone phosphate, iminoaspartate analogues, and quinolinate. *Biochemistry* *55*, 4135–4139.
- (15) Volbeda, A., Darnault, C., Renoux, O., Reichmann, D., Amara, P., Ollagnier de Choudens, S., and Fontecilla-Camps, J. C. (2016) Crystal structures of quinolinate synthase in complex with a substrate analogue, the condensation intermediate, and substrate-derived product. *J. Am. Chem. Soc.* *138*, 11802–11809.
- (16) Esakova, O. A., Silakov, A., Grove, T. L., Saunders, A. H., McLaughlin, M. I., Yennawar, N. H., and Booker, S. J. (2016) Structure of quinolinate synthase from *Pyrococcus horikoshii* in the presence of its product, quinolinic acid. *J. Am. Chem. Soc.* *138*, 7224–7227.
- (17) Suzuki, N., Carlson, J., Griffith, G., and Gholson, R. K. (1973) Studies on the de novo biosynthesis of NAD in *Escherichia coli*. V. Properties of the quinolinic acid synthetase system. *Biochim. Biophys. Acta, Gen. Subj.* *304*, 309–315.
- (18) Curtis, M. D., and Druker, S. H. (1997) Homolytic C–S bond scission in the desulfurization of aromatic and aliphatic thiols mediated by a Mo/Co/S cluster: mechanistic aspects relevant to HDS catalysis. *J. Am. Chem. Soc.* *119*, 1027–1036.
- (19) Obafemi, C. A., and Pfeleiderer, W. (1994) Permanganate oxidation of quinoxaline and its derivatives. *Helv. Chim. Acta* *77*, 1549–1556.
- (20) Holler, T. P., Ruan, F., Spaltenstein, A., and Hopkins, P. B. (1989) Total synthesis of marine mercaptohistidines: othiols A, B, and C. *J. Org. Chem.* *54*, 4570–4575.
- (21) Vernède, X., and Fontecilla-Camps, J. C. (1999) A method to stabilize reduced and/or gas-treated protein crystals by flash-cooling under a controlled atmosphere. *J. Appl. Crystallogr.* *32*, 505–509.
- (22) Gabadinho, J., Beteva, A., Guijarro, M., Rey-Bakaikoa, V., Spruce, D., Bowler, M. W., Brockhauser, S., Flot, D., Gordon, E. J., Hall, D. R., Lavault, B., McCarthy, A. A., McCarthy, J., Mitchell, E., Monaco, S., Mueller-Dieckmann, C., Nurizzo, D., Ravelli, R. B. G., Thibault, X., Walsh, M. A., Leonard, G. A., and McSweeney, S. M. (2010) MxCuBE: a synchrotron beamline control environment customized for macromolecular crystallography experiments. *J. Synchrotron Radiat.* *17*, 700–707.
- (23) Kabsch, W. (2010) XDS. *Acta Crystallogr., Sect. D: Biol. Crystallogr.* *66*, 125–132.
- (24) Evans, P. R., and Murshudov, G. N. (2013) How good are my data and what is the resolution? *Acta Crystallogr., Sect. D: Biol. Crystallogr.* *69*, 1204–1214.
- (25) Winn, M. D., Ballard, C. C., Cowtan, K. D., Dodson, E. J., Emsley, P., Evans, P. R., Keegan, R. M., Krissinel, E. B., Leslie, A. G. W., McCoy, A., McNicholas, S. J., Murshudov, G. N., Pannu, N. S., Potterton, E. A., Powell, H. R., Read, R. J., Vagin, A., and Wilson, K. S. (2011) Overview of the CCP4 suite and current developments. *Acta Crystallogr., Sect. D: Biol. Crystallogr.* *67*, 235–242.
- (26) McCoy, A. J., Grosse-Kunstleve, R. W., Adams, P. D., Winn, M. D., Storoni, L. C., and Read, R. J. (2007) Phaser crystallographic software. *J. Appl. Crystallogr.* *40*, 658–674.
- (27) Murshudov, G. N., Skubák, P., Lebedev, A. A., Pannu, N. S., Steiner, R. A., Nicholls, R. A., Winn, M. D., Long, F., and Vagin, A. A. (2011) REFMAC5 for the refinement of macromolecular crystal structures. *Acta Crystallogr., Sect. D: Biol. Crystallogr.* *67*, 355–367.
- (28) Emsley, P., Lohkamp, B., Scott, W. G., and Cowtan, K. (2010) Features and development of Coot. *Acta Crystallogr., Sect. D: Biol. Crystallogr.* *66*, 486–501.
- (29) Morin, A., Eisenbraun, B., Key, J., Sanschagrin, P. C., Timony, M. A., Ottaviano, M., and Sliz, P. (2013) Collaboration gets the most out of software. *eLife* *2*, e01456.
- (30) Esnouf, R. M. (1999) Further additions to MolScript version 1.4, including reading and contouring of electron-density maps. *Acta Crystallogr., Sect. D: Biol. Crystallogr.* *55*, 938–940.
- (31) Kraulis, P. J. (1991) MOLSCRIPT: a program to produce both detailed and schematic plots of protein structures. *J. Appl. Crystallogr.* *24*, 946–950.
- (32) Merritt, E. A., and Murphy, M. E. (1994) Raster3D Version 2.0. A program for photorealistic molecular graphics. *Acta Crystallogr., Sect. D: Biol. Crystallogr.* *50*, 869–873.
- (33) Schrödinger Release 2016-1: *Jaguar*; Schrödinger, LLC: New York, NY, 2016.
- (34) Vass, M., Tarcsay, Á., and Keserű, G. M. (2012) Multiple ligand docking by Glide: implications for virtual second-site screening. *J. Comput.-Aided Mol. Des.* *26*, 821–834.



# ChemComm

Accepted Manuscript



This article can be cited before page numbers have been issued, to do this please use: S. Ollagnier de Choudens, J. Saez Cabodevilla, A. Volbeda, O. hamelin, J. Latour, O. Gigarel, M. Clémancey, C. Darnault, D. Reichmann, P. Amara and J. C. Fontecilla-Camps, *Chem. Commun.*, 2019, DOI: 10.1039/C8CC09023H.



This is an Accepted Manuscript, which has been through the Royal Society of Chemistry peer review process and has been accepted for publication.

Accepted Manuscripts are published online shortly after acceptance, before technical editing, formatting and proof reading. Using this free service, authors can make their results available to the community, in citable form, before we publish the edited article. We will replace this Accepted Manuscript with the edited and formatted Advance Article as soon as it is available.

You can find more information about Accepted Manuscripts in the [author guidelines](#).

Please note that technical editing may introduce minor changes to the text and/or graphics, which may alter content. The journal's standard [Terms & Conditions](#) and the ethical guidelines, outlined in our [author and reviewer resource centre](#), still apply. In no event shall the Royal Society of Chemistry be held responsible for any errors or omissions in this Accepted Manuscript or any consequences arising from the use of any information it contains.

Journal Name

COMMUNICATION

## Design of Specific Inhibitors of Quinolinate Synthase based on [4Fe-4S] Cluster Coordination

 Received 00th January 20xx,  
Accepted 00th January 20xx

DOI: 10.1039/x0xx00000x

www.rsc.org/

 Jaione Saez Cabodevilla<sup>a,b</sup>, Anne Volbeda<sup>c</sup>, Olivier Hamelin<sup>a</sup>, Jean-Marc Latour<sup>a</sup>, Océane Gigarel<sup>c</sup>, Martin Clémancey<sup>a</sup>, Claudine Darnault<sup>c</sup>, Debora Reichmann<sup>a#</sup>, Patricia Amara<sup>c</sup>, Juan C. Fontecilla-Camps<sup>c</sup> and Sandrine Ollagnier de Choudens<sup>a\*</sup>

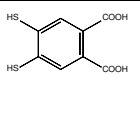
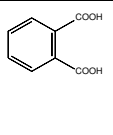
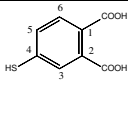
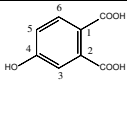
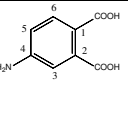
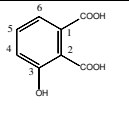
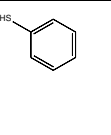
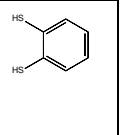
**Quinolinate synthase (NadA) is a [4Fe-4S] cluster-containing enzyme involved in the formation of quinolinic acid, the precursor of the essential NAD coenzyme. Here, we report the synthesis and activity of derivatives of the first inhibitor of NadA. Using multidisciplinary approaches we have investigated their action mechanism and discovered additional specific inhibitors of this enzyme.**

Biosynthesis of nicotinamide adenine dinucleotide (NAD), an essential and ubiquitous cofactor in biology, involves in all living organisms the synthesis of quinolinic acid (QA).<sup>1</sup> In mammals and some bacteria, QA can be synthesized from L-tryptophan<sup>2</sup> whereas in most prokaryotes it is generated from L-aspartate and dihydroxyacetone phosphate (DHAP) through the concerted action of two enzymes: the L-aspartate oxidase NadB that first converts L-aspartate to iminoaspartate (IA), and the quinolinate synthase NadA which condenses IA with DHAP to form QA<sup>3</sup> (Figure S1). Besides these *de novo* pathways for NAD synthesis, salvage pathways exist in some organisms allowing the coenzyme to be recycled from small metabolites such as niacin or nicotinamide.<sup>3</sup> The different pathways for QA biosynthesis in most prokaryotes and eukaryotes, combined with the fact that salvage pathways are absent in some pathogenic microorganisms such as *Mycobacterium leprae* and

*Helicobacter pylori*,<sup>4</sup> makes NadA an ideal target in the search for specific antibacterial drugs. All NadA proteins bind an oxygen-sensitive [4Fe-4S] cluster that is essential for its activity.<sup>5-7</sup> The cluster is ligated by three strictly conserved cysteines and an exchangeable water molecule.<sup>8,9</sup> In 2012, we demonstrated that 4,5 dithiohydroxyphthalic acid (DTHPA), a structural analogue of QA, binds irreversibly to the [4Fe-4S] cluster of *Escherichia coli* (*Ec*) NadA.<sup>10</sup> Binding of DTHPA inhibits *Ec*NadA activity, which strongly suggested that the unique iron site of the [4Fe-4S] cluster was intimately involved in QA synthesis.<sup>10</sup> This was unambiguously demonstrated by crystal structures of *Thermotoga maritima* (*Tm*) [4Fe-4S]-NadA active site mutants in which intermediates bound to the accessible iron site (Figure S1) were trapped.<sup>11,12</sup> DTHPA inhibits NadA activity *in vitro* but also QA formation at 10 μM in *E. coli* cells cultivated in minimal medium.<sup>10</sup> However, at higher concentrations DTHPA also inhibits other essential enzymes.<sup>10</sup>

Here, we have designed and synthesized a series of molecules related to DTHPA, and using biochemical, spectroscopic and crystallographic techniques we have found that two of them are specific NadA inhibitors. DTHPA is characterized by a benzene ring, substituted by two carboxylic acids and two thiolates, in 1,2 and 4,5 positions respectively. The influence of these groups was evaluated by assaying on *in*

**Table 1** IC<sub>50</sub> (μM) determined with [4Fe-4S]-*Ec*NadA (10 μM). (/) = no inhibition (n≥5). PA (phthalic acid), 4MP (4-mercaptophthalic acid), 4HP (4-hydroxyphthalic acid), 4AP (4-aminophthalic acid), 3HP (3-hydroxyphthalic acid), MB (mercaptobenzene), DMB (dimercaptobenzene).

								
DTHPA	PA	4MP	4HP	4AP	3HP	MB	DMB	
IC <sub>50</sub>	10	/	13	175	>5000	/	2000	59

<sup>a</sup> Univ. Grenoble Alpes, CEA, CNRS, BIG-LCBM, UMR5249, 38000, Grenoble, France

<sup>b</sup> Univ. Grenoble Alpes, CNRS, ICMG FR 2607, Département de Pharmacochimie Moléculaire, F-38041, Grenoble, France

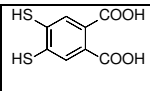
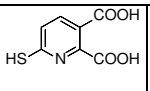
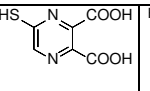
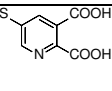
<sup>c</sup> Univ. Grenoble Alpes, CEA, CNRS, IBS, Metalloproteins, F-38000 Grenoble, France

<sup>#</sup> present address: Wachholtzstr. 2, 38106 Braunschweig, Germany

Electronic Supplementary Information (ESI) available: [details of any supplementary information available should be included here]. See DOI: 10.1039/x0xx00000x

*vitro* *EcNadA* activity the effect of commercially available DTHPA derivatives at various concentrations (0-5 mM), using DTHPA as a control (Table 1; Figure S2). First, we investigated the effect of Fe binding ligands. Phthalic acid (PA), which contains the two carboxylate groups of QA but lacks any other potential iron ligands, does not inhibit *NadA* activity even at a 500 equiv. excess relative to *NadA*. Conversely, the addition of an iron binding group at position 4 of the PA ring results in *NadA* inhibition. The strongest inhibitory effect, similar to that of DTHPA, is obtained with a thiolate group (4-mercaptophthalic acid, 4MP), followed by hydroxyl (4-hydroxyphthalic acid, 4HP) and amino groups (4-aminophthalic acid, 4AP). The position of the iron ligand relative to the carboxylate groups is crucial because, in contrast to 4HP, 3-hydroxyphthalic acid (3HP) is not inhibitory. We then considered the effect of carboxylate groups on inhibition because several crystal structures of *NadA* have revealed their involvement in complexes with substrate and intermediates.<sup>11, 12</sup> Mercaptobenzene (MB), which contains one thiolate but no carboxylate substituents, has an inhibitory effect 153 fold lower than 4MP; and dimercaptobenzene (DMB) that contains an extra thiolate inhibited *NadA* 6 times less than DTHPA. Taken together, these results indicate that the minimal chemical and steric requirements of a *NadA* inhibitor are a benzene core with two ortho carboxylates in positions 1 and 2 and at least one high affinity iron ligand (thiolate) in position 4 of the ring. Among the tested DTHPA analogs, 4MP proved to be the best inhibitor, with an  $IC_{50}$  close to that of DTHPA (Table 1). Docking of the Y intermediate in the *TmNadA* X-ray structure, carried out before the structure of the complex became available,<sup>12</sup> suggested that there was an interaction between the nitrogen atom of the pyridine ring and the conserved Asn109 at the active site.<sup>9</sup> According to this model and based on our structure-activity studies, we designed and synthesized 3 nitrogen-containing molecules, expected to be specific and potent *NadA* inhibitors by binding to the *NadA* [4Fe-4S] cluster: 6-mercaptopyridine-2,3-dicarboxylic acid (6MPDC), 5-mercaptopyrazine-2,3-dicarboxylic acid (5MPzDC) and 5-mercaptopyridine-2,3-dicarboxylic acid (5MPDC) (Table 2). These molecules were obtained in a few steps and reasonable overall yields (20%, 55% and 18% for 6MPDC, 5MPzDC and 5MPDC, respectively). They were used in aqueous solution under anaerobic conditions to prevent disulfide dimer formation (observed with 5MPDC). The effect of these molecules on *EcNadA* activity was assayed *in vitro* (Table 2, Figure S3). Their activity is in the same range as DTHPA and 4MP (tens of micromolar), showing that the presence of one or two nitrogen atom(s) in the benzene ring has no enhancing effect for *NadA* inhibition.

**Table 2**  $IC_{50}$  ( $\mu$ M) determined on [4Fe-4S]-*EcNadA* with from left to right: DTHPA, 6MPDC, 5MPzDC and 5MPDC ( $n \geq 4$ ).

				
	DTHPA	6MPDC	5MPzDC	5MPDC
$IC_{50}$	10	40	32	45

Crystal structures of complexes of the *TmNadA*\*Y21F variant with 4MP, 6MPDC and 5MPDC were refined at 1.64 Å, 1.9 Å and 2.1 Å resolution, respectively (Table S1). We call *TmNadA*\* the *TmNadA* variant that carries the K219R mutation,<sup>12</sup> which allows crystallization of *NadA* without affecting its biochemical and spectroscopic properties or its *in vivo* and *in vitro* activity.<sup>9</sup> *TmNadA*\*Y21F was incubated anaerobically with a 2-3.5 molar equiv. of the molecules and brown crystals appeared a few days after setting the crystallization drops. The three molecules fit well to omit Fo-Fc electron density maps calculated with phase information from refined models in which they were not included (Figure 1). All *NadA*-complexes display similar features: (i) like QA and the W, X and Y intermediates,<sup>11, 12</sup> the carboxylate groups of the inhibitors interact with active site amino acids from three different protein domains: His19 and Ser36 (domain 1), Ser124 (domain 2) and His193 and Thr210 (domain 3); (ii) all molecules bind to one iron of the cluster with their thiolate moiety with Fe-S distances of 2.2, 2.3 and 2.2 Å for 4MP, 6MPDC and 5MPDC, respectively; (iii) there is no binding between the cluster and the nitrogen atom of the ring of 6MPDC and 5MPDC, an interaction observed for an alternative QA binding mode.<sup>11, 13, 14</sup> Structures of *NadA*-4MP and *NadA*-6MPDC (Figure 1A-B) display very similar interactions with the protein environment, with a water molecule forming an additional hydrogen bond with the nitrogen atom of the ring in *NadA*-6MPDC (Figure 1B). This hydrogen bond likely decreases the electron density on the sulphur atom weakening the S-Fe bond. This might explain the difference in the  $IC_{50}$  between 4MP and 6MPDC. In the *NadA*-5MPDC complex (Figure 1C), there is a hydrogen bond between the pyridine nitrogen atom and His193 that causes a 180° rotation of the molecule when compared to 6MPDC. Because of this rotation, the thiolate group shifts by 2.1 Å (Figure S4), inducing an important structural constraint for iron binding that leads to cluster degradation. This observation underscores the influence of small changes in the binding mode of inhibitors to the *NadA* active site. Due to the slow degradation of 5MPzDC in water, we were unable to crystallize the *Tm*-5MPzDC complex. However, *in silico* docking of this molecule shows that it should bind the unique iron of the *NadA* active site with its thiolate function as 4MP and 6MPDC do (Figure S5).

Crystallographic data clearly define the interactions of inhibitors with *NadA* [4Fe-4S] cluster. We decided also to investigate the interactions of 4MP, 5MPDC, 5MPzDC and 6MPDC with the [4Fe-4S]-*EcNadA* cluster in solution (like the inhibition assays) using spectroscopic analyses. Indeed, previous studies of *EcNadA* with DTHPA revealed substantial spectroscopic changes associated to its binding to the cluster: (i) Mossbauer spectroscopy evidenced the formation of a new subsite ( $IS = 0.63 \text{ mm s}^{-1}$  and  $QS = 2.02 \text{ mm s}^{-1}$ ) and (ii) UV-visible spectroscopy revealed a new absorption at 500 nm together with a blue-shift of the characteristic  $S \rightarrow Fe^{3+}$  charge transfer 420 nm band of [4Fe-4S]-*EcNadA*.<sup>10</sup> Such strong changes were assigned to the chelation of DTHPA by its two thiolates and weaker ones are expected to be induced by the present

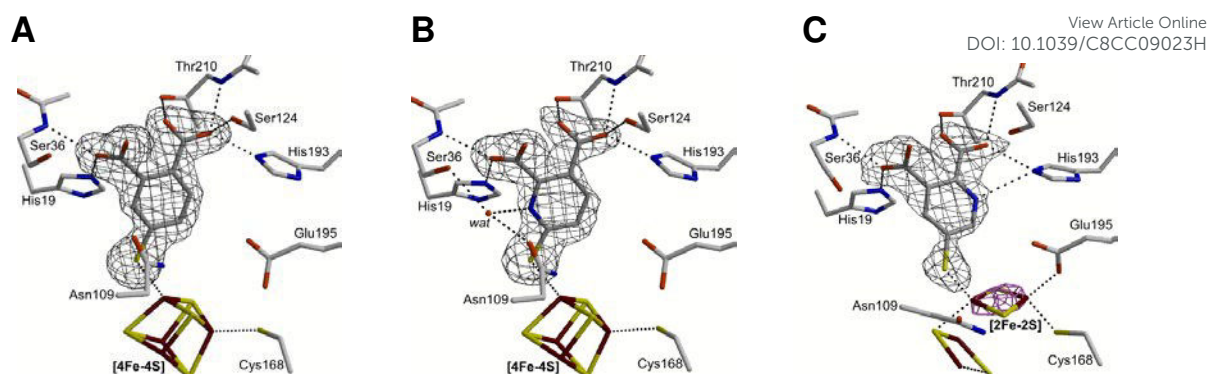


**Fig. 1** Electron density ( $F_{\text{obs}} - F_{\text{calc}}$ ) omit maps for three *TmNadA*\*-bound molecules. **A.** 4MP. **B.** 6MPDC. **C.** 5MPDC. The omit maps are indicated with a black mesh contoured at the 4.0  $\sigma$  level in **(B)** and 3.5  $\sigma$  level in **(A)** and **(C)**. In **(C)** an anomalous difference map shown in pink and contoured at 3.5 $\sigma$  indicates that the [4Fe-4S] cluster has been converted to a relatively well-defined fully occupied [2Fe-2S] cluster in which one Fe atom is bound to the thiolate of 5MPDC and the other to the carboxylate group of Glu195. Much weaker density is observed for the two other Fe atoms of the original [4Fe-4S] cluster and for one of its two remaining S atoms, which were each refined with 50% occupancies.

monothiolate inhibitors. Mossbauer spectra of  $^{57}\text{Fe}$ -labelled [4Fe-4S]-*EcNadA* incubated with an excess of these inhibitors are very similar to each other and consist of a quadrupole doublet similar to that of as-isolated *EcNadA* (Figures S6-S7) and to those of the [4Fe-4S]-LytB/IspH enzyme in complex with its substrate and two inhibitors.<sup>10, 15</sup> Simulations of the present spectra and those of as-isolated *NadA* were performed by taking into account three different contributions for each cluster: two Fe ions from a delocalized  $\text{Fe}^{2.5+}$  pair, and one  $\text{Fe}^{3+}$  and one  $\text{Fe}^{2+}$  ion both from a localized pair due to inhibitor binding. All spectra were satisfactorily accounted for (Figure S8) and in all cases the best-fit parameters reveal the presence of a differentiated Fe site within the cluster which is unveiled by altered IS and QS values vs those of the delocalized pair. Remarkably, whereas DTHPA, taken as a control, induces strong increases in IS and QS values (IS = 0.79  $\text{mm s}^{-1}$  and QS = 1.74  $\text{mm s}^{-1}$ ), 5- and 6MPDC and 5MPzDC cause far weaker changes similar in magnitude (IS =  $0.46 \pm 0.05 \text{ mm s}^{-1}$  and QS =  $0.86 \pm 0.09 \text{ mm s}^{-1}$ ) which is in line with their similar structures. Between these two extremes, 4MP exhibits the same isomer shift as as-isolated *NadA* (IS = 0.60  $\text{mm s}^{-1}$  vs 0.61  $\text{mm s}^{-1}$ , respectively) and the difference in their quadrupole splittings (QS = 1.21  $\text{mm s}^{-1}$  vs 1.14  $\text{mm s}^{-1}$ , respectively) is at the uncertainty level ( $\pm 0.07 \text{ mm s}^{-1}$ ) estimated from statistical analysis of fit results (see SI paragraph 1.6). As a result an interaction between 4MP and the *NadA* cluster in solution is not definitely evidenced by the data. We then resorted to UV-vis. absorption spectroscopy to further probe 4MP ligation taking 6MPDC for comparison. When an excess of both inhibitors is added to [4Fe-4S]-*EcNadA*, slight changes are noted in the 450-700 nm range where cluster absorptions are expected and difference spectra exhibit weak but clear absorptions (Figure S9). Thus, combination of Mossbauer and UV-vis. studies support that the four inhibitors bind to *NadA*'s [4Fe-4S] cluster in solution, likely through their single thiolate, in agreement with both the available crystal structures and docking data.

Next, we investigated the inhibition specificity of 4MP, 6MPDC, 5MPzDC, 5MPDC and DTHPA by testing their effects on the *in vitro* Aconitase B (AcnB) activity. *EcAcnB* was selected as a model to investigate the inhibition specificity because this

bacterial enzyme contains a [4Fe-4S] cluster that displays high functional and structural similarities with the *NadA* cluster.<sup>16</sup> Indeed, both clusters are catalytically involved in a dehydration process and are coordinated by three cysteine residues and solvent molecule(s) in their resting state.<sup>9,16</sup> While 1 equiv. of DTHPA inhibits 50% of *EcNadA* activity,<sup>10</sup> 5 equiv. of DTHPA were required to observe such an inhibition of the aconitase (Figure S10, black bars). When *EcNadA* and *EcAcnB* were incubated in a 1:1 ratio and in the presence of increasing amounts of DTHPA (Figure S10, grey bars), we observed 40% inhibition of *EcAcnB* activity for 20 equiv. of DTHPA. This experiment shows that although DTHPA can also inhibit *EcAcnB*, it is a better inhibitor of *NadA*, which explains some of the *in vivo* results.<sup>10</sup> Concerning DTHPA analogues, 6MPDC and 5MPzDC display 50% and 60% inhibition of *AcnB* activity with 20 and 10 equiv. respectively. Conversely, no inhibition is observed with 5MPDC and 4MP even at 50 equiv. (Figure 2). Taken together, these results show that, in addition to being good inhibitors, 4MP and 5MPDC are also specific to *NadA*.

Owing to differences in the structural and inhibiting specificities between 4MP and 6MPDC, we decided to further investigate their binding to *NadA* through a comparison to both [4Fe-4S]- and apo-*EcAcnB* using UV-visible spectroscopy at the low concentration conditions used for inhibition studies (Figure S11 and Figure 3). Addition of 5 equiv. of 4MP to [4Fe-4S]-*EcNadA*, apo-*EcAcnB* and [4Fe-4S]-*EcAcnB* does not provide clear-cut spectroscopic changes (Figure S11). However, close

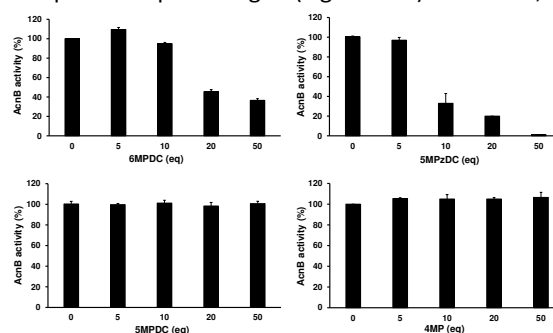


**Fig. 2** Inhibition of *EcAcnB* activity (%) by 6MPDC, 5MPzDC, 5MPDC and 4MP. *EcAcnB* (3  $\mu\text{M}$ ) was incubated with molecules (0-50 eq) for 15 min. and its activity measured. Each point is the average of three independent experiments.

examination of the 250–350 nm region reveals a small but significant absorption detected only in the [4Fe–4S]-EcNadA complex, consistent with the binding specificity of 4MP for NadA inhibition (Figure 3). This absorption can be associated either to the [4Fe–4S] cluster or to 4MP itself, but the absence of a spectroscopic change in the visible region suggests that it is due to a  $\pi$ – $\pi^*$  ligand transition of 4MP. Further analysis revealed that it is due to a ca 400  $\text{cm}^{-1}$  shift of the 4MP absorption in this region (Figure 3 and Table S4). By contrast, in both apo and [4Fe–4S]-EcAcnB, this 4MP absorption is almost not affected by the presence of the protein (the difference in energy maxima is about  $45 \pm 4 \text{ cm}^{-1}$ , Table S4). These data further confirm the interaction of 4MP with the NadA cluster in solution. The same UV-vis experiments in the presence of 5 equiv. of 6MPDC did not show any significant difference between the three proteins (Figure S11). A similar analysis of the absorptions revealed that the intensities of the 6MPDC ligand transitions are strongly enhanced in all cases. This suggests that under these experimental conditions 6MPDC interacts non-specifically with the three proteins through its carboxyl and/or thiol groups, which alters its own electronic transitions ( $\pi$ – $\pi^*$ ,  $n$ – $\pi^*$ ), without apparently affecting the electronic transitions of the cluster in the cases of [4Fe–4S]-EcNadA and [4Fe–4S]-EcAcnB. The absence of detectable interaction for 6MPDC can probably be traced to the low concentration used in these experiments. Indeed, in our different experiments we have studied the interaction of NadA with inhibitors over a wide range of concentrations of both, going from crystallography down to Mossbauer and then UV-visible spectroscopies. This allowed us to evidence interactions at the molecular level for some inhibitors, at a more global level for all of them and a specific interaction for a single one in line with the inhibition studies.

In summary, here we report an enzymatic, structural and spectroscopic study of the [4Fe–4S]-NadA enzyme in the

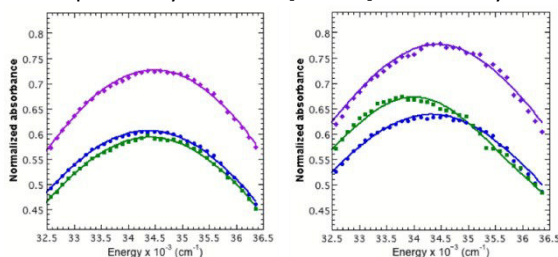


**Fig. 3** Experimental UV-visible spectra (dotted lines) and Gaussian simulations (solid lines) of 4MP in the absence (left) and in the presence (right) of protein: apo AcnB (blue), Fe-S AcnB (violet) and Fe-S NadA (green).

presence of a family of DTHPA analogs that show an inhibitory activity on NadA by binding to the catalytic iron site of the [4Fe–4S] cluster through their thiolate. Even though these molecules do not display a better inhibitory effect than the previously reported DTHPA, we highlight that two of them, 5MPDC and 4MP are more specific NadA inhibitors, which could be used as a base for further drug design. Indeed, identification of specific inhibitors is of great interest in the context of designing new antibacterials against the *M. leprae* and *H. pylori* pathogens.

Our efforts will be now concentrated on their optimization as well as the *in cellulo* activity of the optimized molecules.

This work was supported by the Agence Nationale pour la Recherche for the NADIN contract ANR-16-CE18-0026, the partial financial supports from the ARCANÉ Labex and CBH-EUR-GS (ANR-17-EURE-0003), GRAL Labex (ANR-10-LABEX-04).

## Conflicts of interest

There are no conflicts to declare.

## Notes and references

1. P. Frey and A. D. Hegeman, *Enzymatic Reaction Mechanisms*, Oxford University Press, New York, NY., 2007.
2. J. W. Foster and A. G. Moat, *Microbiol rev*, 1980, **44**, 83–105.
3. T. P. Begley, C. Kinsland, R. A. Mehl, A. Osterman and P. Dorrestein, *Vitamins and hormones*, 2001, **61**, 103–119.
4. S. Y. Gerdes, M. D. Scholle, M. D'Souza, A. Bernal, M. V. Baev, M. Farrell, O. V. Kurnasov, M. D. Daugherty, F. Mseeh, B. M. Polanuyer, J. W. Campbell, S. Anantha, K. Y. Shatalin, S. A. Chowdhury, M. Y. Fonstein and A. L. Osterman, *J bacteriol*, 2002, **184**, 4555–4572.
5. S. Ollagnier-de Choudens, L. Loiseau, Y. Sanakis, F. Barras and M. Fontecave, *FEBS Lett.*, 2005, **579**, 3737–3743.
6. A. H. Saunders, A. E. Griffiths, K. H. Lee, R. M. Cicchillo, L. Tu, J. A. Stromberg, C. Krebs and S. J. Booker, *Biochemistry*, 2008, **47**, 10999–11012.
7. R. M. Cicchillo, L. Tu, J. A. Stromberg, L. M. Hoffart, C. Krebs and S. J. Booker, *J. Am. Chem. Soc.*, 2005, **127**, 7310–7311.
8. C. Rousset, M. Fontecave and S. Ollagnier de Choudens, *FEBS Lett.*, 2008, **582**, 2937–2944.
9. M. V. Cherrier, A. Chan, C. Darnault, D. Reichmann, P. Amara, S. Ollagnier de Choudens and J. C. Fontecilla-Camps, *J Am Chem Soc*, 2014, **136**, 5253–5256.
10. A. Chan, M. Clemancey, J. M. Mouesca, P. Amara, O. Hamelin, J. M. Latour and S. Ollagnier de Choudens, *Angew Chem Int Ed Engl*, 2012, **51**, 7711–7714.
11. A. Volbeda, C. Darnault, O. Renoux, D. Reichmann, P. Amara, S. Ollagnier de Choudens and J. C. Fontecilla-Camps, *J Am Chem Soc*, 2016, **138**, 11802–11809.
12. A. Volbeda, J. S. Cabodevilla, C. Darnault, O. Gigarel, T. H. L. Han, O. Renoux, O. Hamelin, S. Agnier-de-Choudens, P. Amara and J. C. Fontecilla-Camps, *ACS Chemical Biology*, 2018, **13**, 1209–1217.
13. O. A. Esakova, A. Silakov, T. L. Grove, A. H. Saunders, M. I. McLaughlin, N. H. Yennawar and S. J. Booker, *J Am Chem Soc*, 2016, **138**, 7224–7227.
14. M. K. Fenwick and S. E. Ealick, *Biochemistry*, 2016, **55**, 4135–4139.
15. A. Ahrens-Botzong, K. Janthawornpong, J. A. Wolny, E. N. Tambou, M. Rohmer, S. Krasutsky, C. D. Poulter, V. Schunemann and M. Seemann, *Angew Chem Int Ed Engl*, 2011, **50**, 11976–11979.
16. H. Beinert, M. C. Kennedy and C. D. Stout, *Chem. Rev.*, 1996, **96**, 2335–2374.